Title

Novel Antimicrobial Compositions and Mathematical Models for Reducing Microbial Contamination of Fresh Produce and Food Contact Surfaces

Author

Yi, Jiyoon

Publication Date

2021

Peer reviewed|Thesis/dissertation

Novel Antimicrobial Compositions and Mathematical Models for Reducing Microbial Contamination of Fresh Produce and Food Contact Surfaces

By

JI YOON YI

DISSERTATION

Submitted in partial satisfaction of the requirements for the degree of

DOCTOR OF PHILOSOPHY

in

Food Science

in the

OFFICE OF GRADUATE STUDIES

of the

UNIVERSITY OF CALIFORNIA

DAVIS

Approved:

Nitin Nitin, Chair

Christopher W. Simmons

Mukund V. Karwe

Committee in Charge

2021

ACKNOWLEDGMENTS

I would like to express my gratitude to all faculty, staff, and supporters who have provided me with countless opportunities and fellowships and have facilitated my learning during PhD.

First, I would like to thank my major professor, Dr. Nitin Nitin, for his support, encouragement, and motivation throughout my PhD study. I am deeply grateful for his guidance and mentoring in research and will be taking his advice with me past the PhD.

I would also like to thank Drs. Chris Simmons, Tina Jeoh, Erin DiCaprio, Ameer Taha, and Juliana Bell for their service on my qualifying examination and insightful advice of my research and professional growth. For my dissertation committee, I'd like to thank Drs. Mukund Karwe and Chris Simmons for their support and feedback through the dissertation writing process. Additionally, I would like to acknowledge my research collaborators and staff who worked with me for my dissertation project: Dr. Gang Sun, Dr. Glenn Young, Dr. Johan Leveau, Dr. Atul Parikh, Dr. Hung Doan, Yue Ma, Matt Ford, Dr. Mike Clegg, and Sam Hakim.

I would like to thank those around me who also supported me during my PhD: FST/BAE friends and all lab mates in the Nitin lab. Many thanks to Dr. Kang Huang for patience and support in my early PhD and Dr. Achyut Adhikari for mentoring in my career. I'd also like to thank all the mentors from Ewha Womans University for their continuous support.

I benefited from immense support from these next groups, and I am grateful for their contributions to my developing definition of service: people at Graduate Studies, Public Scholarship and Engagement, SoFE-SD co-founders, CPS Executive Board, IAFP staff and SPDG board members, IAFP Affiliate Council, and CalFP members.

A special thank you to my family, Dr. Keon Young Yi, Myung Hee Kim, Dr. Kwang Moo Yi, and Dr. Heewon Bahng, whose incredible love and care keep me going. And to all my friends, thank you for your encouragement, commiseration, and support.

Novel Antimicrobial Compositions and Mathematical Models for Reducing Microbial Contamination of Fresh Produce and Food Contact Surfaces

ABSTRACT

Microbial contamination of fresh produce is one of the key risk factors that can lead to a nationwide outbreak of foodborne diseases. Microbial pathogens can be transmitted to fresh produce by cross-contamination during postharvest processing, which has been traced to the contamination of food contact surfaces and the growth of biofilms on these surfaces. Thus, there is an unmet need to understand the dynamics of bacterial transfer from food contact surfaces to fresh produce and improve decontamination processes to reduce cross-contamination. To address this need, this dissertation is focused on: (i) quantitative analysis of cross-contamination between fresh produce and food contact surfaces; (ii) development of antimicrobial food contact surfaces and evaluation of their efficacy in reducing cross-contamination; (iii) mechanistic mathematical modeling of targeted antimicrobial delivery systems for improved biofilm inactivation; and (iv) advancing a fundamental understanding of barriers to decontamination of fresh produce.

In this research, a reproducible methodology was elaborated to simulate cross-contamination with varying physical contact conditions. Using this method, bacterial transfer between fresh produce and food contact surfaces with different hydrophobicity was quantified. Moreover, antimicrobial plastics were developed for food contact surfaces using chlorine-based sanitizer, and their effectiveness in reducing cross-contamination was evaluated. A poly(vinyl alcohol-co-ethylene) film was selected as a model hydrophilic plastic, and chlorine was chemically bound to these films with *N*-halamine precursors. A polypropylene coupon was selected as a model hydrophobic plastic, and food-grade coatings were deposited on these coupons to charge chlorine using biobased *N*-halamine precursors. Furthermore, a mathematical modeling framework was

established to understand decontamination processes. Biofilm inactivation was modeled for a conventional sanitizer (free chlorine) and biobased targeted delivery systems (chlorine stabilized with yeast microparticles) based on mass transport and biochemical reaction kinetics. A system of partial differential equations was computed using COMSOL Multiphysics® software, and the simulation results were validated with experimental data. Similarly, microbial inactivation on a leaf surface was modeled for the same conventional sanitizer and the biobased targeted delivery systems, using topomimetic leaf replicasts prepared by microfabrication.

The results of these investigations using a combination of experimental and mathematical modeling approaches illustrate the followings: (i) Cross-contamination of fresh produce was a rapid process (< 5 s), which exponentially increased with the contact time, and the applied contact force resulted in a linear increase in bacterial transfer from a contaminated leaf to other surfaces; (ii) Development of antimicrobial plastics with chemically bound chlorine or food-grade coatings both significantly reduced the risk of cross-contamination between fresh produce and food contact surfaces; (iii) Design of biobased targeted delivery systems for chlorine-based sanitizers significantly enhanced the antibiofilm activity. The simulation results showed that this enhancement was attributed to propertied of yeast microparticles, which improved chemical stability of chlorine and provided binding affinity to deliver the stabilized chlorine to target biofilms; (iv) Microscale topographical features and compositions of a leaf surface could be critical barriers to decontamination of fresh produce using conventional sanitizers. Effective decontamination may require novel sanitizer compositions that can target microbes in the macroscale crevices along protruding veins or microscale grooves of a leaf surface.

Overall, this research demonstrates that microbial contamination of fresh produce can be reduced by immobilizing antimicrobials on food contact surfaces using *N*-halamine formulations

with enhanced chemical stability. Furthermore, the research mechanistically illustrates the ability of biobased targeted delivery systems in improving decontamination of biofilms or fresh produce. The combination of experimental and mathematical modeling approaches proposed in this dissertation will advance the development of novel antimicrobial compositions and their enhanced delivery to the target microbes.

TABLE OF CONTENTS

LIST OF FIGURES

LIST OF TABLES

NOMENCLATURE

Symbols

	Description	Units
a	Intercept of a linear regression model	-
A	Area of aqueous/biofilm interface	m^2
A_s	Area of sample plastic film/coupon	cm^2
b	Slope of a linear regression model	s^{-1}, N^{-1}
B_0	Initial concentration of live bacteria	kg/m^2, kg/m^3
$B(t)$	Concentration of live bacteria	kg/m^2, kg/m^3
C_0	Initial concentration of free chlorine	kg/m^3
C_∞	Total chlorine concentration initially charged to yeast microparticles	kg/m^3
$C(t)$	Concentration of free chlorine	kg/m^3
$C_S(t)$	Concentration of chlorine charged in a yeast microparticle	kg/kg
D_C	Diffusivity of free chlorine	m^2/s
$D_{C,\mathrm{eff}}$	Effective diffusivity	m^2/s
D_S	Diffusivity of yeast microparticles	m^2/s
F_{app}	Applied contact force	N
k_0	Rate of natural decay of free chlorine	s^{-1}
k_1	Rate of chlorine depletion by nonspecific reactions with organic matter	$m^3/(kg \cdot s)$
k_b	Rate of binding of free yeast microparticles	s^{-1}
k_C	Rate of bacterial inactivation by free chlorine	$m^3/(kg \cdot s)$
k_{r1}	Rate of passive release of chlorine from free yeast microparticles	s^{-1}
k_{r2}	Rate of apparent active release of chlorine from surface-bound yeast microparticles	s^{-1}
k_S	Rate of bacterial inactivation by chlorine-charged yeast microparticles	$m^2/(kg \cdot s)$
m_B	Mass of a bacterium (*Escherichia coli*)	kg
N	Concentration of sodium thiosulfate used in chlorine titration	mol/L
N_0	Initial number of bacteria on a contaminated leaf	CFU/cm^2
N_t	Number of bacteria on a non-contaminated leaf after contact	CFU/cm^2
O_0	Initial concentration of organic matter	kg/m^3
O_l	Concentration of plant organic matter on the leaf surface	kg/m^2
$O(t)$	Concentration of organic matter	kg/m^3
$O_B(t)$	Concentration of dead bacteria	kg/m^2
r	Radius of biofilm	m
S_0	Initial concentration of yeast microparticles	kg/m^3
$S_{\mathrm{b},\infty}$	Maximum concentration of biofilm-bound yeast microparticles within 1 h incubation	kg/m^2
$S(t)$	Concentration of free yeast microparticles	kg/m^3
$S_\mathrm{b}(t)$	Concentration of surface-bound yeast microparticles	kg/m^2
t	Time	s
V	Volume of iodine solution used in chlorine titration (control)	L
V_b	Volume of biofilm	m^3

V_s	Volume of iodine solution used in chlorine titration (sample)	L
V_w	Volume of aqueous phase	m^3
z_b	Height of biofilm	m
z_l	Maximum height of leaf surface structure	m
z_w	Height of aqueous phase	m

Greek letters

	Description	Units
ρ_N	Density of bacteria in biofilm	kg/m^3
ρ_O	Density of organic matter in biofilm	kg/m^3
ϕ	Biofilm porosity	-
τ	Biofilm tortuosity	-

CHAPTER 1:

Introduction and Literature Review

1.1. Microbial Contamination of Fresh Produce

1.1.1. Microbial pathogens in the fresh produce industry

Contamination of fresh produce by microbial pathogens is a critical food safety challenge, as it has been associated with nationwide outbreaks of foodborne illnesses (Berg, Erlacher, Smalla, & Krause, 2014; Havelaar et al., 2010; Painter et al., 2013; Yeni, Yavaş, Alpas, & Soyer, 2016). It was reported that 46% of foodborne illnesses between 1998–2008 in the United States were attributed to fresh produce, including leafy greens and fruits (Painter et al., 2013). Most of these fresh produce-related outbreaks have been associated with leafy greens, such as romaine lettuce, spinach, and iceberg lettuce (Marshall et al., 2020; Painter et al., 2013). Consumer demand for fresh produce has increased over the past decades because of its beneficial effects on reducing chronic human diseases (Berger et al., 2010; Gustat, O'Malley, Luckett, & Johnson, 2015). However, these commodities are typically minimally processed and consumed raw to maximize the nutritional benefits of essential vitamins and minerals, high fiber content, and low energy density (Goodburn & Wallace, 2013; Gustat et al., 2015; Rickman, Barrett, & Bruhn, 2007a; Rickman, Bruhn, & Barrett, 2007b). Consequently, sanitation steps in postharvest processing of fresh produce aim at 2–3 log reduction of potential microbial pathogens rather than intensive sterilization and mainly focuses on limiting cross-contamination during the process steps.

Microbial pathogens could be introduced to the postharvest processing environment via various routes, including fresh produce, wash water, equipment and other food contact surfaces, and human (Garner & Kathariou, 2016; Gil et al., 2015; Lynch, Tauxe, & Hedberg, 2009; Rajwar, Srivastava, & Sahgal, 2016; Yeni et al., 2016). Contaminated fresh produce could be collected

from farms where soil and irrigation water quality is poor, or organic fertilizers such as animal manures or abattoir wastes are used (Alegbeleye, Singleton, & Sant'Ana, 2018; Gil et al., 2015; Lynch et al., 2009; Rajwar et al., 2016). Due to the lack of adequate reduction in microbial load, the contaminated produce can disseminate microbial pathogens to other produce during handling, storage, transportation, and cleaning steps (Gil et al., 2015; Lynch et al., 2009; Rajwar et al., 2016; Yeni et al., 2016). Moreover, the washing step is designed to remove field dirt and debris, but it could also transfer microbial pathogens to fresh produce (Gil et al., 2015; Lynch et al., 2009). Chlorine-based sanitizers are typically used to control microbes in wash water, yet their antimicrobial efficacy could be insufficient in the presence of high organic matter coming from farm debris and plant materials (Fu, Li, Awad, Zhou, & Liu, 2018; Shen, Luo, Nou, Wang, & Millner, 2013; Weng et al., 2016; Zhou, Luo, Nou, Lyu, & Wang, 2015). Furthermore, food contact surfaces, such as conveyor belts, knives, and reusable containers, can be other sources of microbial cross-contamination (Gil et al., 2015; Rajwar et al., 2016; Yeni et al., 2016). Specifically, reusable plastic containers that are used during handling, transportation, and storage steps can contain microbial pathogens and may not be regularly sanitized during work hours (Izumi, Poubol, Hisa, & Sera, 2016; Izumi, Tsukada, Poubol, & Hisa, 2016; Shi et al., 2016; Singla, Goel, & Ganguli, 2014). Other studies have also reported that agricultural workers with improper hygiene practices could also cause cross-contamination (Gil et al., 2015; Lynch et al., 2009; Rajwar et al., 2016). Overall, microbial pathogens in postharvest processing environments can persist and transferred to fresh produce, resulting in foodborne illness.

The major foodborne pathogens associated with fresh produce are *Listeria monocytogenes,* pathogenic *Escherichia coli*, *Salmonella* spp., *Shigella* spp., *Yersinia* spp., *Staphylococcus aureus*, *Clostridium* spp. (Alegbeleye et al., 2018; Harris et al., 2003; Yeni et al., 2016). Among these

microbes, *L. monocytogenes* is known for its high mortality rate of 20–30% in immunocompromised individuals (Alegbeleye et al., 2018; Painter et al., 2013; Zhu, Gooneratne, & Hussain, 2017). This microbial pathogen is a Gram-positive bacterium, and it causes an infection called listeriosis that is vulnerable to elderly people, infants and toddlers, pregnant women, and the unborn (Zhu et al., 2017). Moreover, *L. monocytogenes* can survive in postharvest processing environments for an extended time since they can form biofilms, persist in cold temperature, and resistant to physiological stresses (Blackman & Frank, 2016; Garner & Kathariou, 2016; Mafu, Roy, Goulet, & Savoie, 1991; Yeni et al., 2016). Thus, monitoring and controlling the survival and colonization of *L. monocytogenes* on equipment and food contact surfaces is an essential task in the fresh produce industry. Another major concern in the fresh produce industry, especially for leafy greens, is a Gram-negative Shiga toxin-producing *E. coli* (Marshall et al., 2020; Olaimat & Holley, 2012; Yeni et al., 2016). This type of pathogenic *E. coli* annually causes more than 265000 illnesses and corresponding economic losses in the United States, and leafy greens are one of the most dominant sources of foodborne *E. coli* outbreaks (Marshall et al., 2020). To this end, many studies on the washing and sanitation process of leafy greens have focused on reducing pathogenic *E. coli*, such as *E. coli* O157:H7 (Doan, Antequera-Gómez, Parikh, & Leveau, 2020; Fu et al., 2018; Huang, Tian, Salvi, Karwe, & Nitin, 2018; Luo et al., 2011; N. Singh, Singh, Bhunia, & Stroshine, 2002). In addition, *Salmonella* spp. are Gram-negative bacteria that have more than 2700 serovars and abundant in nature, and they have also been associated with contamination of fresh produce (Alegbeleye et al., 2018; Bennett et al., 2018; Harris et al., 2003; Yeni et al., 2016). Depending on their serovars, *Salmonella* spp. can survive a wide range of temperatures and extremely acidic environments so that they may contaminate fresh produce throughout the supply

chain, including preharvest, postharvest, storage, and handling conditions (Alegbeleye et al., 2018; Yeni et al., 2016).

1.1.2. Microbial adhesion mechanisms

Cross-contamination of fresh produce begins with the adhesion of microbial pathogens to the produce surface. In this section, the underlying mechanisms of microbial adhesion to substratum surfaces (e.g., fresh produce, food contact surfaces, or any other surfaces) are described by a combination of physicochemical interactions and biochemical binding. Since physicochemical interaction energy between two adjacent bodies causes the initial nonspecific microbe–substratum surface interactions, physicochemical surface properties influencing microbial adhesion are also discussed.

1.1.2.1. Microbial adhesion to fresh produce

Previous studies have reported that microbial adhesion to a substratum surface can be divided into two steps: (i) initial nonspecific physicochemical interactions and (ii) the following specific adhesin–receptor binding (Abdallah et al., 2014; Jaglic et al., 2014; Krachler & Orth, 2013). The initial nonspecific interactions involve reversible physicochemical attachment of microbes to substratum surfaces (Abdallah et al., 2014; Jaglic et al., 2014; Krachler & Orth, 2013). During this process, as shown in Figures 1.1a–b, different types of physicochemical surface properties such as surface topography, roughness, and hydrophobicity can affect the level of the interactions (Abdallah et al., 2014; Bagherifard et al., 2015; Lorenzetti et al., 2015; Perera-Costa, Bruque, González-Martín, Gómez-García, & Vadillo-Rodríguez, 2014). Once a microbe and its substratum surface get closer by this initial step, the microbial adhesin–substratum surface receptor

binding interaction occurs (Abdallah et al., 2014; Jaglic et al., 2014; Krachler & Orth, 2013). In this second step, a rigid cellular and chemical adherence is formed, based on a specificity between the adhesin and receptors (Duque et al., 2013; Jaglic et al., 2014; Mittal et al., 2014).

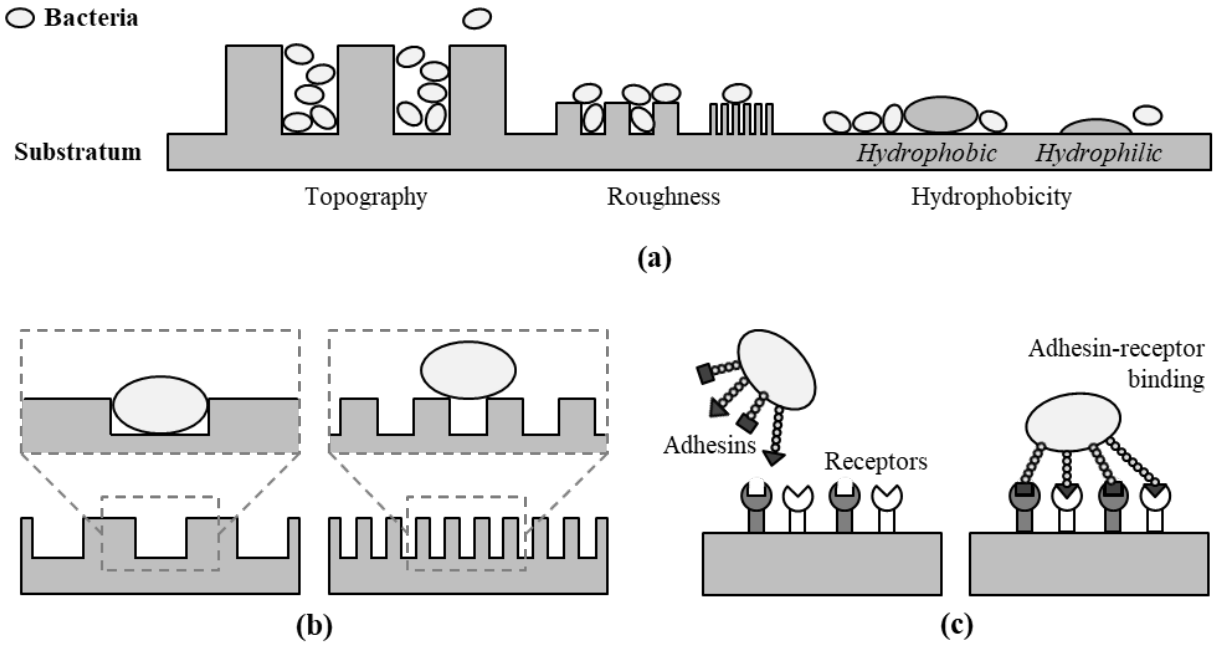

Figure 1.1. Schematic diagrams of microbe–substratum surface interaction. (a) Effect of surface properties on nonspecific physicochemical interactions between microbes and substratum surfaces. Surface topography, roughness, and hydrophobicity are discussed in this chapter (Abdallah et al., 2014; Bagherifard et al., 2015; Lorenzetti et al., 2015; Perera-Costa, Bruque, González-Martín, Gómez-García, & Vadillo-Rodríguez, 2014). (b) Effect of surface roughness on contact area (Lorenzetti et al., 2015). Higher roughness results in the reduced contact area, in turn reducing the interactions. (c) Consequent specific microbial adhesins–substratum surface receptor binding interactions (Krachler & Orth, 2013). After the microbe gets close to the substratum surface via nonspecific physicochemical interactions, bindings are formed with the receptors on the substratum surface through microbial adhesins.

1.1.2.1.1. Nonspecific physicochemical interactions

Microbial adhesion is initiated by reversible and transient nonspecific interactions between a microbe and its substratum surface, and the physicochemical surface properties may play critical roles in governing this process (Abdallah et al., 2014; Jaglic et al., 2014; Krachler & Orth, 2013). In the literature, this initial step of microbial adhesion is described by the Derjaguin, Landau, Verwey, and Overbeek (DLVO) theory, which was originally developed to explain the stability of colloidal suspension with nonspecific physicochemical interactions (Abdallah et al., 2014; Yun Chen, Harapanahalli, Busscher, Norde, & van der Mei, 2014; Lorenzetti et al., 2015). The DLVO theory approximates the interaction energy or potential between two bodies based on the Lifshitz-van der Waals, electrostatic double-layer, Lewis acid-base, and hydration interactions (Israelachvili, 2011). As a microbe moves closer to its substratum surface, the Lifshitz-van der Waals and electrostatic interactions act first (Abdallah et al., 2014; Yun Chen et al., 2014; Lorenzetti et al., 2015). Briefly, the Lifshitz-van der Waals interaction is a dispersive attraction that occurred by dipole and/or induced dipole of each body (the microbe and substratum surface). Electrostatic double-layer interaction is a combination of chemical interactions between each body and ions in media. The levels of these interactions depend on the distance between two bodies and their physicochemical properties (Abdallah et al., 2014). After this initial attachment, the Lewis acid-base and hydration interactions further control the microbial adhesion. The Lewis acid-base interaction is a polar interaction of each body with media by a donation of an unshared electron pair. The hydration interaction comes from the surface hydrophobicity of each body in the presence of aqueous media.

1.1.2.1.2. Specific adhesin-receptor binding

As shown in Figure 1.1c, after the microbe is attached to the substratum surface by nonspecific interactions, a pairing of specific microbial adhesins and substratum receptors occurs (Krachler & Orth, 2013). Common microbial surface adhesins include fimbriae, pili, and flagella, which consist of proteins that have binding ability to other biotic or abiotic surfaces (Adamek, Linke, & Schwartz, 2014; Jaglic et al., 2014; Krachler & Orth, 2013). The production of fimbriae or pili is biochemically controlled, and this governs virulence in foodborne pathogens such as pathogenic *Escherichia coli*, *Salmonella* spp., *Yersinia* spp., *Pseudomonas* spp., *Klebsiella* spp., *Haemophilus* spp. (Krachler & Orth, 2013). In the case of *L. monocytogenes*, it was reported that surface proteins such as biofilm-associated protein L, extracellular DNA, and flagellin FlaA bind to abiotic surfaces, while other proteins like enolase, fibronectin-binding protein, internalin, and cellulose-binding protein bind to biotic cells (Jaglic et al., 2014).

Moreover, several microbial adhesins were reported to bind their receptors on the plant surfaces (Lima, São José, Andrade, Pires, & Ferreira, 2013; Pfeilmeier, Saur, Rathjen, Zipfel, & Malone, 2016; Rossez et al., 2014; Upadhyay, Upadhyaya, Kollanoor-Johny, & Venkitanarayanan, 2013). The flagellum was reported as an adhesin for the attachment of *L. monocytogenes* to plant tissues (Upadhyay et al., 2013), and *E. coli* O157 also used its flagellum to adhere to phospholipids or sulpholipids in plasma membranes of plants (Rossez et al., 2014). Other bacteria such as *Salmonella* Enteritidis secreted chemical compounds of sugars and proteins called mucilage, which helps them adhere and grow on the lettuce leaf surfaces (Lima et al., 2013). For a plant-associated bacterium *Pseudomonas*, it was reported that microbial surface proteins, such as flagellin protein flg22 and EF-Tu protein elf18, bound to their receptors on the plant surfaces, flagellin sensing 2 and EF-Tu receptor, respectively (Pfeilmeier et al., 2016).

1.1.2.2. Physicochemical factors

Since nonspecific physicochemical interactions initiate the microbial adhesion, this could be affected by intrinsic factors, including surface topography/roughness/hydrophobicity (Figure 1.1a), as well as extrinsic factors, including contact time/force and media conditions (Abdallah et al., 2014; Bagherifard et al., 2015; Katsikogianni & Missirlis, 2004; Krachler & Orth, 2013; Lorenzetti et al., 2015; Perera-Costa et al., 2014).

As shown in Figures 1.1a–b, the macroscopic surface topography of the substratum determines the peaks and valleys, where microbes may topographically favor the valleys (Abdallah et al., 2014; Bagherifard et al., 2015; Lorenzetti et al., 2015; Perera-Costa et al., 2014; Sirinutsomboon, Delwiche, & Young, 2011). In contrast, the microscopic surface roughness of a substratum surface can have a size similar to that of microbes (Figures 1.1a–b). Thus, the surface roughness controls the contact area between the microbe and substratum surface, which affects the level of the Lifshitz-van der Waals attraction (Israelachvili, 2011). On the other hand, the change in the shape of the microbial cell wall caused by extrinsic physical impacts can also affect the microbial adhesion process (Yun Chen et al., 2014). This prior study reported that the nanoscale deformation of the cell wall of *Staphylococcus aureus* caused by the applied contact force (1–9 nN) increased the contact area, increasing the Lifshitz-van der Waals force between the microbe and the substratum surface. In the case of Gram-negative *Pseudomonas* spp., however, they had more fluidic outer membranes so that they were less affected by the substratum surface roughness than *Staphylococcus* spp. (Bagherifard et al., 2015).

In addition to the physical factors, microbial surface hydrophobicity and the presence of media may further affect the initial microbial adhesion (Abdallah et al., 2014; Katsikogianni &

Missirlis, 2004; Krachler & Orth, 2013; Lorenzetti et al., 2015). It was reported that hydrophobic surfaces were favored in the adhesion of microbes such as *P. aeruginosa, Staphylococcus aureus* (Abdallah et al., 2014), and *Bacillus subtilis* (Perera-Costa et al., 2014). Since the surface of leafy greens is also hydrophobic due to the epidermal lipid layer of cutin, suberin, and waxes (Lima et al., 2013), the hydration interactions between a microbe and a leaf surface in the presence of water could promote microbial adhesion (Abdallah et al., 2014; Lorenzetti et al., 2015). Furthermore, if the microbial adhesion process occurs in aqueous conditions, organic matter in the media may result in an ionic or pH effect that influences the electrostatic or the Lewis acid-base interactions between microbe and substratum (Abdallah et al., 2014; Yun Chen et al., 2014; Lorenzetti et al., 2015).

1.1.3. Current studies on microbial contamination and unmet needs

Experimental studies on microbial contamination and cross-contamination of fresh produce focused on various sources of contamination, such as wash water, abiotic, or biotic surfaces (Allende, Selma, López-Gálvez, Villaescusa, & Gil, 2008; Bornhorst et al., 2018; Buchholz, Davidson, Marks, Todd, & Ryser, 2012a, 2012b; Y Chen, Jackson, Chea, & Schaffner, 2001; Jensen, Danyluk, Harris, & Schaffner, 2017; Jensen, Friedrich, Harris, Danyluk, & Schaffner, 2013). A study on water-mediated *E. coli* contamination demonstrated that contaminated fresh produce could disseminate *E. coli* to another non-contaminated one by wash water (Allende et al., 2008). This prior study compared different types of wash water, including potable water, diluted recirculated water, and recirculated water with microbes and organic matter. The results showed that the initial contamination level of fresh produce and recirculation of wash water significantly increased cross-contamination, suggesting the use of proper wash water

sanitizers to maintain the water quality. Moreover, studies on the transfer of *E. coli* O157:H7 between leafy greens and equipment surfaces were conducted to understand cross-contamination levels during overall small-and pilot-scale postharvest processing (Buchholz et al., 2012a, 2012b). In their studies, it was reported that most of the inoculated *E. coli* O157:H7 were transferred to wash water and then cross-contaminated to the produce and equipment surfaces, such as shredder, conveyor belt, flume tank, shaker table, and centrifugal dryer. Moreover, the results in these studies showed that one contaminated batch of leafy greens in the processing line led to cross-contamination of following batches, highlighting the risk potential of cross-contamination in postharvest processing environments. In addition, studies have also examined cross-contamination during food preparation, looking into various abiotic food contact surfaces made up of ceramics, metals, glasses, plastics as well as hands (Y Chen et al., 2001; Jensen et al., 2017, 2013). One of these studies reported that the microbial transfer direction, i.e., either from fresh produce or food contact surfaces, significantly influenced the transfer rates (Jensen et al., 2013). Overall, studies on microbial contamination of fresh produce emphasized the importance of effective sanitizers in controlling the microbial and chemical quality of wash water and food contact surfaces.

Nevertheless, there has not been much progress on understanding the influences of physicochemical factors on microbial contamination, as the studies on cross-contamination of fresh produce lack precise control on contact dynamics. For example, an early study on cross-contamination of leafy greens with *E. coli* O157:H7 was conducted by mixing a contaminated leaf with non-contaminated leaves with varying moisture (Wachtel & Charkowski, 2002). The purpose of their study was to simulate a particular scenario, i.e., the lettuce preparation procedure in the restaurant, so the mixing process was performed without exact contact time, force, and the area between leaf surfaces. In contrast, a recent study investigated the influence of contact time on the

cross-contamination from abiotic surfaces to foods, including fresh produce force (Miranda & Schaffner, 2016). However, the food samples in their study were manually dropped on contaminated abiotic surfaces so that the applied contact force in each case would have been different. Similarly, a previous study on cross-contamination of romaine lettuce utilized a sterile weight to press two contacted samples with constant applied contact force, but this process was manually controlled, and the contact time and forces were not varied further (Moore, Sheldon, & Jaykus, 2003). Thus, there is an unmet need to investigate quantitative methods for evaluating the influences of physicochemical factors on microbial contamination of fresh produce.

1.2. Sanitation of Fresh Produce and Food Contact Surfaces

1.2.1. Limitations of sanitation in fresh produce processing

Despite the current efforts in sanitizing wash water and food contact surfaces in fresh produce processing environments, there are still unresolved challenges due to the persistence of microbes entrapped in self-secreted biofilm matrices, organic matter in wash water, and microbes on the fresh produce.

1.2.1.1. Significance of biofilms

Microbes attached to a surface can form biofilms, which are microbes enclosed in a matrix of extracellular polymeric substances (EPS). These biofilms can lead to a critical public health issue, as they accounted for 65% of chronic human infections (Yadav, Song, Singh, & Vidal, 2020). Moreover, biofilms also have been associated with foodborne outbreaks due to their increased resistance to sanitation and cleaning (Meireles, Ferreira, Melo, & Simões, 2017; Srey, Jahid, & Ha, 2013). In the case of fresh produce, biofilms are formed in the postharvest processing

environments, including conveyor belt, drying area, and floor drain, and these could then cross-contaminate to fresh produce (Srey et al., 2013). Furthermore, coliforms and *Escherichia coli* biofilms persist in water distribution systems despite the use of antimicrobials, resulting in a high risk of water safety (Lisle et al., 1998; Murphy, Payne, & Gagnon, 2008; Williams & Braun-Howland, 2003). The resistance of biofilms to sanitation and cleaning could be attributed to their structural and biochemical characteristics (Hall-Stoodley, Costerton, & Stoodley, 2004; Høiby, Bjarnsholt, Givskov, Molin, & Ciofu, 2010; Yadav et al., 2020): (i) As illustrated in Figure 1.2, the self-secreted EPS matrix of biofilms works as organic matter that consumes antimicrobials such as free chlorine (Hall-Stoodley et al., 2004; Kim, 2016; Yadav et al., 2020); (ii) Microbes in biofilms grow at a slower rate than those in suspension (Yadav et al., 2020). This could potentially slow down the effectiveness of antimicrobials that act in ways that interrupt cell division or metabolic cycles (Hall-Stoodley et al., 2004; Yadav et al., 2020); (iii) Biofilms can have dormant, nondividing phenotypic variant cells, which are called persisters (Bigger, 1944). These persister cells can survive antimicrobial treatment and then restart to grow and divide after the depletion of antimicrobials (Yadav et al., 2020). Overall, these properties also make chlorine-based sanitizers less effective in the treatment of biofilms than that of planktonic cells (Lin, Zhu, Wang, & Yu, 2017; Meireles et al., 2017).

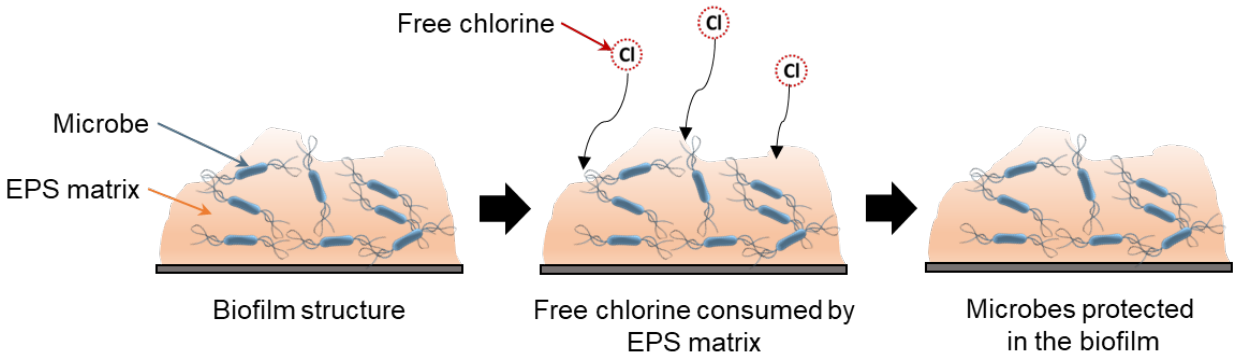

Figure 1.2. A schematic diagram of biofilm inactivation process by free chlorine. EPS: extracellular polymeric substances. The EPS matrix consumes free chlorine upon contact, and thus, microbes entrapped in this self-secreted EPS matrix are protected.

1.2.1.2. Microbes on the fresh produce

Microbes attached to the surface of fresh produce have an increased persistence against chlorine-based sanitizers (Gil, Selma, López-Gálvez, & Allende, 2009; Olaimat & Holley, 2012; Wang, Feng, Liang, Luo, & Malyarchuk, 2009). Chlorine-based sanitizers, such as sodium hypochlorite and hypochlorous acid (also called free chlorine), are commonly used in the fresh produce industry based on their ability to inactivate a wide range of microbes, fast reaction rates, and low cost (Fan & Sokorai, 2015; Luo et al., 2011; Teng et al., 2018; Weng et al., 2016). The antimicrobial efficacy of these chlorine-based sanitizers against microbial pathogens in suspensions has been well established in the literature (Luo et al., 2011; Zhao, Doyle, Zhao, Blake, & Wu, 2001). However, this efficacy can be highly limited against microbes attached to any abiotic (Cabeça, Pizzolitto, & Pizzolitto, 2012; LeChevallier et al., 1988), biotic (Fransisca & Feng, 2012; Fu et al., 2018; Olaimat & Holley, 2012), or biomimetic surfaces (Zhang et al., 2014). This could be because of the substratum surface topography that provides harborage for microbes or the reactivity of the surface that increases chlorine demand (Fu et al., 2018; LeChevallier et al., 1988; Zhang et al., 2014). Previous studies on the leaf surface confirmed that surface topography (Doan, Antequera-Gómez, Parikh, & Leveau, 2020) and compositional characteristics (Fu et al., 2018; Weng et al., 2016) of leafy greens influenced the microbial persistence against chlorine-based sanitizers.

1.2.1.3. Role of organic matter in wash water

Wash water used in postharvest processing of fresh produce is often reused and recirculated, making organic matter accumulate easily and consume free chlorine (Allende et al., 2008; Luo et al., 2011; Nou et al., 2011; Weng et al., 2016; Zhou et al., 2015). Organic matter in

wash water is normally introduced along with fresh produce, which comes from the soil, farm debris, plant exudates, or microbes (Fu et al., 2018; Gil et al., 2009; Huang, Tian, Salvi, Karwe, & Nitin, 2018). The level of organic matter in was water is measured in terms of chemical oxygen demand (COD), and it increases linearly proportional to the amount of fresh produce entering the washing system (Fu et al., 2018; Luo et al., 2012; Munther, Luo, Wu, Magpantay, & Srinivasan, 2015). The COD level may vary among different fresh produce commodities, where chopped or shredded ones release more exudates (Weng et al., 2016). Consequently, the rapid depletion of free chlorine may occur by high COD level in wash water so that microbial pathogens could potentially survive and cross-contaminate fresh produce (Ayebah, Hung, Kim, & Frank, 2006; Fu et al., 2018; Gómez-López, Lannoo, Gil, & Allende, 2014; Korany et al., 2018; Luo et al., 2011; Shen et al., 2013; Weng et al., 2016; Zhou et al., 2015). These reactions between organic matter and free chlorine may also generate byproducts such as chloramines, organochloramines trihalomethanes (Gómez-López, Marín, Medina-Martínez, Gil, & Allende, 2013; López-Gálvez et al., 2010; Zhou et al., 2015). Therefore, researchers have suggested using a total chlorine level higher than the desired final concentration to compensate for chlorine loss by organic matter (Luo et al., 2011). Other studies used chlorine stabilizers such as T-128, which is made up of phosphoric acid and propylene glycol (generally recognized as safe, GRAS) (Nou et al., 2011; Shen et al., 2012; Yang, Luo, Millner, Shelton, & Nou, 2012). This chemical enhanced the chemical stability of free chlorine in wash water, but it showed a limited effect on fresh produce surfaces (Nou et al., 2011).

1.2.2. Developing novel antimicrobial compositions

As a response to the limitations of current sanitation practices discussed in Section 1.2.1, researchers have developed novel antimicrobial materials using different approaches to maximize the microbial inactivation efficiency and economic benefits of conventional chlorine-based sanitizers. These efforts include developing antimicrobial polymers by binding chemicals on the food contact surfaces and utilizing micro-or nano-sized carriers that deliver antimicrobial agents to target cells. More recently, biobased carriers such as yeast cell wall microparticles were investigated to further reduce potential chemical toxicity and meet the needs of the fresh produce industry.

1.2.2.1. Potential of antimicrobial polymers as food contact surfaces

Considering that food contact surfaces mediate cross-contamination of fresh produce (see Section 1.1.3), studies have been conducted to develop various antimicrobial polymers (Appendini & Hotchkiss, 2002; López-Carballo, Higueras, Gavara, & Hernández-Muñoz, 2013; López, Sánchez, Batlle, & Nerín, 2007; Qiao et al., 2017; Si et al., 2017; Sun, Wang, Kadouh, & Zhou, 2014). In these studies, antimicrobial agents such as *N*-halamines, enzymes, essential oils, silver nanoparticles, or phenolic acids were chemically bound to different polymers, showing efficient antimicrobial activity. For example, gallic acid-incorporated chitosan films inactivated 2.5 logs of *L. innocua* by 24-h treatment (Sun et al., 2014), whereas pectin/polylactic acid films containing nisin inactivated 2.1 logs of *L. monocytogenes* by 48-h treatment (Jin, Liu, Zhang, & Hicks, 2009). In contrast, thermoplastic polyurethane (TPU) films modified with *N*-halamine resulted in 6 log reduction of *E. coli* O157:H7 by 2-h treatment (Qiao et al., 2017), and *N*-halamine incorporated poly(vinyl alcohol-co-ethylene) (PVA-co-PE) reduced 5 logs of *E. coli* O157:H7 in 1 h (Si et al.,

2017). These results demonstrated the potential of *N*-halamine polymers in rapid microbial inactivation during dynamic postharvest processing.

N-halamine is a halogen derivative of nitrogen, which has the ability to inactivate a wide range of microbes at low cost (Dong, Wang, Gao, Gao, & Gao, 2017). Previous studies reported that *N*-halamine polymers are not only effective in microbial inactivation but also rechargeable, stable, and non-toxic to humans (Badrossamay & Sun, 2009b, 2009a; Qiao et al., 2017; Si et al., 2017). Moreover, *N*-halamines can be incorporated into various polymers, including polyethylene (Badrossamay & Sun, 2009a), polypropylene (Badrossamay & Sun, 2009b), PVA-co-PE (Si et al., 2017), by reactive extrusion methods. This flexibility may enable diverse options in selecting appropriate food contact surfaces. In addition, unlike conventional sanitizers that may lose antimicrobial efficacy when food materials are present (see Section 1.2.1), *N*-halamine particles or compounds showed effective antimicrobial activity in the presence of fresh produce (Huang & Nitin, 2019) or raw beef (Ren, Qiao, Huang, Weese, & Ren, 2018), respectively. However, prior studies have tested these *N*-halamine materials mostly over long exposure time (Badrossamay & Sun, 2009b; Qiao et al., 2017). A study from Qiao et al. (2017) evaluated the antimicrobial activity of *N*-halamine films made up of thermoplastic polyurethane against *E. coli* O157:H7, showing 6 log reduction within 2 h of incubation. Similarly, Badrossamay & Sun (2009b) investigated various *N*-halamine polypropylene-based polymers in *E. coli* inactivation, and they incubated these polymers with microbes for 1–16 h. Therefore, the effectiveness of *N*-halamine polymers in rapid microbial inactivation, especially in the presence of organic matter, has not been studied. This fast time scale in antimicrobial activity is critical to the postharvest processing of fresh produce, as the operations last for less than 20 min (Gombas et al., 2017; Pérez-Rodríguez et al., 2014). Moreover, *N*-halamine polymers have been studied in the form of films and coatings, which

provide the potential in flexible applications to existing equipment (Dong et al., 2017). Nevertheless, their application to food contact surfaces and the effectiveness in reducing cross-contamination of fresh produce have not been studied.

1.2.2.2. Targeted antimicrobial delivery systems using carriers

To improve sanitation of wash water or biofilms, targeted delivery systems for antimicrobials have been investigated using micro-or nanoparticles as carriers (Choi, Yu, Esteban Fernández, & Hu, 2010; C. Ferreira et al., 2010; Carla Ferreira, Pereira, Pereira, Simões, & Melo, 2013; Li et al., 2008; Sharma et al., 2019). Since these micro-or nanoparticles have a large surface-to-volume ratio, they can be used to load a high concentration of active agents and release these agents in a sustained manner (Barreras-Urbina et al., 2016; Carla Ferreira et al., 2013; Forier et al., 2014). Due to these advantages, micro-and nanoparticles are extensively studied in biomedical, food, and environmental sectors to develop targeted delivery systems. Nonspecific targeting could be achieved by electrostatic interaction or hydrogen bonding of the particles with target microbes or biofilms (Forier et al., 2014), and it delivers antimicrobials for a prolonged time in a controlled manner (Forier et al., 2014; Kim, 2016). However, these nonspecific interactions can be unstable due to the environment, such as the presence of salts and other biomolecules (Cui, Li, Li, Vittayapadung, & Lin, 2016; Joye, Davidov-Pardo, & McClements, 2014). Moreover, both the encapsulation efficiency and the ability to encapsulate diverse antimicrobials can be limited for conventional particles (Forier et al., 2014; Kim, 2016). On the other hand, specific targeting is based on the binding between specific ligands of carriers and target microbes (Forier et al., 2014). In this specific binding, antibodies or lectins are used as ligands, and their respective antigens or carbohydrate residues are used as target receptors (Forier et al., 2014; Stratford & Bond, 1992).

Yet, chemical modification steps are required to achieve this ligand–receptor binding, which may rely on human skills at a high cost (Rukavina & Vanić, 2016). Alternatively, biobased carriers derived from yeast or other microbial cells with a natural bioaffinity to target microbes or biofilms could be used (Huang, Dou, & Nitin, 2019; Hwang et al., 2017; Kuroda, Ueda, Shibasaki, & Tanaka, 2002; Nam et al., 2002). These carriers are discussed in detail in Section 1.2.2.3.

Previous studies on targeted delivery systems for antimicrobials demonstrated that they were effective in biofilm treatment (Cui, Bai, Rashed, & Lin, 2018; Carla Ferreira et al., 2013). A study on calcium carbonate microparticles loaded with benzyldimethyldodecylammonium chloride showed that 1.97 logs of microbes in *P. fluorescens* biofilms were inactivated within 1 h, whereas the free form of this antimicrobials without microparticles inactivated almost nothing within the same treatment time (Carla Ferreira et al., 2013). Similarly, chitosan nanoparticles loaded with clove oil resulted in approximately 2 log reduction of *E. coli* O157:H7 in biofilms by 8-h treatment (Cui et al., 2018). In the same study, *E. coli* O157:H7 in the biofilms were further inactivated by 24-h treatment, resulting in approximately 5 log reduction.

1.2.2.3. Yeast cell wall microparticles as biobased carriers

Yeast cell wall microparticles (or simply yeast microparticles) are derived from food-grade yeast such as *Saccharomyces cerevisiae*, and they have been used as antimicrobial carriers for chlorine and essential oils due to their distinct bioaffinity (da Silva Lima, Maciel, Mendonça, & Costa Junior, 2017; Huang et al., 2019; Paramera, Karathanos, & Konteles, 2014). This natural affinity to bind diverse microbes or their biofilms enables specific targeting of active agents, which originated from specific lectin-carbohydrate binding between yeast microparticles and biofilms (Forier et al., 2014). It has been reported that the surface of the yeast microparticles is rich in

α-mannan and β-glucan (Huang et al., 2019; Kogan & Kocher, 2007), and these carbohydrates have specific binding affinities with lectins on microbial surfaces, such as concanavalin A (Touhami, Hoffmann, Vasella, Denis, & Dufrêne, 2003) and Dectin-1 (Kogan & Kocher, 2007), respectively. Yeast microparticles may also have lectins on their surface (Singh, Bhari, & Kaur, 2011), which can bind to carbohydrates in EPS, such as α-mannopyranosyl and α-glucopyranosyl residue (Forier et al., 2014).

Previous studies using yeast microparticles charged with antimicrobials showed superior biocidal effects against different microbes and biofilms (Dou, Huang, & Nitin, 2021; Huang et al., 2019). Chlorine-charged yeast microparticles showed rapid inactivation of both planktonic cells and biofilms with different species, including *L. innocua*, *E. coli* O157:H7, and *Candida albicans* (Huang et al., 2019). In this prior study, all planktonic cells were inactivated within a few minutes, with or without the presence of organic matter (a high COD level of 2000 mg/L). For biofilms, the same formulation of chlorine-charged yeast microparticles resulted in complete inactivation (> 7 logs) of *E. coli* O157:H7 and *L. innocua* biofilms within 20 and 60 min, respectively. These results were highly effective compared to when an equivalent amount of conventional free chlorine was used. Only 2–3 logs were inactivated in both *E. coli* O157:H7 and *L. innocua* biofilms after 60 min of free chlorine treatment. Similarly, yeast microparticles significantly enhanced the antimicrobial and antibiofilm activities of photosensitizer curcumin (Dou et al., 2021).

1.3. Mathematical Modeling in Antimicrobial Delivery Systems

1.3.1. Mass transport and reaction kinetics in antimicrobial delivery systems

Understanding mechanisms of an antimicrobial delivery system may involve mass transport of active agents and chemical/biochemical reactions involved in the system. Spatial

distributions of antimicrobials could be primarily affected by physical factors that govern mass transport, such as fluid flow or system geometry. For example, a water supply through a pipeline may have biofilms developed near the pipe wall (Figure 1.3) (Fish, Osborn, & Boxall, 2016). These biofilms can be treated with chlorine-based sanitizers injected along with the inlet water flow. However, only a limited amount of chlorine may be accessible to the target microbes in the biofilms due to the heterogeneity in chlorine distribution. Without sufficient mixing in the flow, chlorine may bypass the target microbes since the scale of biofilms is much tiny compared to the entire system. Moreover, as shown in Figures 1.1a–b, the surface topography or roughness can provide harborage to microbes adhered on a substratum surface, including biotic and abiotic surfaces. These surface structures are often heterogeneous, especially in food matrices, which may have structural features at different spatial scales ranging from sub-micron level to centimeter level. Since microbes are microns in size, variations in spatial scales with orders of magnitude may result in different observations across a heterogeneous surface. Thus, it is vital to understand the level of sanitizers accessible to the targets based on mass transport. Furthermore, chemical reactions of sanitizers with organic matter in the system could also limit access to target microbes. In the case of a targeted antimicrobial delivery system with biobased carriers, biochemical reactions could dominate microbial inactivation. The specific binding affinity of carriers may enhance the local mass of antimicrobials near the target microbes, and the reaction time could be prolonged based on controlled release to prevent the regrowth of microbes. Overall, a comprehensive and mechanistic understanding of mass transport and reaction kinetics would determine the spatiotemporal distributions of sanitizers and the efficacy of microbial inactivation.

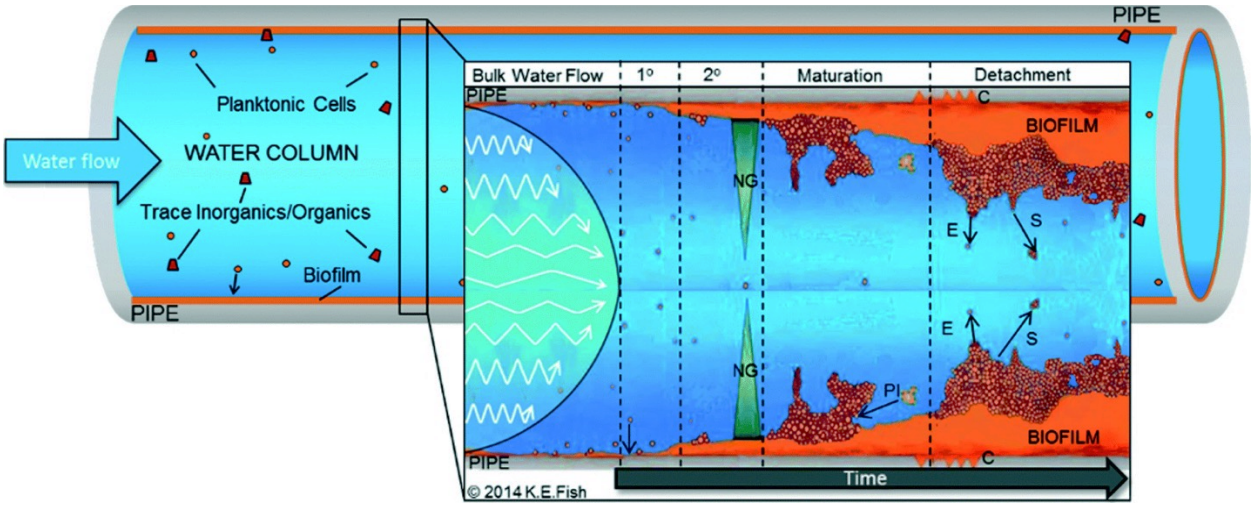

Figure 1.3. Biofilm development within the pipe of drinking water distribution system. Illustration was created by Fish, Osborn, & Boxall (2016).

1.3.2. Sanitation of fresh produce using conventional antimicrobials

Mechanistic mathematical modeling approaches have been applied to understand the postharvest washing and sanitation process of fresh produce since industry-scale experiments are often limited due to the safety issue (Abnavi, Alradaan, Munther, Kothapalli, & Srinivasan, 2019; Kinsinger, Mayton, Luth, & Walker, 2017; Munther et al., 2015; Pérez Rodríguez et al., 2011; Srinivasan, Dehghan Abnavi, Sulak, Kothapalli, & Munther, 2020).

Munther et al. (2015) built a time-dependent model for a well-mixed produce washing system, based on a system of equations describing microbial inactivation in the presence of organic matter in the wash water. In their study, the free chlorine reaction with the organic matter was modeled as second-order kinetics, where the plant organic matter in wash water and microbes were lumped together. The microbial inactivation by free chlorine was also modeled as second-order kinetics with another rate constant obtained from their prior experimental observations (Luo et al., 2012). Furthermore, they modeled planktonic microbes in the wash water and microbes attached to the produce surface separately to account for the net bacterial attachment rate. Their following studies modeled similar systems, while the free chlorine depletion rate by organic matter in wash water was estimated for different commodities, including carrots, cabbage, iceberg lettuce, romaine lettuce, and other leafy greens (Abnavi et al., 2019; Srinivasan et al., 2020). In general, mechanistic modeling approaches by this group established a foundation for understanding chemical reactions in the washing process of fresh produce.

In contrast, Kinsinger et al. (2017) computed spatiotemporal change of chlorine and microbes by a mechanistic modeling approach coupled with 2-dimensional (2D) leaf surface topography. They developed a system of equations describing mass transport and fluid dynamics involved in the washing process but did not include chemical reaction terms. The effect of chlorine

inactivation was combined with microbial removal in terms of the mass transfer rate coefficients. In addition, the 2D geometry of the leaf surface was estimated based on roughness measurement using atomic force microscopy but did not replicate the repeated leaf surface structures such as veins, stomata, and epidermal pavement cells. These structures should be included in future modeling approaches since their influences on the chlorine efficacy were reported in the literature (Doan, Antequera-Gómez, et al., 2020; Zhang et al., 2014). Therefore, future studies may advance by modeling 3D leaf surface topography (see Section 1.3.3) and a combination of mass transport and chemical reactions.

1.3.3. Targeted antimicrobial delivery systems

Traditional mechanistic modeling approaches in targeted delivery systems have focused on biomedical sectors such as drug delivery (Dash, Murthy, Nath, & Chowdhury, 2010; Ying, Wang, Lamm, & Kamei, 2013). These approaches have been recently extended to the targeted delivery of antimicrobials biofilm treatment (Jing et al., 2014; Loo et al., 2016). Biofilms can be a complex domain where physical, chemical, and microbiological processes co-exist (Pérez, Picioreanu, & Van Loosdrecht, 2005). Therefore, previous studies on biofilm inactivation modeling made significant simplifications (Jing et al., 2014; Loo et al., 2016; Peulen & Wilkinson, 2011). Jing et al. (2014) modeled the binding of ceria nanoparticles on a biofilm using a simple pseudo-first-order kinetics equation. They have not included the diffusion term, assuming that physical sorption, or binding, was a dominating process. Similarly, Loo et al. (2016) modeled the release kinetics of silver and curcumin nanoparticles for biofilm treatment using different models (zero-order, first-order, Higuchi, and Hixson-Crowell) but did not couple with mass transport. On the contrary, Peulen and Wilkinson (2011) modeled the diffusion of nanoparticles inside biofilms

using a classical diffusion model in a porous media. However, they did not consider reaction terms, such as binding of nanoparticles to biofilms or release of antimicrobials from nanoparticles. Thus, there is an unmet need to develop a comprehensive mechanistic modeling approach to understand the spatiotemporal information in targeted antimicrobial delivery systems for biofilm treatment. These models should consider design factors, including the size of carriers, chemical stability of antimicrobials against organic matter, binding affinity of carriers to target microbes, and release properties of antimicrobials from carriers (Cui et al., 2016; Forier et al., 2014; Jing et al., 2014; Joye et al., 2014; Loo et al., 2016; Peulen & Wilkinson, 2011).

1.3.4. 3-dimensional (3D) modeling of leaf surfaces

To obtain a reliable spatial prediction on leaf surfaces, it is critical to precisely define the 3D leaf structures. As discussed in Sections 1.1.2.2 and 1.2.1.1, surface topography and roughness affect microbial adhesion and their susceptibility to antimicrobials. However, prior efforts on building a leaf surface geometry have been oversimplified by taking its average surface roughness of relatively smooth zones (Macarisin, Patel, Bauchan, Giron, & Ravishankar, 2013; Wang et al., 2009) or compiling 2D images to reconstruct a 3D image (Wang et al., 2009). These averaging or interpolation methods may not represent the topographical map of leafy greens. Moreover, leaf surface structures are influenced by the species, cultivar, and growth environments (Zhang et al., 2014). Therefore, we would have to connect the topographical properties (distribution of peaks and valleys) and microbial behaviors.

Accordingly, experimental approaches have been made to generate topomimetic surfaces of leafy greens (Doan, Antequera-Gómez, et al., 2020; Doan, Ngassam, et al., 2020; Zhang et al., 2014). In these studies, leaf surface topography was replicated on a silicon-based polymer called

polydimethylsiloxane (PDMS) using a two-step casting method. These PDMS-based leaves were called leaf replicasts, and they reproduced the leaf surface topography at a submicron scale. Zhang et al. (2014) used these leaf replicasts to map the local microbial distribution after chlorine treatment and reported that *E. coli* survived more in the grooves and stomata of the leaf surface. Doan et al. (2020a), on the other hand, reported that the number of *E. coli* surviving from chlorine treatment was influenced by the vein structures. These results highlight the role of surface patterns created by leaf structure, which were not considered in most earlier studies (Fransisca & Feng, 2012; Gómez-López et al., 2013; Horikawa, Chai, Zhao, Wikle, & Chin, 2014; Huang & Nitin, 2019; Palma-Salgado et al., 2020; Zhang et al., 2014).

1.4. Overview of the Dissertation Study

1.4.1. Study hypothesis and objectives

The overall hypothesis of this research was that microbial contamination of fresh produce could be reduced by immobilizing antimicrobials on food contact surfaces and utilizing biobased targeted antimicrobial delivery systems for biofilms and microbes on fresh produce. The specific aims were designed to test the overall hypothesis as follows:

- Develop a reproducible method to quantitatively analyze cross-contamination of fresh produce and determine the influences of physicochemical factors
- Formulate antimicrobial polymers that chemically bind chlorine on food contact surfaces and assess their efficacy in reducing cross-contamination of fresh produce
- Mathematically model targeted delivery systems for biofilm treatment using biobased carriers, evaluate the design parameters, and experimentally validate the simulation results

- Analyze the leaf surface topography and its influence on the antimicrobial efficacy by integrating experimental and simplified mathematical modeling approaches

1.4.2. Study outline

In this dissertation, the work is divided into seven chapters. Chapter 1 provides an overview of microbial contamination of fresh produce, limitations and novel approaches in the sanitation of fresh produce and food contact surfaces, and mathematical modeling in antimicrobial delivery systems. Chapters 2–4 presents experimental works: quantitative analysis of cross-contamination from fresh produce (Chapter 2); evaluation of antimicrobial *N*-halamine incorporated hydrophilic plastic films in reducing cross-contamination of fresh produce (Chapter 3); and development of antimicrobial food-grade coatings on hydrophobic food contact surfaces to reduce cross-contamination (Chapter 4). In Chapter 5, a mechanistic mathematical modeling approach was developed and experimentally validated to design targeted antimicrobial delivery systems for *E. coli* biofilm treatment using yeast microparticles. Chapter 6 combines experimental and mathematical modeling approaches to assess the influence of leaf surface topography on antimicrobial efficacy. Chapter 7 summarizes the key findings of the dissertation and presents directions for future research.

References

Abdallah, M., Benoliel, C., Jama, C., Drider, D., Dhulster, P., & Chihib, N.-E. (2014). Thermodynamic prediction of growth temperature dependence in the adhesion of *Pseudomonas aeruginosa* and *Staphylococcus aureus* to stainless steel and polycarbonate. *Journal of Food Protection*, *77*(7), 1116–1126. https://doi.org/10.4315/0362-028X.JFP-13-365

Abnavi, M. D., Alradaan, A., Munther, D., Kothapalli, C. R., & Srinivasan, P. (2019). Modeling of free chlorine consumption and *Escherichia coli* O157:H7 cross-contamination during fresh-cut produce wash cycles. *Journal of Food Science*, *84*(10), 2736–2744. https://doi.org/10.1111/1750-3841.14774

Adamek, M., Linke, B., & Schwartz, T. (2014). Virulence genes in clinical and environmental *Stenotrophomas maltophilia* isolates: A genome sequencing and gene expression approach. *Microbial Pathogenesis*, *67–68*(1), 20–30. https://doi.org/10.1016/j.micpath.2014.02.001

Alegbeleye, O. O., Singleton, I., & Sant'Ana, A. S. (2018). Sources and contamination routes of microbial pathogens to fresh produce during field cultivation: A review. *Food Microbiology*, *73*, 177–208. https://doi.org/10.1016/j.fm.2018.01.003

Allende, A., Selma, M. V., López-Gálvez, F., Villaescusa, R., & Gil, M. I. (2008). Impact of wash water quality on sensory and microbial quality, including *Escherichia coli* cross-contamination, of fresh-cut escarole. *Journal of Food Protection*, *71*(12), 2514–2518. https://doi.org/10.4315/0362-028X-71.12.2514

Appendini, P., & Hotchkiss, J. H. (2002). Review of antimicrobial food packaging. *Innovative Food Science and Emerging Technologies*, *3*, 113–126. https://doi.org/10.1016/S1466-8564(02)00012-7

Ayebah, B., Hung, Y. C., Kim, C., & Frank, J. F. (2006). Efficacy of electrolyzed water in the inactivation of planktonic and biofilm *Listeria monocytogenes* in the presence of organic matter. *Journal of Food Protection*, *69*(9), 2143–2150. https://doi.org/10.4315/0362-028X-69.9.2143

Badrossamay, M. R., & Sun, G. (2009a). A study on melt grafting of *N*-halamine moieties onto polyethylene and their antibacterial activities. *Macromolecules*, *42*(6), 1948–1954. https://doi.org/10.1021/ma802270b

Badrossamay, M. R., & Sun, G. (2009b). Durable and rechargeable biocidal polypropylene polymers and fibers prepared by using reactive extrusion. *Journal of Biomedical Materials Research - Part B Applied Biomaterials*, *89*(1), 93–101. https://doi.org/10.1002/jbm.b.31191

Bagherifard, S., Hickey, D. J., de Luca, A. C., Malheiro, V. N., Markaki, A. E., Guagliano, M., & Webster, T. J. (2015). The influence of nanostructured features on bacterial adhesion and bone cell functions on severely shot peened 316L stainless steel. *Biomaterials*, *73*, 185–197. https://doi.org/10.1016/j.biomaterials.2015.09.019

Barreras-Urbina, C. G., Ramírez-Wong, B., López-Ahumada, G. A., Burruel-Ibarra, S. E., Martínez-Cruz, O., Tapia-Hernández, J. A., & Rodríguez Félix, F. (2016). Nano- and micro-particles by nanoprecipitation: Possible application in the food and agricultural industries. *International Journal of Food Properties*, *19*(9), 1912–1923. https://doi.org/10.1080/10942912.2015.1089279

Bennett, S. D., Sodha, S. V, Ayers, T. L., Lynch, M. F., Gould, L. H., & Tauxe, R. V. (2018). Produce-associated foodborne disease outbreaks, USA, 1998–2013. *Epidmiology and Infection*, *146*, 1397–1406. https://doi.org/10.1017/S0950268818001620

Berg, G., Erlacher, A., Smalla, K., & Krause, R. (2014). Vegetable microbiomes: is there a

connection among opportunistic infections, human health and our ‘gut feeling’? *Microbial Biotechnology*, *7*(6), 487–495. https://doi.org/10.1111/1751-7915.12159

Berger, C. N., Sodha, S. V., Shaw, R. K., Griffin, P. M., Pink, D., Hand, P., & Frankel, G. (2010). Fresh fruit and vegetables as vehicles for the transmission of human pathogens. *Environmental Microbiology*, *12*(9), 2385–2397. https://doi.org/10.1111/j.1462-2920.2010.02297.x

Bigger, J. W. (1944). Treatment of staphylococcal infections with penicillin by intermittent sterilisation. *Lancet*, *2*, 497–500. https://doi.org/10.1016/S0140-6736(00)74210-3

Blackman, I. C., & Frank, J. F. (2016). Growth of *Listeria monocytogenes* as a biofilm on various food-processing surfaces. *Journal of Food Protection*, *59*(8), 827–831. https://doi.org/10.4315/0362-028x-59.8.827

Bornhorst, E. R., Luo, Y., Park, E., Vinyard, B. T., Nou, X., Zhou, B., … Millner, P. D. (2018). Immersion-free, single-pass, commercial fresh-cut produce washing system: An alternative to flume processing. *Postharvest Biology and Technology*, *146*, 124–133. https://doi.org/10.1016/j.postharvbio.2018.08.008

Buchholz, A. L., Davidson, G. R., Marks, B. P., Todd, E. C. D., & Ryser, E. T. (2012a). Quantitative transfer of *Escherichia coli* O157:H7 to equipment during small-scale production of fresh-cut leafy greens. *Journal of Food Protection*, *75*(7), 1184–1197. https://doi.org/10.4315/0362-028x.jfp-11-489

Buchholz, A. L., Davidson, G. R., Marks, B. P., Todd, E. C. D., & Ryser, E. T. (2012b). Transfer of *Escherichia coli* O157:H7 from equipment surfaces to fresh-cut leafy greens during processing in a model pilot-plant production line with sanitizer-free water. *Journal of Food Protection*, *75*(11), 1920–1929. https://doi.org/10.4315/0362-028X.JFP-11-489

Cabeça, T. K., Pizzolitto, A. C., & Pizzolitto, E. L. (2012). Activity of disinfectants against foodborne pathogens in suspension and adhered to stainless steel surfaces. *Brazilian Journal of Microbiology*, *43*(3), 1112–1119. https://doi.org/10.1590/S1517-83822012000300038

Chen, Y, Jackson, K. M., Chea, F. P., & Schaffner, D. W. (2001). Quantification and variability analysis of bacterial cross-contamination rates in common food service tasks. *Journal of Food Protection*, *64*(1), 72–80. https://doi.org/10.4315/0362-028X-64.1.72

Chen, Yun, Harapanahalli, A. K., Busscher, H. J., Norde, W., & van der Mei, H. C. (2014). Nanoscale cell wall deformation impacts long-range bacterial adhesion forces on surfaces. *Applied and Environmental Microbiology*, *80*(2), 637–643. https://doi.org/10.1128/AEM.02745-13

Choi, O., Yu, C. P., Esteban Fernández, G., & Hu, Z. (2010). Interactions of nanosilver with *Escherichia coli* cells in planktonic and biofilm cultures. *Water Research*, *44*(20), 6095–6103. https://doi.org/10.1016/j.watres.2010.06.069

Cui, H., Bai, M., Rashed, M. M. A., & Lin, L. (2018). The antibacterial activity of clove oil/chitosan nanoparticles embedded gelatin nanofibers against *Escherichia coli* O157:H7 biofilms on cucumber. *International Journal of Food Microbiology*, *266*, 69–78. https://doi.org/10.1016/j.ijfoodmicro.2017.11.019

Cui, H., Li, W., Li, C., Vittayapadung, S., & Lin, L. (2016). Liposome containing cinnamon oil with antibacterial activity against methicillin-resistant *Staphylococcus aureus* biofilm. *Biofouling*, *32*(2), 215–225. https://doi.org/10.1080/08927014.2015.1134516

da Silva Lima, A., Maciel, A. P., Mendonça, C. de J. S., & Costa Junior, L. M. (2017). Use of encapsulated carvacrol with yeast cell walls to control resistant strains of *Rhipicephalus microplus* (Acari: Ixodidae). *Industrial Crops and Products*, *108*, 190–194.

https://doi.org/10.1016/j.indcrop.2017.06.037

Dash, S., Murthy, P. N., Nath, L., & Chowdhury, P. (2010). Kinetic modeling on drug release from controlled drug delivery systems. *Acta Poloniae Pharmaceutica - Drug Research*, *67*(3), 217–223.

Doan, H. K., Antequera-Gómez, M. L., Parikh, A. N., & Leveau, J. H. J. (2020). Leaf surface topography contributes to the ability of *Escherichia coli* on leafy greens to resist removal by washing, escape disinfection with chlorine, and disperse through splash. *Frontiers in Microbiology*, *11*, 1–14. https://doi.org/10.3389/fmicb.2020.01485

Doan, H. K., Ngassam, V. N., Gilmore, S. F., Tecon, R., Parikh, A. N., & Leveau, J. H. J. (2020). Topography-driven shape, spread, and retention of leaf surface water impacts microbial dispersion and activity in the phyllosphere. *Phytobiomes Journal*, *4*(3), 268–280. https://doi.org/10.1094/PBIOMES-01-20-0006-R

Dong, A., Wang, Y. J., Gao, Y., Gao, T., & Gao, G. (2017). Chemical insights into antibacterial *N*-halamines. *Chemical Reviews*, *117*(6), 4806–4862. https://doi.org/10.1021/acs.chemrev.6b00687

Dou, F., Huang, K., & Nitin, N. (2021). Targeted photodynamic treatment of bacterial biofilms using curcumin encapsulated in cells and cell wall particles. *ACS Applied Bio Materials*, *4*(1), 514–522. https://doi.org/10.1021/acsabm.0c01051

Duque, E., de la Torre, J., Bernal, P., Molina-Henares, M. A., Alaminos, M., Espinosa-Urgel, M., … Ramos, J. L. (2013). Identification of reciprocal adhesion genes in pathogenic and non-pathogenic *Pseudomonas*. *Environmental Microbiology*, *15*(1), 36–48. https://doi.org/10.1111/j.1462-2920.2012.02732.x

Fan, X., & Sokorai, K. J. (2015). Formation of trichloromethane in chlorinated water and fresh-

cut produce and as a result of reaction with citric acid. *Postharvest Biology and Technology*, *109*, 65–72. https://doi.org/10.1016/j.postharvbio.2015.06.009

Ferreira, C., Rosmaninho, R., Simoes, M., Pereira, M. C., Bastos, M. M., Nunes, O. C., … Melo, L. F. (2010). Biofouling control using microparticles carrying a biocide. *Biofouling*, *26*(2), 205–212. https://doi.org/10.1080/08927010903419630

Ferreira, Carla, Pereira, A. M., Pereira, M. C., Simões, M., & Melo, L. F. (2013). Biofilm control with new microparticles with immobilized biocide. *Heat Transfer Engineering*, *34*(8–9), 712–718. https://doi.org/10.1080/01457632.2012.739040

Fish, K. E., Osborn, A. M., & Boxall, J. (2016). Characterising and understanding the impact of microbial biofilms and the extracellular polymeric substance (EPS) matrix in drinking water distribution systems. *Environmental Science: Water Research and Technology*, *2*(4), 614–630. https://doi.org/10.1039/c6ew00039h

Forier, K., Raemdonck, K., De Smedt, S. C., Demeester, J., Coenye, T., & Braeckmans, K. (2014). Lipid and polymer nanoparticles for drug delivery to bacterial biofilms. *Journal of Controlled Release*, *190*, 607–623. https://doi.org/10.1016/j.jconrel.2014.03.055

Fransisca, L., & Feng, H. (2012). Effect of surface roughness on inactivation of *Escherichia coli* O157:H7 87-23 by new organic acid-surfactant combinations on alfalfa, broccoli, and radish seeds. *Journal of Food Protection*, *75*(2), 261–269. https://doi.org/10.4315/0362-028X.JFP-11-279

Fu, T., Li, Y., Awad, D., Zhou, T., & Liu, L. (2018). Factors affecting the performance and monitoring of a chlorine wash in preventing *Escherichia coli* O157:H7 cross-contamination during postharvest washing of cut lettuce. *Food Control*, *94*, 212–221. https://doi.org/10.1016/j.foodcont.2018.06.035

Garner, D., & Kathariou, S. (2016). Fresh produce–associated listeriosis outbreaks, sources of concern, teachable moments, and insights. *Journal of Food Protection*, *79*(2), 337–344. https://doi.org/10.4315/0362-028x.jfp-15-387

Gil, M. I., Selma, M. V., López-Gálvez, F., & Allende, A. (2009). Fresh-cut product sanitation and wash water disinfection: Problems and solutions. *International Journal of Food Microbiology*, *134*(1–2), 37–45. https://doi.org/10.1016/j.ijfoodmicro.2009.05.021

Gil, M. I., Selma, M. V., Suslow, T., Jacxsens, L., Uyttendaele, M., & Allende, A. (2015). Pre- and postharvest preventive measures and intervention strategies to control microbial food safety hazards of fresh leafy vegetables. *Critical Reviews in Food Science and Nutrition*, *55*(4), 453–468. https://doi.org/10.1080/10408398.2012.657808

Gombas, D., Luo, Y., Brennan, J., Shergill, G., Petran, R., Walsh, R., … Deng, K. (2017). Guidelines to validate control of cross-contamination during washing of fresh-cut leafy vegetables. *Journal of Food Protection*, *80*(2), 312–330. https://doi.org/10.4315/0362-028X.JFP-16-258

Gómez-López, V. M., Lannoo, A. S., Gil, M. I., & Allende, A. (2014). Minimum free chlorine residual level required for the inactivation of *Escherichia coli* O157: H7 and trihalomethane generation during dynamic washing of fresh-cut spinach. *Food Control*, *42*, 132–138. https://doi.org/10.1016/j.foodcont.2014.01.034

Gómez-López, V. M., Marín, A., Medina-Martínez, M. S., Gil, M. I., & Allende, A. (2013). Generation of trihalomethanes with chlorine-based sanitizers and impact on microbial, nutritional and sensory quality of baby spinach. *Postharvest Biology and Technology*, *85*, 210–217. https://doi.org/10.1016/j.postharvbio.2013.05.012

Goodburn, C., & Wallace, C. A. (2013). The microbiological efficacy of decontamination

methodologies for fresh produce: A review. *Food Control*, *32*(2), 418–427. https://doi.org/10.1016/j.foodcont.2012.12.012

Gustat, J., O'Malley, K., Luckett, B. G., & Johnson, C. C. (2015). Fresh produce consumption and the association between frequency of food shopping, car access, and distance to supermarkets. *Preventive Medicine Reports*, *2*, 47–52. https://doi.org/10.1016/j.pmedr.2014.12.009

Hall-Stoodley, L., Costerton, J. W., & Stoodley, P. (2004). Bacterial biofilms: From the natural environment to infectious diseases. *Nature Reviews Microbiology*, *2*(2), 95–108. https://doi.org/10.1038/nrmicro821

Harris, L. J., Farber, J. N., Beuchat, L. R., Parish, M. E., Suslow, T. V., Garrett, E. H., & Busta, F. F. (2003). Outbreaks associated with fresh produce: incidence, growth and survival of pathogens in fresh and fresh-cut produce. *Comprehensive Reviews in Food Science and Food Safety*, *2*(s1), 78–141. https://doi.org/10.1111/j.1541-4337.2003.tb00031.x

Havelaar, A. H., Brul, S., de Jong, A., de Jonge, R., Zwietering, M. H., & ter Kuile, B. H. (2010). Future challenges to microbial food safety. *International Journal of Food Microbiology*, *139*, S79–S94. https://doi.org/10.1016/j.ijfoodmicro.2009.10.015

Høiby, N., Bjarnsholt, T., Givskov, M., Molin, S., & Ciofu, O. (2010). Antibiotic resistance of bacterial biofilms. *International Journal of Antimicrobial Agents*, *35*(4), 322–332. https://doi.org/10.1016/j.ijantimicag.2009.12.011

Horikawa, S., Chai, Y., Zhao, R., Wikle, H. C., & Chin, B. A. (2014). Effects of food surface topography on phage-based magnetoelastic biosensor detection. *Sensing for Agriculture and Food Quality and Safety VI*, *9108*, 910802. https://doi.org/10.1117/12.2049852

Huang, K., Dou, F., & Nitin, N. (2019). Biobased sanitizer delivery system for improved sanitation of bacterial and fungal biofilms. *ACS Applied Materials & Interfaces*, *11*, 17204–17214.

https://doi.org/10.1021/acsami.9b02428

Huang, K., & Nitin, N. (2019). Antimicrobial particle-based novel sanitizer for enhanced decontamination of fresh produce. *Applied and Environmental Microbiology*, *85*(8), e02599-18. https://doi.org/10.1128/AEM.02599-18

Huang, K., Tian, Y., Salvi, D., Karwe, M., & Nitin, N. (2018). Influence of exposure time, shear stress, and surfactants on detachment of *Escherichia coli* O157:H7 from fresh lettuce leaf surfaces during washing process. *Food and Bioprocess Technology*, *11*, 621–633. https://doi.org/10.1007/s11947-017-2038-5

Hwang, G., Liu, Y., Kim, D., Li, Y., Krysan, D. J., & Koo, H. (2017). *Candida albicans* mannans mediate *Streptococcus mutans* exoenzyme GtfB binding to modulate cross-kingdom biofilm development *in vivo*. *PLoS Pathogens*, *13*(6), 1–25. https://doi.org/10.1371/journal.ppat.1006407

Israelachvili, J. N. (2011). *Intermolecular and surface forces*. Academic press.

Izumi, H., Poubol, J., Hisa, K., & Sera, K. (2016). Potential sources of microbial contamination of satsuma mandarin fruit in Japan, from production through packing shed. *Journal of Food Protection*, *71*(3), 530–538. https://doi.org/10.4315/0362-028x-71.3.530

Izumi, H., Tsukada, Y., Poubol, J., & Hisa, K. (2016). On-farm sources of microbial contamination of persimmon fruit in Japan. *Journal of Food Protection*, *71*(1), 52–59. https://doi.org/10.4315/0362-028x-71.1.52

Jaglic, Z., Desvaux, M., Weiss, A., Nesse, L. L., Meyer, R. L., Demnerova, K., … Knøchel, S. (2014). Surface adhesins and exopolymers of selected foodborne pathogens. *Microbiology*, *160*(12), 2561–2582. https://doi.org/10.1099/mic.0.075887-0

Jensen, D. A., Danyluk, M. D., Harris, L. J., & Schaffner, D. W. (2017). Quantifying bacterial

cross-contamination rates between fresh-cut produce and hands. *Journal of Food Protection*, *80*(2), 213–219. https://doi.org/10.4315/0362-028X.JFP-16-240

Jensen, D. A., Friedrich, L. M., Harris, L. J., Danyluk, M. D., & Schaffner, D. W. (2013). Quantifying transfer rates of *Salmonella* and *Escherichia coli* O157:H7 between fresh-cut produce and common kitchen surfaces. *Journal of Food Protection*, *76*(9), 1530–1538. https://doi.org/10.4315/0362-028x.jfp-13-098

Jin, T., Liu, L., Zhang, H., & Hicks, K. (2009). Antimicrobial activity of nisin incorporated in pectin and polylactic acid composite films against *Listeria monocytogenes*. *International Journal of Food Science and Technology*, *44*(2), 322–329. https://doi.org/10.1111/j.1365-2621.2008.01719.x

Jing, H., Mezgebe, B., Aly Hassan, A., Sahle-Demessie, E., Sorial, G. A., & Bennett-Stamper, C. (2014). Experimental and modeling studies of sorption of ceria nanoparticle on microbial biofilms. *Bioresource Technology*, *161*, 109–117. https://doi.org/10.1016/j.biortech.2014.03.015

Joye, I. J., Davidov-Pardo, G., & McClements, D. J. (2014). Nanotechnology for increased micronutrient bioavailability. *Trends in Food Science and Technology*, *40*(2), 168–182. https://doi.org/10.1016/j.tifs.2014.08.006

Katsikogianni, M., & Missirlis, Y. F. (2004). Concise review of mechanisms of bacterial adhesion to biomaterials and of techniques used in estimating bacteria-material interactions. *European Cells and Materials*, *8*, 37–57. https://doi.org/10.1002/(sici)1097-4636(199823)43:3<338::aid-jbm16>3.0.co;2-b

Kim, M. H. (2016). Nanoparticle-based therapies for wound biofilm infection: Opportunities and challenges. *IEEE Transactions on Nanobioscience*, *15*(3), 294–304.

https://doi.org/10.1109/TNB.2016.2527600

Kinsinger, N. M., Mayton, H. M., Luth, M. R., & Walker, S. L. (2017). Efficacy of post-harvest rinsing and bleach disinfection of *E. coli* O157:H7 on spinach leaf surfaces. *Food Microbiology*, *62*, 212–220. https://doi.org/10.1016/j.fm.2016.10.019

Kogan, G., & Kocher, A. (2007). Role of yeast cell wall polysaccharides in pig nutrition and health protection. *Livestock Science*, *109*, 161–165. https://doi.org/10.1016/j.livsci.2007.01.134

Korany, A. M., Hua, Z., Green, T., Hanrahan, I., El-Shinawy, S. H., El-Kholy, A., … Zhu, M. J. (2018). Efficacy of ozonated water, chlorine, chlorine dioxide, quaternary ammonium compounds and peroxyacetic acid against *Listeria monocytogenes* biofilm on polystyrene surfaces. *Frontiers in Microbiology*, *9*, 1–10. https://doi.org/10.3389/fmicb.2018.02296

Krachler, A. M., & Orth, K. (2013). Targeting the bacteria–host interface. *Virulence*, *4*(4), 284–294. https://doi.org/10.4161/viru.24606

Kuroda, K., Ueda, M., Shibasaki, S., & Tanaka, A. (2002). Cell surface-engineered yeast with ability to bind, and self-aggregate in response to, copper ion. *Applied Microbiology and Biotechnology*, *59*, 259–264. https://doi.org/10.1007/s00253-002-1014-8

LeChevallier, M. W., Cawthon, C. D., Lee, R. G., Lechevallier, M. W., Cawthon, C. D., & Lee, R. G. (1988). Factors promoting survival of bacteria in chlorinated water supplies. *Applied and Environmental Microbiology*, *54*(3), 649–654. https://doi.org/10.1128/aem.54.3.649-654.1988

Li, Q., Mahendra, S., Lyon, D. Y., Brunet, L., Liga, M. V., Li, D., & Alvarez, P. J. J. (2008). Antimicrobial nanomaterials for water disinfection and microbial control: Potential applications and implications. *Water Research*, *42*(18), 4591–4602. https://doi.org/10.1016/j.watres.2008.08.015

Lima, P. M., São José, J. F. B., Andrade, N. J., Pires, A. C. S., & Ferreira, S. O. (2013). Interaction between natural microbiota and physicochemical characteristics of lettuce surfaces can influence the attachment of *Salmonella* Enteritidis. *Food Control*, *30*(1), 157–161. https://doi.org/10.1016/j.foodcont.2012.06.039

Lin, H., Zhu, X., Wang, Y., & Yu, X. (2017). Effect of sodium hypochlorite on typical biofilms formed in drinking water distribution systems. *Journal of Water and Health*, *15*(2), 218–227. https://doi.org/10.2166/wh.2017.141

Lisle, J. T., Broadaway, S. C., Prescott, A. M., Pyle, B. H., Fricker, C., & Mcfeters, G. A. (1998). Effects of starvation on physiological activity and chlorine disinfection resistance in *Escherichia coli* O157:H7. *Applied and Environmental Microbiology*, *64*(12), 4658–4662. https://doi.org/10.1128/aem.64.12.4658-4662.1998

Loo, C. Y., Rohanizadeh, R., Young, P. M., Traini, D., Cavaliere, R., Whitchurch, C. B., & Lee, W. H. (2016). Combination of silver nanoparticles and curcumin nanoparticles for enhanced anti-biofilm activities. *Journal of Agricultural and Food Chemistry*, *64*(12), 2513–2522. https://doi.org/10.1021/acs.jafc.5b04559

López-Carballo, G., Higueras, L., Gavara, R., & Hernández-Muñoz, P. (2013). Silver ions release from antibacterial chitosan films containing in situ generated silver nanoparticles. *Journal of Agricultural and Food Chemistry*, *61*(1), 260–267. https://doi.org/10.1021/jf304006y

López-Gálvez, F., Allende, A., Truchado, P., Martínez-Sánchez, A., Tudela, J. A., Selma, M. V., & Gil, M. I. (2010). Suitability of aqueous chlorine dioxide versus sodium hypochlorite as an effective sanitizer for preserving quality of fresh-cut lettuce while avoiding by-product formation. *Postharvest Biology and Technology*, *55*(1), 53–60. https://doi.org/10.1016/j.postharvbio.2009.08.001

López, P., Sánchez, C., Batlle, R., & Nerín, C. (2007). Development of flexible antimicrobial films using essential oils as active agents. *Journal of Agricultural and Food Chemistry*, *55*(21), 8814–8824. https://doi.org/10.1021/jf071737b

Lorenzetti, M., Dogša, I., Stošicki, T., Stopar, D., Kalin, M., Kobe, S., & Novak, S. (2015). The influence of surface modification on bacterial adhesion to titanium-based substrates. *ACS Applied Materials and Interfaces*, *7*(3), 1644–1651. https://doi.org/10.1021/am507148n

Luo, Y., Nou, X., Millner, P., Zhou, B., Shen, C., Yang, Y., … Shelton, D. (2012). A pilot plant scale evaluation of a new process aid for enhancing chlorine efficacy against pathogen survival and cross-contamination during produce wash. *International Journal of Food Microbiology*, *158*(2), 133–139. https://doi.org/10.1016/j.ijfoodmicro.2012.07.008

Luo, Y., Nou, X., Yang, Y., Alegre, I., Turner, E., Feng, H., … Conway, W. (2011). Determination of free chlorine concentrations needed to prevent *Escherichia coli* O157:H7 cross-contamination during fresh-cut produce wash. *Journal of Food Protection*, *74*(3), 352–358. https://doi.org/10.4315/0362-028X.JFP-10-429

Lynch, M. F., Tauxe, R. V., & Hedberg, C. W. (2009). The growing burden of foodborne outbreaks due to contaminated fresh produce: risks and opportunities. *Epidemiology and Infection*, *137*(3), 307–315. https://doi.org/10.1017/S0950268808001969

Macarisin, D., Patel, J., Bauchan, G., Giron, J. A., & Ravishankar, S. (2013). Effect of spinach cultivar and bacterial adherence factors on survival of *Escherichia coli* O157:H7 on spinach leaves. *Journal of Food Protection*, *76*(11), 1829–1837. https://doi.org/10.4315/0362-028X.JFP-12-556

Mafu, A. A., Roy, D., Goulet, J., & Savoie, L. (1991). Characterization of physicochemical forces involved in adhesion of *Listeria monocytogenes* to surfaces. *Applied and Environmental*

Microbiology, *57*(7), 1969–1973. https://doi.org/10.1128/aem.57.7.1969-1973.1991

Marshall, K. E., Hexemer, A., Seelman, S. L., Fatica, M. K., Blessington, T., Hajmeer, M., … Gieraltowski, L. (2020). Lessons learned from a decade of investigations of Shiga toxin–producing *Escherichia coli* outbreaks linked to leafy greens, United States and Canada. *Emerging Infectious Diseases*, *26*(10), 2319–2328. https://doi.org/10.3201/eid2610.191418

Meireles, A., Ferreira, C., Melo, L., & Simões, M. (2017). Comparative stability and efficacy of selected chlorine-based biocides against *Escherichia coli* in planktonic and biofilm states. *Food Research International*, *102*, 511–518. https://doi.org/10.1016/j.foodres.2017.09.033

Miranda, R. C., & Schaffner, D. W. (2016). Longer contact times increase cross-contamination of *Enterobacter aerogenes* from surfaces to foods. *Applied and Environmental Microbiology*, *82*(21), 6490–6496. https://doi.org/10.1128/AEM.01838-16

Mittal, R., Grati, M., Gerring, R., Blackwelder, P., Yan, D., Li, J. D., & Liu, X. Z. (2014). In vitro interaction of *Pseudomonas aeruginosa* with human middle ear epithelial cells. *PLoS ONE*, *9*(3), 1–11. https://doi.org/10.1371/journal.pone.0091885

Moore, C. M., Sheldon, B. W., & Jaykus, L.-A. (2003). Transfer of *Salmonella* and *Campylobacter* from stainless steel to romaine lettuce. *Journal of Foof Protection*, *66*(12), 2231–2236. https://doi.org/10.4315/0362-028X-66.12.2231

Munther, D., Luo, Y., Wu, J., Magpantay, F. M. G., & Srinivasan, P. (2015). A mathematical model for pathogen cross-contamination dynamics during produce wash. *Food Microbiology*, *51*, 101–107. https://doi.org/10.1016/j.fm.2015.05.010

Murphy, H. M., Payne, S. J., & Gagnon, G. A. (2008). Sequential UV- and chlorine-based disinfection to mitigate *Escherichia coli* in drinking water biofilms. *Water Research*, *42*(8–9), 2083–2092. https://doi.org/10.1016/j.watres.2007.12.020

Nam, J. M., Fujita, Y., Arai, T., Kondo, A., Morikawa, Y., Okada, H., … Tanaka, A. (2002). Construction of engineered yeast with the ability of binding to cellulose. *Journal of Molecular Catalysis - B Enzymatic*, *17*(3–5), 197–202. https://doi.org/10.1016/S1381-1177(02)00028-0

Nou, X., Luo, Y., Hollar, L., Yang, Y., Feng, H., Millner, P., & Shelton, D. (2011). Chlorine stabilizer T-128 enhances efficacy of chlorine against cross-contamination by *E. coli* O157:H7 and *Salmonella* in fresh-cut lettuce processing. *Journal of Food Science*, *76*(3). https://doi.org/10.1111/j.1750-3841.2011.02046.x

Olaimat, A. N., & Holley, R. A. (2012). Factors influencing the microbial safety of fresh produce: A review. *Food Microbiology*, *32*(1), 1–19. https://doi.org/10.1016/j.fm.2012.04.016

Painter, J. A., Hoekstra, R. M., Ayers, T., Tauxe, R. V., Braden, C. R., Angulo, F. J., & Griffin, P. M. (2013). Attribution of foodborne illnesses, hospitalizations, and deaths to food commodities by using outbreak data, United States, 1998-2008. *Emerging Infectious Diseases*, *19*(3), 407–415. https://doi.org/10.3201/eid1903.111866

Palma-Salgado, S., Ku, K. M., Dong, M., Nguyen, T. H., Juvik, J. A., & Feng, H. (2020). Adhesion and removal of *E. coli* K12 as affected by leafy green produce epicuticular wax composition, surface roughness, produce and bacterial surface hydrophobicity, and sanitizers. *International Journal of Food Microbiology*, *334*, 108834. https://doi.org/10.1016/j.ijfoodmicro.2020.108834

Paramera, E. I., Karathanos, V. T., & Konteles, S. J. (2014). *Yeast cells and yeast-based materials for microencapsulation*. *Microencapsulation in the Food Industry*. Elsevier Inc. https://doi.org/10.1016/b978-0-12-404568-2.00023-6

Perera-Costa, D., Bruque, J. M., González-Martín, M. L., Gómez-García, A. C., & Vadillo-Rodríguez, V. (2014). Studying the influence of surface topography on bacterial adhesion

using spatially organized microtopographic surface patterns. *Langmuir*, *30*(16), 4633–4641. https://doi.org/10.1021/la5001057

Pérez-Rodríguez, F., Saiz-Abajo, M. J., Garcia-Gimeno, R. M., Moreno, A., González, D., & Vitas, A. I. (2014). Quantitative assessment of the *Salmonella* distribution on fresh-cut leafy vegetables due to cross-contamination occurred in an industrial process simulated at laboratory scale. *International Journal of Food Microbiology*, *184*, 86–91. https://doi.org/10.1016/j.ijfoodmicro.2014.05.013

Pérez, J., Picioreanu, C., & Van Loosdrecht, M. (2005). Modeling biofilm and floc diffusion processes based on analytical solution of reaction-diffusion equations. *Water Research*, *39*(7), 1311–1323. https://doi.org/10.1016/j.watres.2004.12.020

Pérez Rodríguez, F., Campos, D., Ryser, E. T., Buchholz, A. L., Posada-Izquierdo, G. D., Marks, B. P., … Todd, E. (2011). A mathematical risk model for *Escherichia coli* O157:H7 cross-contamination of lettuce during processing. *Food Microbiology*, *28*(4), 694–701. https://doi.org/10.1016/j.fm.2010.06.008

Peulen, T. O., & Wilkinson, K. J. (2011). Diffusion of nanoparticles in a biofilm. *Environmental Science and Technology*, *45*(8), 3367–3373. https://doi.org/10.1021/es103450g

Pfeilmeier, S., Saur, I. M. L., Rathjen, J. P., Zipfel, C., & Malone, J. G. (2016). High levels of cyclic-di-GMP in plant-associated *Pseudomonas* correlate with evasion of plant immunity. *Molecular Plant Pathology*, *17*(4), 521–531. https://doi.org/10.1111/mpp.12297

Qiao, M., Ren, T., Huang, T., Weese, J., Liu, Y., Ren, X., & Farag, R. (2017). *N*-halamine modified thermoplastic polyurethane with rechargeable antimicrobial function for food contact surface. *RSC Advances*, *7*, 1233–1240. https://doi.org/10.1039/c6ra25502g

Rajwar, A., Srivastava, P., & Sahgal, M. (2016). Microbiology of fresh produce: route of

contamination, detection methods, and remedy. *Critical Reviews in Food Science and Nutrition*, *56*(14), 2383–2390. https://doi.org/10.1080/10408398.2013.841119

Ren, T., Qiao, M., Huang, T. S., Weese, J., & Ren, X. (2018). Efficacy of *N*-halamine compound on reduction of microorganisms in absorbent food pads of raw beef. *Food Control*, *84*, 255–262. https://doi.org/10.1016/j.foodcont.2017.08.006

Rickman, J. C., Barrett, D. M., & Bruhn, C. M. (2007a). Nutritional comparison of fresh, frozen, and canned fruits and vegetables. Part 1. Vitamins C and B and phenolic compounds. *Journal of the Science of Food and Agriculturecience*, *87*, 930–944. https://doi.org/10.1002/jsfa

Rickman, J. C., Bruhn, C. M., & Barrett, D. M. (2007b). Nutritional comparison of fresh, frozen, and canned fruits and vegetables II. Vitamin A and carotenoids, vitamin E, minerals and fiber. *Journal of the Science of Food and Agriculturecience*, *87*, 1185–1196. https://doi.org/10.1002/jsfa

Rossez, Y., Holmes, A., Wolfson, E. B., Gally, D. L., Mahajan, A., Pedersen, H. L., … Holden, N. J. (2014). Flagella interact with ionic plant lipids to mediate adherence of pathogenic *Escherichia coli* to fresh produce plants. *Environmental Microbiology*, *16*(7), 2181–2195. https://doi.org/10.1111/1462-2920.12315

Rukavina, Z., & Vanić, Ž. (2016). Current trends in development of liposomes for targeting bacterial biofilms. *Pharmaceutics*, *8*(2), 1–26. https://doi.org/10.3390/pharmaceutics8020018

Sharma, P., Panghal, A., Gaikwad, V., Jadhav, S., Bagal, A., Jadhav, A., & Chhikara, N. (2019). Nanotechnology: A Boon for Food Safety and Food Defense. In R. Prasad, V. Kumar, M. Kumar, & D. Choudhary (Eds.), *Nanobiotechnology in Bioformulations* (pp. 225–242). Cham: Springer.

Shen, C., Luo, Y., Nou, X., Bauchan, G., Zhou, B., Wang, Q., & Millner, P. (2012). Enhanced inactivation of *Salmonella* and *Pseudomonas* biofilms on stainless steel by use of T-128, a fresh-produce washing aid, in chlorinated wash solutions. *Applied and Environmental Microbiology*, *78*(19), 6789–6798. https://doi.org/10.1128/AEM.01094-12

Shen, C., Luo, Y., Nou, X., Wang, Q., & Millner, P. (2013). Dynamic effects of free chlorine concentration, organic load, and exposure time on the inactivation of *Salmonella*, *Escherichia coli* O157:H7, and non-O157 Shiga toxin–producing *E. coli*. *Journal of Food Protection*, *76*(3), 386–393. https://doi.org/10.4315/0362-028X.JFP-12-320

Shi, Z., Baker, C. A., Lee, S. I., Park, S. H., Kim, S. A., & Ricke, S. C. (2016). Comparison of methods for quantitating *Salmonella enterica* Typhimurium and heidelberg strain attachment to reusable plastic shipping container coupons and preliminary assessment of sanitizer efficacy. *Journal of Environmental Science and Health, Part B*, *51*(9), 602–608. https://doi.org/10.1080/03601234.2016.1181905

Si, Y., Cossu, A., Nitin, N., Ma, Y., Zhao, C., Chiou, B., … Sun, G. (2017). Mechanically robust and transparent *N*-halamine grafted PVA-co-PE films with renewable antimicrobial activity. *Macromolecular Bioscience*, *17*(3), 1600304. https://doi.org/10.1002/mabi.201600304

Singh, N., Singh, R. K., Bhunia, A. K., & Stroshine, R. L. (2002). Effect of inoculation and washing methods on the efficacy of different sanitizers against *Escherichia coli* O157:H7 on lettuce. *Food Microbiology*, *19*(2–3), 183–193. https://doi.org/10.1006/fmic.2001.0471

Singh, R. S., Bhari, R., & Kaur, H. P. (2011). Characteristics of yeast lectins and their role in cell-cell interactions. *Biotechnology Advances*, *29*(6), 726–731. https://doi.org/10.1016/j.biotechadv.2011.06.002

Singla, R., Goel, H., & Ganguli, A. (2014). Novel synergistic approach to exploit the bactericidal

efficacy of commercial disinfectants on the biofilms of *Salmonella enterica* serovar Typhimurium. *Journal of Bioscience and Bioengineering*, *118*(1), 34–40. https://doi.org/10.1016/j.jbiosc.2013.12.025

Sirinutsomboon, B., Delwiche, M. J., & Young, G. M. (2011). Attachment of *Escherichia coli* on plant surface structures built by microfabrication. *Biosystems Engineering*, *108*(3), 244–252. https://doi.org/10.1016/j.biosystemseng.2010.12.007

Srey, S., Jahid, I. K., & Ha, S. Do. (2013). Biofilm formation in food industries: A food safety concern. *Food Control*, *31*(2), 572–585. https://doi.org/10.1016/j.foodcont.2012.12.001

Srinivasan, P., Dehghan Abnavi, M., Sulak, A., Kothapalli, C. R., & Munther, D. (2020). Towards enhanced chlorine control: Mathematical modeling for free chlorine kinetics during fresh-cut carrot, cabbage and lettuce washing. *Postharvest Biology and Technology*, *161*, 111092. https://doi.org/10.1016/j.postharvbio.2019.111092

Stratford, M., & Bond, C. J. (1992). Selective separation of microorganisms by lectins: Yeast and concanavalin A as a model system. *Biotechnology and Bioengineering*, *40*(7), 835–843. https://doi.org/10.1002/bit.260400711

Sun, X., Wang, Z., Kadouh, H., & Zhou, K. (2014). The antimicrobial, mechanical, physical and structural properties of chitosan-gallic acid films. *LWT - Food Science and Technology*, *57*(1), 83–89. https://doi.org/10.1016/j.lwt.2013.11.037

Teng, Z., Luo, Y., Alborzi, S., Zhou, B., Chen, L., Zhang, J., … Wang, Q. (2018). Investigation on chlorine-based sanitization under stabilized conditions in the presence of organic load. *International Journal of Food Microbiology*, *266*, 150–157. https://doi.org/10.1016/j.ijfoodmicro.2017.11.027

Touhami, A., Hoffmann, B., Vasella, A., Denis, F. A., & Dufrêne, Y. F. (2003). Aggregation of

yeast cells: Direct measurement of discrete lectin-carbohydrate interactions. *Microbiology*, *149*(10), 2873–2878. https://doi.org/10.1099/mic.0.26431-0

Upadhyay, A., Upadhyaya, I., Kollanoor-Johny, A., & Venkitanarayanan, K. (2013). Antibiofilm effect of plant derived antimicrobials on *Listeria monocytogenes*. *Food Microbiology*, *36*(1), 79–89. https://doi.org/10.1016/j.fm.2013.04.010

Wachtel, M. R., & Charkowski, A. O. (2002). Cross-contamination of lettuce with *Escherichia coli* O157:H7. *Journal of Food Protection*, *65*(3), 465–470. https://doi.org/10.4315/0362-028X-65.3.465

Wang, H., Feng, H., Liang, W., Luo, Y., & Malyarchuk, V. (2009). Effect of surface roughness on retention and removal of *Escherichia coli* O157:H7 on surfaces of selected fruits. *Journal of Food Science*, *74*(1), 1–8. https://doi.org/10.1111/j.1750-3841.2008.00998.x

Weng, S., Luo, Y., Li, J., Zhou, B., Jacangelo, J. G., & Schwab, K. J. (2016). Assessment and speciation of chlorine demand in fresh-cut produce wash water. *Food Control*, *60*, 543–551. https://doi.org/10.1016/j.foodcont.2015.08.031

Williams, M. M., & Braun-Howland, E. B. (2003). Growth of *Escherichia coli* in model distribution system biofilms exposed to hypochlorous acid or monochloramine. *Applied and Environmental Microbiology*, *69*(9), 5463–5471. https://doi.org/10.1128/AEM.69.9.5463-5471.2003

Yadav, M. K., Song, J.-J., Singh, B. P., & Vidal, J. E. (2020). Microbial biofilms and human disease: A concise review. In M. K. Yadav & B. P. Singh (Eds.), *New and Future Developments in Microbial Biotechnology and Bioengineering: Microbial Biofilms* (Vol. 1, pp. 1–13). Elsevier. https://doi.org/10.1016/b978-0-444-64279-0.00001-3

Yang, Y., Luo, Y., Millner, P., Shelton, D., & Nou, X. (2012). Enhanced chlorine efficacy against

bacterial pathogens in wash solution with high organic loads. *Journal of Food Processing and Preservation*, *36*(6), 560–566. https://doi.org/10.1111/jfpp.12000

Yeni, F., Yavaş, S., Alpas, H., & Soyer, Y. (2016). Most common foodborne pathogens and mycotoxins on fresh produce: A review of recent outbreaks. *Critical Reviews in Food Science and Nutrition*, *56*(9), 1532–1544. https://doi.org/10.1080/10408398.2013.777021

Ying, C. T., Wang, J., Lamm, R. J., & Kamei, D. T. (2013). Mathematical modeling of vesicle drug delivery systems 2: Targeted vesicle interactions with cells, tumors, and the body. *Journal of Laboratory Automation*, *18*(1), 46–62. https://doi.org/10.1177/2211068212458265

Zhang, B., Luo, Y., Pearlstein, A. J., Aplin, J., Liu, Y., Bauchan, G. R., … Millner, P. D. (2014). Fabrication of biomimetically patterned surfaces and their application to probing plant-bacteria interactions. *ACS Applied Materials and Interfaces*, *6*(15), 12467–12478. https://doi.org/10.1021/am502384q

Zhao, T., Doyle, M. P., Zhao, P., Blake, P., & Wu, F. M. (2001). Chlorine inactivation of *Escherichia coli* O157:H7 in water. *Journal of Food Protection*, *64*(10), 1607–1609. https://doi.org/10.4315/0362-028X-64.10.1607

Zhou, B., Luo, Y., Nou, X., Lyu, S., & Wang, Q. (2015). Inactivation dynamics of *Salmonella enterica*, *Listeria monocytogenes*, and *Escherichia coli* O157: H7 in wash water during simulated chlorine depletion and replenishment processes. *Food Microbiology*. https://doi.org/10.1016/j.fm.2015.03.004

Zhu, Q., Gooneratne, R., & Hussain, M. (2017). *Listeria monocytogenes* in fresh produce: outbreaks, prevalence and contamination levels. *Foods*, *6*(21), 1–11. https://doi.org/10.3390/foods6030021

CHAPTER 2:

Quantitative Analysis and Influences of Contact Dynamics on Microbial Cross-Contamination from Contaminated Fresh Produce [1]

Abstract

Cross-contamination of fresh produce during postharvest processing could be a significant risk factor that can lead to foodborne outbreaks. The aim of this study was to simulate cross-contamination from a contaminated lettuce to non-contaminated leaves/abiotic surfaces (glass, polyethylene), quantify the bacterial transfer efficiency to determine the influences of contact time, number of repeated contacts, and applied contact force, and evaluate the influences of surface hydrophobicity and bacterial species. The results demonstrate that bacterial transfer between leaves was instantaneous and bi-directional. The leaf-to-leaf transfer efficiency of *Listeria innocua* increased up to 6.8% with an applied contact force of 20 N, a force equivalent to 2-kg stack of lettuce leaves, while it had limited influence on the transfer of a plant-associated bacterium, *Pseudomonas fluorescens*. The transfer efficiencies for both bacteria increased with the increase in hydrophobicity of abiotic surfaces. Overall, this study illustrates a quantitative approach to characterize the influence of physical and biological factors in influencing cross-contamination and could guide the development of preventive measures for reducing the risk of cross-contamination.

Keywords: Fresh produce; Cross-contamination; Bacterial transfer efficiency; *Listeria innocua*; *Pseudomonas fluorescens*; Lettuce

[1] Note: This chapter has been published in *Journal of Food Engineering* (2020).

2.1. Introduction

Cross-contamination of minimally processed products such as fresh produce and tree-nuts has emerged as a significant risk factor that can lead to a nationwide outbreak of a foodborne illness (Berg, Erlacher, Smalla, & Krause, 2014; Yeni, Yavaş, Alpas, & Soyer, 2016). During postharvest processing or food preparation, cross-contamination of fresh produce can result from contact with a contaminated surface, contaminated wash water, or contaminated fresh produce itself (Gil et al., 2015; Jensen, Friedrich, Harris, Danyluk, & Schaffner, 2013; Lynch, Tauxe, & Hedberg, 2009; Matthews, 2009; Rajwar, Srivastava, & Sahgal, 2016). Previous studies have illustrated the risk of cross-contamination to fresh produce such as lettuce, carrots, celery, and melon from diverse contaminated surfaces, including shredder, conveyor belt, flume tank, shaker table, and kitchen surfaces (Buchholz, Davidson, Marks, Todd, & Ryser, 2012; Chen, Jackson, Chea, & Schaffner, 2001; Jensen et al., 2013). These diverse food contact surfaces represent different materials, including ceramics, glass, plastics, and metals. Similarly, direct contact between a contaminated and a non-contaminated fresh produce can cause potential cross-contamination. Diverse underlying mechanisms can contribute to cross-contamination from contaminated surfaces, including fresh produce (Krachler & Orth, 2013; Lynch et al., 2009). Numerous studies suggested that bacteria are transferred by specific adhesin-ligand interactions (Duque et al., 2013; Krachler & Orth, 2013; Pfeilmeier, Saur, Rathjen, Zipfel, & Malone, 2016) and highlighted roles of surface chemistry, geometry, and non-specific physicochemical interactions, as well as environmental factors such as temperature and humidity (Abdallah et al., 2014; Lopez et al., 2013; Lorenzetti et al., 2015; Perera-Costa, Bruque, González-Martín, Gómez-García, & Vadillo-Rodríguez, 2014; Solomon & Matthews, 2006). Many of these prior studies,

especially those focused on physicochemical mechanisms of bacterial transfer, were conducted using abiotic flat surfaces with defined surface chemistry.

Various experimental approaches have been used to study cross-contamination of fresh produce from the wash water, however, only limited progress has been made in conducting cross-contamination studies with precise control on contact time and force between contaminated and non-contaminated food products or materials commonly forming surfaces of processing equipment or packaging materials. Many of these cross-contamination studies were conducted by mixing fractions of contaminated leaves with non-contaminated leaves or physically dropping or pressing the leaves against a surface. In an early study simulating cross-contamination of lettuce during postharvest handling, one inoculated dry lettuce was mixed with a large volume of non-inoculated leaves with or without water, however, contact time, force, or contact area were not precisely controlled (Wachtel & Charkowski, 2002). A recent study explored the influence of contact time on cross-contamination between different types of food and food-contact surfaces, but this was performed by simply dropping food on contaminated surfaces without controlling the contact force (Miranda & Schaffner, 2016). Thus, to the best of our knowledge, none of the prior studies have evaluated the influences of contact time, number of repeated contacts, and contact force on cross-contamination between contaminated and non-contaminated food materials.

The goals of this study were to 1) evaluate cross-contamination between romaine lettuce leaves as a function of contact time, number of repeated contacts, and applied contact force for the two selected strains of bacteria, and 2) evaluate the influence of physicochemical properties of contact surfaces on cross-contamination from contaminated leaves to non-contaminated leaves or abiotic model surfaces. To achieve these goals, a texture analyzer was adapted to simulate the transfer of *Listeria innocua* or *Pseudomonas fluorescens* from contaminated leaves to non-

contaminated surfaces (both biotic and abiotic surfaces). A texture analyzer is a tool that has been used widely in food research, but only to measure product quality such as firmness and resistance (Arsenault, Letellier, Quessy, & Boulianne, 2007; Lu, Joerger, & Wu, 2014). By utilizing this device, precise control on contact time and applied contact force is achieved, resulting in a reproducible approach to assessing the efficiency of cross-contamination. To investigate the influence of surface hydrophobicity on the bacterial cross-contamination efficiency, the hydrophilic glass surfaces and hydrophobic polyethylene (PE) were selected as model food contact surfaces. Among commercially available food contact surfaces used for food processing or packaging, such as glass, plastics, or stainless steel, these two model surfaces were selected based on the following criteria: 1) a pair of surfaces with a large variation in water contact angle, a measure of surface hydrophobicity and 2) relatively smooth surfaces to minimize the influence of surface roughness. In summary, this study evaluates cross-contamination resulting from leaf-to-leaf and leaf-to-model food contact surfaces under different experimental conditions for the selected model bacteria. The results of this study will aid in assessing the risk of cross-contamination and the role of selected physicochemical parameters in influencing cross-contamination.

2.2. Materials and Methods

2.2.1. Bacterial strain, media, and culture

L. innocua was selected as a surrogate for a Gram-positive human pathogen *L. monocytogenes*, a leading cause of a number of fatal foodborne outbreaks linked to contamination of fresh produce (Garner & Kathariou, 2016; Yeni et al., 2016; Zhu, Gooneratne, & Hussain, 2017). *P. fluorescens* was chosen as a model Gram-negative plant-associated

bacterium that could be found on the leaf surfaces (Lindow & Leveau, 2002), isolated from within plants (Nithya & Babu, 2017; Weyens et al., 2013), or in the roots of plants (Molina, Ramos, & Espinosa-Urgel, 2003; Nithya & Babu, 2017), in addition to forming biofilms (Molina et al., 2003). A rifampicin-resistant *L. innocua* (ATCC, 33090) provided by Dr. Linda Harris (University of California-Davis, USA) and *P. fluorescens* (ATCC, 13525) were stored in this study. A *L. innocua* resistant to 50 µg/ml of rifampicin was prepared by adaptive growth of the bacteria in the presence of increasing amounts of rifampicin (Fisher Scientific, Pittsburg, CA, USA) (Parnell, Harris, & Suslow, 2005; Vandamm, Li, Harris, Schaffner, & Danyluk, 2013). The bacterial stocks were stored in liquid nitrogen in the tryptic soy broth (TSB) (Sigma-Aldrich, St. Louis, MO, USA) and nutrient broth (NB) (Difco, Sparks, MD, USA) supplemented with 15% (v/v) of glycerol, respectively. The bacteria were streaked onto a plate of tryptic soy agar (TSA) (Sigma-Aldrich) supplemented with 50 µg/ml rifampicin and nutrient agar (NA) (Difco) plates for *L. innocua* and *P. fluorescens*, respectively, and then grown in an incubator at 30 ºC for 48 h. To prepare bacteria for each experiment, a colony was isolated, and it was inoculated in 10 ml of a liquid media. TSB media was used for *L. innocua,* and NB media was used for *P. fluorescens*. The inoculated liquid culture was incubated at 30 ºC for 24 h with constant shaking at 250 rpm. The bacterial cells in the stationary phase were isolated from a liquid media and washed three times with sterile phosphate buffered saline (PBS, Fisher Scientific) using centrifugal separation of bacterial cells (Centrifuge 5804, Eppendorf AG, Hamburg, Germany) at 3100 × *g* / 23 ºC, for 8 min. After each wash, the bacterial pellet was re-suspended in a sterile PBS solution to obtain a population of approximately 9 log CFU/ml. The final population of approximately 6 log CFU/ml for inoculation on a leaf surface was achieved by serial dilution of the bacterial suspension. This inoculation level of the bacterial cells was decided based on evaluation of the levels of bacteria on the leaf surface

required for the detection of the lowest level of cross-contamination on model contact surfaces. For this evaluation, glass was selected as the model surface with the lowest level of cross-contamination from the leaf surface. In addition, the inoculated level of bacteria of 4–5 log CFU/cm^2 is within the range of average aerobic microbes present on the leaf surface, typically in the range of 4–6 log CFU/cm^2 (Koseki, Yoshida, Isobe, & Itoh, 2016). The initial inoculated levels of bacteria on the leaf surface were enumerated using the standard plate counting methods as described in Section 2.2.6.

2.2.2. Leaf surface preparation and bacterial inoculation

Romaine lettuce leaves were purchased from a local market and stored at 4 ºC until further use up to seven days. Outer leaves were removed, and the leaves without any visual tissue damage were selected. The selected leaves were cut into a 5 × 5 cm^2 square with a sterile scalpel and then washed with sterile deionized water prior to the experiments. Bacterial inoculation on a leaf surface was performed based on a modified protocol used in our prior study (Huang, Tian, Salvi, Karwe, & Nitin, 2018). A 5 × 5 cm^2 square leaf slice was placed on a Petri dish of a 100 mm diameter, and then 0.5 ml of 6-log CFU/ml bacterial suspension was dropped by pipette and spread with a sterile cell spreader over the adaxial leaf surface (upper surface) for inoculation of bacteria on the surface. Consequently, the Petri dish was sealed by parafilm (Fisher Scientific) and stored at 4 ºC for 24 h to allow bacterial adhesion to the leaf surface. All the leaf samples after incubation were cut into 3 cm diameter disks with a sterile cork borer and then rinsed twice with 5 ml of sterile deionized water by gentle dipping to remove loosely attached bacteria on the leaf surface. Using a similar inoculation and rinsing protocol in our prior study, the results illustrated that bacteria adhered to the leaf surface could not be easily removed by a simple rinse process (Huang et al.,

2018). In this prior study, a high shear simulated washing device was used, and the results showed that the removal efficiency from the leaf surface with high shear washing decreased with extended incubation for 24 h.

2.2.3. Simulated leaf-to-leaf cross-contamination

A TA-XT2 Texture Analyser (Stable Micro Systems, Godalming, Surrey, UK) was used to simulate a highly reproducible leaf-to-leaf cross-contamination event. As shown in Figure 2.1, a contaminated leaf was attached to the bottom of a probe which is placed in the middle of the texture analyzer, an adaxial surface facing down with a double-sided tape. A non-contaminated leaf was placed on a 100 mm diameter Petri dish, the adaxial surface facing up with a double-sided tape, and then the dish was put on the platform of the texture analyzer, aligned with the contaminated leaf. Adaxial surfaces of two leaves were facing each other so that they could overlap when the probe comes down with the preset contact conditions. The Texture Expert Exceed software (version 2.64, Stable Micro Systems) was used to control contact time, number of repeated contacts, and applied contact force, reducing random errors. Different contact times (1, 5, 60, 120 s), numbers of repeated contacts (1, 5, 10, 20), and applied contact forces (1, 5, 9.8, 20 N) were investigated. The contact conditions were chosen based on different scenarios that may be applicable to postharvest processing. For instance, 1 kg of a leaf stack could be placed on top of two contacting leaves during storage and transportation, and this would generate an applied force of 9.8 N. Moreover, after the washing process of leafy greens, the leaves are commonly centrifuged for 2–5 min to remove excess water prior to packaging. In this case, the mechanical force experienced by leaves may even be higher than the forces applied in this study, depending on the range of centrifugal speeds and the size of the centrifuge. All the experiments were

performed at 23 ± 2 ºC, and excess moisture was presented on the leaf surface to simulate conditions during postharvest processing of leaves.

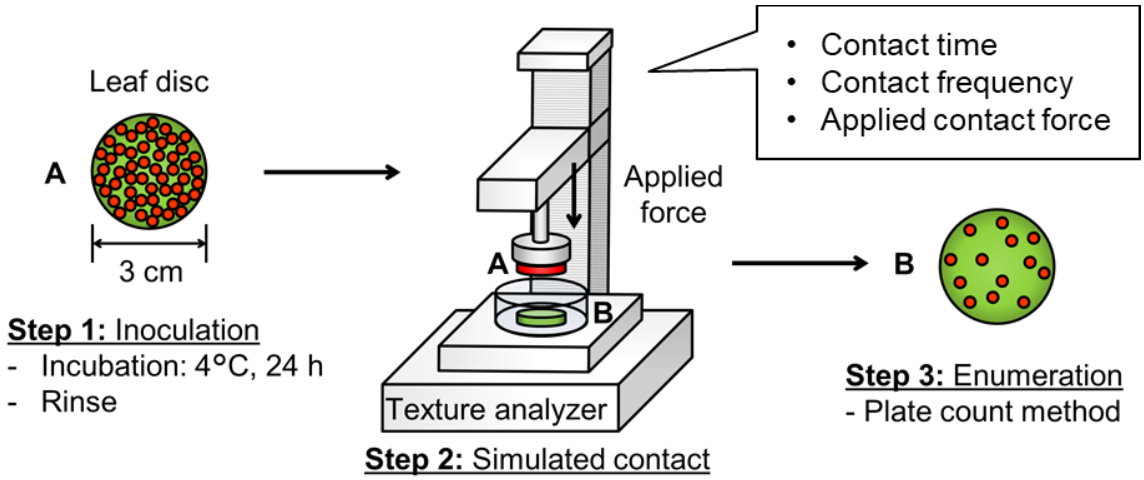

Figure 2.1. Schematic diagram of the experimental approach for simulating leaf-to-leaf cross-contamination. Contact time, frequency, and force were precisely controlled by a modified texture analyzer to perform highly reproducible cross-contamination measurements.

2.2.4. Variations on the surface hydrophobicity

Different abiotic model surfaces were used for leaf-to-surface cross-contamination to evaluate the influence of surface hydrophobicity on bacterial transfer efficiency. Glass and PE surfaces were chosen as a hydrophilic or hydrophobic model surface, respectively, and used as recipient surfaces in simulated leaf-to-surface cross-contamination. A microscope cover glass (0.17–0.25 mm thick, Fisher Scientific) was used as a model glass surface, and a PE film (0.10 mm thick, McMaster-Carr, Santa Fe Springs, CA, USA) cut into a 3 cm diameter disk was used as a model PE surface. All the model surfaces were washed with 70% (v/v) ethanol followed by sterile water before use. These surfaces were placed as recipients on the platform of the texture analyzer for contact experiments, and the source of contamination remained the same as above, a leaf contaminated with bacteria.

2.2.5. Measurement of surface hydrophobicity

The contact angles of deionized water on glass, leaf, and PE were measured to determine the relative surface hydrophobicity using the Theta Optical Tensiometer (Attention, Biolin Scientific, Stockholm, Sweden). For leaf samples, the veins were discarded and 1-cm diameter disks were cut from the middle part of a leaf. A droplet of 15-µl deionized water was then dropped on each selected surface, and the advancing water contact angle was measured at 23 °C using the sessile drop method (OneAttension version 1.8, Biolin Scientific) (Huang et al., 2018).

The cell surface hydrophobicity for bacteria used in this study was also measured as described by previous studies (Huang & Nitin, 2017; Rosenberg, Gutnick, & Rosenberg, 1980). Bacterial cells were prepared as described in Section 2.2.1, and the bacterial suspension of approximately 8 log CFU/ml obtained by dilution was used for this cell surface hydrophobicity

assay. This number was verified by the enumeration method described in Section 2.2.6. The optical density at 640 nm of the original bacterial suspension (OD_1) and the bottom suspension after the phase separation by using Octan (OD_2) were measured using Genesys 10S UV-Vis spectrophotometer (Thermo Scientific, Rochester, NY, USA). The hydrophobicity index (HPBI) was calculated as:

$$\text{HPBI} = \frac{(\text{OD}_1 - \text{OD}_2)}{\text{OD}_1} \times 100 \quad (2.1)$$

All the measurements were performed in triplicates.

2.2.6. Microbiological analysis

The level of bacteria was enumerated by the plate counting method. To recover bacteria from glass, leaf, and PE surfaces, a sterile maximum recovery diluent (MRD, Sigma-Aldrich) solution was used. Each sample was immersed into 10 ml of MRD solution for 2 min and then vortexed at full speed for 1 min using a vortex mixer (Fisher Scientific, Waltham, MA, USA). This process of MRD-based bacterial recovery was verified by comparing recovery efficiencies of bacteria using homogenization of the leaf samples. The MRD-based recovery approach was selected as it could be used for both biotic and abiotic. The isolated bacterial suspension was diluted 10-fold, and both the diluted suspension and the primary isolate from the surfaces were plated on a selective culture media for enumeration. For the plate cultures, TSA supplemented with 50 µg/ml rifampicin and NA were used for *L. innocua* and *P. fluorescens*, respectively. After incubation at 30 ºC for 48 h, the colony forming units (CFU) on the agar plates were enumerated. The detection limit was determined by converting 1 CFU/agar plate into log CFU/cm^2, which resulted in 1.15 log CFU/cm^2. To understand and compare the influences of different contact conditions, the bacterial transfer efficiency was calculated as follows:

$$\text{Bacterial transfer efficiency (BTE, \%)} = \frac{N_t}{N_0} \times 100 \quad (2.2)$$

where N_t is the number of viable bacteria on a non-contaminated leaf after contact (CFU/cm^2) and N_0 is the number of viable bacteria initially on a contaminated leaf (CFU/cm^2). The bacterial transfer efficiency quantifies the propensity of bacteria to transfer from a contaminated leaf to a non-contaminated surface (leaf or model surfaces).

2.2.7. Statistical analysis and quantitative data analysis

Statistical analysis was performed using the SPSS Statistics software (version 24, IBM SPSS, Chicago, IL, USA) to evaluate the measurement sets of microbial enumeration. All the experiments were performed in triplicates. A one- or two-way analysis of variance was used to determine the significant differences among the values of the selected measurements ($p < 0.05$). The bacterial transfer efficiencies calculated by Eq. 2.2 were fitted to kinetic models to determine the influences of experimental variables. A log-linear (Eq. 2.3) and a linear model (Eq. 2.4) was used to describe the influences of contact time and applied contact force, respectively:

$$\log(\text{BTE}) = a_t + b_t t \quad (1 \leq t \leq 120) \quad (2.3)$$

$$\text{BTE} = a_F + b_F F_{\text{app}} \quad \left(1 \leq F_{\text{app}} \leq 20\right) \quad (2.4)$$

where a and b are the intercept and slope of each model, respectively, t is the contact time (s), and F_{app} is the applied contact force (N). The log-linear model has been used in prior studies to describe the transfer of bacteria between food and food contact surfaces (Flores, Tamplin, Marmer, Phillips, & Cooke, 2016; Pérez-Rodríguez et al., 2007). The linear model was selected to evaluate the influence of applied contact force, as it is a simple model that describes the experimental data.

2.3. Results

2.3.1. Bacterial transfer via simulated leaf-to-leaf cross-contamination

The results in Figure 2.2 show that *L. innocua* and *P. fluorescens* were transferred from a contaminated lettuce leaf to a non-contaminated leaf after a single 5-s contact with an applied contact force of 9.8 N. This force corresponds to the force applied by a 1-kg stack of lettuce leaves on top of a contaminated leaf in contact with a non-contaminated leaf and application of this force improves contact between the leaf surfaces. It is important to note that the applied contact forces used in this study did not significantly influence ($p > 0.05$) the turgor of the leaf tissue measured based on the electrolyte leakage assay before and after contact for the longest time period used in this study (data not shown) or cause any visual damage to the leaf. The results illustrate that from 4.45 and 4.97 log CFU/cm^2 of *L. innocua* and *P. fluorescens* on the contaminated leaves, respectively, 3.21 and 3.46 log CFU/cm^2 of bacteria were transferred to non-contaminated leaves upon contact. Based on the experimental results, the efficiencies of cross-contamination for *L. innocua* and *P. fluorescens* were 4.3% and 3.8%, respectively. These results reveal that there was no significant difference ($p > 0.05$) in the efficiency of transfer for two diversely-related species of bacteria: one a Gram-positive bacterium which can reside on a leaf surface but cannot infect the leaf tissue or cause spoilage; and the other a Gram-negative and a plant-associated bacterium that can invade and affect the plant tissue. These results further illustrate that transfer of bacteria from a contaminated leaf to a non-contaminated leaf is rapid, within a 5-s contact.

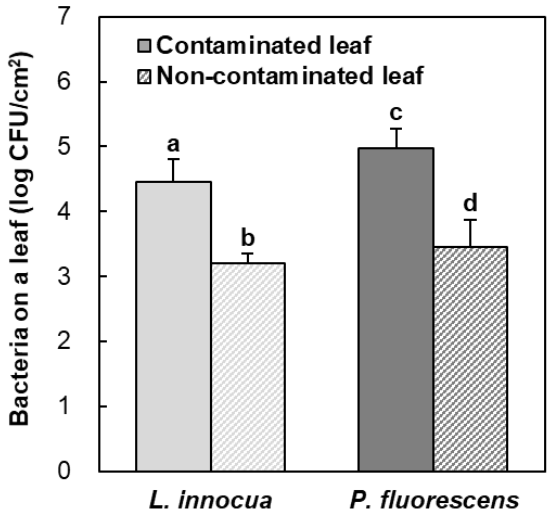

Figure 2.2. Bacterial transfer from a contaminated leaf to a non-contaminated leaf using the simulated cross-contamination process. A fresh romaine lettuce leaf was contaminated with 6-log CFU/ml suspension of *Listeria innocua* or *Pseudomonas fluorescens*. The transfer of bacteria from a contaminated leaf to a non-contaminated leaf was quantified using a single contact between the leaves with an applied contact force of 9.8 N for 5 s. The results represent the mean values and their standard deviations ($n \geq 3$). Different letters indicate significant differences between the values ($p < 0.05$).

Results in Figure 2.3 show that a contaminated leaf can transfer bacteria not only to a single non-contaminated leaf but also to multiple non-contaminated leaves upon sequential contacts. The level of *L. innocua* transferred upon sequential contacts with constant contact conditions–from a single contaminated leaf of 4.45 log CFU/cm^2 to different non-contaminated leaves that were successively introduced–were 3.48, 3.37, 3.35, 3.16, and 2.78 log CFU/cm^2 on leaves upon 1st, 2nd, 3rd, 4th, and 5th contact, respectively. In the case of *P. fluorescens*, from a contaminated leaf of 4.97 log CFU/cm^2, 3.79, 3.64, 3.57, 3.26, and 3.30 log CFU/cm^2 were transferred on non-contaminated leaves upon 1st, 2nd, 3rd, 4th, and 5th contact, respectively. These results illustrate that the level of bacterial transfer from a contaminated leaf to multiple non-contaminated leaves did not change significantly ($p > 0.05$) upon successive contacts and was high for at least the first five contacts. Similar trends in the transfer efficiency were observed for *L. innocua* and *P. fluorescens*. Overall, these results suggest that a single leaf contaminated at a high level (4–5 log CFU/cm^2) can rapidly transfer its bacteria to multiple non-contaminated leaves upon sequential contacts.

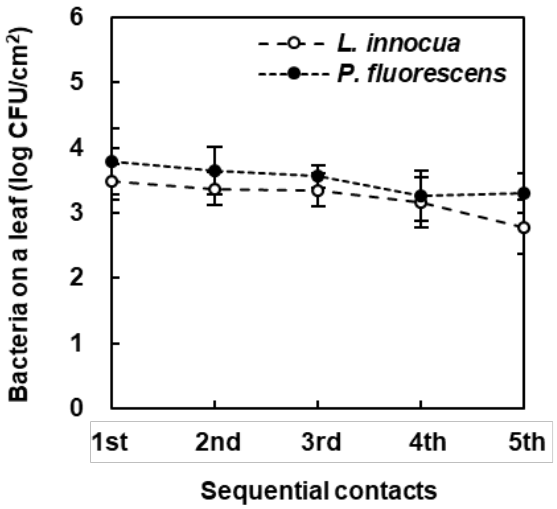

Figure 2.3. Bacterial transfer from a single contaminated leaf to multiple non-contaminated leaves with sequential contacts. A contaminated lettuce leaf inoculated with either *L. innocua* or *P. fluorescens* was used to transfer bacteria, and non-contaminated recipient leaves were sequentially introduced at each contact. To simulate multiple leaves, a new non-contaminated leaf was introduced upon each contact. All contacts were performed using an applied contact force of 9.8 N for 5 s. The data represents mean values and their standard deviations (n = 3). There was no significant difference among the values for the same bacterial species ($p > 0.05$).

2.3.2. Influences of contact time and the number of repeated contacts on leaf-to-leaf cross-contamination

Figures 2.4a–b illustrate the influence of contact time and the number of repeated contacts on leaf-to-leaf cross-contamination, respectively. The results in Figure 2.4a illustrate that bacterial transfer from a contaminated to a non-contaminated leaf was instantaneous (less than 5 s), and the transfer efficiency increased with the contact time for a fixed applied contact force of 9.8 N. From the 4.45-log CFU/cm^2 of *L. innocua* on a contaminated leaf, 3.01, 3.24, 3.58, and 3.84 log CFU/cm^2 were transferred to a non-contaminated leaf with a contact time of 1, 5, 60, and 120 s, respectively. Similarly, from the 4.97-log CFU/cm^2 of *P. fluorescens,* 3.08, 3.45, 3.38, and 3.96 log CFU/cm^2 were transferred to a non-contaminated leaf with a contact time of 1, 5, 60, and 120 s, respectively. Accordingly, the transfer efficiencies for *L. innocua* with a single contact with contact times of 1, 5, 60, and 120 s at an applied contact force of 9.8 N were 2.6%, 4.4%, 9.8%, and 18%, respectively, and the efficiencies for *P. fluorescens* were 1.4%, 4.4%, 2.9%, and 8.9%, respectively. Significant increases ($p < 0.05$) in the transfer efficiency were observed for both the selected bacteria. In contrast, results in Figure 4b illustrate that repeated contacts between a single contaminated leaf and a single non-contaminated leaf did not significantly increase ($p > 0.05$) the bacterial transfer efficiency. Overall, these results highlight that leaf-to-leaf cross-contamination is an efficient process as single contact can transfer a significant number of bacteria from a contaminated to a non-contaminated leaf.

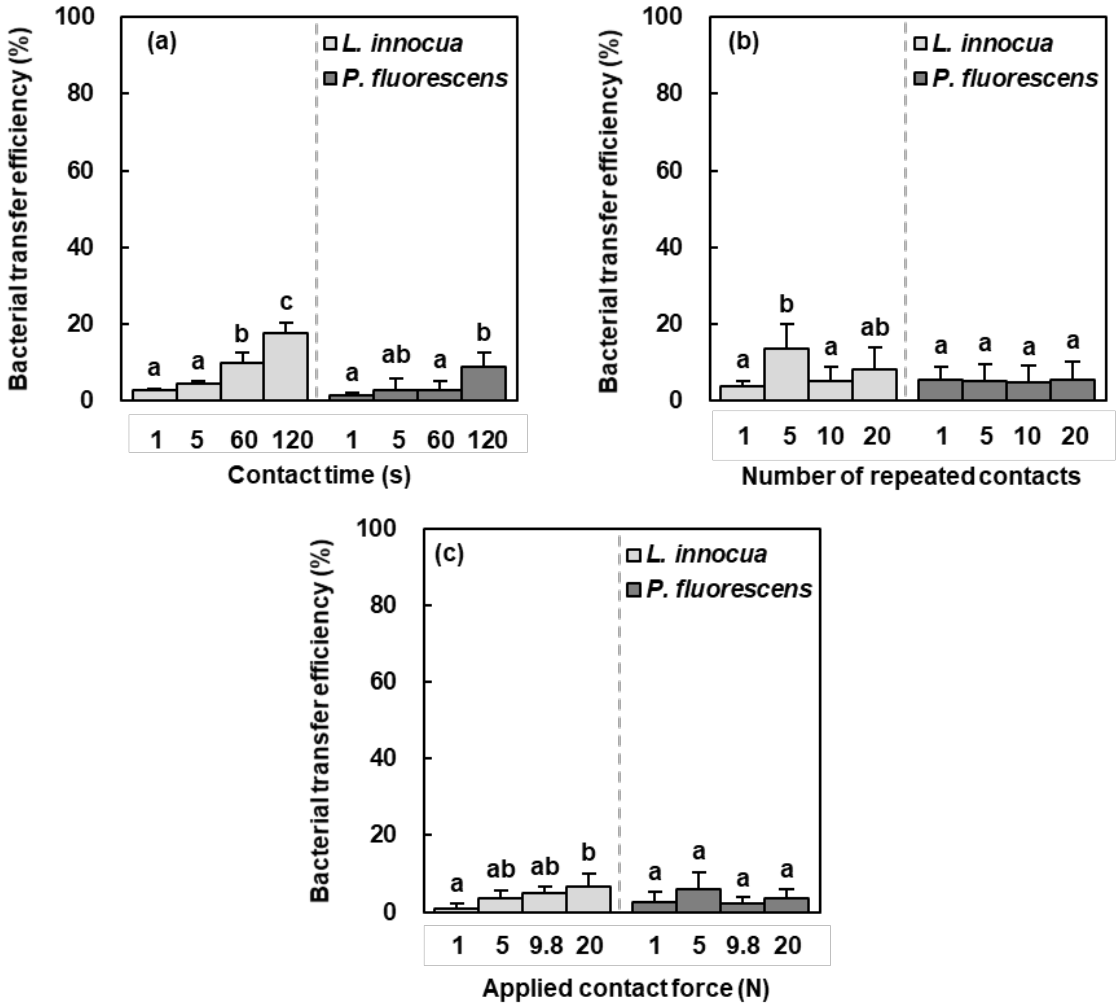

Figure 2.4. Bacterial transfer efficiencies from a contaminated leaf to a non-contaminated leaf using the simulated cross-contamination process: (a) the influence of contact time on bacterial transfer efficiency between surfaces with a constant applied contact force of 9.8 N, (b) the influence of the number of repeated contact at a fixed contact force of 9.8 N for 5 s, and (c) the influence of applied contact force with a single 5-s contact. The bacterial transfer efficiency was defined as the ratio of bacteria on a non-contaminated leaf after contact with bacteria initially on a contaminated leaf. The data are mean values and their standard deviations ($n = 3$). Different letters indicate significant differences between the mean values for the same bacterial species ($p < 0.05$).

2.3.3. Influence of applied contact force on leaf-to-leaf cross-contamination

The results in Figure 4c show the influence of applied contact force on bacterial transfer from a contaminated leaf to a non-contaminated leaf for the selected model bacteria in this study. Unlike other factors discussed above, variations in the applied contact force resulted in differences in transfer of *L. innocua* from a contaminated leaf to a non-contaminated leaf compared to transfer of *P. fluorescens* under the same set of experimental conditions, including the contact time of 5 s. The results for the transfer of the *L. innocua* show an increase in bacterial transfer from contaminated to non-contaminated leaves with an increase in applied contact force. The transferred bacteria (*L. innocua)* increased from 2.14 to 3.39 log CFU/cm^2 with an increase in applied contact forces of 1 to 20 N, respectively. However, in the case of *P. fluorescens*, a limited increase in the transferred bacteria was observed with an increase in applied contact force. The levels of bacterial transfer were in the range of 3.24–3.51 log CFU/cm^2 as the applied contact force was increased from 1 to 20 N. In addition, the transfer efficiencies for *L. innocua* under applied contact forces of 1, 5, 9.8, and 20 N were 0.89%, 3.4%, 4.8%, and 6.8%, and the efficiencies for *P. fluorescens* under the same set of conditions were 2.7%, 5.8%, 2.3%, and 3.6%, respectively. These results suggest that the transfer efficiency of *L. innocua* was influenced by the applied contact force at relatively lower levels of applied contact force, but the influence of the applied contact force was significantly reduced ($p < 0.05$) above a certain threshold level. However, in the case of *P. fluorescens,* the applied contact force did not significantly influence ($p > 0.05$) the bacterial transfer efficiency from a contaminated to a non-contaminated leaf. Furthermore, the level of bacteria transferred was relatively higher for *P. fluorescens* strain as compared to *L. innocua* at the levels of applied contact force lower than 5 N. These differences in the transfer efficiency with the

applied contact force were further explored with various surfaces selected to represent model hydrophobic and hydrophilic surfaces.

2.3.4. Quantitative data analysis for bacterial transfer efficiency

Table 2.1 indicates the quantitative data analysis for bacterial transfer efficiency as a function of different contact conditions. The influence of contact time on bacterial transfer efficiency was fitted to a log-linear model as described in Eq. 2.3. The *b* values (Table 2.1) representing the slopes of bacterial transfer efficiency as a function of contact time were similar for the two selected bacterial species. This implies that the influence of contact time on the bacterial transfer efficiency was similar among the two selected species. In contrast, the influence of applied contact force was fitted to a linear model as described in Eq. 2.4, where the *b* values varied with the changes in both contact surfaces and bacterial species. Furthermore, the data for the transfer of *P. fluorescens* in some cases were not fitted to a kinetic model, as there was no significant change in the bacterial transfer efficiency with increasing applied contact force.

Table 2.1. Parameters and goodness-of-fit for the bacterial transfer efficiency models

Variables	Surfaces	*L. innocua*			*P. fluorescens*		
		a	*b*	R^2	*a*	*b*	R^2
Contact time (Eq. 2.3)	Leaf-to-leaf	0.5235	0.0063	0.93	0.0742	0.0065	0.92
Applied contact force (Eq. 2.4)	Leaf-to-glass	2.3904	0.8114	0.94	-1.358	0.5885	0.97
	Leaf-to-leaf	1.3933	0.2899	0.92	n/a	n/a	n/a
	Leaf-to-PE	17.82	2.7787	0.96	n/a	n/a	n/a

A log-linear (Eq. 2.3) and a linear (Eq. 2.4) model were used to fit the data to determine the influences of contact time and applied contact force, respectively. PE: Polyethylene. n/a: Not applicable, as bacterial transfer efficiency was independent of the applied contact force for *P. fluorescens*.

2.3.5. Bacterial cross-contamination with different surface hydrophobicity

Figures 2.5a–b illustrate the role of surface contact angle or surface hydrophobicity on the efficiency of bacterial transfer from a contaminated leaf to a non-contaminated model surface for the selected bacteria. Although both bacterial species significantly preferred ($p < 0.05$) hydrophobic surfaces, the transfer efficiencies of a plant-associated bacterium (*P. fluorescens*) and a non-plant bacterium (*L. innocua*) showed different trends with increasing applied contact force for each of the model surfaces. The surface hydrophobicity of model surfaces was characterized according to the contact angle measurement method. The contact angles of deionized water on glass, leaf, and PE surfaces were 42.81 ± 3.26º (mean ± standard deviation), 69.50 ± 3.97º, and 72.40 ± 1.63º, respectively. These results indicate that glass is a relatively hydrophilic surface while the leaf and plastic are relatively hydrophobic. The cell surface hydrophobicity of selected bacteria was determined by measuring HPBI as described in Section 2.2.5. The values of HPBI for *L. innocua* and *P. fluorescens* were 56.76 ± 0.58 and 62.31 ± 0.39, respectively. The results in Figure 5a illustrate that for *L. innocua*, a hydrophobic PE surface was dramatically favored, and the influence of the applied contact force on the bacterial transfer efficiency was significant ($p < 0.05$) on flat surfaces above certain threshold levels of applied contact force. From a contaminated leaf of 4.45 log CFU/cm^2, 3.28, 3.28, 3.50, and 3.88 log CFU/cm^2 were transferred on a non-contaminated glass surface, and 3.90, 4.01, 4.28, and 4.42 log CFU/cm^2 were transferred on a non-contaminated PE surface, upon a single 5-s contact at applied contact forces of 1, 5, 9.8, and 20 N, respectively. These values correspond to the transfer efficiencies of 4.8%, 5.7%, 8.4%, and 20% for glass surfaces, and 20%, 28%, 52%, and 71% for PE surfaces, respectively. The results suggest that the transfer of *L. innocua* was enhanced upon contact with a smooth hydrophobic surface. Similarly, the results in Figure 5b show that for *P. fluorescens,* a

hydrophobic PE surface was favored in general. Moreover, the efficiency of bacterial transfer to a hydrophilic glass surface was not favored but increased for the applied contact force higher than 9.8 N. From a contaminated leaf of 4.97 log CFU/cm^2, 1.76, 2.32, 3.60, and 3.56 log CFU/cm^2 were transferred to a non-contaminated glass surface, while 3.13, 3.95, 4.24, and 4.17 log CFU/cm^2 were transferred to a non-contaminated PE surface, upon a single 5-s contact at applied contact forces of 1, 5, 9.8, 20 N, respectively. These values also mean that the transfer efficiencies of *P. fluorescens* with a single 5-s contact at 1, 5, 9.8, and 20 N from a contaminated leaf to a non-contaminated glass surface were 0.11%, 0.48%, 4.4%, and 11%, while the transfer efficiencies to a PE surface were 4.3%, 18%, 18%, and 15%, respectively. The results suggest that *P. fluorescens,* the plant-associated bacterium which can invade and affect the leaf tissue, is transferred to a leaf or plastic surface easily even with the lower applied contact force but requires more force for transferring to a less hydrophobic surface such as glass. Overall, these results suggest that the bacterial transfer from a contaminated leaf to a non-contaminated model surface favors a hydrophobic surface.

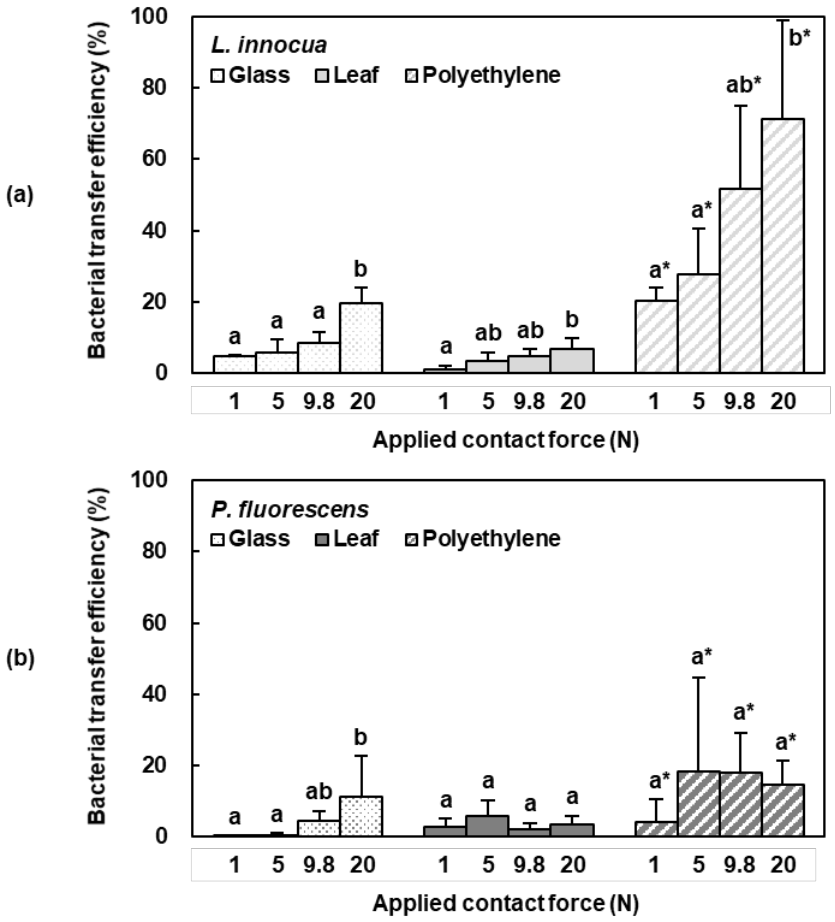

Figure 2.5. Bacterial transfer efficiencies from a contaminated leaf to non-contaminated model surfaces (glass, leaf, polyethylene) as a result of a single 5-s contact at different applied contact forces for (a) *L. innocua* and (b) *P. fluorescens.* The data are mean values and their standard deviations ($n = 3$). Different letters indicate significant differences between the values for the same recipient surface ($p < 0.05$), and asterisks indicate the significant difference among different recipient surfaces ($p < 0.05$).

2.4. Discussion

2.4.1. Leaf-to-leaf or leaf-to-surface cross-contamination is rapid and bi-directional

The experimental approach developed in this study illustrates that the transfer of bacteria from a contaminated leaf to a non-contaminated leaf or abiotic model surfaces is rapid, regardless of bacterial species explored. The results show that significant transfer of bacteria occurred within 5 s and the transfer efficiency increased exponentially at a similar rate with an increase in contact time for both the selected bacterial species. This finding is consistent with the results from prior studies that have reported rapid bacterial transfer between food materials and abiotic surfaces upon contact (Jensen et al., 2013; Miranda & Schaffner, 2016; Moore, Sheldon, & Jaykus, 2003; Zilelidou, Tsourou, Poimenidou, Loukou, & Skandamis, 2015). However, the transfer efficiency of bacteria from a contaminated leaf to a non-contaminated leaf or non-contaminated abiotic model surface was significantly lower (3–4%) than that reported in an earlier study evaluating the transfer of bacteria to a leaf surface from a contaminated stainless steel surface (31–36%) using similar levels of an applied contact force (1 N). These differences suggest that the transfer of bacteria from a contaminated abiotic surface to leafy greens is significantly more efficient compared to the transfer of bacteria from a contaminated leaf to non-contaminated leaves or non-contaminated surfaces. This has a significant impact as it indicates that the risk of cross-contamination of fresh produce is significantly higher from the contaminated surface as compared to contaminated fresh produce.

This study also evaluates the influence of repeated contacts between a contaminated leaf and non-contaminated leaves and the potential of a single contaminated leaf to transfer bacteria to multiple non-contaminated leaves. The lack of influence of repeated contacts on the bacterial transfer efficiency suggests that the transfer process of bacteria from one leaf to another is a

dynamic bi-directional process. Furthermore, this bi-directional process may be influenced by a local contact between the leaf surfaces and a relative location of the bacteria in addition to the total number of bacterial cells on a given leaf surface. As a result, this process of leaf-to-leaf bacterial transfer can also take place from a leaf surface with relatively fewer bacteria to a surface with relatively more bacteria, and the net number of bacteria transferred between the surfaces would not change upon repeated contacts. Previous studies reported that bacteria were transferred upon contact instantaneously and evenly distributed over the available surface area, resulting in a constant number of transferable bacteria for repeated contacts (Greene et al., 2018; Ivanek, Grohn, Wiedmann, & Wells, 2004). These results are consistent with the present study and suggest that a single contaminated leaf can transfer bacteria to multiple non-contaminated leaves.

2.4.2. The influence of applied contact force depends on relative binding affinity

The applied contact force significantly affected ($p < 0.05$) the bacterial transfer efficiency, however, the influence of the applied contact force on the bacterial transfer efficiency was depending on the relative binding affinity of bacteria with the leaf surface. The variation in bacterial transfer efficiency as a function of applied contact force was dependent on contact surface hydrophobicity and bacterial species. The transfer efficiency of *L. innocua* increased with an increase in the applied contact force up to a certain threshold level, while that of *P. fluorescens* remained unchanging regardless of the applied contact force. The selected bacterial species are distinct in that *Pseudomonas* is a plant-associated bacterium, which is reported to adhere dominantly to lettuce among the various bacterial population (King, Magnuson, Török, & Goodman, 1991). Moreover, the lower transfer efficiency of *L. innocua* to a non-contaminated leaf surface at the applied contact forces under 5 N may be due to the roughness of a leaf surface and

physical differences in the size of bacteria. In addition to surface hydrophobicity, surface roughness is reported as the other important factor influencing bacterial adhesion (Abdallah et al., 2014; Katsikogianni & Missirlis, 2004; Krachler & Orth, 2013). Similarly, the size and shape of bacteria and their affinity for plant microstructures may influence their localization (Sirinutsomboon, Delwiche, & Young, 2011). Thus, the bacteria placed in a valley of a leaf surface may not be quite approachable to another recipient surface. Furthermore, the affinity of bacteria to a recipient surface may also influence the transfer efficiency. However, as increasing applied contact force flattens a leaf so that bacteria and the recipient surface get closer, the adhesion force between them becomes stronger enough to transfer bacteria (Razatos, Ong, Sharma, & Georgiou, 1998). This is also supported by the previous studies, which highlighted that the role of contact force in the release of the bacteria trapped in a rough leaf surface (Lorenzetti et al., 2015; Pérez-Rodríguez, Valero, Carrasco, García, & Zurera, 2008). In conclusion, an enhanced applied contact force promotes bacterial transfer up to certain threshold levels.

2.4.3. Bacterial transfer efficiency from a contaminated leaf is increased on hydrophobic surfaces

The results of this study also demonstrate a significant ($p < 0.05$) influence of the recipient's surface hydrophobicity on the bacterial transfer efficiency as a function of the applied contact force. Abiotic model surfaces of different hydrophobicity were tested in this study since surface hydrophobicity has been known as one of the major factors influencing bacterial adhesion (Abdallah et al., 2014; Katsikogianni & Missirlis, 2004; Krachler & Orth, 2013). For both the selected bacterial species, the hydrophobic PE surface was significantly preferred ($p < 0.05$), where *L. innocua* showed a rapid increase in the transfer efficiency with an increase in the applied

contact force. This is in consistent with the literature that suggests preference of hydrophobic surface for various bacteria such as *P. aeruginosa, Staphylococcus aureus* (Abdallah et al., 2014), and *Bacillus subtilis* (Perera-Costa et al., 2014). These bacteria, as well as our selected bacteria, are hydrophobic (Ahimou, Paquot, Jacques, Thonart, & Rouxhet, 2001; Bruinsma, Rustema-Abbing, Van der Mei, & Busscher, 2001; Hogt, Dankert, & Feijen, 1985; Rosenberg et al., 1980) so that the hydrophobic interactions between bacteria and a non-contaminated surface may be promoted when a hydrophobic surface is used as a recipient, and consequently, resulting in the enhanced bacterial transfer.

2.5. Conclusion

This study illustrates a novel approach to simulate cross-contamination between leafy greens and between leaf and abiotic surfaces with precise controls on contact time, number of repeated contacts, and applied contact force. The results demonstrate that bacterial transfer from a contaminated leaf to either non-contaminated leaf or abiotic surface is instantaneous, and the extent of contact time has limited influence on the bacterial transfer efficiency. The results also illustrate that a single contaminated leaf can cross-contaminate multiple leaves. The study also evaluates the influence of applied contact force between the surfaces. The results indicate that with an increase in the applied contact force, the transfer efficiency of *L. innocua* from a contaminated leaf to a non-contaminated leaf or abiotic surfaces increases. However, leaf-to-leaf transfer of a plant-associated, *P. fluorescens*, remains unchanged regardless of the applied contact force. In addition, the results also illustrate the significance of a recipient's surface hydrophobicity in increasing the bacterial transfer efficiency from a contaminated leaf to abiotic surfaces. Overall, the results of this study illustrate a quantitative approach to characterize the cross-contamination

process as a function of the physical, chemical, and biological properties of the system. This quantitative approach can be extended to understand the risk of cross-contamination as well as to develop preventive measures for reducing the risk of cross-contamination.

Acknowledgements

This project was supported by Agriculture and Food Research Initiative grant no. 2015-68003-23411 from the USDA National Institute of Food and Agriculture (USDA-NIFA) Program Enhancing Food Safety through Improved Processing Technologies (A4131).

References

Abdallah, M., Benoliel, C., Jama, C., Drider, D., Dhulster, P., & Chihib, N.-E. (2014). Thermodynamic prediction of growth temperature dependence in the adhesion of *Pseudomonas aeruginosa* and *Staphylococcus aureus* to stainless steel and polycarbonate. *Journal of Food Protection*, *77*(7), 1116–1126. https://doi.org/10.4315/0362-028X.JFP-13-365

Ahimou, F., Paquot, M., Jacques, P., Thonart, P., & Rouxhet, P. G. (2001). Influence of electrical properties on the evaluation of the surface hydrophobicity of *Bacillus subtilis*. *Journal of Microbiological Methods*, *45*, 119–126. https://doi.org/10.1016/S0167-7012(01)00240-8

Arsenault, J., Letellier, A., Quessy, S., & Boulianne, M. (2007). Prevalence and risk factors for *Salmonella* and *Campylobacter* spp. carcass contamination in broiler chickens slaughtered in Quebec, Canada. *Journal of Food Protection*, *70*(8), 1820–1828. https://doi.org/10.4315/0362-028X-70.8.1820

Berg, G., Erlacher, A., Smalla, K., & Krause, R. (2014). Vegetable microbiomes: is there a connection among opportunistic infections, human health and our 'gut feeling'? *Microbial Biotechnology*, *7*(6), 487–495. https://doi.org/10.1111/1751-7915.12159

Bruinsma, G. M., Rustema-Abbing, M., Van der Mei, H. C., & Busscher, H. J. (2001). Effects of cell surface damage on surface properties and adhesion of *Pseudomonas aeruginosa*. *Journal of Microbiological Methods*, *45*, 95–101. https://doi.org/10.1016/S0167-7012(01)00238-X

Buchholz, A. L., Davidson, G. R., Marks, B. P., Todd, E. C. D., & Ryser, E. T. (2012). Transfer of *Escherichia coli* O157:H7 from equipment surfaces to fresh-cut leafy greens during processing in a model pilot-plant production line with sanitizer-free water. *Journal of Food Protection*, *75*(11), 1920–1929. https://doi.org/10.4315/0362-028X.JFP-11-489

Chen, Y., Jackson, K. M., Chea, F. P., & Schaffner, D. W. (2001). Quantification and variability analysis of bacterial cross-contamination rates in common food service tasks. *Journal of Food Protection*, *64*(1), 72–80. https://doi.org/10.4315/0362-028X-64.1.72

Duque, E., de la Torre, J., Bernal, P., Molina-Henares, M. A., Alaminos, M., Espinosa-Urgel, M., … Ramos, J. L. (2013). Identification of reciprocal adhesion genes in pathogenic and non-pathogenic *Pseudomonas*. *Environmental Microbiology*, *15*(1), 36–48. https://doi.org/10.1111/j.1462-2920.2012.02732.x

Flores, R. A., Tamplin, M. L., Marmer, B. S., Phillips, J. G., & Cooke, P. H. (2016). Transfer coefficient models for *Escherichia coli* O157:H7 on contacts between beef tissue and high-density polyethylene surfaces. *Journal of Food Protection*, *69*(6), 1248–1255. https://doi.org/10.4315/0362-028x-69.6.1248

Garner, D., & Kathariou, S. (2016). Fresh produce–associated listeriosis outbreaks, sources of concern, teachable moments, and insights. *Journal of Food Protection*, *79*(2), 337–344. https://doi.org/10.4315/0362-028x.jfp-15-387

Gil, M. I., Selma, M. V., Suslow, T., Jacxsens, L., Uyttendaele, M., & Allende, A. (2015). Pre- and postharvest preventive measures and intervention strategies to control microbial food safety hazards of fresh leafy vegetables. *Critical Reviews in Food Science and Nutrition*, *55*(4), 453–468. https://doi.org/10.1080/10408398.2012.657808

Greene, C., Ceron, N. H., Eisenberg, M. C., Koopman, J., Miller, J. D., Xi, C., & Eisenberg, J. N. S. (2018). Asymmetric transfer efficiencies between fomites and fingers: impact on model parameterization. *American Journal of Infection Control*, *46*, 620–626. https://doi.org/10.1016/j.ajic.2017.12.002

Hogt, A. H., Dankert, J., & Feijen, J. (1985). Adhesion of *Staphylococcus epidermidis* and

Staphylococcus saprophyticus to a hydrophobic biomaterial. *Journal of General Microbiology*, *131*, 2485–2491. https://doi.org/10.1099/00221287-131-9-2485

Huang, K., & Nitin, N. (2017). Enhanced removal of *Escherichia coli* O157:H7 and *Listeria innocua* from fresh lettuce leaves using surfactants during simulated washing. *Food Control*, *79*, 207–217. https://doi.org/10.1016/j.foodcont.2017.03.032

Huang, K., Tian, Y., Salvi, D., Karwe, M., & Nitin, N. (2018). Influence of exposure time, shear stress, and surfactants on detachment of *Escherichia coli* O157:H7 from fresh lettuce leaf surfaces during washing process. *Food and Bioprocess Technology*, *11*, 621–633. https://doi.org/10.1007/s11947-017-2038-5

Ivanek, R., Grohn, Y. T., Wiedmann, M., & Wells, M. T. (2004). Mathematical model of *Listeria monocytogenes* cross-contamination in a fish processing plant. *Journal of Food Protection*, *67*(12), 2688–2697. https://doi.org/10.4315/0362-028X-67.12.2688

Jensen, D. A., Friedrich, L. M., Harris, L. J., Danyluk, M. D., & Schaffner, D. W. (2013). Quantifying transfer rates of *Salmonella* and *Escherichia coli* O157:H7 between fresh-cut produce and common kitchen surfaces. *Journal of Food Protection*, *76*(9), 1530–1538. https://doi.org/10.4315/0362-028x.jfp-13-098

Katsikogianni, M., & Missirlis, Y. F. (2004). Concise review of mechanisms of bacterial adhesion to biomaterials and of techniques used in estimating bacteria-material interactions. *European Cells and Materials*, *8*, 37–57. https://doi.org/10.1002/(sici)1097-4636(199823)43:3<338::aid-jbm16>3.0.co;2-b

King, A. D., Magnuson, J. A., Török, T., & Goodman, N. (1991). Microbial flora and storage quality of partially processed lettuce. *Journal of Food Science*, *56*(2), 459–461. https://doi.org/10.1111/j.1365-2621.1991.tb05303.x

Koseki, S., Yoshida, K., Isobe, S., & Itoh, K. (2016). Decontamination of lettuce using acidic electrolyzed water. *Journal of Food Protection*, *64*(5), 652–658. https://doi.org/10.4315/0362-028x-64.5.652

Krachler, A. M., & Orth, K. (2013). Targeting the bacteria–host interface. *Virulence*, *4*(4), 284–294. https://doi.org/10.4161/viru.24606

Lindow, S. E., & Leveau, J. H. J. (2002). Phyllosphere microbiology. *Current Opinion in Biotechnology*, *13*(3), 238–243. https://doi.org/10.1016/S0958-1669(02)00313-0

Lopez, G. U., Gerba, C. P., Tamimi, A. H., Kitajima, M., Maxwell, S. L., & Rose, J. B. (2013). Transfer efficiency of bacteria and viruses from porous and nonporous fomites to fingers under different relative humidity conditions. *Applied and Environmental Microbiology*, *79*(18), 5728–5734. https://doi.org/10.1128/aem.01030-13

Lorenzetti, M., Dogša, I., Stošicki, T., Stopar, D., Kalin, M., Kobe, S., & Novak, S. (2015). The influence of surface modification on bacterial adhesion to titanium-based substrates. *ACS Applied Materials and Interfaces*, *7*(3), 1644–1651. https://doi.org/10.1021/am507148n

Lu, Y., Joerger, R., & Wu, C. (2014). Similar reduction of *Salmonella enterica* Typhimurium on grape tomatoes and its cross-contamination in wash water by washing with natural antimicrobials as compared with chlorine treatment. *Food and Bioprocess Technology*, *7*(3), 661–670. https://doi.org/10.1007/s11947-013-1105-9

Lynch, M. F., Tauxe, R. V., & Hedberg, C. W. (2009). The growing burden of foodborne outbreaks due to contaminated fresh produce: risks and opportunities. *Epidemiology and Infection*, *137*(3), 307–315. https://doi.org/10.1017/S0950268808001969

Matthews, K. R. (2009). Leafy vegetables. In *The Produce Contamination Problem: Causes and Solutions* (pp. 165–187). Elsevier, New York.

Miranda, R. C., & Schaffner, D. W. (2016). Longer contact times increase cross-contamination of *Enterobacter aerogenes* from surfaces to foods. *Applied and Environmental Microbiology*, *82*(21), 6490–6496. https://doi.org/10.1128/AEM.01838-16

Molina, M. A., Ramos, J. L., & Espinosa-Urgel, M. (2003). Plant-associated biofilms. *Reviews in Environmental Science and Biotechnology*, *2*(2–4), 99–108. https://doi.org/10.1023/B:RESB.0000040458.35960.25

Moore, C. M., Sheldon, B. W., & Jaykus, L.-A. (2003). Transfer of *Salmonella* and *Campylobacter* from stainless steel to romaine lettuce. *Journal of Foof Protection*, *66*(12), 2231–2236. https://doi.org/10.4315/0362-028X-66.12.2231

Nithya, A., & Babu, S. (2017). Prevalence of plant beneficial and human pathogenic bacteria isolated from salad vegetables in India. *BMC Microbiology*, *17*(1), 1–16. https://doi.org/10.1186/s12866-017-0974-x

Parnell, T. L., Harris, L. J., & Suslow, T. V. (2005). Reducing *Salmonella* on cantaloupes and honeydew melons using wash practices applicable to postharvest handling, foodservice, and consumer preparation. *International Journal of Food Microbiology*, *99*(1), 59–70. https://doi.org/10.1016/j.ijfoodmicro.2004.07.014

Perera-Costa, D., Bruque, J. M., González-Martín, M. L., Gómez-García, A. C., & Vadillo-Rodríguez, V. (2014). Studying the influence of surface topography on bacterial adhesion using spatially organized microtopographic surface patterns. *Langmuir*, *30*(16), 4633–4641. https://doi.org/10.1021/la5001057

Pérez-Rodríguez, F., Valero, A., Carrasco, E., García, R. M., & Zurera, G. (2008). Understanding and modelling bacterial transfer to foods: A review. *Trends in Food Science and Technology*, *19*(3), 131–144. https://doi.org/10.1016/j.tifs.2007.08.003

Pérez-Rodríguez, F., Valero, A., Todd, E. C. D., Carrasco, E., García-Gimeno, R. M., & Zurera, G. (2007). Modeling transfer of *Escherichia coli* O157:H7 and *Staphylococcus aureus* during slicing of a cooked meat product. *Meat Science*, *76*(4), 692–699. https://doi.org/10.1016/j.meatsci.2007.02.011

Pfeilmeier, S., Saur, I. M. L., Rathjen, J. P., Zipfel, C., & Malone, J. G. (2016). High levels of cyclic-di-GMP in plant-associated *Pseudomonas* correlate with evasion of plant immunity. *Molecular Plant Pathology*, *17*(4), 521–531. https://doi.org/10.1111/mpp.12297

Rajwar, A., Srivastava, P., & Sahgal, M. (2016). Microbiology of fresh produce: route of contamination, detection methods, and remedy. *Critical Reviews in Food Science and Nutrition*, *56*(14), 2383–2390. https://doi.org/10.1080/10408398.2013.841119

Razatos, A., Ong, Y. L., Sharma, M. M., & Georgiou, G. (1998). Molecular determinants of bacterial adhesion monitored by atomic force microscopy. *Proceedings of the National Academy of Sciences of the United States of America*, *95*(19), 11059–11064. https://doi.org/10.1002/jmr.618

Rosenberg, M., Gutnick, D., & Rosenberg, E. (1980). Adherence of bacteria to hydrocarbons: a simple method for measuring cell-surface hydrophobicity. *FEMS Microbiology Letters*, *9*, 29–33. https://doi.org/10.1111/j.1574-6968.1980.tb05599.x

Sirinutsomboon, B., Delwiche, M. J., & Young, G. M. (2011). Attachment of *Escherichia coli* on plant surface structures built by microfabrication. *Biosystems Engineering*, *108*(3), 244–252. https://doi.org/10.1016/j.biosystemseng.2010.12.007

Solomon, E. B., & Matthews, K. R. (2006). Interaction of live and dead *Escherichia coli* O157:H7 and fluorescent microspheres with lettuce tissue suggests bacterial processes do not mediate adherence. *Letters in Applied Microbiology*, *42*(2), 88–93. https://doi.org/10.1111/j.1472-

765X.2005.01816.x

Vandamm, J. P., Li, D., Harris, L. J., Schaffner, D. W., & Danyluk, M. D. (2013). Fate of *Escherichia coli* O157: H7, *Listeria monocytogenes*, and *Salmonella* on fresh-cut celery. *Food Microbiology*, *34*(1), 151–157. https://doi.org/10.1016/j.fm.2012.11.016

Wachtel, M. R., & Charkowski, A. O. (2002). Cross-contamination of lettuce with *Escherichia coli* O157:H7. *Journal of Food Protection*, *65*(3), 465–470. https://doi.org/10.4315/0362-028X-65.3.465

Weyens, N., Beckers, B., Schellingen, K., Ceulemans, R., Croes, S., Janssen, J., … Vangronsveld, J. (2013). Plant-associated bacteria and their role in the success or failure of metal phytoextraction projects: First observations of a field-related experiment. *Microbial Biotechnology*, *6*(3), 288–299. https://doi.org/10.1111/1751-7915.12038

Yeni, F., Yavaş, S., Alpas, H., & Soyer, Y. (2016). Most common foodborne pathogens and mycotoxins on fresh produce: A review of recent outbreaks. *Critical Reviews in Food Science and Nutrition*, *56*(9), 1532–1544. https://doi.org/10.1080/10408398.2013.777021

Zhu, Q., Gooneratne, R., & Hussain, M. (2017). *Listeria monocytogenes* in fresh produce: outbreaks, prevalence and contamination levels. *Foods*, *6*(21), 1–11. https://doi.org/10.3390/foods6030021

Zilelidou, E. A., Tsourou, V., Poimenidou, S., Loukou, A., & Skandamis, P. N. (2015). Modeling transfer of *Escherichia coli* O157:H7 and *Listeria monocytogenes* during preparation of fresh-cut salads: Impact of cutting and shredding practices. *Food Microbiology*, *45*(PB), 254–265. https://doi.org/10.1016/j.fm.2014.06.019

CHAPTER 3:

Antimicrobial *N*-Halamine Incorporated Poly(Vinyl Alcohol-co-Ethylene) Films for Reducing Cross-Contamination of Fresh Produce [2]

Abstract

Cross-contamination of fresh produce can lead to nationwide foodborne outbreaks. Despite using current sanitation practices, several studies have shown that reusable plastic containers used during the harvest and postharvest processing can be contaminated with pathogenic bacteria. These contaminated surfaces of plastic containers can lead to cross-contamination of fresh produce. The overall objective of this study was to develop a rechargeable antimicrobial plastic film that could be used to reduce cross-contamination of fresh produce in a dynamic postharvest processing environment. An *N*-halamine precursor incorporated poly(vinyl alcohol-co-ethylene) film was used to charge chlorine via immersion in a dilute bleach to achieve a chlorine-charged plastic film. Cross-contamination was simulated using baby spinach inoculated with 5-log CFU/cm^2 *Listeria innocua* to contact a non-contaminated film, which was then contacted by another non-contaminated leaf at different contact times (5–1200 s) and applied forces (1 and 9.8 N). Bacteria on different surfaces were quantified, and quality attributes of leaves such as color, texture, and total phenolic content were measured. The active chlorine content in the charged plastic films reached 445.8 ± 7.2 nmol/cm^2 after 1 h chlorination in a 10% dilute bleach solution and remained constant for at least 3 recharging cycles. The self-cleaning activity of the charged plastic films was demonstrated (> 2 log reduction of inoculated bacteria) after a 20-min contact and reduced approximately 2 logs of inoculated *L. innocua* on leaves. The charged plastic films were also effective for reducing cross-contamination of leaves, preventing bacterial transfer from

[2] Note: This chapter has been published in *Food Control* (2021).

contaminated leaves to non-contaminated leaves without causing a significant quality loss. Thus, the antimicrobial plastic films used in this study can effectively reduce cross-contamination of leafy greens and be potentially used as a liner material or moldable plastic for reusable containers during harvesting and postharvest processing.

Keywords: Cross-contamination; Fresh produce; Baby spinach; *Listeria*; *N*-halamine; Antimicrobial plastic film

3.1. Introduction

Foodborne illness associated with fresh produce contamination is a major societal challenge (Havelaar et al., 2010; Painter et al., 2013; Yeni, Yavaş, Alpas, & Soyer, 2016). The consumption of fresh produce has increased with an increasing awareness of its health benefits (Berger et al., 2010; Olaimat & Holley, 2012). As postharvest fresh produce processing does not have a kill step, cross-contamination is a significant food safety concern during harvest and postharvest processing. Cross-contamination from food contact surfaces, equipment, humans, and contaminated product can lead to contamination of fresh produce with pathogens (Garner & Kathariou, 2016; Yeni et al., 2016). Prior studies have shown that reusable plastic containers used for storage, transportation, and handling of fresh produce can be a source of cross-contamination (Izumi, Poubol, Hisa, & Sera, 2016; Izumi, Tsukada, Poubol, & Hisa, 2016; Shi et al., 2016; Singla, Goel, & Ganguli, 2014). Among various foodborne pathogens associated with fresh produce, *Listeria monocytogenes* is one of the common contaminating pathogens that has been associated with various disease outbreaks (Alegbeleye, Singleton, & Sant'Ana, 2018; Painter et al., 2013; Zhu, Gooneratne, & Hussain, 2017). Based on its ability to form biofilms, persistence in cold temperature, and resistance to various physiological stresses, including osmotic stress, *Listeria* can survive on the surface of food processing equipment for an extended time (Blackman & Frank, 2016; Garner & Kathariou, 2016; Mafu, Roy, Goulet, & Savoie, 1991; Yeni et al., 2016). Thus, developing approaches to mitigate the survival and colonization of food contact surfaces by *Listeria* can help reduce the incidence of foodborne illness.

One of the potential approaches to limit cross-contamination of fresh produce from food contact surfaces is to develop antimicrobial polymers. Various studies have investigated different antimicrobial polymers for the inactivation of inoculated microbes as well as the reduction of

biofilm formation (Appendini & Hotchkiss, 2002; López-Carballo, Higueras, Gavara, & Hernández-Muñoz, 2013; Qiao et al., 2017; Xinbo Sun, Cao, Porteous, & Sun, 2012). Antimicrobial agents such as *N*-halamines, enzymes, essential oils, silver nanoparticles, and phenolic acids have been incorporated into different polymer matrices to develop antimicrobial films and coatings (Appendini & Hotchkiss, 2002; López-Carballo et al., 2013; López, Sánchez, Batlle, & Nerín, 2007; Qiao et al., 2017; Xiuxiu Sun, Wang, Kadouh, & Zhou, 2014). Despite various studies focused on evaluating the antimicrobial properties of these films and coatings over extended time periods, there is a lack of quantitative information on their effectiveness in providing rapid microbial inactivation in the presence of organic matter. The need for rapid kill is significant as prior studies have shown that a short contact period with a contaminated surface (less than 20 min) may be adequate for bacteria to transfer to a batch of fresh produce (Yi, Huang, Young, & Nitin, 2020; Zilelidou, Tsourou, Poimenidou, Loukou, & Skandamis, 2015). However, many of the prior studies with antimicrobial polymers have focused on microbial inactivation after a relatively long exposure time, for example, a study by Qiao et al. (2017) illustrated that *N*-halamine polymers inactivated 6 logs of *Escherichia coli* within 2-h contact on thermoplastic polyurethane (TPU) films. In another case, chitosan films containing gallic acid reduced *L. innocua* 2.5 logs after 24 h of contact (Borges, Ferreira, Saavedra, & Simões, 2013). Further, the antimicrobial characteristics of these polymers could be influenced by contact with food, considering that many of the prior antimicrobial studies were conducted without the presence of food or organic matter. The presence of food may attenuate the antimicrobial properties (Appendini & Hotchkiss, 2002), which is vital for evaluating the translation of these antimicrobial polymer compositions to practical applications, such as the development of antimicrobial liner materials or modified plastic

compositions for harvest bins, storage boxes, packaging turntables, and conveyor belts to control cross-contamination of minimally processed foods.

To address these knowledge gaps, the objectives of this study were to 1) evaluate an antimicrobial *N*-halamine incorporated plastic film in preventing cross-contamination of a model fresh produce, 2) determine the influence of contact time and applied contact force on bacterial transfer, and 3) evaluate quality attributes of the model fresh produce upon contact with modified plastic films. In this study, *N*-halamine was selected as an antimicrobial agent since it has a superior performance in terms of biocidal activity, stability, rechargeability, and non-toxicity to humans (Qiao et al., 2017; Si et al., 2017). In this study, *N*-halamine precursor incorporated poly(vinyl alcohol-co-ethylene) (PVA-co-PE) plastic film was selected and examined for its potential to inactivate *L. innocua*, a surrogate of human pathogenic *L. monocytogenes*, on a model fresh produce. Baby spinach was selected as a model fresh produce since it represents one of the major crops among leafy greens and has been associated with disease outbreaks from foodborne pathogens (Painter et al., 2013). In summary, this study comprehensively evaluated the application of the plastic film modified with *N*-halamine to prevent cross-contamination of fresh produce. These results are expected to guide the selection of this modified plastic as a liner material or a moldable plastic for reusable containers, such as totes, bins, and crates used during the harvest and postharvest processing of fresh produce.

3.2. Materials and Methods

3.2.1. Bacterial strain, media, and growth conditions

A Gram-positive bacterial strain *L. innocua* (ATCC 33090) was selected in this study as a surrogate for a human pathogenic *L. monocytogenes*. A stock of rifampicin-resistant *L. innocua*

was provided by Dr. Linda Harris (University of California-Davis, USA) and stored frozen (-80 ºC) in tryptic soy broth (TSB) (Sigma-Aldrich, St. Louis, MO, USA) supplemented with 15% v/v of glycerol in liquid nitrogen. The bacteria were then streaked onto tryptic soy agar (TSA) (Sigma-Aldrich) plates supplemented with 50 µg/mL rifampicin and grown at 30 ºC for 48 h before use. One colony was picked from the agar plate, cultured in TSB, and incubated with a constant shaking of 250 rpm at 30 ºC for 22 h to achieve the stationary phase cultures. A 10 mL of bacterial culture was then centrifuged at 3100 × *g* for 8 min at room temperature, and the pellet was suspended in 10 mL of phosphate buffered saline (PBS, Fisher Scientific, Pittsburg, CA, USA) solution. This step was repeated twice to wash the cells before experiments, and the final bacterial concentration of 6 log CFU/mL (assessed by plate counting) was achieved by serial dilutions.

3.2.2. Preparation and inoculation of baby spinach

Fresh baby spinach (*Spinacia oleracea*) leaves (fresh-cut, commercially washed) were purchased from a local market and stored at 4 °C until further use up to seven days. Leaves without tissue damage were selected and cut into 5 cm × 5 cm square leaf slice, and then washed with sterile deionized water prior to use. A 0.5 mL of bacterial suspension was dropped on the leaf samples and spread with a sterile cell spreader. The inoculated leaf samples were incubated for 1 h at room temperature to allow bacterial attachment. The leaves were cut into 1-cm diameter discs with a sterile borer after inoculation and then rinsed with 1 mL of sterile deionized water by a quick dip to wash off loosely attached bacteria, and therefore, excess moisture was presented on the leaf surfaces.

3.2.3. Preparation of antimicrobial plastic films

3.2.3.1. Modification of PVA-co-PE films with N-halamine precursor

An uncharged polymerized high-strength PVA-co-PE grafting film was prepared as previously described (Si et al., 2017). Briefly, PVA-co-PE powders, 2,4-diamino-6-diallylamino-1,3,5-triazine (DAM) precursor (4% w/w of PVA-co-PE), and dicumyl peroxide initiator (0.04% w/w of PVA-co-PE) were first mixed and extruded. The extrudates of poly(vinyl alcohol-co-ethylene-g-diallylmelamine) (PVA-co-PE-g-DAM) were pelletized. The as-prepared pellets were hot-pressed using a Carver automatic hydraulic presses (AutoFour/30-15H) with a pressure of 260 MPa at 190 ºC for 5 min. The *N*-halamine precursor amount in the PVA-co-PE film was 4% w/w, and the thickness of the film was 0.15 mm.

3.2.3.2. Chlorination of N-halamine incorporated plastic films

A 0.1 g of uncharged plastic film was immersed in 30 mL of dilute household bleach (10% v/v of 8.25% commercial sodium hypochlorite solution at pH 5) at room temperature and incubated under constant shaking at 250 rpm for a predetermined duration (15 min–2 h for testing total active chlorine content and 1 h for the other experiments). After chlorination, the chlorine-charged plastic film was washed three times with sterile deionized water to remove any free hypochlorous moieties and dried in the air.

3.2.4. Total active chlorine content and rechargeability of plastic films

The total active chlorine content of charged plastic films was quantified by the iodometric titration method. Briefly, 0.1 g of charged plastic film was added to 15 mL of 0.001-N sodium thiosulfate solution with shaking for 30 min. The residual sodium thiosulfate was subsequently

titrated with a 0.001-N iodine standard solution. The total active chlorine content of the charged plastic films (nmol/cm^2) was calculated according to:

$$\text{Total active chlorine content} = \frac{(V_0 - V_s) \times 10^9 N}{2A_s} \quad (3.1)$$

where V_0 and V_s are the volumes of the iodine solution consumed in titration without and with a charged plastic film (L), respectively, N is the concentration of sodium thiosulfate solution (mol/L), and A_s is the surface area (cm^2) of the charged plastic film.

For the rechargeability tests, plastic films were first charged for 1 h, then treated with an excess amount of sodium thiosulfate solution (1% w/v) for 1 h to quench any active chlorine. Then the quenched films were recharged in a chlorination solution for another 1 h, and the total active chlorine content of the film was measured as described above.

3.2.5. Microbial inactivation by charged plastic films

The inactivation efficacy of the charged plastic films against *L. innocua* was evaluated. Uncharged plastic films were used as a control group. *L. innocua* suspension at a concentration of approximately 5 log CFU/mL was prepared by serial dilution with sterile PBS, and a plastic coupon (1 cm × 1 cm) was fixed at the bottom of each well in a 24-well microplate. A 1 mL of bacterial suspension was added to each well, where the liquid level of suspension was 1 mm higher than the plastic coupons. After incubation at room temperature for 5, 10, and 20 min, respectively, the plastic coupons were collected with sterile forceps and rinsed twice by sterile deionized water to remove loosely attached bacteria. Each plastic coupon was then transferred to a sterile test tube containing 1 mL of maximum recovery diluent (MRD, Sigma-Aldrich) with 1% w/v sodium thiosulfate, and allowed to stand for 2 min. After vortexing at full speed for 1 min by a vortex mixer (Fisher Scientific, Waltham, MA, USA), the isolated bacterial suspension was diluted

10-fold, and both the diluted suspension and the primary isolate from the coupons were plated on TSA plates supplemented with 50 μg/mL rifampicin. The plates were incubated at 30 °C for 48 h prior to bacterial enumeration. The colony forming unit (CFU) on a plate was counted, and this was converted to log CFU/cm^2 based on the surface area of the plastic coupon (1 cm^2). The detection limit of the assay in this section was determined by converting 1 CFU per agar plate into log CFU/cm^2, which was 1 log CFU/cm^2.

3.2.6. Effect of charged plastic films in reducing cross-contamination of baby spinach

The efficacy of the charged plastic films in reducing cross-contamination of baby spinach leaves was evaluated, as shown in Figure 3.1. Uncharged plastic films were used as a control group. The process of leaf-film-leaf cross-contamination was divided into two steps; (1) leaf-to-film bacterial transfer, which was from a contaminated leaf to a non-contaminated plastic film (uncharged or charged) by contact, followed by (2) film-to-leaf bacterial transfer, which was from the film used in the first step to a non-contaminated leaf by another contact. The contact process was simulated using a TA-XT2 Texture Analyser (Stable Micro Systems, Godalming, Surrey, UK) according to the method described in our previous work (Yi et al., 2020). A plastic film (diameter = 1 cm) was attached to the bottom of a probe of the texture analyzer, facing down with double-sided tape. A donor or recipient leaf was placed on a 100-mm diameter Petri dish facing up, and then the dish was put on a platform of the device aligned with the film. The film and the leaf were overlapping when the probe comes down with the preset contact conditions controlled by the Texture Expert Exceed software (version 2.64, Stable Micro Systems). Different combinations of contact times (5–20 min) and applied contact forces (1 and 9.8 N) were explored.

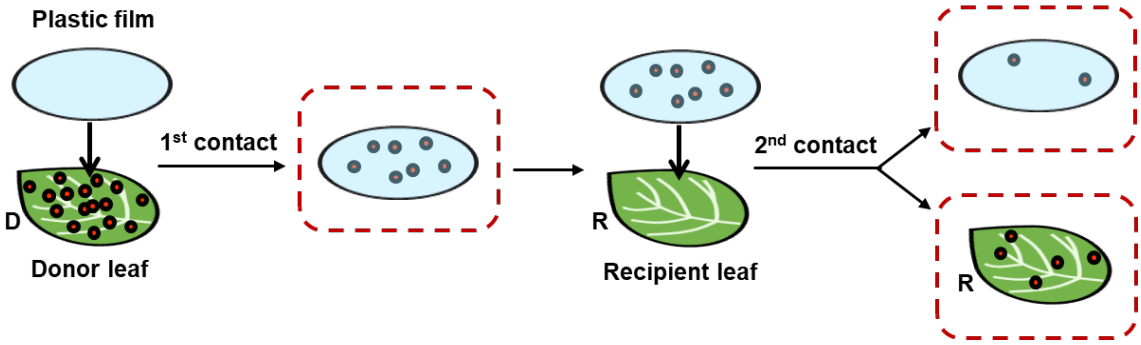

Figure 3.1. A schematic diagram of simulated cross-contamination of baby spinach and plastic films. An uncharged *N*-halamine precursor incorporated poly(vinyl alcohol-co-ethylene) film and a chlorine-charged plastic film were used. Red dotted boxes indicate samples analyzed for microbiological enumeration.

For enumeration of viable bacteria on leaves or plastic films, the samples were transferred to a sterile test tube containing 10 mL of MRD with 1 % w/v sodium thiosulfate, which stops the chlorine reaction, and allowed it to stand for 2 min. After vortexing at full speed for 1 min by a vortex mixer, quantification of viable bacteria was performed by serial dilutions and plating on TSA plates supplemented with 50 μg/mL rifampicin as described in Section 3.2.6. Bacterial counts were determined after incubation at 37 ºC for 48 h. The colony forming unit on a plate was counted, and this was converted to log CFU/cm^2 based on the surface area of the film or the leaf with a diameter of 1 cm. The detection of this assay in this section was determined by converting 1 CFU per agar plate into log CFU/cm^2, which was 1.10 CFU/cm^2.

3.2.7. Characterization of charged plastic films upon contact with baby spinach

3.2.7.1. Self-cleaning activity

The self-cleaning activity of the charged plastic films was demonstrated by extended incubation of the films after leaf-to-film contact with contaminated donor leaves at an applied contact force of 9.8 N for 20 min. After a non-contaminated film contacted the donor leaf, it was incubated at room temperature for 5–20 min. The number of viable bacteria on each film after contact was enumerated as a function of incubation time after contact, and the results for the uncharged and charged plastic films were compared.

3.2.7.2. X-ray photoelectron spectroscopy

The surface chlorine content of the charged plastic films before and after contact with a leaf at an applied contact force of 9.8 N for 20 min was characterized by the X-ray photoelectron spectroscopy (XPS, PHI 5600, Perkin Elmer, USA). A single 100 μm spot was analyzed from each

coupon at an angle of 45º relative to the plastic film surface with Al Kα excitation. Survey scans were collected at a pass energy of 187.35 eV. The reported XPS results were representative spectra of 3 scans on each film.

3.2.8. Quality evaluations of baby spinach upon contact with charged plastic films

3.2.8.1. Color analysis

For the color measurement, baby spinach leaves were analyzed using the ColorFlex EZ Spectrophotometer (Hunter Lab, Reston, VA, USA). Hunter's color values (L, a, b) were measured by the EasymatchQC software (Hunter Lab, Reston, VA, USA). Fresh leaves were used as a reference, and the colors of leaves after contact with plastic films at an applied contact force of 9.8 N for 20 min were evaluated. Total color difference (ΔE) before and after contact was determined using the following equation:

$$\Delta E_{ab}^{*} = [(L_1^{*} - L_0^{*})^2 + (a_1^{*} - a_0^{*})^2 + (b_1^{*} - b_0^{*})^2]^{\frac{1}{2}} \quad (3.2)$$

where L_0^{*}, a_0^{*}, and b_0^{*} are Hunter's color values from a reference (fresh baby spinach) and L_1^{*}, a_1^{*}, and b_1^{*} are Hunter's color values from a leaf after contact with either an uncharged or a charged plastic film.

3.2.8.2. Texture analysis

The compressibility of baby spinach was measured using the TA-XT2 Texture Analyser. A spinach leaf was positioned on the platform and then compressed by the probe to a depth of 2 mm at a speed of 1 mm/s. The maximum compression force was recorded using the Texture Expert Exceed software (version 2.64, Stable Micro Systems). The maximum compression force of leaves after different treatments were compared, including fresh leaves, leaves after contact with

uncharged plastic films at an applied contact force of 9.8 N for 20 min, and leaves after the same contact with the charged plastic films.

3.2.8.3. Quantification of total phenolic content

The phenolic compounds of baby spinach were extracted following the modified method of (Edenharder, Keller, Platt, & Unger, 2001) before quantification. A 1 g of the leaf was chopped into small pieces and then homogenized using a homogenizer (T18 digital ULTRA TURRAX, IKA, Germany) at 3,000 rpm for 2 min. The homogenized sample was extracted with 10 mL of 70 % v/v aqueous methanol on a mechanical shaker at 40°C for 2 h, followed by centrifugation at 10,000 rpm for 15 min. The supernatant of the mixture was decanted into a test tube, and the same cycle was repeated for the pellet. The mixture of supernatants was then filtered through a Whatman No. 1 filter paper to obtain a clear extract for further analysis.

The total phenolic contents of the leaves were determined according to the modified Folin-Ciocalteu assay (Velioglu, Mazza, Gao, & Oomah, 1998). The Folin-Ciocalteu reagent (Sigma-Aldrich) was diluted 10-fold with deionized water, and then 0.75 mL of the reagent was mixed with 100 μL of the extract in a test tube. After standing at room temperature for 5 min, 0.75 mL of sodium carbonate (60 g/L) (Sigma-Aldrich) solution was added to the mixture. The mixture was allowed to stand at room temperature in the dark for 90 min, and a 100 μL aliquot was placed within a well of a 96-well plate. The absorbance was measured at 750 nm using a Spectramax340 device (Molecular Devices LLC, Sunnyvale, CA, USA) versus a blank. The standard calibration (0.05–0.5 g/L) curve was plotted using gallic acid (Sigma-Aldrich), and the total phenolic content was expressed as gallic acid equivalents (GAE) g on a fresh weight basis, i.e., per 1 kg of baby spinach. Fresh leaves, leaves after contact with uncharged plastic films at an applied contact force

of 9.8 N for 20 min, and leaves after the same contact with the charged plastic films were evaluated.

3.2.9. Statistical analysis

Statistical analysis was performed using the GraphPad Prism software (version 5.04, GraphPad Software, Inc., La Jolla, CA, USA). All experiments were performed in triplicates unless otherwise specified. The significant differences between treatments were determined through one-way analysis of variance, followed by Tukey's pairwise comparisons with a 95 % confidence interval.

3.3. Results and Discussion

3.3.1. Antimicrobial activity of charged plastic films

3.3.1.1. Chlorine loading capacity of plastic films

To evaluate the chlorine loading capacity of the plastic films, the total active chlorine content after charging the films with a dilute bleach solution and rechargeability of the films were evaluated. Results in Figure 3.2a illustrate an increase in the total active chlorine content of the plastic films as a function of incubation time with a concentrated chlorine solution. The total active chlorine content reached 445.8 ± 7.2 nmol/cm^2 after 1 h of chlorination. With extended chlorination time of more than 1 h, no significant increase ($p > 0.05$) in the chlorine concentration of the films was observed. The results in Figure 3.2b indicate that the total active chlorine content did not decrease significantly ($p > 0.05$) over 3 repeated charging cycles. Overall, the plastic films could be charged with more than 445 nmol/cm^2 (or more than 15.8 μg/cm^2) of total active chlorine and recharged multiple times. In this study, PVA-co-PE was used as hydrophilic plastic, but it is

possible to extend this concept to other commodity vinyl polymers. Based on reactive extrusion principles and using diverse forms of *N*-halamine precursors, polyethylene (Badrossamay & Sun, 2009a) and polypropylene (Badrossamay & Sun, 2009b) plastic materials were modified to create rechargeable antimicrobial *N*-halamine polymers in prior studies. Thus, future studies may include these different plastics to examine their abilities to reduce cross-contamination of fresh produce.

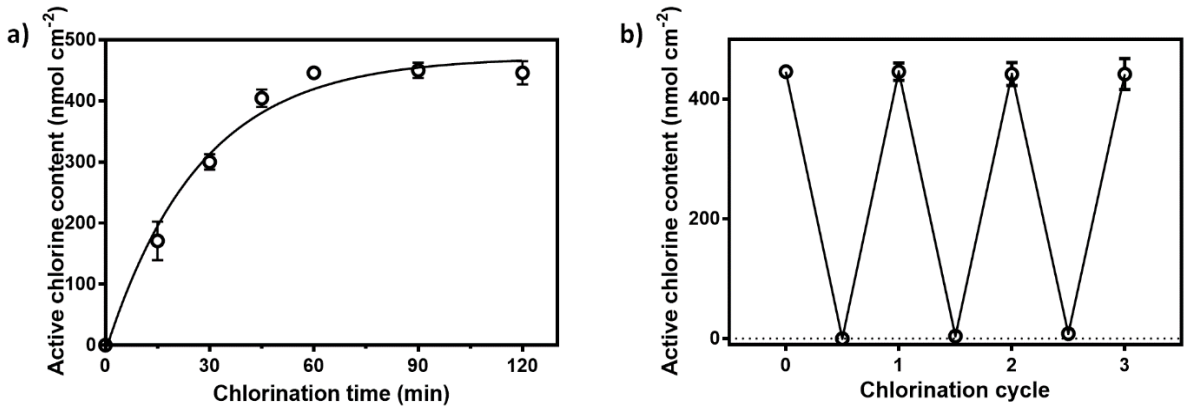

Figure 3.2. The chlorine loading capacity of an *N*-halamine precursor incorporated poly(vinyl alcohol-co-ethylene) film. a) The total active chlorine content of a chlorine-charged plastic film as a function of the chlorination time; b) Rechargeability of the plastic films. The results represent the mean values and their standard deviations (n = 3).

3.3.1.2. Rapid microbial inactivation upon contact with charged plastic films

To assess the antimicrobial efficacy of the charged plastic films, the bacterial suspension of *L. innocua* was selected as a model system. Results in Table 3.1 show the survival of *L. innocua* upon exposure to the plastic film as a function of incubation time. For this measurement, bacterial suspension was added to the surface of a film, as described in Section 3.2.5. After a 5-min exposure of bacterial suspension to the control uncharged plastic film, 3.01 ± 0.09 log CFU/cm^2 of *L. innocua* were detected on the control uncharged plastic film. There were no significant changes ($p > 0.05$) in the number of viable bacteria on the uncharged and charged plastic films with an increase in the exposure time. In the case of the chlorine-charged plastic films, the numbers of viable bacteria on the films were less than the limit of detection, indicating that all the bacteria attached to the films were inactivated after 5 min of incubation. These results suggest that the charged plastic films were effective for the inactivation of *L. innocua* within a short contact time.

Table 3.1. Antimicrobial efficacy of the plastic films against *Listeria innocua*

	5 min exposure	10 min exposure	20 min exposure
Viable bacteria on an uncharged plastic film (log CFU/cm^2)	3.01 ± 0.09	2.84 ± 0.31	3.11 ± 0.17
Viable bacteria on a charged plastic film (log CFU/cm^2)	UDL	UDL	UDL

UDL: under the limit of detection (1 log CFU/cm^2). A 1 mL suspension of 5-log CFU/mL *L. innocua* was used as an initial load. The results represent the mean values and their standard deviations (n = 3). There were no significant differences among the values for the same row (p > 0.05).

This level of microbial inactivation was higher and faster compared to those of the previously reported antimicrobial polymers. A prior study has reported < 1 log reduction of *Escherichia coli* in a 30-min exposure to chlorine-charged *N*-halamine TPU films (Qiao et al., 2017). The differences in the antimicrobial activity of our charged plastic films compared to the *N*-halamine incorporated TPU films could be attributed to the differences in the total level of active chlorine content in the films. In the previous study, the maximum level of total active chlorine content in the antimicrobial TPU film was approximately 5.5 μg/cm^2 (Qiao et al., 2017). In contrast, the charged plastic film used in the current study was more than 445 nmol/cm^2 (or more than 15.8 μg/cm^2) of total active chlorine (Figure 3.a). These differences in total active chlorine levels could influence the overall surface density of chlorine molecules and thus impact the rate of bacterial inactivation. Moreover, the inactivation rate of the charged plastic films used in this study was significantly higher than that of polymers containing antimicrobial agents other than *N*-halamine, such as gallic acid or nisin, as reported in the literature (Jin, Liu, Zhang, & Hicks, 2009; Xiuxiu Sun et al., 2014). For example, a prior study reported a 2.5 log reduction of *L. innocua* after 24-h exposure using gallic acid as an antimicrobial incorporated into a chitosan film (Xiuxiu Sun et al., 2014). Similarly, a nisin incorporated pectin/polylactic acid film resulted in a 2.1 log reduction of *L. monocytogenes* after 48 h of exposure (Jin et al., 2009). Therefore, the results in this study suggest that the chlorine-charged plastic films can achieve higher levels of microbial inactivation in a short contact period. Rapid inactivation is a major requirement for using antimicrobial polymers in fresh produce processing lines since the products may undergo rapid movement within a short contact time and can be rapidly cross-contaminated (Gombas et al., 2017; Pérez-Rodríguez et al., 2014). With different chemistries using *N*-halamine precursors, the balance between the stability and reactivity of the antimicrobial polymers can be further engineered to meet

the needs of the applications (Qian & Sun, 2003). The *N*-halamine precursor (2,4-diamino-6-diallylamino-1,3,5-triazine) used in this study is a primary amine that behaves as an amide (Si et al., 2017). This type of *N*-halamine provides rapid inactivation based on its reactivity but may have reduced stability in water (Dong, Wang, Gao, Gao, & Gao, 2017). For applications in moist environments, secondary amide precursors, such as *N-tert*-butylacrylamide, could be used to enhance the stability of the *N*-halamine polymers.

3.3.2. Reduction of cross-contamination of baby spinach by charged plastic films

In addition to the inactivation of microbial suspension, the charged plastic films were further tested for the efficacy in preventing cross-contamination of baby spinach as a function of contact time. To mimic a practical use of the charged plastic films as a liner material on food contact surfaces, a leaf-film-leaf cross-contamination process was evaluated. In the process of leaf-film-leaf cross-contamination, a contaminated leaf first made contact with a non-contaminated plastic film (leaf-to-film bacterial transfer), and then this contaminated film was used to make another contact with a non-contaminated leaf (film-to-leaf bacterial transfer).

3.3.2.1. Reduction of leaf-to-film bacterial transfer

The results in Figure 3.3 show leaf-to-film bacterial transfer from a contaminated leaf (donor) to a non-contaminated plastic film. The initial concentration of *L. innocua* on a donor leaf was 5.27 ± 0.12 log CFU/cm^2. Upon contact with the donor leaf, the control uncharged plastic films had a bacterial count of 3.94 ± 0.24, 3.80 ± 0.21, 3.95 ± 0.13 log CFU/cm^2 of *L. innocua,* while the charged plastic films had a bacterial count of 3.50 ± 0.10, 2.13 ± 0.34, 2.12 ± 0.40 log CFU/cm^2 of *L. innocua* for the contact times of 5, 10, 20 min, respectively. To

ensure uniform contact between a leaf and a film, a force of 1 N was applied on top of the two contacting surfaces using a texture analyzer. The results illustrate that with increasing contact time, there was no significant change ($p > 0.05$) in the number of viable bacteria on uncharged plastic films. However, bacterial transfer significantly decreased ($p < 0.05$) for the charged plastic films after 10 min of contact with the contaminated leaf, resulting in 1.67–1.83 log reduction. Considering that a typical level of *Listeria* contamination of fresh produce is 1–2 log CFU/g (Zhu et al., 2017), which is much lower than our initial load, this level of log reduction could be considered as an effective antimicrobial approach. These results suggest the potential of the charged plastic films to reduce cross-contamination of food contact surfaces upon contact with contaminated fresh produce.

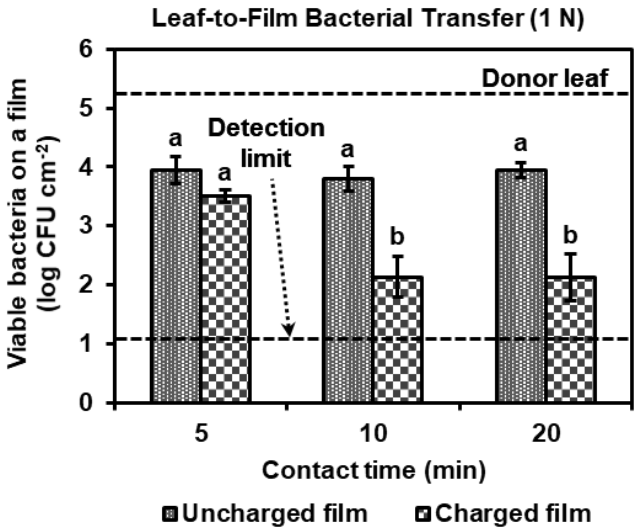

Figure 3.3. Effect of charged plastic films in reducing the transfer of *Listeria innocua* from baby spinach after the 1st contact (from a contaminated leaf to a non-contaminated plastic film). The applied contact force between the leaf and the film was 1 N. The initial bacterial load on a contaminated (donor) leaf was 5.27 ± 0.12 log CFU/cm^2, and the detection limit was 1.10 log CFU/cm^2. The results represent the mean values and their standard deviations ($n = 3$). Different letters indicate significant differences between the values ($p < 0.05$).

3.3.2.2. Reduction of film-to-leaf bacterial transfer

The results in Figure 3.4 show film-to-leaf bacterial transfer from uncharged or charged plastic films inoculated upon contact with a contaminated leaf (Figure 3.3). The initial load of bacteria on the film was the same as described in Section 3.3.2.1. As illustrated in Figure 3.4a, the residual numbers of viable bacteria on the uncharged plastic films were 4.07 ± 0.35, 3.87 ± 0.16, 3.68 ± 0.19 log CFU/cm^2 upon contact with a non-contaminated leaf for the selected contact times of 5, 10, 20 min, respectively. In the case of the charged plastic films, the residual number of viable bacteria was 1.79 ± 0.43 log CFU/cm^2 after a 5-min contact with a recipient leaf, while the numbers of viable bacteria on the charged plastic films after 10- and 20-min contact were less than the limit of detection. Figure 3.4b illustrates the level of viable bacteria transferred to a recipient leaf upon contact with a contaminated film with an applied contact force of 1 N. For the uncharged plastic films, 3.66 ± 0.04, 3.36 ± 0.27, 3.63 ± 0.09 log CFU/cm^2 were transferred to the leaf following the contact periods of 5, 10, 20 min between a leaf and a film. For the charged plastic films, 1.99 ± 0.17 log CFU/cm^2 were transferred after a 5-min contact between a leaf and a film. The numbers of bacteria on the recipient leaves upon contact for 10 and 20 min with the charged plastic films were less than the detection limit. Overall, the charged plastic films significantly reduced ($p < 0.05$) the level of viable bacteria on their surfaces (> 2.77 log reduction) as well as bacterial transfer to a recipient leaf (> 2.26 log reduction) within 10 min. Thus, using the charged plastic films can be an effective intervention method to control the risk of cross-contamination of fresh produce in a dynamic processing environment.

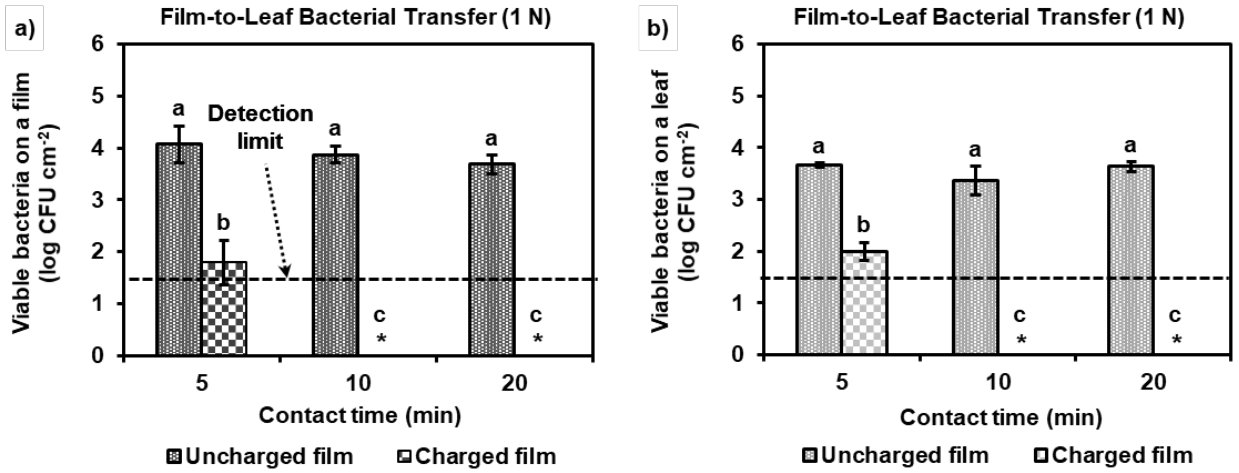

Figure 3.4. Effect of charged plastic films in reducing the transfer of *L. innocua* from a contaminated film to a non-contaminated leaf after the 2nd contact (from the film contaminated by the 1st contact in Figure 3.3 to a non-contaminated leaf). a) The number of viable bacteria remaining on a film and b) the number of viable bacteria on a leaf transferred from the film upon contact. The experimental conditions (applied contact force, detection limit) were maintained the same as in Figure 3.3. The results represent the mean values and their standard deviations (n = 3), and the asterisks indicate that the number of viable bacteria was less than the limit of detection. Different letters indicate significant differences between the values ($p < 0.05$).

3.3.3. Influence of an increased applied contact force on prevention effect

Contact force applied to a leaf can influence the contact area between a leaf and a film, which could be affected by the inherent compressibility, curvature, and surface roughness of the leaf. The applied contact force may influence the contact area between a leaf and a film, thus influencing the interactions of both organic matter and bacteria on a leaf with the food contact surface. The results in Figure 3.5 show leaf-to-film bacterial transfer from a contaminated leaf to a non-contaminated film using an applied contact force of 9.8 N. This applied contact force was chosen based on our prior study, where we defined the range of applied contact forces related to postharvest processing (Yi et al., 2020). For example, 1 kg of a leaf stack could be placed on top of a leaf contacting a film during the storage or transportation, and this may generate an applied force of 9.8 N. Upon contact with a contaminated leaf with the initial load of 5.25 ± 0.11 log CFU/cm^2, the uncharged plastic films received 4.06 ± 0.23, 4.11 ± 0.32, 4.18 ± 0.12 log CFU/cm^2 of viable bacteria, while the charged plastic films received 3.43 ± 0.24, 2.82 ± 0.10, 2.90 ± 0.06 log CFU/cm^2, for the contact times of 5, 10, 20 min, respectively. There were no significant changes ($p > 0.05$) in the number of viable bacteria on an uncharged plastic film as a function of contact time. In contrast, the charged plastic films significantly reduced ($p < 0.05$) the number of viable bacteria on the film after 10 min of contact. The ability of the charged plastic films to reduce the number of viable bacteria on the film was significantly reduced ($p < 0.05$) with an increase in the applied contact force from 1 N to 9.8 N. Overall, these results suggest that the charged plastic films were effective in reducing cross-contamination, while the overall efficiency of these antimicrobial plastic films was reduced with an increased in applied contact force.

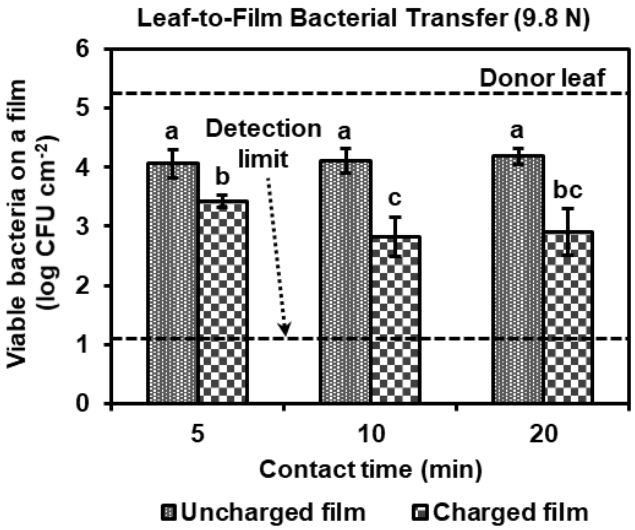

Figure 3.5. Influence of an increased applied contact force on the transfer of *L. innocua* from baby spinach. The applied contact force between the contaminated leaf (donor) and a non-contaminated film was 9.8 N. The initial bacterial load on a donor leaf was 5.25 ± 0.11 log CFU/cm^2, and the detection limit was 1.10 log CFU/cm^2. The results represent the mean values and their standard deviations (n = 3). Different letters indicate significant differences between the values ($p < 0.05$).

During the postharvest processing of fresh produce, the contact force between fresh produce and a food contact surface may vary depending on the application and the type of surfaces. For example, fresh produce in contact with the walls of a harvest bin may experience normal forces due to the load of the produce. Similarly, during the conveying and handling processes, fresh produce may experience an enhanced force acting on its contact with the food contact surface, due to a range of factors, including human handling. The increased applied contact force is expected to enhance the contact of fresh produce with the food contact surface. In the case of leafy greens such as baby spinach, the enhanced contact may increase the contact area between the leaf and food contact surfaces. Consequently, the enhanced contact can increase the effective organic load exposed to the contact surface from the leaves. The increased exposure to organic load can then deplete chlorine on the surface of the antimicrobial polymers (Bastarrachea, Denis-Rohr, & Goddard, 2015; Ren, Qiao, Huang, Weese, & Ren, 2018). Based on the results presented in Figures 3.3 and 3.5, it could be concluded that the antimicrobial effect was reduced when a higher contact force was applied between the film and the leaf. These results suggest that the diffusion of antimicrobial agents within the plastic films is much slower than the depletion of the surface chlorine by fresh produce samples. This observation is in agreement with the literature since a charged plastic film used in this study was an amine halamine (Si et al., 2017), and it was reported that the intermolecular chlorine diffusion from amine halamine is a slow reaction (Qian & Sun, 2005). This limitation in the film design could be potentially reduced by developing polymeric materials with higher surface area and reduced thickness, such as fiber matrices (Deng, Si, & Sun, 2020). Thus, future studies evaluating the potential of the antimicrobial polymers may consider some of these approaches to improve the antimicrobial effectiveness against an organic matter of food.

3.3.4. Characteristics of charged plastic films upon contact with baby spinach

3.3.4.1. Self-cleaning activity

The self-cleaning activity of the charged plastic films was evaluated after contact between a contaminated donor leaf and a non-contaminated film at an applied contact force of 9.8 N for 20 min. For this test, the film was maintained under ambient conditions after the initial contamination with the leaf samples. The results in Figure 3.6a show that the number of viable bacteria on the films did not change significantly ($p > 0.05$) with an extended incubation after contact with a contaminated leaf. However, the number of viable bacteria on the charged plastic films decreased as a function of time ($p < 0.05$), and the numbers of viable bacteria on the charged plastic films were less than the limit of detection after 20 min of an extended incubation. These results illustrate that the chlorine-charged plastic films can self-clean their surfaces by inactivating bacteria with extended incubation time. This self-cleaning ability is one of the significant advantages of the chlorine-charged plastic film, since it could reduce labor and the cost required for sanitation and cleaning of surfaces. Future studies may be designed to evaluate the reduction in microbial load on modified surfaces with extended use in a food processing environment.

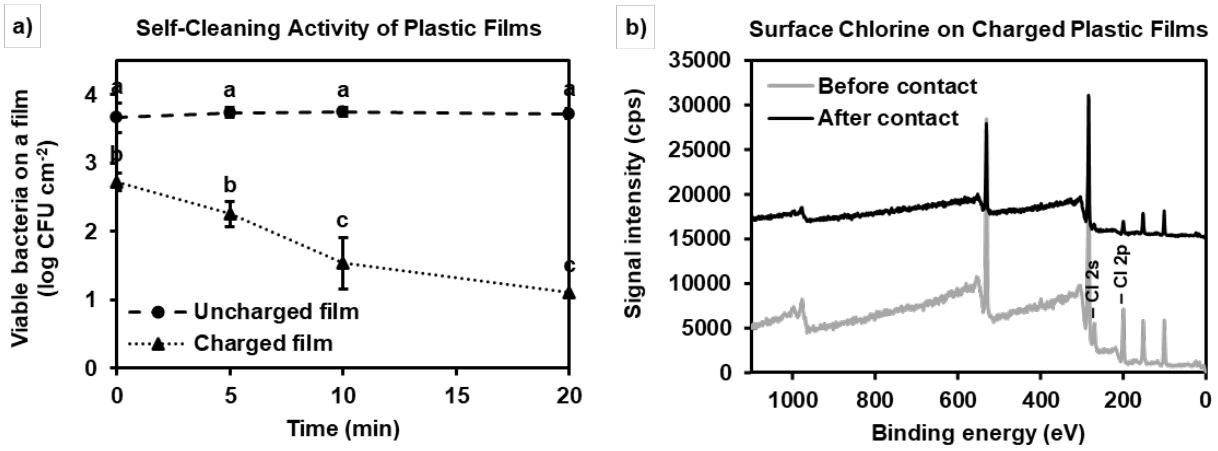

Figure 3.6. Characteristics of charged plastic films upon contact with baby spinach at an applied contact force of 9.8 N for 20 min. a) The self-cleaning activity of charged plastic films. b) X-ray photoelectron spectroscopy survey scans of charged plastic film surfaces before and after contact. The results represent the mean values, and error bars indicate their standard deviations ($n = 3$). Different letters indicate significant differences between the values ($p < 0.05$).

3.3.4.2. Chlorine consumption by contacting baby spinach

Changes in active chlorine content on the charged plastic film surfaces following contact with a non-contaminated leaf were determined using XPS. The applied contact force of 9.8 N and contact time of 20 min were selected for this measurement. The results in Figure 3.6b and Table 3.2 show that the active chlorine level on the charged plastic film surfaces before and after contact with a non-contaminated leaf changed from 9.53 atomic % to 3.87 atomic %. Since the leaves used for this assay were not contaminated with bacteria, this change in active chlorine content might have resulted from a reaction between chlorine on the charged plastic film surface and the leaf itself. This could be supported by previous studies on the organic matter of baby spinach (Weng et al., 2016) and its reactivity with chlorine (Gómez-López, Marín, Medina-Martínez, Gil, & Allende, 2013). A prior study reported that baby spinach extracts prepared by blending had a high level of organic matter (Weng et al., 2016). Since baby spinach has a large surface-to-volume ratio (Bergquist, 2006), diverse organic matter on the leaf surface, including cutin biopolymers or other structural cell wall carbohydrates, could be accessible to chlorine that comes into contact. This may lead to rapid consumption of chlorine on the leaf surface. Similarly, it was reported that whole-leaf baby spinach reacted with free chlorine to generate trihalomethanes (Gómez-López et al., 2013). On the other hand, the results in Table 3.2 indicate only a partial level of chlorine was reduced by contact with the leaf, and chlorine was still detected on the charged film surfaces. This could be further reduced if chopped or shredded leafy greens were used, which are known to release more organic matter (Weng et al., 2016). Overall, the results suggest that organic matter on a leaf surface can reduce the active chlorine content on the charged plastic film surfaces. These results, combined with the results in Figure 3.5, suggest that diffusion of active

chlorine within the charged plastic films to the surface of the film is a rate-limiting process, which limited the recovery of surface chlorine as it was consumed by the organic matter in fresh produce.

Table 3.2. Atomic compositions of charged plastic film surface as determined by X-ray photoelectron spectroscopy

	% atomic composition (atomic %)				
Sample	O	C	Si	Cl	N
Before contact	44.90 ± 6.07a	30.40 ± 5.28a	13.16 ± 5.91a	9.53 ± 1.06a	2.00 ± 0.66a
After contact	50.67 ± 4.80a	29.17 ± 3.67a	14.97 ± 1.86a	3.87 ± 0.71b	1.33 ± 0.47a

The results represent the mean values and their standard deviations (n = 3). Different letters within the same column indicate significant differences between the values ($p < 0.05$).

3.3.5. Quality evaluations of baby spinach before and after contact with charged plastic films

The quality attributes of the leaves upon contact with the charged plastic films were assessed based on the measurements of color, texture, and total phenolic contents. For these measurements, the contact between a leaf and a charged plastic film was conducted with an applied contact force of 9.8 N for a total time of 20 min. The results in Figure 3.7a represent the total color differences between a fresh leaf and a leaf upon contact with a film, and there were no significant differences in the total color of the leaves contacted with uncharged and charged films ($p > 0.05$). The results in Figure 3.7b show no significant differences ($p > 0.05$) between the maximum compression forces of a fresh leaf, a leaf after contact with an uncharged plastic film, and a leaf after contact with a charged plastic film. There was also no significant loss of total phenolic contents of leaves. Thus, the results show that there was no quality loss of baby spinach upon contact with the charged plastic films.

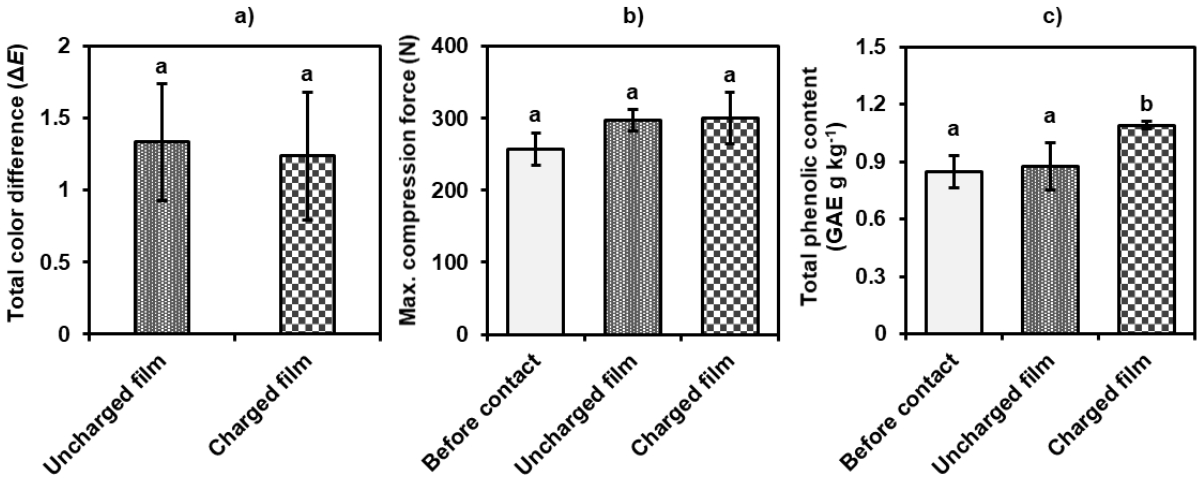

Figure 3.7. Quality evaluations of baby spinach before and after contact with plastic films at an applied force of 9.8 N for 20 min. a) The total color difference of leaves after contact with the films compared to fresh leaves, b) maximum compression forces, and c) total phenolic contents. The results represent the mean values and their standard deviations ($n = 3$). Different letters indicate significant differences between the values ($p < 0.05$).

3.4. Conclusions

In summary, this study demonstrates the potential of an antimicrobial *N*-halamine incorporated plastic film that can effectively reduce the cross-contamination of fresh produce during rapid postharvest processes. The study shows that chlorine-charged plastic films resulted in rapid and significant inactivation of bacteria inoculated on the surface (> 2 log reduction in 10 min) as well as reducing cross-contamination of baby spinach (approximately 2 log reduction in 10 min) without negatively influencing the leaf quality. In the presence of a higher applied contact force, which resulted in an enhanced organic load exposed to the plastic films, the antimicrobial efficiency of the charged plastic films was reduced. Even under these conditions, a significant reduction in the transfer of bacteria from contaminated leaf to film was observed within 20 min of contact as compared to uncharged plastic films. The reduced rate of bacterial inactivation in a high organic load environment suggests limited chlorine diffusion from the film to its surface as the surface exposed chlorine is being consumed by organic matter. These constraints may be reduced by increasing the surface area of the plastic material, such as fibers, and thus improving the contact between food and chlorine bound to the material. Overall, the results in this study illustrate the potential use of the charged plastic film as a liner material for food contact surfaces or moldable plastic containers to reduce cross-contamination of fresh produce during the harvest and postharvest processing.

Acknowledgements

This project was supported by the United States Department of Agriculture-National Institute of Food and Agriculture NIFA Award [grant number 2015-68003-23411]; the Center for Produce Safety Award [grant number 2018CPS07]. XPS microscopy was performed at the Biomolecular

Nanotechnology Center of the California Institute for Quantitative Biosciences (QB3) at the University of California, Berkeley.

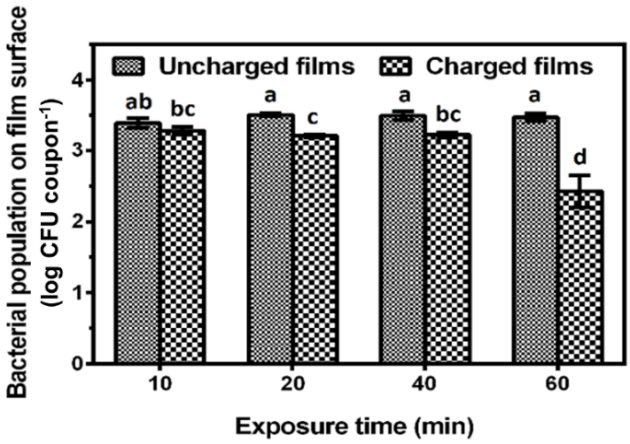

Figure 3.8. Antimicrobial efficacy of charged plastic films against *L. innocua* in the presence of organic matter (COD = 500 mg/L). Different letters indicate significant differences between the values ($p < 0.05$).

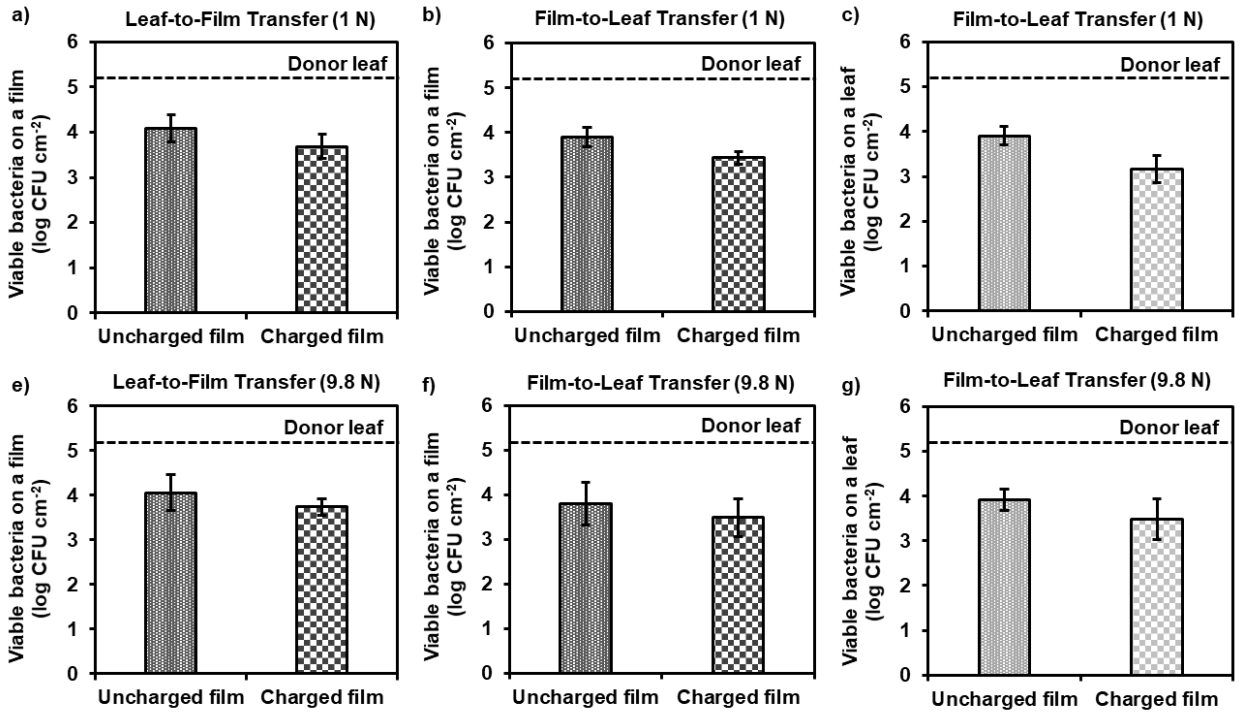

Figure 3.9. Effect of charged plastic films in reducing cross-contamination from contaminated baby spinach upon 5-s contact at applied contact forces of (a–c) 1 N or (e–g) 9.8 N. a,e) The number of viable bacteria on a film after the initial leaf-to-film transfer, b,f) the number of viable bacteria on a film after the following film-to-leaf transfer, and c,g) the number of viable bacteria on a leaf after the film-to-leaf transfer. The initial bacterial load on a contaminated leaf (donor) was 5.27 ± 0.12 log CFU/cm^2, and the detection limit was 1.10 log CFU/cm^2. The results represent the mean values and their standard deviations (n = 3). There were no significant differences among the values (p > 0.05).

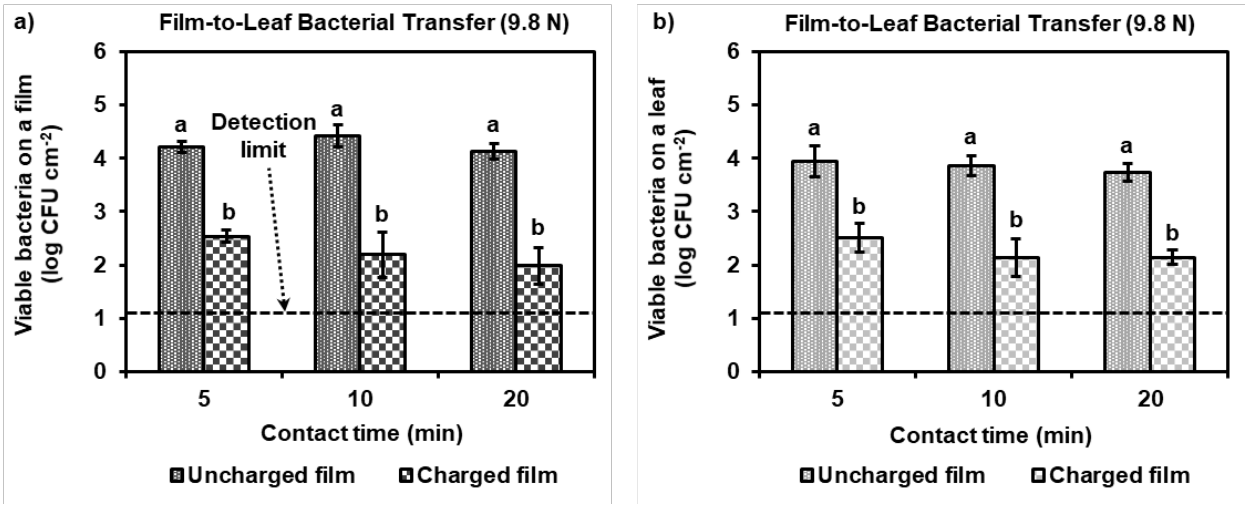

Figure 3.10. Effect of charged plastic films in reducing the transfer of *L. innocua* from a contaminated film to a non-contaminated leaf at an increased applied contact force. a) The number of viable bacteria remaining on a film and b) the number of viable bacteria on a leaf transferred from the film upon contact. The plastic films resulting from the leaf-to-film bacterial transfer (Figure 3.5) were used as the contaminated film, and the experimental conditions were maintained the same as in Figure 3.5. The results represent the mean values and their standard deviations ($n = 3$). Different letters indicate significant differences between the values ($p < 0.05$).

References

Alegbeleye, O. O., Singleton, I., & Sant'Ana, A. S. (2018). Sources and contamination routes of microbial pathogens to fresh produce during field cultivation: A review. *Food Microbiology*, *73*, 177–208. https://doi.org/10.1016/j.fm.2018.01.003

Appendini, P., & Hotchkiss, J. H. (2002). Review of antimicrobial food packaging. *Innovative Food Science and Emerging Technologies*, *3*, 113–126. https://doi.org/10.1016/S1466-8564(02)00012-7

Badrossamay, M. R., & Sun, G. (2009a). A study on melt grafting of *N*-halamine moieties onto polyethylene and their antibacterial activities. *Macromolecules*, *42*(6), 1948–1954. https://doi.org/10.1021/ma802270b

Badrossamay, M. R., & Sun, G. (2009b). Durable and rechargeable biocidal polypropylene polymers and fibers prepared by using reactive extrusion. *Journal of Biomedical Materials Research - Part B Applied Biomaterials*, *89*(1), 93–101. https://doi.org/10.1002/jbm.b.31191

Bastarrachea, L. J., Denis-Rohr, A., & Goddard, J. M. (2015). Antimicrobial food equipment coatings: Applications and challenges. *Annual Review of Food Science and Technology*, *6*, 97–118. https://doi.org/10.1146/annurev-food-022814-015453

Berger, C. N., Sodha, S. V., Shaw, R. K., Griffin, P. M., Pink, D., Hand, P., & Frankel, G. (2010). Fresh fruit and vegetables as vehicles for the transmission of human pathogens. *Environmental Microbiology*, *12*(9), 2385–2397. https://doi.org/10.1111/j.1462-2920.2010.02297.x

Bergquist, S. (2006). *Bioactive compounds in baby spinach (Spinacia oleracea L.)* (Vol. 2006).

Blackman, I. C., & Frank, J. F. (2016). Growth of *Listeria monocytogenes* as a biofilm on various food-processing surfaces. *Journal of Food Protection*, *59*(8), 827–831. https://doi.org/10.4315/0362-028x-59.8.827

Borges, A., Ferreira, C., Saavedra, M. J., & Simões, M. (2013). Antibacterial activity and mode of action of ferulic and gallic acids against pathogenic bacteria. *Microbial Drug Resistance*, *19*(4), 256–265. https://doi.org/10.1089/mdr.2012.0244

Deng, Y., Si, Y., & Sun, G. (2020). Fibrous materials for antimicrobial applications. In J. Hu, B. Kumar, & J. Lu (Eds.), *Handbook of Fibrous Materials* (pp. 927–951). https://doi.org/10.1002/9783527342587.ch33

Dong, A., Wang, Y. J., Gao, Y., Gao, T., & Gao, G. (2017). Chemical insights into antibacterial *N*-halamines. *Chemical Reviews*, *117*(6), 4806–4862. https://doi.org/10.1021/acs.chemrev.6b00687

Edenharder, R., Keller, G., Platt, K. L., & Unger, K. K. (2001). Isolation and characterization of structurally novel antimutagenic flavonoids from spinach (*Spinacia oleracea*). *Journal of Agricultural and Food Chemistry*, *49*, 2767–2773. https://doi.org/10.1021/jf0013712

Garner, D., & Kathariou, S. (2016). Fresh produce–associated listeriosis outbreaks, sources of concern, teachable moments, and insights. *Journal of Food Protection*, *79*(2), 337–344. https://doi.org/10.4315/0362-028x.jfp-15-387

Gombas, D., Luo, Y., Brennan, J., Shergill, G., Petran, R., Walsh, R., … Deng, K. (2017). Guidelines to validate control of cross-contamination during washing of fresh-cut leafy vegetables. *Journal of Food Protection*, *80*(2), 312–330. https://doi.org/10.4315/0362-028X.JFP-16-258

Gómez-López, V. M., Marín, A., Medina-Martínez, M. S., Gil, M. I., & Allende, A. (2013). Generation of trihalomethanes with chlorine-based sanitizers and impact on microbial, nutritional and sensory quality of baby spinach. *Postharvest Biology and Technology*, *85*, 210–217. https://doi.org/10.1016/j.postharvbio.2013.05.012

Havelaar, A. H., Brul, S., de Jong, A., de Jonge, R., Zwietering, M. H., & ter Kuile, B. H. (2010). Future challenges to microbial food safety. *International Journal of Food Microbiology*, *139*, S79–S94. https://doi.org/10.1016/j.ijfoodmicro.2009.10.015

Izumi, H., Poubol, J., Hisa, K., & Sera, K. (2016). Potential sources of microbial contamination of satsuma mandarin fruit in Japan, from production through packing shed. *Journal of Food Protection*, *71*(3), 530–538. https://doi.org/10.4315/0362-028x-71.3.530

Izumi, H., Tsukada, Y., Poubol, J., & Hisa, K. (2016). On-farm sources of microbial contamination of persimmon fruit in Japan. *Journal of Food Protection*, *71*(1), 52–59. https://doi.org/10.4315/0362-028x-71.1.52

Jin, T., Liu, L., Zhang, H., & Hicks, K. (2009). Antimicrobial activity of nisin incorporated in pectin and polylactic acid composite films against *Listeria monocytogenes*. *International Journal of Food Science and Technology*, *44*(2), 322–329. https://doi.org/10.1111/j.1365-2621.2008.01719.x

López-Carballo, G., Higueras, L., Gavara, R., & Hernández-Muñoz, P. (2013). Silver ions release from antibacterial chitosan films containing in situ generated silver nanoparticles. *Journal of Agricultural and Food Chemistry*, *61*(1), 260–267. https://doi.org/10.1021/jf304006y

López, P., Sánchez, C., Batlle, R., & Nerín, C. (2007). Development of flexible antimicrobial films using essential oils as active agents. *Journal of Agricultural and Food Chemistry*, *55*(21), 8814–8824. https://doi.org/10.1021/jf071737b

Mafu, A. A., Roy, D., Goulet, J., & Savoie, L. (1991). Characterization of physicochemical forces involved in adhesion of *Listeria monocytogenes* to surfaces. *Applied and Environmental Microbiology*, *57*(7), 1969–1973. https://doi.org/10.1128/aem.57.7.1969-1973.1991

Olaimat, A. N., & Holley, R. A. (2012). Factors influencing the microbial safety of fresh produce: A review. *Food Microbiology*, *32*(1), 1–19. https://doi.org/10.1016/j.fm.2012.04.016

Painter, J. A., Hoekstra, R. M., Ayers, T., Tauxe, R. V., Braden, C. R., Angulo, F. J., & Griffin, P. M. (2013). Attribution of foodborne illnesses, hospitalizations, and deaths to food commodities by using outbreak data, United States, 1998-2008. *Emerging Infectious Diseases*, *19*(3), 407–415. https://doi.org/10.3201/eid1903.111866

Pérez-Rodríguez, F., Saiz-Abajo, M. J., Garcia-Gimeno, R. M., Moreno, A., González, D., & Vitas, A. I. (2014). Quantitative assessment of the *Salmonella* distribution on fresh-cut leafy vegetables due to cross-contamination occurred in an industrial process simulated at laboratory scale. *International Journal of Food Microbiology*, *184*, 86–91. https://doi.org/10.1016/j.ijfoodmicro.2014.05.013

Qian, L., & Sun, G. (2003). Durable and regenerable antimicrobial textiles: Synthesis and applications of 3-methylol-2,2,5,5-tetramethylimidazolidin-4-one (MTMIO). *Journal of Applied Polymer Science*, *89*(9), 2418–2425. https://doi.org/10.1002/app.12405

Qian, L., & Sun, G. (2005). Durable and regenerable antimicrobial textiles: Chlorine transfer among halamine structures. *Industrial and Engineering Chemistry Research*, *44*(4), 852–856. https://doi.org/10.1021/ie049493x

Qiao, M., Ren, T., Huang, T., Weese, J., Liu, Y., Ren, X., & Farag, R. (2017). *N*-halamine modified thermoplastic polyurethane with rechargeable antimicrobial function for food contact surface. *RSC Advances*, *7*, 1233–1240. https://doi.org/10.1039/c6ra25502g

Ren, T., Qiao, M., Huang, T. S., Weese, J., & Ren, X. (2018). Efficacy of *N*-halamine compound on reduction of microorganisms in absorbent food pads of raw beef. *Food Control*, *84*, 255–262. https://doi.org/10.1016/j.foodcont.2017.08.006

Shi, Z., Baker, C. A., Lee, S. I., Park, S. H., Kim, S. A., & Ricke, S. C. (2016). Comparison of methods for quantitating *Salmonella enterica* Typhimurium and heidelberg strain attachment to reusable plastic shipping container coupons and preliminary assessment of sanitizer efficacy. *Journal of Environmental Science and Health, Part B*, *51*(9), 602–608. https://doi.org/10.1080/03601234.2016.1181905

Si, Y., Cossu, A., Nitin, N., Ma, Y., Zhao, C., Chiou, B., … Sun, G. (2017). Mechanically robust and transparent *N*-halamine grafted PVA-co-PE films with renewable antimicrobial activity. *Macromolecular Bioscience*, *17*(3), 1600304. https://doi.org/10.1002/mabi.201600304

Singla, R., Goel, H., & Ganguli, A. (2014). Novel synergistic approach to exploit the bactericidal efficacy of commercial disinfectants on the biofilms of *Salmonella enterica* serovar Typhimurium. *Journal of Bioscience and Bioengineering*, *118*(1), 34–40. https://doi.org/10.1016/j.jbiosc.2013.12.025

Sun, Xinbo, Cao, Z., Porteous, N., & Sun, Y. (2012). An N-halamine-based rechargeable antimicrobial and biofilm controlling polyurethane. *Acta Biomaterialia*, *8*(4), 1498–1506. https://doi.org/10.1016/j.actbio.2011.12.027

Sun, Xiuxiu, Wang, Z., Kadouh, H., & Zhou, K. (2014). The antimicrobial, mechanical, physical and structural properties of chitosan-gallic acid films. *LWT - Food Science and Technology*, *57*(1), 83–89. https://doi.org/10.1016/j.lwt.2013.11.037

Velioglu, Y. S., Mazza, G., Gao, L., & Oomah, B. D. (1998). Antioxidant activity and total phenolics in selected fruits, vegetables, and grain products. *Journal of Agricultural and Food Chemistry*, *46*, 4113–4117. https://doi.org/10.1021/jf9801973

Weng, S., Luo, Y., Li, J., Zhou, B., Jacangelo, J. G., & Schwab, K. J. (2016). Assessment and speciation of chlorine demand in fresh-cut produce wash water. *Food Control*, *60*, 543–551. https://doi.org/10.1016/j.foodcont.2015.08.031

Yeni, F., Yavaş, S., Alpas, H., & Soyer, Y. (2016). Most common foodborne pathogens and mycotoxins on fresh produce: A review of recent outbreaks. *Critical Reviews in Food Science and Nutrition*, *56*(9), 1532–1544. https://doi.org/10.1080/10408398.2013.777021

Yi, J., Huang, K., Young, G. M., & Nitin, N. (2020). Quantitative analysis and influences of contact dynamics on bacterial cross-contamination from contaminated fresh produce. *Journal of Food Engineering*, *270*, 109771. https://doi.org/10.1016/j.jfoodeng.2019.109771

Zhu, Q., Gooneratne, R., & Hussain, M. (2017). *Listeria monocytogenes* in fresh produce: outbreaks, prevalence and contamination levels. *Foods*, *6*(21), 1–11. https://doi.org/10.3390/foods6030021

Zilelidou, E. A., Tsourou, V., Poimenidou, S., Loukou, A., & Skandamis, P. N. (2015). Modeling transfer of *Escherichia coli* O157:H7 and *Listeria monocytogenes* during preparation of fresh-cut salads: Impact of cutting and shredding practices. *Food Microbiology*, *45*, 254–265. https://doi.org/10.1016/j.fm.2014.06.019

CHAPTER 4:

Antimicrobial Food-Grade Coatings on Hydrophobic Plastics for Reducing Cross-Contamination of Fresh Produce

Abstract

Antimicrobial coatings using food-grade compositions were developed to reduce the risk of cross-contamination from hydrophobic plastic surfaces. The objectives were to develop antimicrobial food-grade coatings on plastics, evaluate their antimicrobial activity in the presence of water and organic matter, and determine their efficacy in reducing cross-contamination. Wax-based coating solutions were prepared by mixing 5 or 10% Bio-Mos (yeast-derived *N*-halamine precursor that binds chlorine), ethanol, glycerol, Tween 80, and beeswax at 70 °C. Polypropylene coupons were dip-coated three times for 10 s, and surface-bound chlorine compositions (*N*-halamine) were generated by reacting the Bio-Mos/beeswax coatings with commercial bleach for 1 h. The level of surface-bound chlorine and the coating's antimicrobial efficacy was enhanced by encapsulating ε-poly-L-lysine (EPL) into Bio-Mos. Uncoated and uncharged coupons were used as controls. The antimicrobial activity was evaluated against *Escherichia coli* O157:H7 (10^6 CFU/mL, 20 μL) for 2–10 min. The stability was tested after water immersion (1–8 h) or in the presence of organic matter (500–20000 mg/L chemical oxygen demand). Cross-contamination was simulated using baby spinach. Submillimeter-scale uniform coatings were achieved on plastic coupons, resulting in the surface-bound chlorine concentration of 262.50–700.00 nmol/cm^2, depending on the Bio-Mos composition. The chlorine-charged 5% Bio-Mos/beeswax coatings resulted in > 4 log reduction of inoculated bacteria within 2 min. The coatings with 10% Bio-Mos/beeswax modified with EPL maintained their antimicrobial activity after water immersion for 8 h or in the presence of high organic load (20000 mg/L). These coatings significantly reduced cross-contamination

(> 2 log reduction) of baby spinach from the plastic surfaces. The antimicrobial food-grade coatings developed in this study would enable stable and rapid deposition on existing food contact surfaces, reducing cross-contamination of fresh produce.

Keywords: Antimicrobial; Food-grade coatings; *N*-halamine; Cross-contamination; Fresh produce; *Escherichia coli* O157:H7

4.1. Introduction

Cross-contamination of fresh produce is a significant food safety concern during postharvest processing. Fresh produce has been associated with nearly half (46%) of foodborne illnesses between 1998–2008 in the United States, and most of these cases were attributed to leafy greens (Marshall et al., 2020; Painter et al., 2013). To preserves its nutritional benefits, fresh produce is consumed raw or minimally processed with limited inactivation of microbes on the surface of fresh produce (Goodburn & Wallace, 2013; Gustat, O'Malley, Luckett, & Johnson, 2015; Rickman, Barrett, & Bruhn, 2007; Rickman, Bruhn, & Barrett, 2007). In several instances, food contact surfaces were identified as a major route for cross-contamination of fresh produce (Gil et al., 2015; Rajwar, Srivastava, & Sahgal, 2016; Ripolles-Avila, Hascoët, Ríos-Castillo, & Rodríguez-Jerez, 2019; Yeni, Yavaş, Alpas, & Soyer, 2016). Foodborne pathogens introduced in fresh produce during preharvest, harvest, or postharvest processing can persist on food contact surfaces, including shredder, conveyor belt, flume washer, centrifugal dryer, packing table, and reusable plastic containers (Buchholz, Davidson, Marks, Todd, & Ryser, 2012a, 2012b; Zhu, Wu, Trmcic, Wang, & Warriner, 2020). These pathogens could then be disseminated to multiple batches of fresh produce during harvest and postharvest processing. Thus, there is an unmet need to develop an effective intervention strategy that could be applied to existing food contact surfaces and maintain antimicrobial activity in a sustained manner.

Previous studies have developed antimicrobial coatings on diverse food contact surfaces to reduce cross-contamination during food processing (Bastarrachea, Denis-Rohr, & Goddard, 2015; Qiao et al., 2018; Torres Dominguez, Nguyen, Hunt, & Mustapha, 2019). Materials used for food processing equipment are typically selected based on their chemical inertness in processing environments, and thus, the deposition of antimicrobials on these surfaces may require surface

modification to generate stable coatings (Bastarrachea et al., 2015). This surface modification includes bulk modification (e.g., alloys, extrusion) or functionalization (e.g., plasma, corona, UV treatment) (Bastarrachea et al., 2015; Kugel, Stafslien, & Chisholm, 2011; Vartiainen, Rättö, & Paulussen, 2005; Woskowicz et al., 2020), which could not be easily done on existing food contact surfaces in a processing facility. As an alternative to surface modification, coating matrices could be used to immobilize antimicrobial compounds on these surfaces. Some examples include: a coating composition on a stainless-steel surface that combines *N*-halamine antimicrobials and dopamine polymers for adhesive functionalities (Qiao et al., 2018); polylactic acid-chitosan films combined with antimicrobial agents such as lauric arginate ester and nisin (Guo, Jin, Wang, Scullen, & Sommers, 2014); and coatings with silver nanoparticles in different types of polymeric matrices (Carbone, Donia, Sabbatella, & Antiochia, 2016). However, there has been limited progress in the commercial adaptation of these coating approaches due to several factors, including (i) the regulatory approval for coating materials, (ii) cost and time required for the coating process, and (iii) antimicrobial efficacy under rapid food processing conditions (Bastarrachea et al., 2015). Therefore, antimicrobial coatings using food-grade materials that can be rapidly applied to existing food contact surfaces and stable under processing conditions would promote the commercial adoption of these technologies.

In this study, antimicrobial food-grade coatings on plastic surfaces were developed using yeast-derived particles as an antimicrobial *N*-halamine precursor and beeswax as a coating polymer. Among diverse antimicrobial compounds that can be embedded into coating polymers, *N*-halamine coatings have been studied extensively because of their stability and rechargeability (Bastarrachea et al., 2015; Hui & Debiemme-Chouvy, 2013; Qiao et al., 2018). It was reported that yeast cell wall particles derived from *Saccharomyces cerevisiae* are food-grade precursors for

N-halamine functional groups (N-Cl linkage) (Huang, Dou, & Nitin, 2019). Bio-Mos is a commercially available form of these yeast cell wall particles derived from *S. cerevisiae*, and therefore, it was chosen as a food-grade antimicrobial precursor that could be charged with chlorine. Moreover, a hydrophobic polypropylene (PP) plastic surface was selected as a model food contact surface since it is widely used plastic, especially for the fabrication of conveyor belt, reusable plastic containers that are used most frequently during the postharvest processing. Furthermore, beeswax was selected as a food-grade coating polymer for these hydrophobic plastics, as it is known for excellent moisture resistance and therefore used for diverse edible films (Liu et al., 2016; Zhang, Xiao, & Qian, 2014). Utilizing these food-grade ingredients, the Bio-Mos/beeswax solutions with different compositions were deposited on PP surfaces by dip coating.

The objectives of this study were to (i) to develop antimicrobial food-grade coatings on hydrophobic plastics, (ii) evaluate the antimicrobial activity of these coatings and the stability under simulated processing conditions, and (iii) determine their efficacy in reducing cross-contamination of fresh produce. Baby spinach leaves were used as a model fresh produce, and *Escherichia coli* O157:H7 was selected as a model bacterium for a foodborne pathogen since it is a major source of foodborne illnesses associated with leafy greens (Marshall et al., 2020; Yeni et al., 2016). The antimicrobial activity of the Bio-Mos/beeswax coatings on PP surfaces was evaluated after water immersion or in the presence of organic matter to simulate processing conditions. To enhance chlorine loading capacity and improve stability of the *N*-halamine compositions under these conditions, Bio-Mos was encapsulated with food-grade polymer ε-poly-L-lysine (EPL). Overall, the results of this study illustrate the potential of an effective and rapid antimicrobial coating approach that is stable under processing conditions and significantly reduces cross-contamination of fresh produce.

4.2. Material and Methods

4.2.1. Chemicals and reagents

Acetic acid, ethanol, glycerol, hydrochloric acid (HCl), Luria-Bertani (LB) broth, phosphate-buffered saline (PBS), potassium phosphate dibasic (K_2HPO_4), potassium phosphate monobasic (KH_2PO_4), tryptic soy broth (TSB), and tryptic soy agar (TSA) were purchased from Fisher Scientific (Waltham, MA, USA). Beeswax, bicinchoninic acid (BCA) protein assay kit, maximum recovery diluent (MRD), 10% sodium hypochlorite, Triton-X 100, and Tween 80 were purchased from Millipore Sigma (St. Louis, MO, USA). Bio-Mos was purchased from Alltech (Nicholasville, KY, USA). EPL was purchased from Biosynth Carbosynth (Berkshire, UK). Rifampicin was purchased from TCI America (Portland, OR, USA). Ultrapure water (18 MΩ cm) was obtained using the in-lab Milli-Q RG water ultra purification system from EMD Millipore (Billerica, MA, USA).

4.2.2. Bacterial strain, media, and growth conditions

A rifampicin-resistant and Shiga toxin-negative *E. coli* O157:H7 (ATCC 700728) provided by Dr. Linda Harris (University of California-Davis, USA) was used in this study. The bacteria were stored in a TSB supplemented with 15% v/v glycerol at –80 °C before use and then streaked onto a TSA plate supplemented with 50 μg/mL rifampicin and grown at 37 °C for 24 h. One colony was isolated from this TSA plate, cultured in 10 mL of TSB at 250 rpm/37 °C for 18 h to reach the stationary phase. The bacterial suspension was then washed three times with 10 mL of sterile PBS using centrifugal separation at 3100 × g/23 °C for 8 min. The concentration of the bacterial

suspension was assessed by plate counting (approximately 9 log CFU/mL), and this was serially diluted with sterile PBS to obtain the concentration of 6 log CFU/mL for further use.

4.2.3. Antimicrobial food-grade coatings on hydrophobic plastics

4.2.3.1. Preparation of the Bio-Mos/beeswax coating solution

Bio-Mos/beeswax coating solutions were prepared using 3 different Bio-Mos compositions, including 5 % w/v Bio-Mos (5% BM), 10% w/v Bio-Mos (10% BM), and 10% w/v Bio-Mos encapsulated with EPL (10% BM-EPL). The powdered Bio-Mos particles were washed twice with absolute ethanol using centrifugal separation at 5700 × g for 5 min before use. In the case of the 10% BM-EPL coating composition, the washed Bio-Mos particles were encapsulated with EPL (BM-EPL) via vacuum infusion. For 3 g of the washed Bio-Mos particles, a 15 mL of 1% w/v EPL encapsulation solution consisting of absolute ethanol and 9.75 mL of phosphate buffer (100 mM, pH 6.5) was used. The vacuum infusion was performed at 99% vacuum for 5 min, and the resulting BM-EPL particles were washed twice by absolute ethanol using centrifugal separation at 5700 × g for 5 min. The washed Bio-Mos or BM-EPL particles were dissolved in 100 mL of absolute ethanol with 0.2 g of glycerol and 0.2 g of Tween 80 by stirring at 300 rpm/23 °C for 30 min. This mixture was further homogenized using a homogenizer (T18 digital ULTRA TURRAX, IKA, Germany) at 10000 rpm for 5 min. A 10 g of beeswax was then added to this mixture and dissolved at 70 °C for 15 min to obtain the final coating solution.

4.2.3.2. Deposition of the Bio-Mos/beeswax coatings on PP coupons

A sheet of PP (8742K431, McMaster-Carr, Santa Fe Springs, CA, USA) was used as a model hydrophobic food contact surface. This PP sheet was cut into coupons of 1 × 1 cm^2 and

cleaned with 70% ethanol and sterile deionized (DI) water. The cleaned plastic coupons were dip-coated by full immersion into the Bio-Mos/beeswax coating solution for 10 s, followed by 1-min drying at 4 °C until the coating solution was cured. This process was repeated three times to ensure homogeneous deposition of the coatings on plastic coupons. The coated plastic coupons were transferred to a clean petri dish and kept at 23 °C for overnight to fully evaporate the remaining ethanol. Then the coated plastic coupons were rinsed with sterile DI water twice by vortexing at full speed to remove excess coating solutions that were not firmly attached to the plastic coupons. The thickness of uncoated and coated plastic coupons was measured using calipers.

4.2.3.3. Chlorination of the Bio-Mos/beeswax coatings on plastic coupons

The Bio-Mos/beeswax coatings on plastic coupons were immersed in 1% free chlorine solution at pH 5 to generate surface-bound chlorine in the form of *N*-halamine compositions. The chlorination solution was prepared by diluting a commercial household bleach (8.25% sodium hypochlorite). The coated plastic coupons were immersed in 1% free chlorine solution, covered with aluminum foil to protect from light, and incubated with a constant shaking of 250 rpm at 23 °C for a predetermined period (15–60 min). After chlorination, the coated plastic coupons were washed three times with sterile DI water.

4.2.4. Characterization of the Bio-Mos/beeswax coatings on plastic coupons

4.2.4.1. Total protein content

The total protein content of the coated plastic coupons was determined using the BCA protein assay kit and following the modified manufacturer protocol of the kit. Briefly, two pieces of the coated plastic coupons were immersed in 2 mL of agent A and 40 μL of agent B of the BCA

protein assay kit. The mixture was incubated at 60 °C for 30 min, and plastic coupons coated without Bio-Mos were used as a control. Different concentrations of Bio-Mos were used to generate a standard curve, and the Bio-Mos equivalent protein level was determined based on the absorbance at 562 nm.

4.2.4.2. Total active chlorine content

The total active chlorine content of the chlorine-charged Bio-Mos/beeswax coatings on plastic coupons was measured by titration using sodium thiosulfate and iodine standard solutions, following a method in our previous study (Yi et al., 2021). A piece of sample plastic coupon was incubated with 15 mL of 0.001 N sodium thiosulfate, 30 mL of DI water, and 1 mL acetic acid at a constant shaking of 200 rpm/23 °C for 24 h. After incubation, the residual sodium thiosulfate was titrated with 0.001 N iodine standard solution. The active chlorine content of the Bio-Mos/beeswax coating on a plastic coupon (nmol/cm^2) was calculated as follows:

$$\text{Total active chlorine content} = \frac{(V_0 - V_s) \times 10^9 N}{2A_s} \quad (4.1)$$

where V_0 and V_s are the volumes of the iodine solution consumed in titration without and with a sample plastic coupon (L), respectively, N is the concentration of sodium thiosulfate solution (mol/L), and A_s is the surface area (cm^2) of the sample plastic coupon.

4.2.5. Antimicrobial activity of the Bio-Mos/beeswax coatings on plastic coupons

The antimicrobial activity of the chlorine-charged Bio-Mos/beeswax coatings on plastic coupons was evaluated by inoculating bacterial suspension on them. A 20 μL of a bacterial suspension at the concentration of 6 log CFU/mL was spotted on the plastic coupon, and after incubation at 23 °C for different times (2, 5, 10 min), the coupon was immersed into the bacterial

recovery solution supplemented with sodium thiosulfate for bacterial enumeration, which is described in Section 4.2.8. Uncoated plastic coupons were used as a control (negative control), and the uncharged coupons coated with the 5% BM coating solution were tested to examine the influence of the coating itself on antimicrobial activity (positive control).

4.2.6. Stability of the Bio-Mos/beeswax coatings on plastic coupons

The stability of the chlorine-charged Bio-Mos/beeswax coatings on plastic coupons and their respective antimicrobial activity was evaluated after water immersion for extended times. A piece of the plastic coupon was immersed in 2 mL sterile DI water in a sterile 24-well microplate after 1 h chlorination. The plate was covered with aluminum foil to protect from light and incubated at 23 °C for 1, 4, and 8 h. After incubation, the plastic coupons were taken out and gently dried, followed by total chlorine content assay and antimicrobial test for 10 min as described in Sections 4.2.4.2 and 4.2.5, respectively. The uncharged plastic coupons were used to analyze the total protein content after water immersion, as described in Section 4.2.4.1.

Similarly, the presence of organic matter was assessed in terms of the chemical stability of chlorine and the respective antimicrobial activity. LB broth was selected as a source of simulated organic content in wash water since it is a homogenous and well-defined organic matter (Cossu, Ercan, Tikekar, & Nitin, 2016). The as-prepared sterile LB broth was used to simulate the chemical oxygen demand (COD) level of 20000 mg/L, and it was further diluted with sterile DI water to simulate lower COD levels of 500 and 1000 mg/L. For the total chlorine content assay, 20 µL of the LB solution was spotted on the coated plastic coupons after 1 h chlorination. After 10-min treatment at 23 °C, the plastic coupon was rinsed three times with sterile DI water by vortexing at full speed. The rinsed plastic coupons were then analyzed as described in Section 4.2.4.2. The

respective antimicrobial activity was assessed by spotting 20 μL of bacterial suspension diluted by LB broth at 23 °C for 10 min following the protocol described in Section 4.2.5.

4.2.7. Reduction of cross-contamination of baby spinach

The effect of the Bio-Mos/beeswax coatings on plastic coupons for reducing cross-contamination of fresh produce was investigated using baby spinach (*Spinacia oleracea*) leaves. Fresh leaves were purchased from a local market and stored at 4 °C until further use up to seven days. These leaves were inoculated following a method in our previous study (Yi et al., 2021). Briefly, the leaves were cut into 5 × 5 cm^2 slices and washed with sterile DI water before use. A 0.5 mL of a bacterial suspension at the concentration of 6 log CFU/mL was inoculated on the leaves by the droplet-spreading method. The inoculated leaves were incubated at 23 °C for 1 h to allow bacterial attachment. After incubation, the leaves were cut into a smaller piece (1 × 1 cm^2) by selecting a region where the bacterial suspension was homogeneously spread. The leaves were then gently rinsed twice with sterile DI water by a quick dip to remove loosely attached bacteria and maintain excess moisture on the leaf surfaces.

The leaf-plastic-leaf cross-contamination process was simulated using a TA-XT2 Texture Analyser (Stable Micro Systems, Godalming, Surrey, UK), following a method in our previous study (Yi, Huang, Young, & Nitin, 2020). As shown in Figure 4.9a, the initial bacterial transfer was from the contaminated leaf to a clean plastic coupon (1st contact), and this was performed at an applied contact force of 1 N for 10 min. The resulting plastic coupon was then used to transfer bacteria to another clean leaf under the same contact conditions (2nd contact). The plastic coupon and the leaf after the 2nd contact were immersed into the bacterial recovery solution supplemented with sodium thiosulfate for bacterial enumeration, which is described in Section 4.2.8.

4.2.8. Microbiological assay

Bacteria on the coupons or leaf surfaces was recovered by sterile MRD solution, and the number of viable bacteria was measured based on the plate count method, following a method in our previous study (Yi et al., 2021, 2020). After each treatment, the sample plastic coupon or leaf was immersed in 1 mL of sterile MRD solution supplemented with 1% w/v sodium thiosulfate for 2 min to quench the residual chlorine and recover bacteria. Then this mixture was vortexed at full speed for 1 min. A 100 μL of the recovered bacterial suspension was plated on a TSA plate supplemented with 50 μg/mL rifampicin with serial dilution. The TSA plates were incubated at 37 °C for 24 h, and the colony forming units (CFUs) were counted and converted to log CFU/cm^2 using the surface area of the sample. The detection limit was determined by converting 1 CFU of a TSA plate into this unit, which was 1 log CFU/cm^2.

4.2.9. Statistical analysis

The measure data were evaluated using the SPSS Statistics software (version 27, IBM SPSS, Chicago, IL, USA). The significant differences ($p < 0.05$) among data were determined by one-way analysis of variance and Tukey's test. All the experiments were performed in triplicates.

4.3. Results

4.3.1. Characterization of the Bio-Mos/beeswax coatings on plastic coupons

The PP plastic coupons were dip-coated with the Bio-Mos/beeswax solutions, and these coated coupons were characterized by measuring their thickness and total protein content. The results in Figure 4.1 show the physical appearance of the Bio-Mos/beeswax coatings of different

compositions, including the 5% BM, 10% BM, and 10% BM-EPL coatings, which were rapidly (< 2 min) and uniformly deposited on plastic coupons. As shown in Figure 4.2a, the average thickness of the uncoated plastic coupons was 1.44 ± 0.03 mm. After coating, the thickness of the plastic coupons coated with 5% BM, 10% BM, and 10% BM-EPL solutions increased to 1.55 ± 0.03, 1.53 ± 0.02, and 1.61 ± 0.02 mm, respectively. The results in Figures 4.2b and 4.3 show the total protein content of the coated plastic coupons in terms of the Bio-Mos equivalent protein. The Bio-Mos equivalent protein levels of the as-prepared plastic coupons coated with the 5% BM, 10% BM, and 10% BM-EPL solutions were 0.87 ± 0.38, 1.58 ± 0.07, and 20.46 ± 0.89 mg/cm^2, respectively. The results in Figure 4.3 illustrate that increasing the mass of Bio-Mos in the coating solution from 5% to 10% led to a higher content of Bio-Mos equivalent protein on the coated plastic coupons. Furthermore, using the 10% BM-EPL coating solution resulted in a much higher Bio-Mos equivalent protein level deposited on the coated plastic coupons. This increase could be attributed to a higher protein content of EPL encapsulated into Bio-Mos. Overall, the results demonstrate that encapsulation of EPL significantly ($p < 0.05$) increased the total protein content of the Bio-Mos/beeswax coatings on plastic coupons.

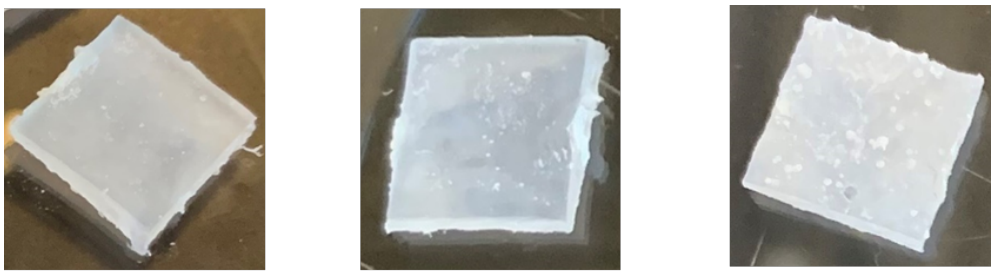

Figure 4.1. Images of the Bio-Mos/beeswax coatings on polypropylene plastic coupons. 5% BM: plastic coupons coated with the 5% Bio-Mos/beeswax solution. 10% BM: plastic coupons coated with the 10% Bio-Mos/beeswax solution. 10% BM-EPL: plastic coupons coated with the 10% Bio-Mos/beeswax solution modified with ε-poly-L-lysine (EPL).

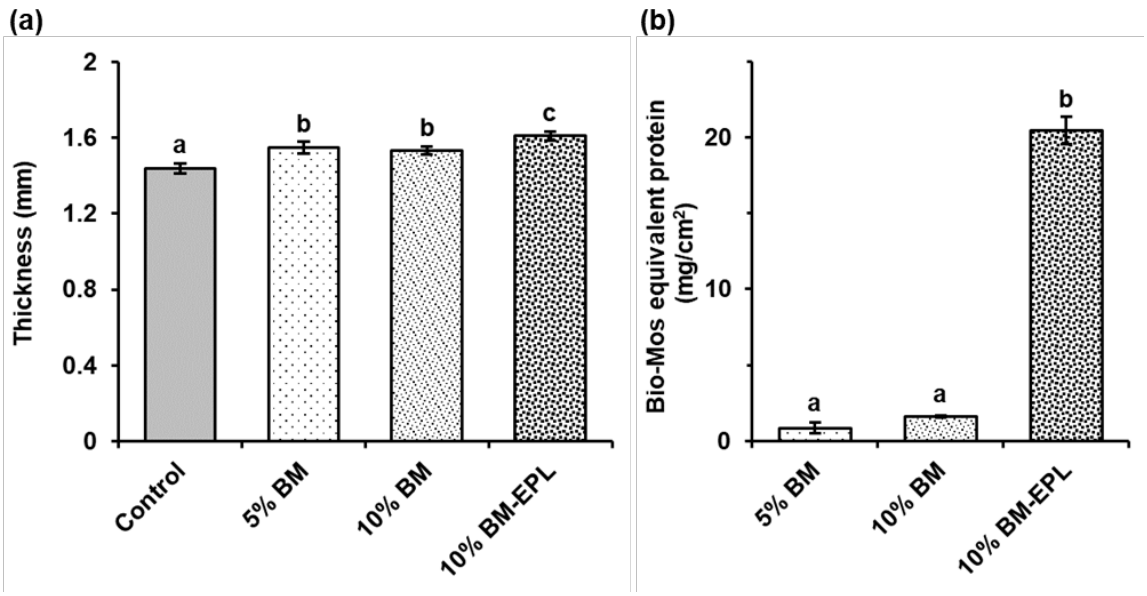

Figure 4.2. Properties of the Bio-Mos/beeswax coatings on plastic coupons. (a) The average thickness of uncoated/coated plastic coupons; (b) The level of Bio-Mos equivalent protein deposited on each plastic coupon. Control: uncoated plastic coupons. The results represent the mean values and their standard deviations (n = 3). Different letters indicate significant differences between values ($p < 0.05$).

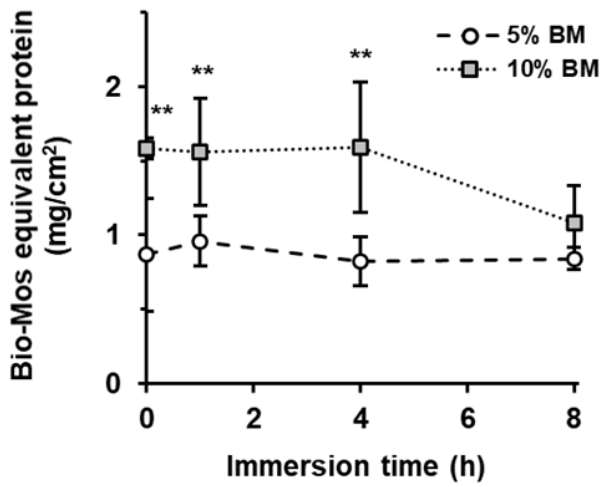

Figure 4.3. Pairwise comparison of the level of Bio-Mos equivalent protein deposited on polypropylene plastic coupons coated with the 5% or 10% Bio-Mos/beeswax solution. The results represent the mean values and their standard deviations (n = 3). The double asterisks indicate significant differences between values ($p < 0.05$).

4.3.2. Total chlorine content and antimicrobial activity of the Bio-Mos/beeswax coatings

The Bio-Mos/beeswax coatings on plastic coupons were charged with 1% free chlorine (pH 5) to form surface-bound chlorine compositions between the primary amines and secondary imines from Bio-Mos and chlorine, which is called as *N*-halamine functional groups. Figure 4.4 shows the change in total active chlorine content of the 5% BM coatings on plastic coupons as a function of chlorination time. These results illustrate that 262.50 ± 25.00 nmol/cm^2 of active chlorine was bound to the coatings on the plastic coupon after 60 min of chlorination at 23 °C. The extended chlorination time did not significantly ($p > 0.05$) increase the total active chlorine of the coated plastic coupons (data not shown).

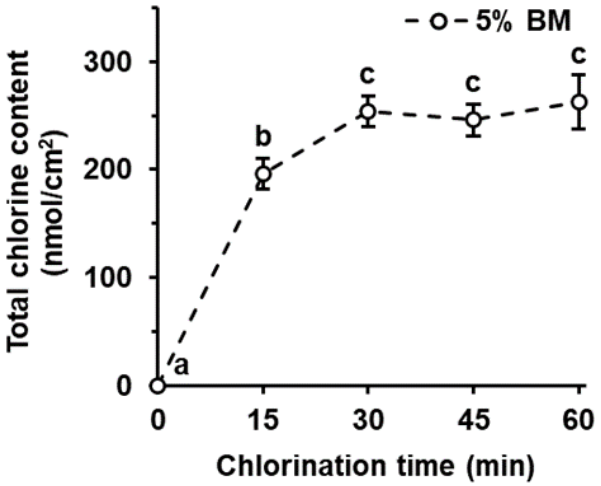

Figure 4.4. Chlorination of the Bio-Mos/beeswax coatings on plastic coupons. The results represent the mean values and their standard deviations ($n = 3$). Different letters indicate significant differences between values ($p < 0.05$).

The results in Figure 4.5 demonstrate the antimicrobial activity of the chlorine-charged 5% BM coatings on plastic coupons against *E. coli* O157:H7. As shown in Figure 4.5a, uncoated plastic coupons (negative control) resulted in 4.7 log CFU/cm^2 of *E. coli* O157:H7 after 10 min of incubation. This level did not significantly ($p > 0.05$) change by depositing the 5% BM coatings on plastic coupons. However, the chlorine-charged 5% BM coatings inactivated all the inoculated bacteria within 10 min. Moreover, the results in Figure 4.5b illustrate that the same level of bacterial inactivation was achieved for shorter treatment times (2, 5 min). Therefore, the 5% BM coatings on the plastic coupons were effective in rapid inactivation of inoculated *E. coli* O157:H7, resulting in > 4 log reduction within 2 min.

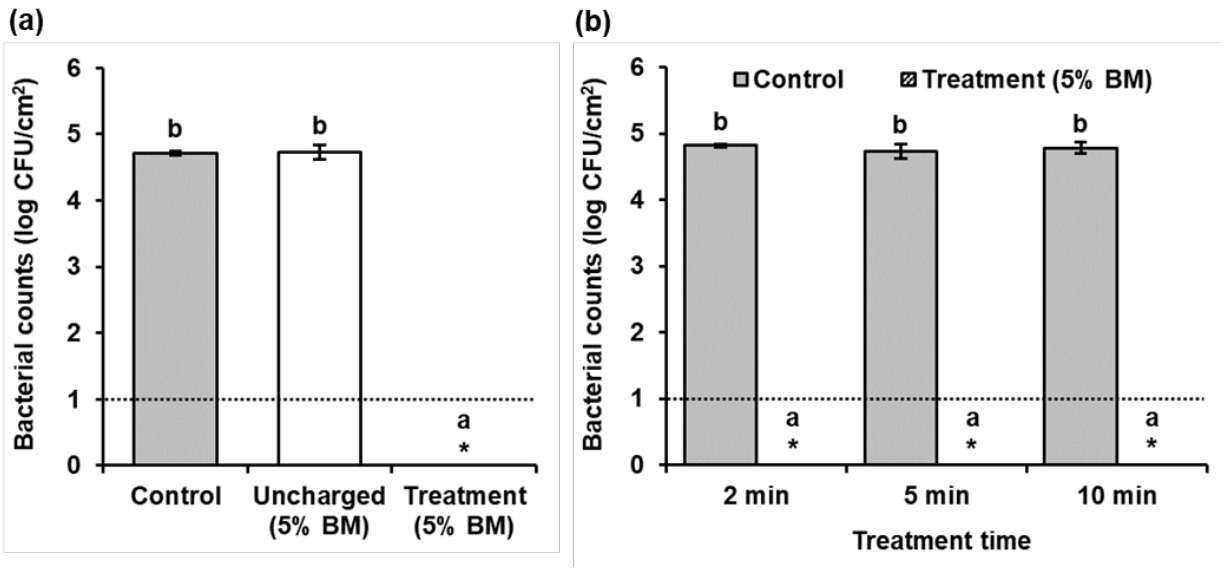

Figure 4.5. Antimicrobial activity of the Bio-Mos/beeswax coatings on plastic coupons. (a) Bacterial counts on each plastic coupon 10 min after inoculation of *Escherichia coli* O157:H7. (b) Bacterial reduction on the coated coupons for shorter treatment times (2, 5, 10 min). Uncharged: plastic coupons coated with the 5% Bio-Mos/beeswax solution. Treatment: plastic coupons coated with the 5% Bio-Mos/beeswax solution and charged with 1% free chlorine at pH 5 for 1 h. The results represent the mean values and their standard deviations (n = 3). Different letters indicate significant differences between values ($p < 0.05$), and the asterisks indicate that the bacterial counts were less than the limit of detection. The detection limit of bacterial counts was 1 log CFU/cm^2.

4.3.3. Stability under aqueous conditions

The chlorine stability and antimicrobial activity of the Bio-Mos/beeswax coatings on plastic coupons in an aqueous environment were tested for three different compositions, including the 5% BM, 10% BM, and 10% BM-EPL coatings. The coated coupons after water immersion for 1, 2, 4, and 8 h were analyzed for the changes in the total protein content, total active chlorine content, and antimicrobial activity for 10 min treatment. The results in Figure 4.6a illustrate that there was no significant ($p > 0.05$) loss of the total protein content for all the coated plastic coupons by water immersion. In contrast, the results in Figure 4.6b show that the total active chlorine content of all the coated plastic coupons decreased as a function of immersion time. The initial concentrations of 262.50 ± 25.00, 354.17 ± 52.04, and 700.00 ± 43.30 nmol/cm^2 for the 5% BM, 10% BM, and 10% BM-EPL coatings significantly ($p < 0.05$) decreased to 154.17 ± 38.19, 212.50 ± 50.00, and 408.33 ± 38.19 nmol/cm^2 after 8-h water immersion. Similarly, the results in Figure 4.6c illustrate that the antimicrobial activity of the 5% BM coatings decreased as a function of water immersion time, resulting in only 1.4 and 1.0 log reduction after 4-and 8-h immersion. An increase in the mass of Bio-Mos in the coating solution from 5% to 10% resulted in improved bacterial inactivation after 4-h immersion (> 4 log reduction), yet < 1 log reduction was achieved after 8-h immersion. On the contrary, the 10% BM-EPL coatings resulted in complete inactivation of inoculated bacteria even after 8-h immersion. Overall, the results demonstrate that the Bio-Mos/beeswax coatings were physically stable, but the surface-bound chlorine was released to water as a function of time, resulting in less effective antimicrobial activity. This was improved by the encapsulation of EPL, which significantly ($p < 0.05$) increased the chlorine loading capacity so that antimicrobial activity was maintained after water immersion for 8 h.

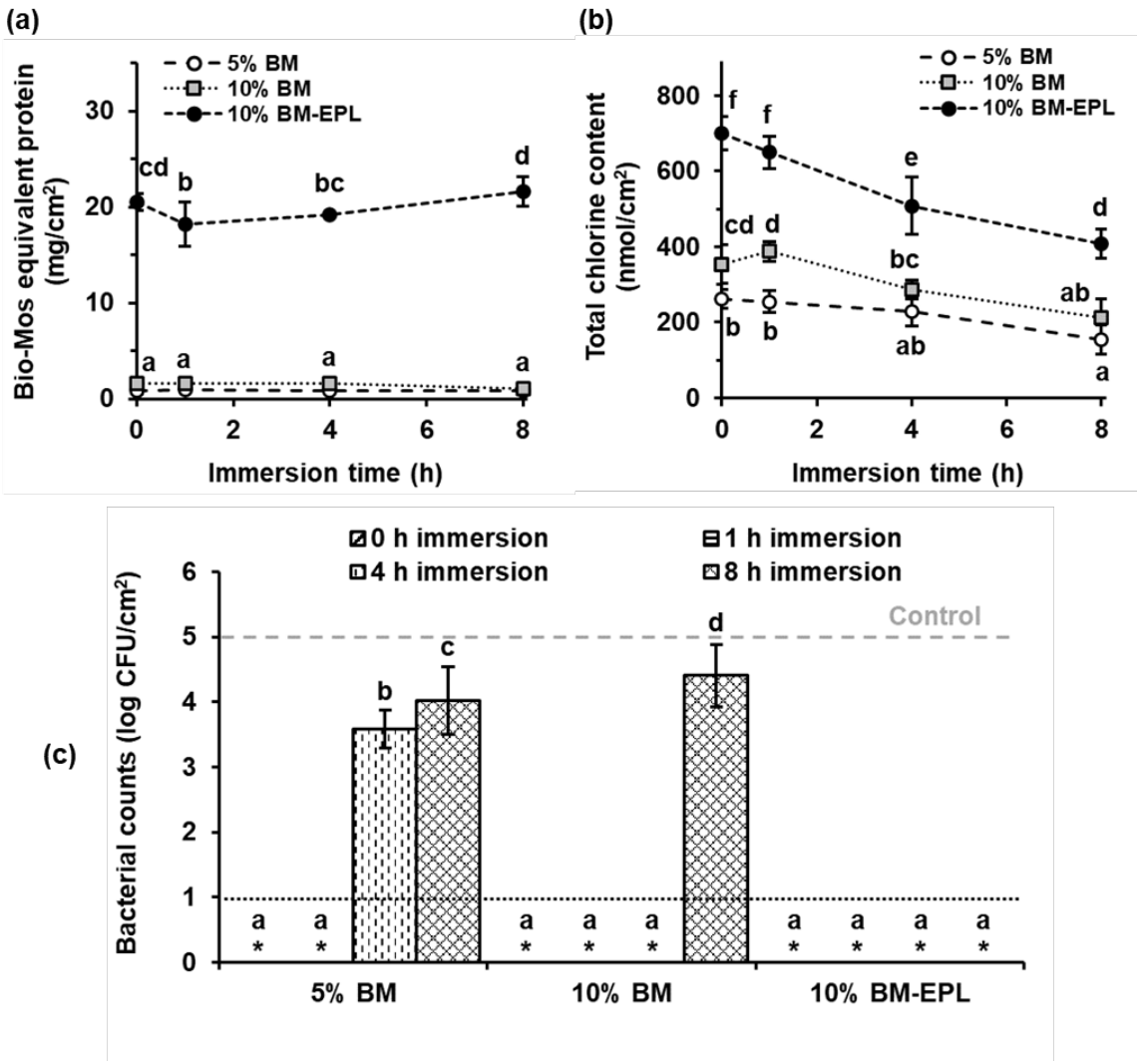

Figure 4.6. Stability of the Bio-Mos/beeswax coatings after water immersion for different times (0, 1, 4, 8 h): (a) the level of the Bio-Mos equivalent protein on each plastic coupon, (b) total chlorine content, and (c) antimicrobial activity against *E. coli* O157:H7 for 10 min treatment. All plastic coupons were charged with 1% free chlorine (pH 5) for 1 h before water immersion. The results represent the mean values and their standard deviations (n = 3). Different letters indicate significant differences between values ($p < 0.05$), and the asterisks indicate that the bacterial counts were less than the limit of detection. The detection limit was 1 log CFU/cm^2, and the number of bacteria on the control plastic coupon was 5 log CFU/cm^2.

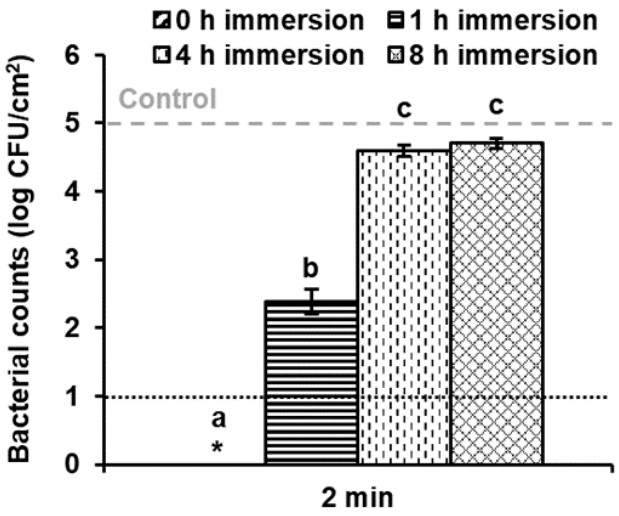

Figure 4.7. Antimicrobial activity of the Bio-Mos/beeswax coatings against *E. coli* O157:H7 for 2 min treatment after water immersion for different times (0, 1, 4, 8 h). All plastic coupons were charged with 1% free chlorine (pH 5) for 1 h before water immersion. The results represent the mean values and their standard deviations (n = 3). Different letters indicate significant differences between values ($p < 0.05$), and the asterisks indicate that the bacterial counts were less than the limit of detection. The detection limit was 1 log CFU/cm^2, and the number of bacteria on the control plastic coupon was 5 log CFU/cm^2.

4.3.4. Stability in the presence of organic matter

The chlorine stability and antimicrobial activity of the Bio-Mos/beeswax coatings were also tested in the presence of organic matter. The coated coupons after 1-h chlorination were exposed to different COD levels (500–20000 mg/L) for 10 min, and the total active chlorine content and antimicrobial activity were assessed. The results in Figure 4.8a illustrate that the presence of 500 mg/L COD reduced the total chlorine contents of the 5% BM and 10% BM coatings from 262.50 ± 25.00 and 354.17 ± 52.04 nmol/cm^2 to 162.50 ± 25.00 and 187.50 ± 25.00 nmol/cm^2, respectively. In contrast, the total chlorine content of the 10% BM-EPL coatings was 658.33 ± 80.36 nmol/cm^2 under the same condition. Moreover, the total chlorine contents of these 10% BM-EPL coatings were maintained high against increased COD levels, i.e., 683.33 ± 38.19 and 558.33 ± 38.19 nmol/cm^2 in the presence of 1000 and 20000 mg/L COD, respectively. The results in Figure 4.8b demonstrate the respective antimicrobial activity in the presence of organic matter. There were no bacteria detected on the 10% BM-EPL coatings in the presence of 500–20000 mg/L COD. Overall, the antimicrobial activity of the 10% BM-EPL coatings was maintained in an organic-rich environment.

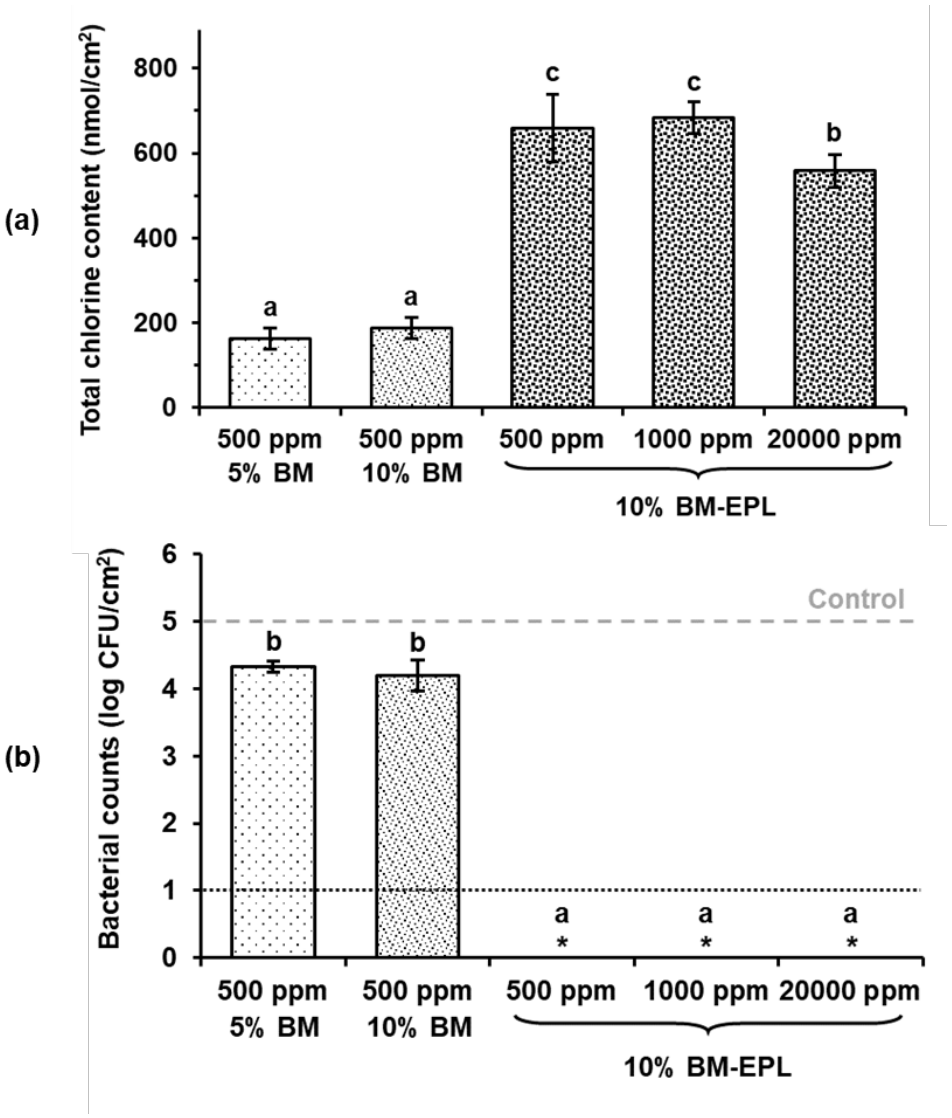

Figure 4.8. (a) Chlorine stability of the Bio-Mos/beeswax coatings on the presence of organic matter at different chemical oxygen demand (COD) levels and (b) their respective antimicrobial activity against *E. coli* O157:H7 for 10 min treatment. 500, 1000, and 20000 ppm indicate the COD levels in the unit of mg/L. The results represent the mean values and their standard deviations ($n = 3$). Different letters indicate significant differences between values ($p < 0.05$), and the asterisks indicate that the bacterial counts were less than the limit of detection. The detection limit of the bacterial counts was 1 log CFU/cm^2, and the number of bacteria on the control plastic coupon was 5 log CFU/cm^2.

4.3.5. Reduction of cross-contamination of baby spinach

As shown in Figure 4.9a, the cross-contamination process between baby spinach and plastic food contact surfaces was simulated using plastic coupons that were uncoated or coated with the 10% BM-EPL coating solution. The results in Figure 4.9b demonstrate that from the initial inoculum of 4.7 ± 0.4 log CFU/cm^2 on the contaminated leaf surface, 2.7 ± 0.2 and 3.0 ± 0.2 log CFU/cm^2 were transferred to the non-contaminated recipient plastic coupon and leaf upon leaf-plastic-leaf contact, respectively. In contrast, the 10% BM-EPL coatings resulted in a complete bacterial inactivation (> 2 log reduction) on both the recipient plastic coupon and leaf within 10 min. Thus, the results demonstrate that the 10% BM-EPL coatings could be used to significantly ($p < 0.05$) reduce the risk of cross-contamination of fresh produce.

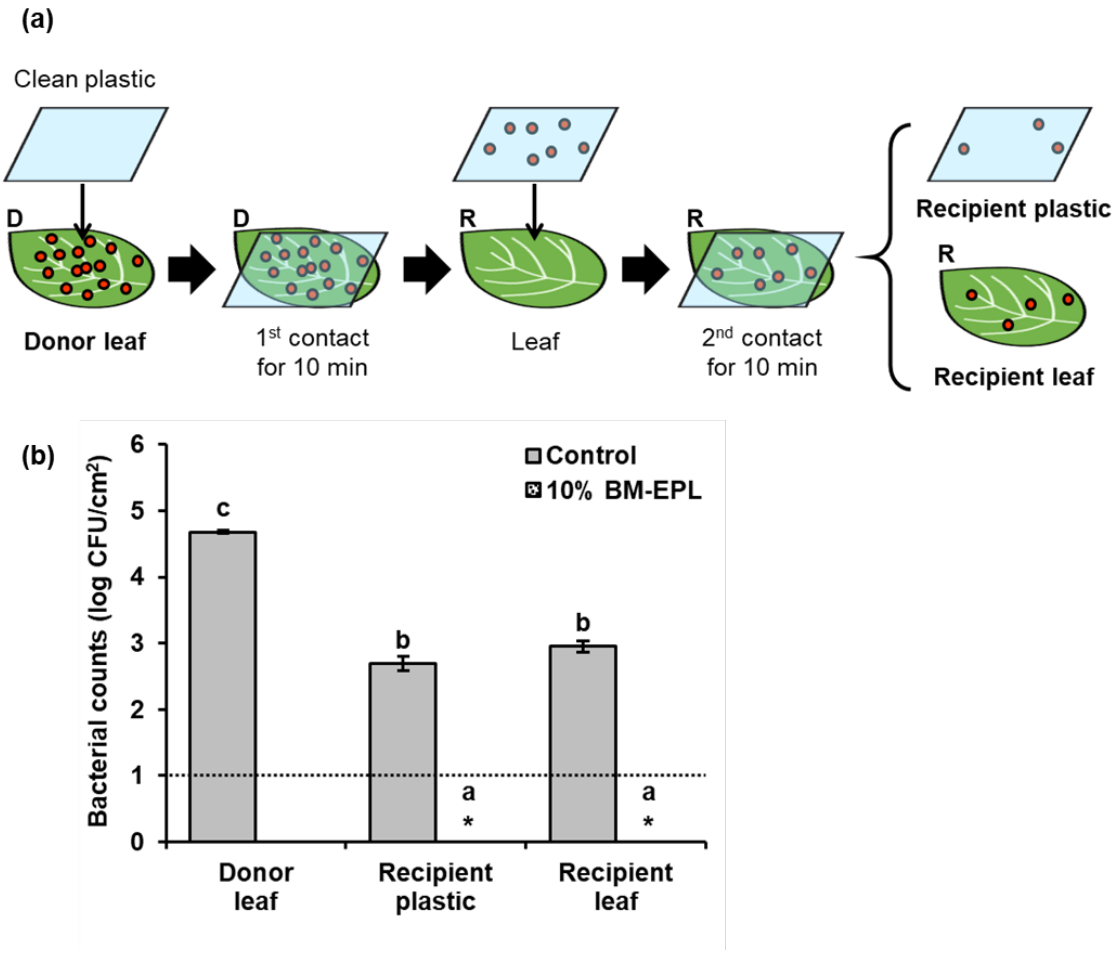

Figure 4.9. Effect of the Bio-Mos/beeswax coatings on reducing cross-contamination of fresh produce. (a) A schematic diagram of the simulated cross-contamination process. A leaf contaminated with *E. coli* O157:H7 and a clean plastic coupon contacted for 10 min at an applied contact force of 1 N, and this resulting plastic coupon was used to contaminate a clean leaf. All samples were cut into the size of 1 × 1 cm^2. (b) Bacterial counts on the selected samples (donor leaf, recipient plastic/leaf). The results represent the mean values and their standard deviations ($n = 3$). Different letters indicate significant differences between values ($p < 0.05$), and the asterisks indicate that the bacterial counts were less than the limit of detection. The detection limit of the bacterial counts was 1 log CFU/cm^2.

4.4. Discussion

4.4.1. Rapid and simple process of uniform antimicrobial coatings on hydrophobic plastics

In this study, hydrophobic PP plastic coupons were dip-coated with the Bio-Mos/beeswax coating solution to generate uniform distribution and rapid deposition of antimicrobial compounds. Figures 4.1–4.2a illustrate that this process resulted in submillimeter-scale uniform Bio-Mos/beeswax coatings on plastic coupons, which were obtained without extended drying time to cure the coatings or additional surface modification of plastics. Previous studies on antimicrobial coatings typically required several hours to dry and cure the coating solution (Denis-Rohr, Bastarrachea, & Goddard, 2015; López-carballo, Hernández-muñoz, Gavara, & Ocio, 2008). However, the Bio-Mos/beeswax coatings were cured within a few minutes due to a significantly lower temperature of the coating process as compared to the melting point of beeswax (62–64 °C). Moreover, prior approaches for antimicrobial coatings on hydrophobic plastics such as PP were made after the initial functionalization step by plasma (Vartiainen et al., 2005; Woskowicz et al., 2020) or UV treatments (Egodage et al., 2017), which may not be feasible for industry application. The use of beeswax allowed simple dip-coating without these surface modification techniques. Similar approaches with beeswax-based coatings were reported: beeswax-chitosan coatings were deposited on paper as a barrier to water (Zhang et al., 2014); or beeswax was used to immobilize Ag nanoparticles on paper for antimicrobial activity (Liu et al., 2016) while the present study utilized food-grade antimicrobials. Overall, the antimicrobial food-grade coating approach developed in this study is simple, rapid, and robust enough to promote commercial adaptation.

4.4.2. Enhanced antimicrobial activity in simulated processing environments

The results in this study illustrate an enhanced antimicrobial activity of the Bio-Mos/beeswax coatings under various conditions. As shown in Figure 4.5b, the 5% BM coatings resulted in > 4 log reduction by 2-min contact. This was significantly efficient and appropriate for rapid processing environments of fresh produce, given that antimicrobial coatings reported in the literature require several hours to achieve this level of bacterial inactivation (Bastarrachea & Goddard, 2015; Dogra et al., 2015; Qiao et al., 2017; Yemmireddy, Farrell, & Hung, 2015). Moreover, the encapsulation of EPL into Bio-Mos further improved the stability of the Bio-Mos/beeswax coatings after water immersion. The results in Figures 4.6a–4.6b show that the Bio-Mos deposited on the coated surface was stable under aqueous conditions, but the surface-bound chlorine of the coatings was released as a function of time. However, EPL significantly ($p < 0.05$) increased the chlorine loading capacity so that the 10% BM-EPL after 8-h water immersion had a higher level of chlorine than the 5% BM before water immersion. This increase in the chlorine loading capacity is due to the chemical structure of EPL that is rich in primary and secondary amine groups (Shukla et al., 2012), which can form additional N halamine compositions by reaction with chlorine (Dong et al., 2017; Huang, Yi, & Nitin, 2021). Consequently, the 10% BM-EPL coatings maintained their antimicrobial efficacy (> 4 log reduction in 10 min) even after water immersion for 8 h. Our prior study on hydrophilic antimicrobial coatings that consist of yeast cell wall particles and chitosan had similar observations (Huang, Yi, Young, & Nitin, 2021). In this prior study, the antimicrobial coatings resulted in > 4 log reduction in 10 min after water immersion for 4 h, and this activity was reduced when the immersion time was extended to 8 h (approximately 2 log reduction in 10 min). Considering that the fresh produce industry uses a large volume of water during preharvest, harvest, and postharvest processing, the results of the

hydrophobic coating compositions proposed in this study demonstrate promising advantages in aqueous environments. In addition, the Bio-Mos/beeswax coatings modified with EPL showed remarkable improvement in antimicrobial activity in the presence of organic matter. As shown in Figure 4.8, the 10% BM-EPL coatings resulted in > 4 log reduction in 10 min under organic-rich environments with the COD levels of 500–20000 mg/L. It was reported that yeast cell wall particles from *S. cerevisiae* can protect chlorine from nonspecific reactions with organic matter in aqueous environments (Huang et al., 2019). Since Bio-Mos is a commercial extract of yeast cell wall particles, similar observations were obtained in this study. The results in Figures 4.6b and 4.8a illustrate that the presence of organic matter consumed only a limited level of chlorine charged to the Bio-Mos/beeswax coatings. Overall, the Bio-Mos/beeswax coatings have enhanced antimicrobial activity under simulated pre-and postharvest processing conditions.

4.4.3. Reduction of cross-contamination of baby spinach

This study demonstrates the potential of the Bio-Mos/beeswax coatings for reducing cross-contamination of fresh produce. The results in Figure 4.9 illustrate that the 10% BM-EPL coatings led to > 2 log reduction on both leaf and plastic surfaces in 10 min during the simulated cross-contamination process. These levels of bacterial reduction are similar or greater than those reported in our previous study with *N*-halamine incorporated hydrophilic plastic films (Yi et al., 2021). In this previous study, *N*-halamine compositions were chemically incorporated into poly(vinyl alcohol-co-ethylene) films, and these films resulted in > 2 log reduction and approximately 2 log reduction on the plastic and leaf surfaces in 10 min, respectively. Moreover, the time scale of these bacterial reduction levels was significantly faster than the literature of other antimicrobial polymers (Boyacı et al., 2019; Ren, Qiao, Huang, Weese, & Ren, 2018). The results

of a prior work showed that bacterial reduction on melon surfaces by essential oil-based antimicrobial coatings took 1–2 days (Boyacı et al., 2019). Similarly, a prior study on *N*-halamine polymer reported that its antimicrobial activity was reduced by contact with food samples such as meat, and therefore bacterial inactivation took more than 1 day (Ren et al., 2018). Thus, the Bio-Mos/beeswax coatings developed in the present study may provide equivalent or better effects on reducing cross-contamination compared to prior technologies and enable a broader application option in terms of the hydrophobicity of the food contact surfaces.

4.5. Conclusions

This study presents antimicrobial food-grade coatings that allow rapid deposition on existing food contact surfaces, maintain antimicrobial efficacy under simulated processing conditions, and effectively reduce cross-contamination of fresh produce. A yeast-derived food-grade *N*-halamine precursor, Bio-Mos, was mixed with beeswax to provide physically stable coatings on hydrophobic plastic surfaces. Surface-bound chlorine charged to these Bio-Mos/beeswax coatings enabled rapid inactivation of *E. coli* O157:H7, resulting in > 4 log reduction in 2 min. The stability of these coatings under simulated processing conditions was further improved by encapsulating food-grade polymer EPL into Bio-Mos, which significantly increased the chlorine loading capacity. The Bio-Mos/beeswax coatings modified with EPL resulted in > 4 log reduction after water immersion for 8 h or in the presence of 20000 mg/L COD. Based on these advantages, these coatings significantly reduced cross-contamination between fresh produce and plastic surfaces. The findings in this study illustrate the potential for commercial adaption of the Bio-Mos/beeswax coatings on existing food contact surfaces to reduce cross-contamination of fresh produce.

Acknowledgements

This work was supported by the Center for Produce Safety Award [grant number 2021CPS08].

References

Bastarrachea, L. J., Denis-Rohr, A., & Goddard, J. M. (2015). Antimicrobial food equipment coatings: Applications and challenges. *Annual Review of Food Science and Technology*, *6*(1), 97–118. https://doi.org/10.1146/annurev-food-022814-015453

Bastarrachea, L. J., & Goddard, J. M. (2015). Antimicrobial coatings with dual cationic and *N*-halamine character: Characterization and biocidal efficacy. *Journal of Agricultural and Food Chemistry*, *63*(16), 4243–4251. https://doi.org/10.1021/acs.jafc.5b00445

Boyacı, D., Iorio, G., Sozbilen, G. S., Alkan, D., Trabattoni, S., Pucillo, F., … Yemenicioğlu, A. (2019). Development of flexible antimicrobial zein coatings with essential oils for the inhibition of critical pathogens on the surface of whole fruits: Test of coatings on inoculated melons. *Food Packaging and Shelf Life*, *20*, 100316. https://doi.org/10.1016/j.fpsl.2019.100316

Buchholz, A. L., Davidson, G. R., Marks, B. P., Todd, E. C. D., & Ryser, E. T. (2012a). Quantitative transfer of *Escherichia coli* O157:H7 to equipment during small-scale production of fresh-cut leafy greens. *Journal of Food Protection*, *75*(7), 1184–1197. https://doi.org/10.4315/0362-028x.jfp-11-489

Buchholz, A. L., Davidson, G. R., Marks, B. P., Todd, E. C. D., & Ryser, E. T. (2012b). Transfer of *Escherichia coli* O157:H7 from equipment surfaces to fresh-cut leafy greens during processing in a model pilot-plant production line with sanitizer-free water. *Journal of Food Protection*, *75*(11), 1920–1929. https://doi.org/10.4315/0362-028X.JFP-11-489

Carbone, M., Donia, D. T., Sabbatella, G., & Antiochia, R. (2016). Silver nanoparticles in polymeric matrices for fresh food packaging. *Journal of King Saud University - Science*, *28*(4), 273–279. https://doi.org/10.1016/j.jksus.2016.05.004

Cossu, A., Ercan, D., Tikekar, R. V., & Nitin, N. (2016). Antimicrobial effect of photosensitized rose bengal on bacteria and viruses in model wash water. *Food and Bioprocess Technology*, *9*(3), 441–451. https://doi.org/10.1007/s11947-015-1631-8

Denis-Rohr, A., Bastarrachea, L. J., & Goddard, J. M. (2015). Antimicrobial efficacy of *N*-halamine coatings prepared via dip and spray layer-by-layer deposition. *Food and Bioproducts Processing*, *96*, 12–19. https://doi.org/https://doi.org/10.1016/j.fbp.2015.06.002

Dogra, N., Choudhary, R., Kohli, P., Haddock, J. D., Makwana, S., Horev, B., … Rodov, V. (2015). Polydiacetylene nanovesicles as carriers of natural phenylpropanoids for creating antimicrobial food-contact surfaces. *Journal of Agricultural and Food Chemistry*, *63*(9), 2557–2565. https://doi.org/10.1021/jf505442w

Dong, A., Wang, Y. J., Gao, Y., Gao, T., & Gao, G. (2017). Chemical insights into antibacterial *N*-halamines. *Chemical Reviews*, *117*(6), 4806–4862. https://doi.org/10.1021/acs.chemrev.6b00687

Egodage, D. P., Jayalath, H. T. S., Samarasekara, A. M. P. B., Amarasinghe, D. A. S., Madushani, S. P. A., & Senerath, S. M. N. S. (2017). Novel antimicrobial nano coated polypropylene based materials for food packaging systems. *3rd International Moratuwa Engineering Research Conference, MERCon 2017*, 88–92. https://doi.org/10.1109/MERCon.2017.7980462

Gil, M. I., Selma, M. V., Suslow, T., Jacxsens, L., Uyttendaele, M., & Allende, A. (2015). Pre- and postharvest preventive measures and intervention strategies to control microbial food safety hazards of fresh leafy vegetables. *Critical Reviews in Food Science and Nutrition*, *55*(4), 453–468. https://doi.org/10.1080/10408398.2012.657808

Goodburn, C., & Wallace, C. A. (2013). The microbiological efficacy of decontamination methodologies for fresh produce: A review. *Food Control*, *32*(2), 418–427. https://doi.org/10.1016/j.foodcont.2012.12.012

Guo, M., Jin, T. Z., Wang, L., Scullen, O. J., & Sommers, C. H. (2014). Antimicrobial films and coatings for inactivation of *Listeria innocua* on ready-to-eat deli turkey meat. *Food Control*, *40*(1), 64–70. https://doi.org/10.1016/j.foodcont.2013.11.018

Gustat, J., O'Malley, K., Luckett, B. G., & Johnson, C. C. (2015). Fresh produce consumption and the association between frequency of food shopping, car access, and distance to supermarkets. *Preventive Medicine Reports*, *2*, 47–52. https://doi.org/10.1016/j.pmedr.2014.12.009

Huang, K., Dou, F., & Nitin, N. (2019). Biobased sanitizer delivery system for improved sanitation of bacterial and fungal biofilms. *ACS Applied Materials & Interfaces*, *11*, 17204–17214. https://doi.org/10.1021/acsami.9b02428

Huang, K., Yi, J., & Nitin, N. (2021). Enhanced decontamination of fresh produce using novel bio-based sanitizer. Unpublished.

Huang, K., Yi, J., Young, G. M., & Nitin, N. (2021). Cell-based carriers incorporated edible antimicrobial coatings on diverse food contact surfaces for preventing cross-contamination of fresh produce. Unpublished.

Hui, F., & Debiemme-Chouvy, C. (2013). Antimicrobial *N*-halamine polymers and coatings: A review of their synthesis, characterization, and applications. *Biomacromolecules*, *14*(3), 585–601. https://doi.org/10.1021/bm301980q

Kugel, A., Stafslien, S., & Chisholm, B. J. (2011). Antimicrobial coatings produced by "tethering" biocides to the coating matrix: A comprehensive review. *Progress in Organic Coatings*, *72*(3), 222–252. https://doi.org/10.1016/j.porgcoat.2011.07.004

Liu, K., Liang, H., Nasrallah, J., Chen, L., Huang, L., & Ni, Y. (2016). Preparation of the CNC/Ag/beeswax composites for enhancing antibacterial and water resistance properties of paper. *Carbohydrate Polymers*, *142*, 183–188. https://doi.org/10.1016/j.carbpol.2016.01.044

López-carballo, G., Hernández-muñoz, P., Gavara, R., & Ocio, M. J. (2008). Photoactivated chlorophyllin-based gelatin films and coatings to prevent microbial contamination of food products. *International Journal of Food Microbiology*, *126*, 65–70. https://doi.org/10.1016/j.ijfoodmicro.2008.05.002

Marshall, K. E., Hexemer, A., Seelman, S. L., Fatica, M. K., Blessington, T., Hajmeer, M., … Gieraltowski, L. (2020). Lessons learned from a decade of investigations of Shiga toxin–producing *Escherichia coli* outbreaks linked to leafy greens, United States and Canada. *Emerging Infectious Diseases*, *26*(10), 2319–2328. https://doi.org/10.3201/eid2610.191418

Painter, J. A., Hoekstra, R. M., Ayers, T., Tauxe, R. V., Braden, C. R., Angulo, F. J., & Griffin, P. M. (2013). Attribution of foodborne illnesses, hospitalizations, and deaths to food commodities by using outbreak data, United States, 1998-2008. *Emerging Infectious Diseases*, *19*(3), 407–415. https://doi.org/10.3201/eid1903.111866

Qiao, M., Liu, Q., Yong, Y., Pardo, Y., Worobo, R., Liu, Z., … Ma, M. (2018). Scalable and rechargeable antimicrobial coating for food safety applications. *Journal of Agricultural and Food Chemistry*, *66*, 11441–11450. https://doi.org/10.1021/acs.jafc.8b03864

Qiao, M., Ren, T., Huang, T., Weese, J., Liu, Y., Ren, X., & Farag, R. (2017). *N*-halamine modified thermoplastic polyurethane with rechargeable antimicrobial function for food contact surface. *RSC Advances*, *7*, 1233–1240. https://doi.org/10.1039/c6ra25502g

Rajwar, A., Srivastava, P., & Sahgal, M. (2016). Microbiology of fresh produce: route of contamination, detection methods, and remedy. *Critical Reviews in Food Science and Nutrition*, *56*(14), 2383–2390. https://doi.org/10.1080/10408398.2013.841119

Ren, T., Qiao, M., Huang, T. S., Weese, J., & Ren, X. (2018). Efficacy of *N*-halamine compound on reduction of microorganisms in absorbent food pads of raw beef. *Food Control*, *84*, 255–262. https://doi.org/10.1016/j.foodcont.2017.08.006

Rickman, J. C., Barrett, D. M., & Bruhn, C. M. (2007). Nutritional comparison of fresh, frozen, and canned fruits and vegetables. Part 1. Vitamins C and B and phenolic compounds. *Journal of the Science of Food and Agriculturecience*, *87*, 930–944. https://doi.org/10.1002/jsfa

Rickman, J. C., Bruhn, C. M., & Barrett, D. M. (2007). Nutritional comparison of fresh, frozen, and canned fruits and vegetables II. Vitamin A and carotenoids, vitamin E, minerals and fiber. *Journal of the Science of Food and Agriculturecience*, *87*, 1185–1196. https://doi.org/10.1002/jsfa

Ripolles-Avila, C., Hascoët, A. S., Ríos-Castillo, A. G., & Rodríguez-Jerez, J. J. (2019). Hygienic properties exhibited by single-use wood and plastic packaging on the microbial stability for fish. *LWT - Food Science and Technology*, *113*, 108309. https://doi.org/10.1016/j.lwt.2019.108309

Shukla, S. C., Singh, A., Pandey, A. K., & Mishra, A. (2012). Review on production and medical applications of ε-polylysine. *Biochemical Engineering Journal*, *65*, 70–81. https://doi.org/10.1016/j.bej.2012.04.001

Torres Dominguez, E., Nguyen, P. H., Hunt, H. K., & Mustapha, A. (2019). Antimicrobial coatings for food contact surfaces: Legal framework, mechanical properties, and potential

applications. *Comprehensive Reviews in Food Science and Food Safety*, *18*(6), 1825–1858. https://doi.org/10.1111/1541-4337.12502

Vartiainen, J., Rättö, M., & Paulussen, S. (2005). Antimicrobial activity of glucose oxidase-immobilized plasma-activated polypropylene films. *Packaging Technology and Science*, *18*(5), 243–251. https://doi.org/10.1002/pts.695

Woskowicz, E., Łożyńska, M., Kowalik-Klimczak, A., Kacprzyńska-Gołacka, J., Osuch-Słomka, E., Piasek, A., & Gradoń, L. (2020). Plasma deposition of antimicrobial coatings based on silver and copper on polypropylene. *Polimery/Polymers*, *65*(1), 33–43. https://doi.org/10.14314/POLIMERY.2020.1.5

Yemmireddy, V. K., Farrell, G. D., & Hung, Y. C. (2015). Development of titanium dioxide (TiO_2) nanocoatings on food contact surfaces and method to evaluate their durability and photocatalytic bactericidal property. *Journal of Food Science*, *80*(8), N1903–N1911. https://doi.org/10.1111/1750-3841.12962

Yeni, F., Yavaş, S., Alpas, H., & Soyer, Y. (2016). Most common foodborne pathogens and mycotoxins on fresh produce: A review of recent outbreaks. *Critical Reviews in Food Science and Nutrition*, *56*(9), 1532–1544. https://doi.org/10.1080/10408398.2013.777021

Yi, J., Huang, K., Ma, Y., Sun, G., Young, G. M., & Nitin, N. (2021). Antimicrobial *N*-halamine incorporated poly(vinyl alcohol-co-ethylene) films for reducing cross-contamination of fresh produce. *Food Control*, *124*, 107880. https://doi.org/10.1016/j.foodcont.2021.107880

Yi, J., Huang, K., Young, G. M., & Nitin, N. (2020). Quantitative analysis and influences of contact dynamics on bacterial cross-contamination from contaminated fresh produce. *Journal of Food Engineering*, *270*, 109771. https://doi.org/10.1016/j.jfoodeng.2019.109771

Zhang, W., Xiao, H., & Qian, L. (2014). Beeswax-chitosan emulsion coated paper with enhanced water vapor barrier efficiency. *Applied Surface Science*, *300*, 80–85. https://doi.org/10.1016/j.apsusc.2014.02.005

Zhu, Y., Wu, F., Trmcic, A., Wang, S., & Warriner, K. (2020). Microbiological status of reusable plastic containers in commercial grower/packer operations and risk of *Salmonella* cross-contamination between containers and cucumbers. *Food Control*, *110*, 107021. https://doi.org/10.1016/j.foodcont.2019.107021

CHAPTER 5:

Modeling Bioaffinity-Based Targeted Delivery of Antimicrobials to *Escherichia coli* Biofilms Using Yeast Microparticles

Part 1. Model Development and Numerical Simulation

Abstract

Biofilms are potential reservoirs for pathogenic microbes leading to a significant challenge for food safety, ecosystems, and human health. Various micro-and nanoparticles have been experimentally evaluated to improve biofilm inactivation by developing targeted delivery systems. However, the role of transport processes and reaction kinetics of these delivery systems are not well understood. In this study, a mechanistic modeling approach was developed to understand the targeted delivery of chlorine to an *Escherichia coli* biofilm using a novel bioaffinity-based yeast microparticle. Biofilm inactivation by this delivery system was numerically simulated as a combination of reaction kinetics and transport phenomena. Simulation results demonstrate that the targeted delivery system achieved 7 log reduction within 16.2 min, while the equivalent level of conventional free chlorine achieved 3.6 log reduction for the same treatment time. These numerical results matched with the experimental observations in our previous study. This study illustrates the potential of a mechanistic modeling approach to improve fundamental understanding of biofilm inactivation by targeted antimicrobial delivery systems and guide the design of these systems using biobased particles.

Keywords: Biofilm; Antimicrobial; Targeted delivery; Yeast microparticle; Binding affinity; Mechanistic modeling

5.1. Introduction

A biofilm is a community of microbes embedded in a self-secreted matrix of extracellular polymeric substances (EPS). Biofilms contribute to a significant number of cases (> 65%) in healthcare-associated infections (Yadav, Song, Singh, & Vidal, 2020) and are also a leading contributor to foodborne outbreaks (Srey, Jahid, & Ha, 2013). These biofilms are resistant to removal or disinfection due to the protective effect of their EPS matrix, a slow growth rate of bacteria in biofilms, and the presence of persister cells (Hall-Stoodley, Costerton, & Stoodley, 2004; Høiby, Bjarnsholt, Givskov, Molin, & Ciofu, 2010; Yadav et al., 2020). The EPS matrix provides protection since it comprises polymers that neutralize or bind antimicrobial agents (Hall-Stoodley et al., 2004; Kim, 2016; Yadav et al., 2020). Moreover, since microbes in biofilms have a slower growth rate than planktonic cells (Yadav et al., 2020), they are more resistant to antimicrobials that inactivate microbes by disrupting cell division and their metabolic cycles (Hall-Stoodley et al., 2004; Yadav et al., 2020). Furthermore, persister cells in biofilms can survive antimicrobial treatment, and then grow and divide in the presence of favorable conditions (Yadav et al., 2020). Therefore, highly localized delivery of stabilized antimicrobials to the biofilm interface and their controlled release within the biofilm may enhance the inactivation of bacteria in the biofilm.

To address these needs, numerous studies have focused on enhancing the targeted delivery of antimicrobials to biofilms in aqueous systems, using micro-and nanoparticles as carriers (Choi, Yu, Esteban Fernández, & Hu, 2010; C. Ferreira et al., 2010; Carla Ferreira, Pereira, Pereira, Simões, & Melo, 2013; Li et al., 2008; Sharma et al., 2019). These particles have gained significant interest in biomedical, food, and environmental applications for targeted delivery, due to their large surface-to-volume ratio, which is optimal for concentrating active agents, and the sustained release

of active agents over time (Barreras-Urbina et al., 2016; Carla Ferreira et al., 2013; Forier et al., 2014). Among them, yeast microparticles derived from cell walls of baker's yeasts (*Saccharomyces cerevisiae*) have been used as efficient carriers to encapsulate active ingredients (da Silva Lima, Maciel, Mendonça, & Costa Junior, 2017; Paramera, Karathanos, & Konteles, 2014) or chemically bind antimicrobials such as chlorine (Huang, Dou, & Nitin, 2019). These yeast microparticles also enhanced the antibiofilm activity of the loaded chlorine (Huang et al., 2019). However, to the best of our knowledge, quantitative and mechanistic understandings of the enhanced biofilm inactivation by microparticle-based antimicrobial delivery systems have not been studied, which is vital for advancing the development of these antimicrobial particles.

Mechanistic modeling of biofilm inactivation requires an understanding of physical, chemical, and biological processes that influence the interaction of antimicrobial delivery systems with biofilms. (Pérez, Picioreanu, & Van Loosdrecht, 2005). A prior study modeled the sorption of ceria nanoparticles on a bacterial biofilm using a pseudo-first-order kinetics equation, but their diffusion was not included in explaining the overall antimicrobial activity (Jing et al., 2014). In contrast, another study modeled the diffusion of nanoparticles inside a biofilm, but the binding of nanoparticles to biofilms or the release of antimicrobials was not considered (Peulen & Wilkinson, 2011). However, for the biobased antimicrobial particles, both the specific binding affinity of the particle and the release of antimicrobials could play key roles in modulating the antibiofilm activity (Huang et al., 2019). Thus, to address the knowledge gaps in the current mathematical models, a mechanistic modeling approach for biobased particles was developed in this study using a combination of diffusion and binding/release/inactivation reactions.

The overall goals of this study were to numerically simulate (i) the delivery of antimicrobial yeast microparticles to *E. coli* biofilms and (ii) subsequent inactivation of bacteria

in the biofilms. The extension of this study, which focused on the key factors influencing the biofilm inactivation by the targeted delivery system and its experimental validation, is presented in a companion paper (Yi, Huang, & Nitin, 2021).

5.2. Materials and Methods

5.2.1. Chemicals and reagents

Acetone, ethanol, hydrochloric acid (HCl), isopropanol, phosphate-buffered saline (PBS), potassium phosphate dibasic (K_2HPO_4), potassium phosphate monobasic (KH_2PO_4), sodium hydroxide (NaOH), sodium thiosulfate, tryptic soy broth (TSB), and tryptic soy agar (TSA) were purchased from Fisher Scientific (Waltham, MA, USA). Branched polyethylenimine, calcofluor white stain, M9 minimal salts medium, and 10% sodium hypochlorite were purchased from Millipore Sigma (St. Louis, MO, USA). D-glucose was purchased from Research Products International (Mout Prospect, IL, USA). Tryptone was purchased from Amresco (VWR, Radnor, PA, USA). *N*,*N*-Diethyl-*p*-phenylenediamine (DPD)-free chlorine reagent powder was obtained from Hach (Loveland, CO, USA). Fleischmann's Active Dry Yeast (*S. cerevisiae*) was purchased from a local grocery store. Ultrapure water (18 MΩ cm) was obtained using the in-lab Milli-Q RG water ultrapurification system from EMD Millipore (Billerica, MA, USA).

5.2.2. Characterization of kinetics parameters

5.2.2.1. Preparation of antimicrobial yeast microparticles

Yeast microparticles were selected as biobased carriers and charged with chlorine using a dilute sodium hypochlorite solution (1% v/v). To ensure the high chlorine loading capacity and binding affinity to the target biofilm, polyethylenimine was encapsulated into yeast microparticles and then charged with chlorine, generating yeast microparticle–polyethylenimine–chlorine (YPC).

In Part 1, only these YPC particles were used, while two different types of antimicrobial yeast microparticles were used in Part 2, i.e., YPC and yeast microparticle–chlorine (YC). Both selected forms of antimicrobial yeast microparticles were prepared by the methods reported in our previous study (Huang et al., 2019): (i) chemical hydrolysis of yeasts to obtain yeast microparticles, (ii) encapsulation of polyethylenimine into yeast microparticles to increase binding affinity, followed by (iii) chlorination of the prepared microparticles. In the case of preparation of YC, step (ii) was bypassed.

Baker's yeasts were first chemically hydrolyzed to attain yeast microparticles (Soto & Ostroff, 2008). Briefly, 20 g of baker's yeast was suspended in 200 mL of 1 M NaOH solution, stirred and heated to 80 °C. After 1 h, the suspension was cooled down at room temperature with stirring for 10–15 min, followed by centrifugal separation at 2500 × *g* for 10 min. The pellet was collected and then resuspended in 200 mL of 1 mM HCl at pH 4.2 and 55 °C. After 1 h of stirring, the pellet was collected by centrifugation at 2500 × *g* for 10 min. Using the same centrifugal conditions, the pellet was washed twice with water, four times with isopropanol, and then twice with acetone. The resulting slurry was dried under vacuum at room temperature for 24 h to acquire yeast microparticle powder. The yeast microparticle powder was rehydrated and washed three times with Milli-Q water by centrifugation at 2500 × *g* for 5 min before each experiment.

Prior to the chlorination of yeast microparticles, polyethylenimine was encapsulated into yeast microparticles to obtain yeast microparticle–polyethylenimine via vacuum infusion. A 0.5 g of washed yeast microparticles were mixed with 3.25 mL of 100 mM phosphate buffer (pH 6.5), 1 mL of absolute ethanol, and 0.75 mL of 200 g/L polyethylenimine in ethanol. The mixture was vortexed and then subjected to a 99% vacuum for 10 min. After encapsulation, the polyethylenimine-encapsulated yeast microparticles were washed twice with Milli-Q water.

The chlorination of the selected microparticles (yeast microparticles and yeast microparticle–polyethylenimine) was performed by immersing them into a chlorination solution, based on the formation of the *N*-halamine functional group (N–Cl linkage) between yeast microparticle or yeast microparticle–polyethylenimine and chlorine. The washed microparticles were resuspended into 5 mL of sterile Milli-Q water and then mixed with 10 mL of 1% sodium hypochlorite (pH = 5) at 200 rpm and room temperature for 1 h. After chlorination, the chlorine-charged microparticles were washed twice with sterile Milli-Q water to obtain the final products.

5.2.2.2. Bacterial strain and biofilm formation

A Shiga toxin-negative, rifampicin-resistant liquid nitrogen stock of *E. coli* O157:H7 (ATCC 700728) (*E. coli*) was streaked onto TSA plates supplemented with 50 μg/mL rifampicin and grown at 37 °C for 24 h before use. One colony was then isolated from the plates and cultured in TSB media with constant shaking (250 rpm) at 37 °C for 18 h to reach the stationary phase. The bacterial cells were washed three times with sterile PBS using centrifugal separation at 3100 × *g*, room temperature for 8 min, and then resuspended in sterile PBS at a concentration of approximately 9 log CFU/mL. The *E. coli* biofilm was grown in a sterile 24-well polystyrene plate (Corning Inc., Corning, NY, USA). A 0.1 mL of bacterial suspension and 0.9 mL of the M9 medium supplemented with 0.4% D-glucose and 0.4% tryptone were added to each well to achieve the final concentration of approximately 7 log CFU/mL. After incubation at room temperature for 4 days, each well was gently washed three times with 1 mL of sterile PBS to remove the planktonic cells.

5.2.2.3. Binding affinity of yeast microparticles to E. coli biofilms

To quantify the binding affinity of the selected yeast microparticles to this *E. coli* biofilm, the proportion of biofilm-bound yeast microparticles was measured using a fluorescence-based binding assay, following the methods in our prior study (Huang et al., 2019). Yeast microparticle–polyethylenimine was labeled with calcofluor white staining, followed by washing three times with Milli-Q water. A 0.01 g of fluorescence-labeled yeast microparticle–polyethylenimine was suspended in 1 mL of sterile Milli-Q water to obtain an equivalent concentration of microparticles in the biofilm inactivation assay. This concentration was determined based on the results of our prior study (Huang et al., 2019). The mixture was then gently added to the biofilm grown in a 24-well plate and incubated at room temperature. After incubation for different times (0, 15, 30, 45, and 60 min), the yeast microparticle–polyethylenimine solution was gently removed, and each well was washed twice with sterile Milli-Q water. A 1 mL of 0.01 g/mL fluorescence-labeled yeast microparticle–polyethylenimine solution was added into an empty well as a control. The fluorescence intensity of yeast microparticle–polyethylenimine bound to the biofilm was measured by a plate reader with an excitation/emission wavelength at 350/440 nm. All experiments were performed in triplicates at room temperature. Based on the absorbance data, the ratio of biofilm-bound yeast microparticles to initial yeast microparticles was determined for each time point and then converted into the surface concentration of bound yeast microparticles [$S_b(t)$] in the unit of kg/m^2. The maximum concentration of biofilm-bound yeast microparticles within 1 h incubation ($S_{b,\infty}$) was determined by using the data at 60 min.

The set of converted data was then fitted to the pseudo-first-order kinetics equation, which is one of the simplest models used to describe the particle adsorption in the literature (Jing et al., 2014; Simonin, 2016):

$$S_{\mathrm{b}}(t) = S_{\mathrm{b},\infty}(1 - e^{-k_{\mathrm{b}}t}) \quad (5.1)$$

where $S_{\mathrm{b}}(t)$ is the concentration of yeast microparticles bound to biofilm (kg/m^2), t is the time (s), $S_{\mathrm{b},\infty}$ is the maximum concentration of biofilm-bound yeast microparticles within 1 h incubation (kg/m^2), and k_{b} is the binding rate of free yeast microparticles to biofilm (s^{-1}).

5.2.2.4. Controlled release of chlorine from yeast microparticles

The measurement of chlorine release from the yeast microparticles was divided into two cases: 1) passive release of chlorine from free yeast microparticles in the aqueous phase or 2) apparent active release of chlorine from biofilm-bound yeast microparticles.

The passive chlorine release rate from free yeast microparticles in the aqueous phase was quantified by the *N*,*N*-Diethyl-*p*-phenylenediamine (DPD) colorimetric method (Helbling & VanBriesen, 2007; Huang et al., 2019). A 0.01 g/mL of YPC suspended in Milli-Q water was incubated at room temperature with constant shaking at 250 rpm for 10 min. The solution was then centrifuged at 2500 × *g* for 5 min, and the supernatant was evaluated for the released free chlorine. The pellet was resuspended in 1 mL of Milli-Q water, and the same procedure was repeated as needed to determine chlorine release as a function of time. All experiments were performed in triplicates at room temperature. Based on the absorbance data, the standard curve with different levels of free chlorine was generated, and the chlorine concentration of the aqueous sample (kg/m^3) at different time points was estimated from the standard curve. All the concentrations used in this measurement were the same as in the numerical simulation, and the total chlorine concentration initially charged to yeast microparticles (C_∞) was pre-determined by the results in the prior study (Huang et al., 2019).

The measured data were fitted to typical drug release kinetics equations, such as the first-order, Higuchi, and Hixson-Crowell models (Costa & Sousa Lobo, 2001; Dash, Murthy, Nath, & Chowdhury, 2010; Loo et al., 2016). Among these models, the simplest model (the first-order kinetics) with high R^2 values (data not shown) was selected:

$$[C_\infty - C(t)] = C_\infty e^{-k_{r1}t} \quad (5.2)$$

where $C(t)$ is the chlorine concentration in the aqueous phase or biofilm (kg/m^3), C_∞ is the total chlorine level initially charged to yeast microparticles (kg/m^3), and k_{r1} is the passive chlorine release rate from free yeast microparticles in the aqueous phase (s^{-1}). The left-hand side corresponds to the total chlorine remaining in the yeast microparticles.

The apparent active chlorine release rate from the biofilm-bound yeast microparticles was assessed by measuring the antimicrobial activity of chlorine-charged yeast microparticles. The chlorine level was not directly measured due to its reactivity, where chlorine release cannot be isolated from its concurrent reactions, including irreversible binding of yeast microparticle to the biofilm, chlorine depletion due to organic matter and bacterial inactivation in the biofilm. Therefore, the bacterial inactivation was measured, and it was assumed that all the released chlorine was used for the bacterial inactivation by decoupling other reactions. These other reactions, i.e., binding process and chlorine depletion by organic matter in the biofilm, were eliminated using planktonic cells at the same concentration level as the biofilm in a well-mixed system for the biofilm inactivation. In addition, biofilm inactivation by the chlorine-charged yeast microparticles can be attributed to both direct contact of the microparticles with bacteria and chlorine actively released from the microparticles upon binding the biofilm (Dong, Wang, Gao, Gao, & Gao, 2017). In this study, these two mechanisms were combined together to represent the apparent active release rate, followed by the biofilm inactivation by this released chlorine. This

apparent active release rate was then determined based on the time and the equivalent free chlorine concentration required to inactivate planktonic cells at the same concentration level as the biofilm. Briefly, 0.5 mL of bacterial suspension with approximately 7 log CFU/mL was added to 4.5 mL of the chlorine-charged yeast microparticle solution in a stirred 5-mL beaker. After different time points (0, 5, 10, 15, or 20 s), 0.5 mL of 0.1 M sodium thiosulfate was added to quench the residual chlorine and stop the reaction. A 100 μL of the mixture was inoculated onto TSA plates and enumerated after incubation at 37 °C for 24 h. All experiments were performed in triplicates at room temperature. The time required for 7 log reduction of planktonic cells was selected from the resulting data, and the equivalent free chlorine concentration required for the same bacterial inactivation was measured as 3 mg/L from the preliminary study (data not shown). Assuming that the chlorine-charged yeast microparticles released this equivalent free chlorine concentration of 3 mg/L within the selected time required for bacterial inactivation, the apparent active chlorine release rate was determined.

The set of time-equivalent free chlorine concentration data was fitted to the first-order kinetics equation as follows:

$$C_S(t) = C_{S,0} e^{-k_{r2} t} \tag{5.3a}$$

where $C_S(t)$ is concentration of chlorine charged to a yeast microparticle (kg/kg), $C_{S,0}$ is the initial level of chlorine charged to a yeast microparticle (kg/kg) and $C_{S,0} = C_\infty/S_0$ by definition, S_0 is the initial level of yeast microparticles in the aqueous phase (kg/m^3), and k_{r2} is the apparent active chlorine release rate from biofilm-bound yeast microparticles (s^{-1}). This value of $C_S(t)$ had the following relationship with $C(t)$ and $S(t)$:

$$C(t) = \left[C_{S,0} - C_S(t)\right] S(t) \tag{5.3b}$$

where $S(t)$ is the yeast microparticle concentration in the aqueous phase (kg/m^3). The left-hand side represents the level of chlorine released in the aqueous phase during the measurement, while the right-hand side represents the loss of total level of chlorine from the yeast microparticles.

5.2.3. Model development

COMSOL Multiphysics® software version 5.5 (or simply COMSOL) was used to numerically simulate transport processes of chlorine and yeast microparticles and consequent bacterial inactivation in the biofilms. The free chlorine model was selected as a conventional biofilm inactivation system since it is the most commonly used antimicrobial. The YPC model was selected as a targeted delivery system to improve mass transfer near the aqueous/biofilm interface using yeast microparticles. In the biofilm, live/dead bacteria and EPS were assumed to be contained and fixed. The variables and parameters used in this study are indicated in Tables 5.1 and 5.2, respectively. The simulation results were plotted in terms of chlorine distributions and bacterial counts. For bacterial counts, the raw data obtained in the simulation were expressed in units of the number of bacteria in the biofilm (equivalent to CFU/m^3), and these were converted to the bacterial counts (equivalent to CFU) by multiplying the biofilm volume (m^3). Then, these bacterial counts (CFU) were divided by the volume of microbial recovery solution (1 mL) to convert them to the standard unit in the experimental microbiological analysis (CFU/mL). This process of unit conversion assumed equivalent conditions to experimental measurements, and thus, 1 CFU in bacterial counts of the numerical simulation was equivalent to 1 CFU/mL of the experimental measurement.

Table 5.1. List of variables

Symbol	Description	Units
$C(t)$	Chlorine concentration in the aqueous phase or biofilm	kg/m^3
$C_S(t)$	Concentration of chlorine charged to a yeast microparticle	kg/kg
$B(t)$	Live bacterial concentration in biofilm	kg/m^3
$O(t)$	Organic matter concentration in the aqueous phase (chemical oxygen demand) or biofilm (EPS + dead bacteria)	kg/m^3
$S(t)$	Yeast microparticle concentration in the aqueous phase	kg/m^3
$S_\mathrm{b}(t)$	Concentration of yeast microparticles bound to aqueous/biofilm interface	kg/m^2

All the variables are nonnegative and *t* is the time (s). EPS: Extracellular polymeric substances.

Table 5.2. List of input parameters used in the numerical simulation

Symbol	Description	Value & units	Source
A	Area of aqueous/biofilm interface	1.77×10^{-4} m^2	Calculated [a]
B_0	Initial level of bacteria in biofilm	1.56 kg/m^3	Calculated [b]
C_0	Initial level of free chlorine	0.05 kg/m^3	(Huang et al., 2019)
C_∞	Total chlorine level initially charged to yeast microparticles	0.05 kg/m^3	(Huang et al., 2019)
D_C	Diffusivity of free chlorine at 23°C	1.0489×10^{-9} m^2/s	(Chao, 1968)
D_S	Diffusivity of yeast microparticles	8.584×10^{-14} m^2/s	(Ju, Liu, Yang, & Sun, 2014)
k_0	Natural decay rate of free chlorine	2.83×10^{-5} s^{-1}	(Munther et al., 2015)
k_1	Depletion rate of chlorine by nonspecific reactions with organic matter	8.97×10^{-3} m^3/(kg·s)	(Munther et al., 2015)
k_C	Bacterial inactivation rate of by free chlorine	12.5 m^3/(kg·s)	(Munther et al., 2015)
m_B	Mass of an *E. coli* cell	9.5×10^{-16} kg	(Neidhardt, Ingraham, & Schaechter, 1990)
O_0	Initial level of organic matter in biofilm	279.93 kg/m^3	(Stine et al., 2013) [c]
r	Radius of biofilm	7.5×10^{-3} m	Measured
S_0	Initial level of yeast microparticles	10 kg/m^3	Assumed [d]
V_b	Volume of biofilm	6.08×10^{-9} m^3	Calculated [e]
V_w	Volume of aqueous phase	10^{-6} m^3	Assumed [d]
z_b	Thickness of biofilm	3.44×10^{-5} m	(Hung et al., 2013)
z_w	Thickness of aqueous phase	5.66×10^{-3} m	Calculated [f]
ρ_B	Density of bacteria in biofilm	1025 kg/m^3	(Landa-Marbán et al., 2019)
ρ_O	Density of organic matter in biofilm	1012.5 kg/m^3	(Landa-Marbán et al., 2019)
ϕ	Biofilm porosity	0.722	(Gou et al., 2019)

[a] Area of the circle with a radius of r. [b] $B_0 = 10^7$ CFU $\times \frac{m_B}{V_\mathrm{b}}$. [c] $\frac{O_0}{\rho_O} + \frac{B_0}{\rho_B} + \phi = 1$. [d] The values were assumed to match the experimental validation conditions in Part 2 of this study (Yi et al., 2021). [f] Volume of the cylinder with a radius of r and a height of z_b. [e] Height of the cylinder with a volume of V_w and a radius of r.

5.2.3.1. Geometry

The three-dimensional geometry depicting *E. coli* biofilm formed in a 24-well plate filled with the aqueous solution is shown in Figure 5.1a. As the geometry is rotationally symmetric, a 3D cylindrical geometry (Figure 5.1a) was reduced to a 2D axisymmetric plane (Figure 5.1b) to save on computational time. As shown in Figure 5.1b, the system was divided into two domains: aqueous and biofilm. The selected antimicrobial yeast microparticles were contained in the aqueous phase. The biofilm was assumed to be a porous medium. All boundaries were fixed. The dimensions were as follows: (i) A radius of the system was the same as the radius of a well in the 24-well plastic plate (r = 0.75 cm), (ii) the thickness of the *E. coli* biofilm was assumed to be fixed at z_b = 34.4 μm (Hung et al., 2013), and (iii) the height of the aqueous phase was calculated as $z_w = 5.66 \times 10^{-3}$ m. This was obtained from the volume of the aqueous phase (1 mL) and the radius r (see Table 5.2).

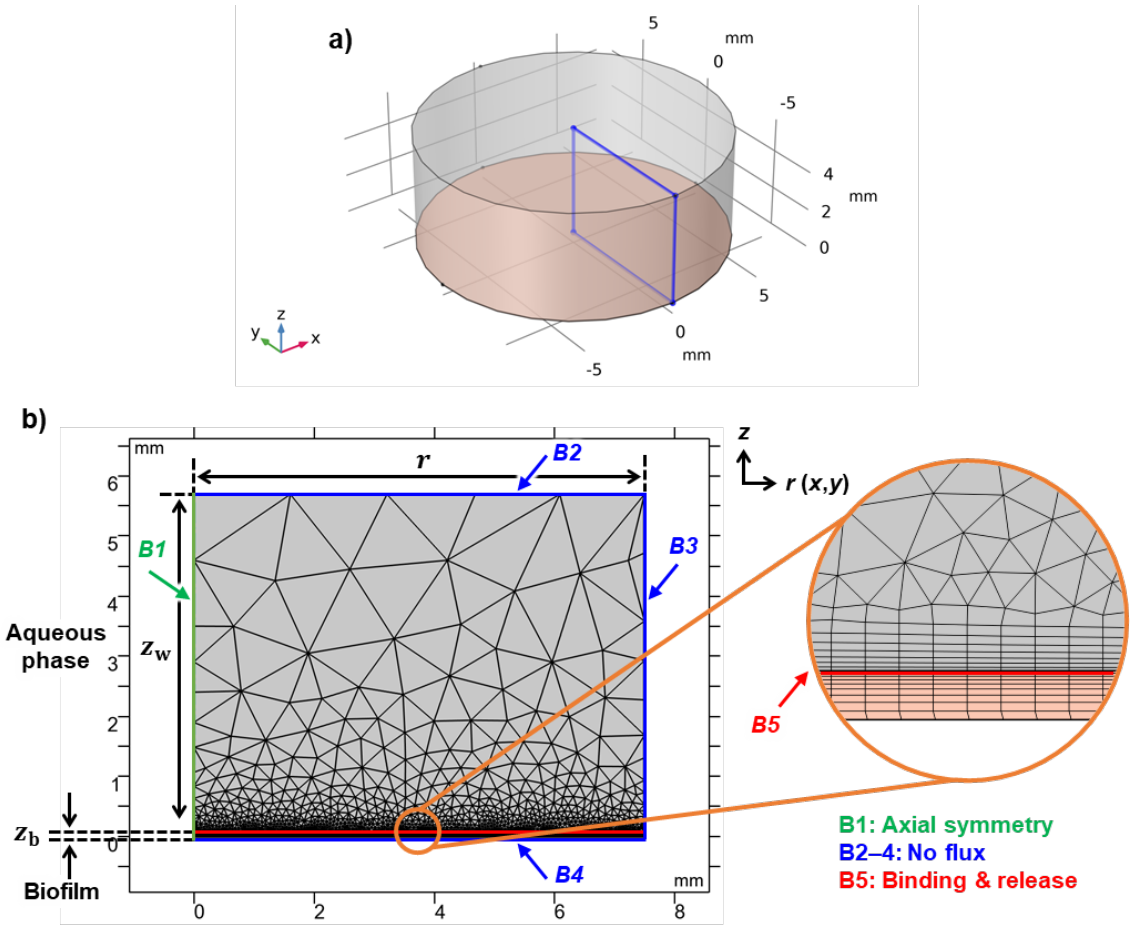

Figure 5.1. Geometry, boundary conditions, mesh for numerical simulation of antimicrobial delivery systems for biofilm inactivation using COMSOL Multiphysics® software. (a) The 3D geometry and radial cross-section for the 2D axis-symmetric model (b) The 2D radial cross-section, boundary conditions, and mesh.

5.2.3.2. Free chlorine model – a conventional system

5.2.3.2.1. Governing equations

The mass balance of free chlorine was divided into three parts: diffusion, natural decay of chlorine, and chlorine depletion by reactions with the biofilm components. The aqueous phase was at rest so that the convection was neglected. Organic matter in the biofilm consisted of EPS and dead bacteria. It was assumed that organic content was not depleting by reaction with chlorine since it has multiple sites that can participate in nonspecific reactions with chlorine (Deborde & von Gunten, 2008; Munther, Luo, Wu, Magpantay, & Srinivasan, 2015).

The rate of change of chlorine in the aqueous domain was as follows:

$$\left.\frac{\partial C(t)}{\partial t}\right|_{\text{Aqueous}} = D_C \nabla^2 C(t) - k_0 C(t) - k_1 O(t) C(t) \tag{5.4}$$

where $O(t)$ is organic matter concentration (kg/m^3), D_C is the diffusivity of free chlorine in water (m^2/s), k_0 is the natural decay rate of chlorine (s^{-1}), and k_1 is the depletion rate of chlorine by nonspecific reactions with organic matter [m^3/(kg·s)] (see Table 5.2). On the right-hand side, the first term is the chlorine diffusion, the second term is the natural chlorine decay reaction, and the last term is the chlorine depletion by nonspecific reactions with organic matter in the aqueous phase.

In the biofilm domain, chlorine diffusion in a porous medium was applied (Peulen & Wilkinson, 2011), and adsorption of free chlorine to the biofilm interface was assumed to be negligible. All reactions in the biofilm were assumed to occur in the pore volume.

$$\left.\frac{\partial C(t)}{\partial t}\right|_{\text{Biofilm}} = \frac{1}{\phi} D_{C,\text{eff}} \nabla^2 C(t) - k_0 C(t) - k_1 [B(t) + O(t)] C(t) \tag{5.5a}$$

$$D_{C,\text{eff}} = \left(\frac{\phi}{\tau}\right) D_C, \qquad \tau = \phi^{-1/3} \tag{5.5b}$$

where $B(t)$ is the live bacterial concentration in biofilm (kg/m^3) and ϕ is the biofilm porosity. On the right-hand side of Eq. 5.5a, the first term corresponds to the diffusion in a porous media defined by the Millington and Quirk model (Millington & Quirk, 1961), where the effective diffusivity and tortuosity are calculated as Eq. 5.5b. This model was selected as it is widely used in the literature (Incollingo et al., 2020) and suggested as a default setting in COMSOL. The second term is the same as Eq. 5.4. The last term is the chlorine depletion by reactions with live bacteria and organic matter in the biofilm.

The bacterial population in the biofilm was described as follows (Munther et al., 2015):

$$\left.\frac{\partial B(t)}{\partial t}\right|_{\text{Biofilm}} = -k_C B(t) C(t) \tag{5.6}$$

where k_C is the bacterial inactivation rate by chlorine [m^3/(kg·s)] (see Table 5.2). Considering that mature biofilms at equilibrium were used and the treatment time (≤ 1 h) was relatively shorter than biofilm development, net bacterial growth and death in the biofilm were assumed negligible.

Since the inactivated bacteria became organic matter as dead bacteria, the mass balance of the organic matter in the biofilm was acquired as follows by the mass conservation law:

$$\left.\frac{\partial O(t)}{\partial t}\right|_{\text{Biofilm}} = k_C B(t) C(t) \tag{5.7}$$

where the variables and parameters are the same as those in Eqs. 5.5–5.6.

5.2.3.2.2. Initial and boundary conditions

The initial and boundary conditions of the free chlorine model are shown in Table 5.3 and Figure 5.1, respectively. The initial free chlorine level of C_0 was homogenously distributed in the aqueous domain, while there was initially no free chlorine in the biofilm domain. In contrast, the initial level of B_0 and O_0 were homogeneously distributed in the biofilm domain for live bacteria

and organic matter (EPS and dead bacteria), respectively. As shown in Figure 5.1, axial symmetry was applied to the boundary B1, and no flux conditions were applied at the boundaries B2–4. At the aqueous/biofilm interface (boundary B5), continuity of mass transfer was applied for free chlorine (Stewart & Raquepas, 1995).

Table 5.3. Initial conditions for the free chlorine and yeast microparticle–polyethylenimine–chlorine (YPC) models

Model	Domain	$C(t)$	$B(t)$	$O(t)$	$S(t)$	$S_{\mathrm{b}}(t)$
Free chlorine	Aqueous	$C(0) = C_0$	n/a	$O(0) = 0$	n/a	n/a
	Biofilm	$C(0) = 0$	$B(0) = B_0$	$O(0) = O_0$	n/a	n/a
YPC	Aqueous	$C(0) = 0$	n/a	$O(0) = 0$	$S(0) = S_0$	$S_{\mathrm{b}}(0) = 0$
	Biofilm	$C(0) = 0$	$B(0) = B_0$	$O(0) = O_0$	n/a	n/a

YPC: yeast microparticle–polyethylenimine–chlorine. n/a: Not applicable. See Table 5.2 for the parameters.

5.2.3.3. YPC model – a targeted delivery system

In the YPC model, assumptions of the free chlorine model were also applied along with the additional assumptions based on our prior experimental observations (Huang et al., 2019): (i) Chlorine was not initially present in the aqueous phase but charged to yeast microparticles with a high concentration in the form of *N*-halamine (N-Cl); (ii) This *N*-halamine composition of yeast microparticles did not react with organic matter in the aqueous phase; (iii) Yeast microparticles in the aqueous phase followed free diffusion and did not diffuse into biofilm due to the treatment time scale (≤ 1 h) and particle size; (iv) Specific binding reaction of yeast microparticles to biofilm was irreversible and followed the experimentally measured rate; (v) Limited amount of chlorine was released from free yeast microparticles in the aqueous phase following the passive release rate, while the active release was triggered by the bacteria and organic matter upon binding the biofilm and followed the apparent active release rate.

5.2.3.3.1. Governing equations

The delivery process of YPC was divided into four sub-steps: (i) Free diffusion of the yeast microparticles in the aqueous domain (Eq. 5.8); (ii) Passive release of chlorine from these microparticles (Eq. 5.9); (iii) Binding of yeast microparticles at the aqueous/biofilm interface (given as boundary conditions; Eqs. 5.10–5.11); and (iv) Apparent active release of chlorine from biofilm-bound yeast microparticles (Eq. 5.12).

Free diffusion of the yeast microparticles in the aqueous phase was defined as:

$$\left.\frac{\partial S(t)}{\partial t}\right|_{\text{Aqueous}} = D_S \nabla^2 S(t) \tag{5.8}$$

Where D_S is the diffusivity of yeast microparticles in water (m^2/s) (see Table 5.2). Based on this diffusion, the biofilm-bound yeast microparticles released chlorine at local points (see Eqs. 5.10–5.12).

The passive chlorine release from the microparticles in the aqueous phase was described by the first-order kinetics as in Eq. 5.2, and thus, the chlorine distribution in the aqueous phase of the YPC model was as follows, in analogy to Eq. 5.4 of the free chlorine model:

$$\left.\frac{\partial C(t)}{\partial t}\right|_{\text{Aqueous}} = D_C \nabla^2 C(t) - k_0 C(t) + k_{\text{r1}}[C_\infty - C(t)] \tag{5.9}$$

where the variable and parameters are the same as those in Eqs. 5.2 and 5.4.

Once chlorine was released from yeast microparticles by the passive release in the aqueous phase (Eq. 5.9) or the apparent active release at the aqueous/biofilm interface (Eqs. 5.10–5.12), the rate of change of chlorine followed the same equation in the free chlorine model (Eq. 5.5). Similarly, the rates of change of bacteria and organic matter in the biofilm domain followed Eqs. 5.6 and 5.7, respectively.

5.2.3.3.2. Initial and boundary conditions

The initial and boundary conditions of the YPC model are shown in Table 5.3 and Figure 5.1, respectively. Most of these conditions are the same as the free chlorine model, but the initial level of Y_0 was applied in the aqueous domain for free yeast microparticles instead of free chlorine, and the following equations were added to describe the binding of yeast microparticles to the biofilm and chlorine release from the biofilm-bound yeast microparticles.

The concentration of free yeast microparticles in the aqueous phase decreased as they were bound to the aqueous/biofilm interface (boundary B5, Figure 5.1). This binding affinity was

described by the pseudo-first-order kinetics (Eq. 5.1). By taking derivatives of Eq. 5.1, the rate of change of the bound microparticles at the boundary B5 was described as:

$$\left.\frac{\partial S_{\mathrm{b}}(t)}{\partial t}\right|_{B5} = k_{\mathrm{b}}\left[S_{\mathrm{b},\infty} - S_{\mathrm{b}}(t)\right] \tag{5.10}$$

where the variable and parameters are the same as those in Eq. 5.1.

By the mass conservation law, the rate of change of the free yeast microparticles at the boundary B5 resulting from the binding reaction was written as follows:

$$\left.\frac{\partial S(t)}{\partial t}\right|_{B5} = -k_{\mathrm{b}}\left[S_{\mathrm{b},\infty} - S_{\mathrm{b}}(t)\right] \tag{5.11}$$

Then, the level of chlorine in the aqueous phase released from the biofilm-bound microparticles at the aqueous/biofilm interface (boundary B5, Figure 5.1) was described as Eq. 5.12a, given that the relationship between the charged chlorine and yeast microparticles follows Eq. 5.3b:

$$C(t)|_{B5} = \left[C_{S,0} - C_S(t)\right]S_{\mathrm{b}}(t) \tag{5.12a}$$

where the variables and parameters are the same as those in Eqs. 5.1 and 5.3.

The concentration of chlorine remaining in a single yeast microparticle was determined by Eq. 5.3a, assuming that the apparent active chlorine release follows the first-order kinetics. By taking derivatives of Eq. 5.3a,

$$\left.\frac{\partial C_S(t)}{\partial t}\right|_{B5} = -k_{\mathrm{r}2}C_S(t) \tag{5.12b}$$

where the variable and parameters are the same as those in Eq. 5.3.

5.2.3.4. Computational mesh convergence

The mesh convergence was tested to confirm that simulation results are independent of the meshes, and the convergence criteria were set to 0.005 (the difference between simulation results

from two sequential meshes be less than 0.5%). The computational mesh was designed using a combination of predefined meshes in COMSOL and its built-in adaptive mesh refinement algorithm. The initial mesh was developed using free triangular meshes with the predefined size of extremely coarse in the aqueous domain, free quad meshes with the predefined size of extremely fine in the biofilm domain, and adding a boundary layer at the aqueous/biofilm interface. This initial mesh was further refined by a COMSOL-provided adaptive mesh refinement algorithm (longest edge refinement method). This algorithm determines the longest edge of the mesh elements that have the largest errors, and then bisect this longest edge to increase the mesh element number (Chandler et al., 2011; COMSOL, 2008). The final mesh for the free chlorine model consisted of 1686 triangular elements, 7355 quadrilateral elements, 1006 edge elements, and 6 vertex elements with an average element quality of 0.8528. The mesh quality greater than 0.3 should not affect the quality of the solution (COMSOL, 2008; Lin et al., 2017; Santos et al., 2011). The final mesh for the YPC model consisted of 2129 triangular elements, 5382 quadrilateral elements, 699 edge elements, and 6 vertex elements with an average element quality of 0.9148.

5.3. Results

5.3.1. Characterization of kinetics parameters

The results in Figure 5.2 and Table 5.4 show the kinetics parameters that were experimentally measured for characterizing the binding and release rate of chlorine-charged yeast microparticles in an aqueous environment. These parameters were used to develop the model for biofilm inactivation by the targeted delivery system (YPC model). As shown in Figure 5.2a, the binding ratio data of yeast microparticles to the *E. coli* biofilm were fitted to the pseudo-first-order kinetics ($R^2 = 0.97$), which resulted in the binding rate (k_b) of 6.16×10^{-4} s^{-1}. Moreover, the

maximum concentration of biofilm-bound yeast microparticles with 1 h of incubation ($S_{b,\infty}$) was determined to be 0.054 kg/m^2 based on experimental observations (Table 5.4). Results in Figure 5.2b show the rate of decrease of chlorine remaining in free yeast microparticles in the aqueous phase, which represents the passive chlorine release rate from free microparticles to water. The data were fitted to the first-order kinetics ($R^2 = 0.98$), and the passive chlorine release rate (k_{r1}) of 1.06×10^{-5} s^{-1} was obtained. In contrast, the apparent active chlorine release rate from biofilm-bound yeast microparticles was determined by measuring the time and equivalent free chlorine concentration required to inactivate bacteria (see Section 5.2.2.4). This dataset was then fitted to the first-order kinetics, resulting in the apparent active chlorine release rate (k_{r2}) of 4.13×10^{-3} s^{-1}. This apparent active release rate of chlorine was 100 times faster than the passive release rate.

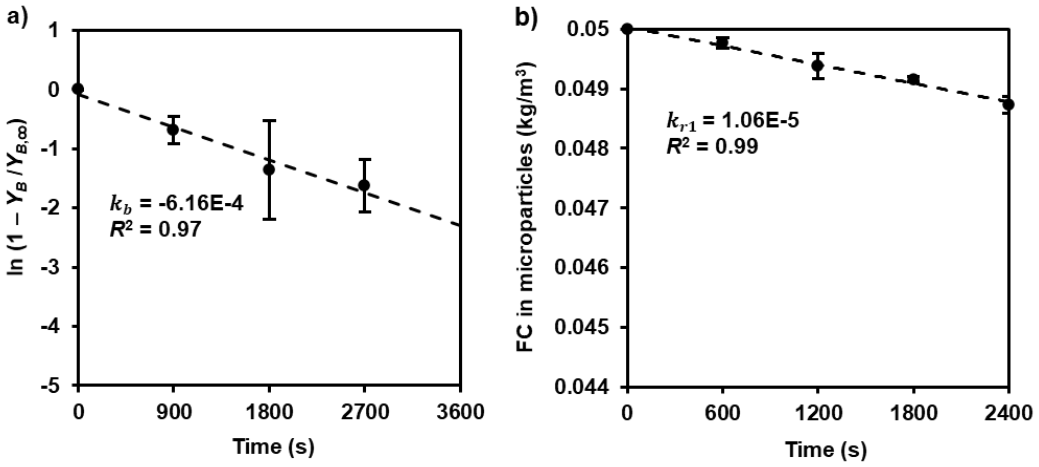

Figure 5.2. Reaction kinetics of the selected antimicrobial yeast microparticles, i.e., yeast microparticle–polyethylenimine–chlorine (YPC), as a function of incubation time: (a) binding of yeast microparticles to the *Escherichia coli* O157:H7 (*E. coli*) biofilm and (b) passive release of chlorine from free yeast microparticles in the aqueous phase. Data were fitted to (a) the pseudo-first-order kinetics equation (dotted lines) with the binding rate k_b, and (b) the first-order kinetics equation (dotted lines) to attain the passive release rate parameter in the aqueous phase k_{r1}. The data are mean values and their standard deviations (n = 3).

Table 5.4. List of experimentally measured parameters of the YPC model

Symbol	Description	Value & units
k_{b}	Binding rate of free yeast microparticles to biofilm	6.16×10^{-4} s^{-1}
k_{r1}	Passive chlorine release rate from free yeast microparticles in the aqueous phase	1.06×10^{-5} s^{-1}
k_{r2}	Apparent active chlorine release rate from biofilm-bound yeast microparticles	4.13×10^{-3} s^{-1}
$S_{\mathrm{b},\infty}$	Maximum concentration of biofilm-bound yeast microparticles within 1 h incubation	0.054 kg/m^2

Rate parameters were measured as described in Section 5.2.2.

5.3.2. Simulated spatiotemporal distribution of chlorine

The simulation results in Figure 5.3 show the spatiotemporal changes in chlorine concentrations within the biofilm for the free chlorine model (conventional system) and YPC model (targeted delivery system). To compare the chlorine delivery efficiency of two selected models, the initial chlorine concentration in the free chlorine model was set to be equivalent to the total chlorine level initially charged to yeast microparticles in the YPC model. The major differences between these two models are described in Section 5.2.3.3. The results in Figures 5.3a–5.3d show a rapid chlorine depletion at the top section of the biofilm in the free chlorine model. As shown in Figure 5.3i, the initial free chlorine concentration at the top section of the biofilm was relatively higher (0.028 kg/m^3). However, this level decreased rapidly (< 1.5 min) to 0.1-fold (0.003 kg/m^3), before the effective penetration of free chlorine to the bottom section of the biofilm. In the case of the YPC model, the results in Figures 5.3e–h show that chlorine concentration at the top section of the biofilm increased gradually as a function of time for the first 6 min, reaching the maximum chlorine concentration of 0.004 kg/m^3. This level decreased slowly compared to the free chlorine model, as the chlorine concentration reached 0.001 kg/m^3 after 46 min. Thus, more chlorine was delivered along the biofilm depth than the free chlorine model. Overall, chlorine was rapidly depleted upon reaching the biofilm, but yeast microparticles increased mass transfer at the interface, resulting in sustained chlorine level within the biofilm.

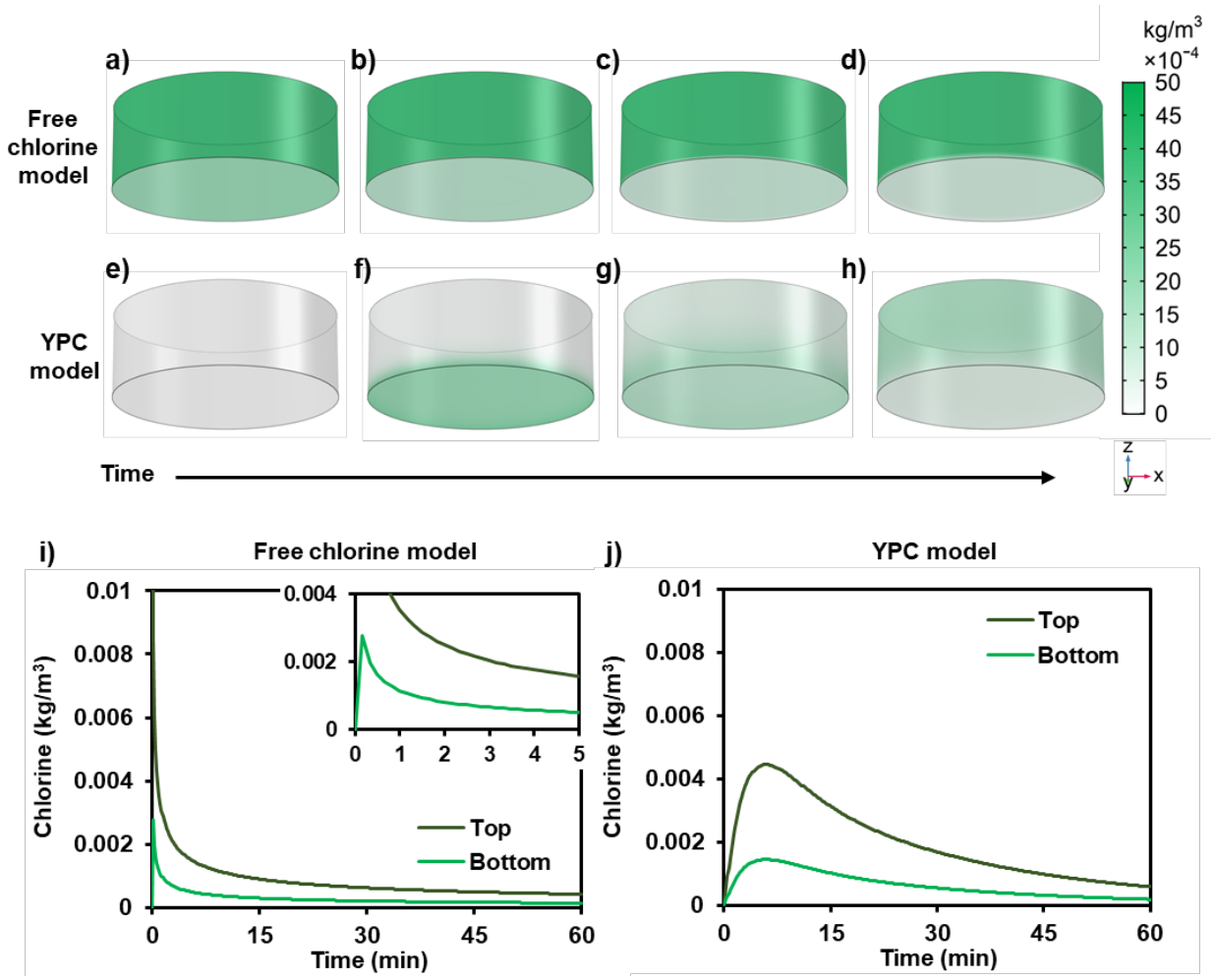

Figure 5.3. Simulated spatiotemporal chlorine distributions of (a–d) the free chlorine model and (e–h) the YPC model: (a,e) 0 min, (b,f) 5 min, (c,g) 20 min, (d,h) 60 min. The bottom two plots are the chlorine concentrations as a function of time at different locations in the *E. coli* biofilm for (i) the free chlorine model and (j) the YPC model.

5.3.3. Simulated biofilm inactivation efficacy

Figure 5.4 illustrates the simulated bacterial inactivation in the biofilm in each model. The inactivation level of *E. coli* in the biofilm was calculated by subtracting the mean log CFU/mL after the treatment from the initial log CFU/mL (7 log CFU/mL). The details of the unit conversion of bacterial counts in the biofilm are described in Section 5.2.3. As shown in Figure 5.4a, the volumetric average inactivation level of *E. coli* in the biofilm was 3.4 log by 15 min of treatment in the free chlorine model. This volumetric average inactivation level increased to 6.4 log after 60 min. Moreover, the spatial variations in bacterial survival after the treatment were observed. The inactivation level at the top section of the biofilm was 7 log after 8.7 min of free chlorine treatment, while the inactivation level at the bottom section of the biofilm was only 2.1 log within the same treatment time. On the contrary, the results in Figure 5.4b show that the volumetric average inactivation level reached 7 log within 16.2 min treatment in the YPC model. In this case, the inactivation level at the top and bottom sections reached 7 log within 5.3 and 18.8 min, respectively. Overall, YPC enhanced the delivery and chemical stability of chlorine and resulted in improved inactivation of the biofilm.

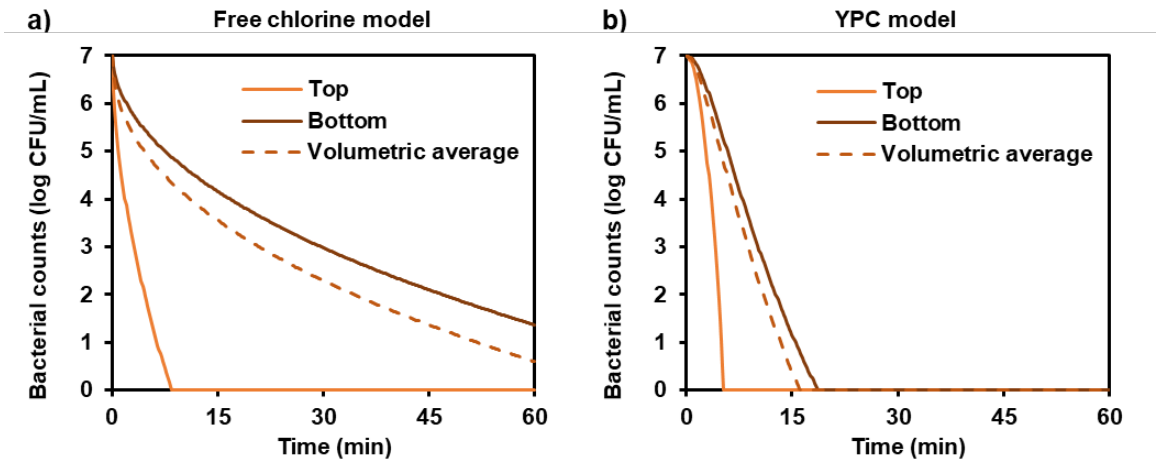

Figure 5.4. Simulated bacterial inactivation in the *E. coli* biofilm of (a) the free chlorine model and (b) the YPC model.

5.4. Discussion

5.4.1. A mechanistic modeling approach to improve targeted delivery of chlorine to biofilms

In this study, a mechanistic modeling approach was developed to understand the simultaneous effect of the factors influencing the targeted delivery of antimicrobials to the biofilm. Designing a targeted delivery system for biofilm inactivation may involve multiple factors since physical, chemical, and biological processes are co-occurring in the biofilm ecosystems (Pérez et al., 2005). Previous studies have indicated the following as major factors influencing the targeted delivery of antimicrobials to biofilms: (i) size of particles used to deliver antimicrobials (Forier et al., 2014; Joye, Davidov-Pardo, & McClements, 2014; Peulen & Wilkinson, 2011); (ii) chemical stability of antimicrobials in the presence of organic matter (Cui, Li, Li, Vittayapadung, & Lin, 2016; Forier et al., 2014; Joye et al., 2014); (iii) binding affinity of particles to target biofilms (Forier et al., 2014; Jing et al., 2014); (iv) controlled release of antimicrobials from the particles (Forier et al., 2014; Loo et al., 2016). The particle size is important since it affects the physicochemical stability, biological activity of particles, release kinetics (Joye et al., 2014), as well as the penetration of the particles into biofilms by diffusion (Forier et al., 2014; Peulen & Wilkinson, 2011). However, this was not included in the present study since the yeast cell wall-derived microparticles had a fixed size. Delivery systems with particles may also increase the chemical stability of antimicrobials susceptible to realistic environments (Cui et al., 2016; Forier et al., 2014; Joye et al., 2014). The same principle was applied as an extension in Part 2 of this study (Yi et al., 2021), where yeast microparticles protected chlorine from nonspecific chemical reactions with organic matter. Furthermore, mathematical modeling studies on targeted delivery systems for biofilm inactivation emphasized either the binding affinity of particles to the biofilm

(Jing et al., 2014) or the controlled release of antimicrobials from particles (Loo et al., 2016). In the present study, these two factors were both included by using a mechanistic modeling approach.

5.4.2. Spatiotemporal distributions of chlorine delivery for biofilm inactivation using yeast microparticles

The simulation results in Figure 5.4 show the overall effect of using yeast microparticles on improved biofilm inactivation. The rates of biofilm inactivation in the free chlorine and YPC models were compared, assuming the same level of total chlorine was used. While the free chlorine model had survivor bacteria after a 60-min treatment, the volumetric average inactivation level of *E. coli* in the biofilm reached 7 log (all bacteria inactivated) within 16.2 min in the YPC model. Our prior experimental observations supported these simulation results, where the same level of YPC microparticles resulted in a 7 log reduction in an *E. coli* biofilm within the 20-min treatment (Huang et al., 2019). In the same study, free chlorine at a lower concentration of 0.02 kg/m^3 was examined, which was equivalent to the concentration of released free chlorine from the yeast microparticles. Therefore, an additional simulation was performed in this study using this lower free chlorine concentration. The simulation results in Figure 5.5 show that 2–3 log reduction was achieved after a 60-min treatment, and this was the same level reported in the prior experimental observations (Huang et al., 2019). Overall, we could conclude that our mechanistic model can be used as a tool to understand the improved biofilm inactivation by yeast microparticles.

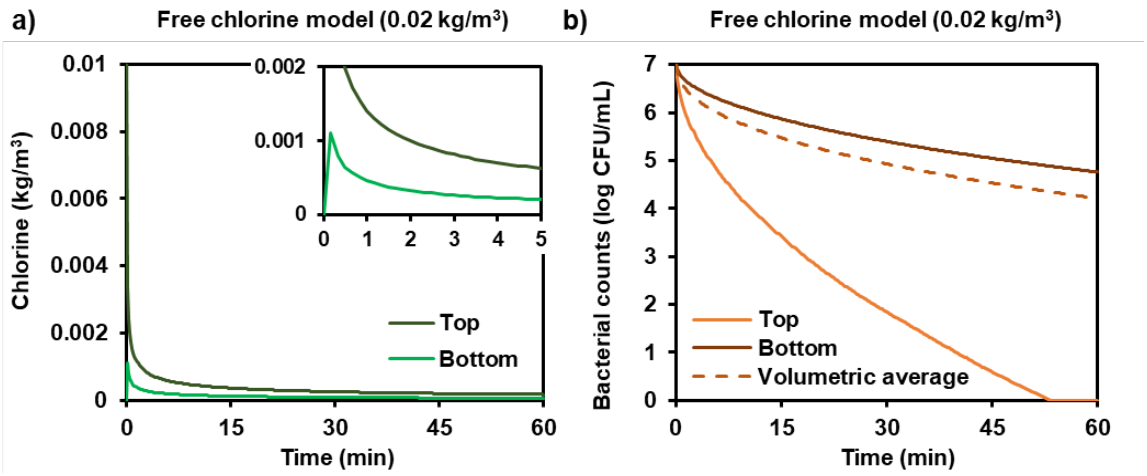

Figure 5.5. Simulated results of the free chlorine model at a lower concentration of 0.02 kg/m^3: (a) chlorine concentrations as a function of time at different locations in the *E. coli* biofilm and (b) bacterial inactivation in the biofilm.

Furthermore, it should be noted that this improvement is remarkable considering that previous studies of targeted delivery for biofilm inactivation resulted in only 2–3 log reduction without an extended treatment time (Cui, Bai, Rashed, & Lin, 2018; Carla Ferreira et al., 2013). A previous study on the biofilm inactivation using clove oil-loaded chitosan nanoparticles resulted in approximately 2 log reduction of *E. coli* biofilm after 8 h (Cui et al., 2018). Another study on the biofilm control using calcium carbonate microparticles charged with benzyldimethyldodecylammonium chloride resulted in a 1.97 log reduction of *Pseudomonas fluorescens* biofilm after 1 h (Carla Ferreira et al., 2013). To determine the key factors that contributed to the improvement in biofilm inactivation, it is important to understand the spatiotemporal delivery of antimicrobials. The results in Figure 5.3 show that the use of yeast microparticles increased a localized chlorine concentration at the biofilm interface for a prolonged time, and consequently, more chlorine was delivered to the bottom section of the biofilm. As shown in Figure 5.4, this enhanced chlorine delivery resulted in an improved bacterial inactivation at the bottom section of the biofilm, which was essential for the complete inactivation of the biofilm. Thus, the enhanced chlorine delivery to the biofilm interface was a key factor, and this was further discussed in our companion paper (Yi et al., 2021) in terms of the following factors: the chemical stability of chlorine in yeast microparticles, binding affinity of yeast microparticles to the biofilm, controlled release of chlorine from yeast microparticles.

5.5. Conclusions

This study proposes a mechanistic modeling approach to numerically simulate the biofilm inactivation. The targeted delivery of chlorine to an *E. coli* biofilm using yeast microparticles was modeled; as a combination of diffusion in a porous media, and reaction equations for binding of

yeast microparticles to the biofilm, chlorine release from these particles, and bacterial inactivation by the released chlorine. The simulation results demonstrate the spatiotemporal chlorine distribution in the system, as well as bacterial inactivation in the biofilm that matched the experimental observations in the literature. These results support that our mechanistic modeling approach could be used as a tool to predict the biofilm inactivation efficacy of a targeted delivery system using bioaffinity of microparticles. Furthermore, by changing the parameters involved in major physicochemical properties, such as chemical stability, binding affinity, controlled release, the proposed model could potentially simulate the system behavior and determine the key factors, as it will be discussed in Part 2 of this study.

Acknowledgements

This work was supported by the United States Department of Agriculture National Institute of Food and Agriculture [grant number 2015-68003-23411].

References

Barreras-Urbina, C. G., Ramírez-Wong, B., López-Ahumada, G. A., Burruel-Ibarra, S. E., Martínez-Cruz, O., Tapia-Hernández, J. A., & Rodríguez Félix, F. (2016). Nano- and micro-particles by nanoprecipitation: Possible application in the food and agricultural industries. *International Journal of Food Properties*, *19*(9), 1912–1923. https://doi.org/10.1080/10942912.2015.1089279

Chandler, D., Maldonado, G. I., Primm, R. T., & Freels, J. D. (2011). Neutronics modeling of the high flux isotope reactor using COMSOL. *Annals of Nuclear Energy*, *38*(11), 2594–2605. https://doi.org/10.1016/j.anucene.2011.06.002

Chao, M. S. (1968). The diffusion coefficients of hypochlorite, hypochlorous acid, and chlorine in aqueous media by chronopotentiometry. *Journal of The Electrochemical Society*, *115*(11), 1172. https://doi.org/10.1149/1.2410933

Choi, O., Yu, C. P., Esteban Fernández, G., & Hu, Z. (2010). Interactions of nanosilver with *Escherichia coli* cells in planktonic and biofilm cultures. *Water Research*, *44*(20), 6095–6103. https://doi.org/10.1016/j.watres.2010.06.069

COMSOL. (2008). *COMSOL Multiphysic User's Guide Version 3.5a*.

Costa, P., & Sousa Lobo, J. M. (2001). Modeling and comparison of dissolution profiles. *European Journal of Pharmaceutical Sciences*, *13*(2), 123–133. https://doi.org/10.1016/S0928-0987(01)00095-1

Cui, H., Bai, M., Rashed, M. M. A., & Lin, L. (2018). The antibacterial activity of clove oil/chitosan nanoparticles embedded gelatin nanofibers against *Escherichia coli* O157:H7 biofilms on cucumber. *International Journal of Food Microbiology*, *266*, 69–78. https://doi.org/10.1016/j.ijfoodmicro.2017.11.019

Cui, H., Li, W., Li, C., Vittayapadung, S., & Lin, L. (2016). Liposome containing cinnamon oil with antibacterial activity against methicillin-resistant *Staphylococcus aureus* biofilm. *Biofouling*, *32*(2), 215–225. https://doi.org/10.1080/08927014.2015.1134516

da Silva Lima, A., Maciel, A. P., Mendonça, C. de J. S., & Costa Junior, L. M. (2017). Use of encapsulated carvacrol with yeast cell walls to control resistant strains of *Rhipicephalus microplus* (Acari: Ixodidae). *Industrial Crops and Products*, *108*, 190–194. https://doi.org/10.1016/j.indcrop.2017.06.037

Dash, S., Murthy, P. N., Nath, L., & Chowdhury, P. (2010). Kinetic modeling on drug release from controlled drug delivery systems. *Acta Poloniae Pharmaceutica - Drug Research*, *67*(3), 217–223.

Deborde, M., & von Gunten, U. (2008). Reactions of chlorine with inorganic and organic compounds during water treatment-Kinetics and mechanisms: A critical review. *Water Research*, *42*, 13–51. https://doi.org/10.1016/j.watres.2007.07.025

Dong, A., Wang, Y. J., Gao, Y., Gao, T., & Gao, G. (2017). Chemical insights into antibacterial *N*-halamines. *Chemical Reviews*, *117*(6), 4806–4862. https://doi.org/10.1021/acs.chemrev.6b00687

Ferreira, C., Rosmaninho, R., Simoes, M., Pereira, M. C., Bastos, M. M., Nunes, O. C., … Melo, L. F. (2010). Biofouling control using microparticles carrying a biocide. *Biofouling*, *26*(2), 205–212. https://doi.org/10.1080/08927010903419630

Ferreira, Carla, Pereira, A. M., Pereira, M. C., Simões, M., & Melo, L. F. (2013). Biofilm control with new microparticles with immobilized biocide. *Heat Transfer Engineering*, *34*(8–9), 712–718. https://doi.org/10.1080/01457632.2012.739040

Forier, K., Raemdonck, K., De Smedt, S. C., Demeester, J., Coenye, T., & Braeckmans, K. (2014). Lipid and polymer nanoparticles for drug delivery to bacterial biofilms. *Journal of Controlled Release*, *190*, 607–623. https://doi.org/10.1016/j.jconrel.2014.03.055

Gou, Y., Liu, W., Wang, J. J., Tan, L., Hong, B., Guo, L., … Zhao, Y. (2019). CRISPR-Cas9 knockout of *qseB* induced asynchrony between motility and biofilm formation in *Escherichia coli*. *Canadian Journal of Microbiology*, *65*(9), 691–702. https://doi.org/10.1139/cjm-2019-0100

Hall-Stoodley, L., Costerton, J. W., & Stoodley, P. (2004). Bacterial biofilms: From the natural environment to infectious diseases. *Nature Reviews Microbiology*, *2*(2), 95–108. https://doi.org/10.1038/nrmicro821

Helbling, D. E., & VanBriesen, J. M. (2007). Free chlorine demand and cell survival of microbial suspensions. *Water Research*, *41*(19), 4424–4434. https://doi.org/10.1016/j.watres.2007.06.006

Høiby, N., Bjarnsholt, T., Givskov, M., Molin, S., & Ciofu, O. (2010). Antibiotic resistance of bacterial biofilms. *International Journal of Antimicrobial Agents*, *35*(4), 322–332. https://doi.org/10.1016/j.ijantimicag.2009.12.011

Huang, K., Dou, F., & Nitin, N. (2019). Biobased sanitizer delivery system for improved sanitation of bacterial and fungal biofilms. *ACS Applied Materials & Interfaces*, *11*, 17204–17214. https://doi.org/10.1021/acsami.9b02428

Hung, C., Zhou, Y., Pinkner, J. S., Dodson, K. W., Crowley, J. R., Heuser, J., … Hultgren, S. J. (2013). *Escherichia coli* biofilms have an organized and complex extracellular matrix structure. *MBio*, *4*(5), 1–10. https://doi.org/10.1128/mBio.00645-13

Incollingo, S., Ferrari, A., & Musso, G. (2020). Numerical investigation on water exchange of shale samples. *E3S Web of Conferences*, *195*, 1–6. https://doi.org/10.1051/e3sconf/202019502025

Jing, H., Mezgebe, B., Aly Hassan, A., Sahle-Demessie, E., Sorial, G. A., & Bennett-Stamper, C. (2014). Experimental and modeling studies of sorption of ceria nanoparticle on microbial biofilms. *Bioresource Technology*, *161*, 109–117. https://doi.org/10.1016/j.biortech.2014.03.015

Joye, I. J., Davidov-Pardo, G., & McClements, D. J. (2014). Nanotechnology for increased micronutrient bioavailability. *Trends in Food Science and Technology*, *40*(2), 168–182. https://doi.org/10.1016/j.tifs.2014.08.006

Ju, T., Liu, S., Yang, J., & Sun, D. (2014). Rapidly exploring random tree algorithm-based path planning for robot-aided optical manipulation of biological cells. *IEEE Transactions on Automation Science and Engineering*, *11*(3), 649–657. https://doi.org/10.1109/TASE.2013.2289311

Karalis, K., Karkalos, N., Antipas, G. S. E., & Xenidis, A. (2015). Electromagnetic phenomena in an electric submerged arc furnace. *METAL 2015 - 24th International Conference on Metallurgy and Materials*, *Conference Proceedings*, 60–66.

Kim, M. H. (2016). Nanoparticle-based therapies for wound biofilm infection: Opportunities and challenges. *IEEE Transactions on Nanobioscience*, *15*(3), 294–304. https://doi.org/10.1109/TNB.2016.2527600

Landa-Marbán, D., Liu, N., Pop, I. S., Kumar, K., Pettersson, P., Bødtker, G., … Radu, F. A. (2019). A pore-scale model for permeable biofilm: Numerical simulations and laboratory

experiments. *Transport in Porous Media*, *127*(3), 643–660. https://doi.org/10.1007/s11242-018-1218-8

Li, Q., Mahendra, S., Lyon, D. Y., Brunet, L., Liga, M. V., Li, D., & Alvarez, P. J. J. (2008). Antimicrobial nanomaterials for water disinfection and microbial control: Potential applications and implications. *Water Research*, *42*(18), 4591–4602. https://doi.org/10.1016/j.watres.2008.08.015

Lin, B., Li, H., Chen, Z., Zheng, C., Hong, Y., & Wang, Z. (2017). Sensitivity analysis on the microwave heating of coal: A coupled electromagnetic and heat transfer model. *Applied Thermal Engineering*, *126*, 949–962. https://doi.org/10.1016/j.applthermaleng.2017.08.012

Loo, C. Y., Rohanizadeh, R., Young, P. M., Traini, D., Cavaliere, R., Whitchurch, C. B., & Lee, W. H. (2016). Combination of silver nanoparticles and curcumin nanoparticles for enhanced anti-biofilm activities. *Journal of Agricultural and Food Chemistry*, *64*(12), 2513–2522. https://doi.org/10.1021/acs.jafc.5b04559

Millington, R. J., & Quirk, J. P. (1961). Permeability of porous solids. *Transactions of the Faraday Society*, *57*, 1200–1207. https://doi.org/10.1039/TF9615701200

Munther, D., Luo, Y., Wu, J., Magpantay, F. M. G., & Srinivasan, P. (2015). A mathematical model for pathogen cross-contamination dynamics during produce wash. *Food Microbiology*, *51*, 101–107. https://doi.org/10.1016/j.fm.2015.05.010

Neidhardt, F. C., Ingraham, J. L., & Schaechter, M. (1990). *Physiology of the Bacterial Cell*. Sinauer Associates, Sunderland, MA.

Paramera, E. I., Karathanos, V. T., & Konteles, S. J. (2014). *Yeast cells and yeast-based materials for microencapsulation*. *Microencapsulation in the Food Industry*. Elsevier Inc. https://doi.org/10.1016/b978-0-12-404568-2.00023-6

Pérez, J., Picioreanu, C., & Van Loosdrecht, M. (2005). Modeling biofilm and floc diffusion processes based on analytical solution of reaction-diffusion equations. *Water Research*, *39*(7), 1311–1323. https://doi.org/10.1016/j.watres.2004.12.020

Peulen, T. O., & Wilkinson, K. J. (2011). Diffusion of nanoparticles in a biofilm. *Environmental Science and Technology*, *45*(8), 3367–3373. https://doi.org/10.1021/es103450g

Santos, T., Valente, M. A., Monteiro, J., Sousa, J., & Costa, L. C. (2011). Electromagnetic and thermal history during microwave heating. *Applied Thermal Engineering*, *31*(16), 3255–3261. https://doi.org/10.1016/j.applthermaleng.2011.06.006

Sharma, P., Panghal, A., Gaikwad, V., Jadhav, S., Bagal, A., Jadhav, A., & Chhikara, N. (2019). Nanotechnology: A Boon for Food Safety and Food Defense. In R. Prasad, V. Kumar, M. Kumar, & D. Choudhary (Eds.), *Nanobiotechnology in Bioformulations* (pp. 225–242). Cham: Springer.

Simonin, J. P. (2016). On the comparison of pseudo-first order and pseudo-second order rate laws in the modeling of adsorption kinetics. *Chemical Engineering Journal*, *300*, 254–263. https://doi.org/10.1016/j.cej.2016.04.079

Soto, E. R., & Ostroff, G. R. (2008). Characterization of multilayered nanoparticles encapsulated in yeast cell wall particles for DNA. *Bioconjugate Chemistry*, *19*(4), 840–848. https://doi.org/10.1021/bc700329p

Srey, S., Jahid, I. K., & Ha, S. Do. (2013). Biofilm formation in food industries: A food safety concern. *Food Control*, *31*(2), 572–585. https://doi.org/10.1016/j.foodcont.2012.12.001

Stewart, P. S., & Raquepas, J. B. (1995). Implications of reaction-diffusion theory for the disinfection of microbial biofilms by reactive antimicrobial agents. *Chemical Engineering Science*, *50*(19), 3099–3104. https://doi.org/10.1016/0009-2509(95)00143-S

Stine, A. E., Nassar, D., Miller, J. K., Clemons, C. B., Wilber, J. P., Young, G. W., … Milsted, A. (2013). Modeling the response of a biofilm to silver-based antimicrobial. *Mathematical Biosciences*, *244*, 29–39. https://doi.org/10.1016/j.mbs.2013.04.006

Yadav, M. K., Song, J.-J., Singh, B. P., & Vidal, J. E. (2020). Microbial biofilms and human disease: A concise review. In M. K. Yadav & B. P. Singh (Eds.), *New and Future Developments in Microbial Biotechnology and Bioengineering: Microbial Biofilms* (Vol. 1, pp. 1–13). Elsevier. https://doi.org/10.1016/b978-0-444-64279-0.00001-3

Yi, J., Huang, K., & Nitin, N. (2021). Modeling bioaffinity-based targeted delivery of antimicrobials to *Escherichia coli* biofilms using yeast microparticles. Part 2: parameter evaluation and validation. Manuscript submitted for publication.

Part 2. Parameter Evaluation and Validation

Abstract

Design of bioaffinity-based targeted delivery systems for biofilm inactivation may require a comprehensive understanding of various factors: the chemical stability of antimicrobials in biobased particles, binding affinity of biobased particles to biofilms, and controlled release of antimicrobials. In this study, *Escherichia coli* biofilm inactivation by chlorine-charged yeast microparticles was numerically simulated, and the roles of design factors of this targeted delivery system were assessed by parameter evaluation. The simulation results were further validated using two different types of yeast microparticles. The results of this study illustrate that the chemical stability of chlorine achieved by yeast microparticles was a key factor for improved biofilm inactivation in an organic-rich environment (> 6 additional log reduction in 20 min compared to the free chlorine treatment). Moreover, the binding affinity of yeast microparticles to the biofilms was another key factor for enhanced inactivation, as a 10-fold increase in binding rate resulted in 4.2-fold faster inactivation. Overall, the mechanistic modeling framework developed in this study could guide the design and development of biobased particles for targeted inactivation of biofilms.

Keywords: Biofilm; Antimicrobial; Targeted delivery; Yeast microparticle; Binding affinity; Mechanistic modeling

5.6. Introduction

Biofilms are a critical issue influencing food and water safety as well as public health (Lisle et al., 1998; Murphy, Payne, & Gagnon, 2008; Srey, Jahid, & Ha, 2013; Williams & Braun-Howland, 2003; Yadav, Song, Singh, & Vidal, 2020). Micro-and nanoparticles have been used to develop targeted antimicrobial delivery systems for biofilm inactivation, by stabilizing antimicrobials and enabling a highly localized and sustained delivery to the biofilm (Choi, Yu, Esteban Fernández, & Hu, 2010; C. Ferreira et al., 2010; Carla Ferreira, Pereira, Pereira, Simões, & Melo, 2013; Li et al., 2008; Sharma et al., 2019). To enable targeted delivery, specific binding interaction could be achieved by modifying the particles using antibody or lectin to form bonds with specific antigen or carbohydrate residues in biofilms, respectively (Forier et al., 2014; Stratford & Bond, 1992). Nevertheless, the chemical synthesis methods, such as bioconjugation of affinity molecules to these engineered particles, are often complex and expensive (Rukavina & Vanić, 2016). In contrast, yeast or other fungal cells have a natural affinity to bind bacteria and their biofilms (Huang, Dou, & Nitin, 2019; Hwang et al., 2017). The binding affinity of these yeast microparticles has been attributed to specific interactions among lectins on yeast cells with bacterial polysaccharides (Forier et al., 2014; Singh, Bhari, & Kaur, 2011; Touhami, Hoffmann, Vasella, Denis, & Dufrêne, 2003) and vice versa (Huang et al., 2019; Kogan & Kocher, 2007; Touhami et al., 2003). Other microbe-derived microparticles may be generated from naturally existing microbes or genetically engineered microbes that express specific binding ligands on their cell wall surfaces (Huang et al., 2019; Kuroda, Ueda, Shibasaki, & Tanaka, 2002; Nam et al., 2002). The use of these bioaffinity-based microparticles may lead to diverse combinations of particles with different binding affinities and antimicrobials with varying controlled release rates.

Thus, a mechanistic understanding of these factors for the targeted antimicrobial delivery is needed for the rational selection of biobased particles.

Prior studies have developed simplified mathematical models for antimicrobial delivery systems to predict biofilm inactivation using inorganic particles (Jing et al., 2014; Loo et al., 2016; Peulen & Wilkinson, 2011). However, these models did not involve biological factors originated from biobased particles, including binding affinity and controlled release. Moreover, inorganic particles used in these prior studies were chemically stable, while common antimicrobials such as chlorine can be consumed by soluble organic matter in the system. Thus, these prior models have not been used to determine the relative significance of individual factors (e.g., chemical stability, binding affinity, or controlled release) involved in biofilm inactivation. Therefore, in Part 1 of this study, a mechanistic modeling approach was developed to simulate the biofilm inactivation using biobased microparticles based on mass transport and reaction kinetics of binding affinity and controlled release (Yi, Huang, & Nitin, 2021). This enables simultaneous evaluation of the significance of each factor on the biofilm inactivation.

In particular, Part 2 of this study focused on evaluating the role of chemical stability of antimicrobials, binding of yeast microparticles to the biofilms, and controlled release of antimicrobials in influencing biofilm inactivation. The overall goals of this study were to: (i) determine the key factors influencing the biofilm inactivation efficacy of the biobased antimicrobial delivery system; and (ii) experimentally validate the model using two different designs of biobased carriers derived from yeast cell walls. Overall, this study illustrates the application of a mechanistic modeling approach to understand the role of individual design factors in designing the targeted delivery system for biofilm inactivation using yeast microparticles.

5.7. Materials and Methods

5.7.1. Model variations and parameter evaluation

In Part 1 of this study, a conventional system for biofilm inactivation was modeled using free chlorine, whereas a targeted delivery system was modeled using yeast microparticle–polyethylenimine–chlorine (YPC) (Yi et al., 2021). These models were utilized in the present study to determine the key factors that improved biofilm inactivation efficacy based on parameters evaluation using COMSOL Multiphysics® software version 5.5 (or simply COMSOL).

5.7.1.1. Chemical stability of chlorine – the presence of organic matter in the aqueous phase

The chemical stability of chlorine in the presence of organic matter was evaluated by using the free chlorine and YPC models developed in Part 1 of this study (Yi et al., 2021). Unlike the free chlorine, chlorine was charged to YPC particles in the form of *N*-halamine (N-Cl) and did not react with organic matter in the aqueous phase of the YPC model (Huang et al., 2019). Other model assumptions, equations, and input parameters follow the descriptions in Part 1 of this study (Yi et al., 2021), except for the initial organic matter concentration in the aqueous phase, i.e., $O(0) = 2$ kg/m^3.

5.7.1.2. Reaction rates – binding of yeast microparticles and apparent active release of chlorine

To understand the influences of binding affinity and controlled release on biofilm inactivation efficacy, their rate parameters were further evaluated. Two rate parameters, yeast microparticle binding rate to the biofilm (k_b) and the apparent active chlorine release rate from the biofilm-bound yeast microparticles (k_{r2}) were selected. In each case, one of the selected rate parameters was raised 10-folds or lowered 0.1-folds to compute the simulated biofilm inactivation

results. All the other conditions were kept the same as the original YPC model. The results were compared to the average biofilm inactivation of the original YPC model.

5.7.2. Experimental validation

The simulation results were compared to the experimental observations using two different types of antimicrobial yeast microparticles to validate the mechanistic model and determine the significance of design factors, including binding and release properties. YPC and yeast microparticle–chlorine (YC) were used since they have different binding affinity and chlorine release rates. They both were prepared from baker's yeast, but polyethylenimine was encapsulated for YPC to increase binding affinity and improve controlled release. The reaction parameters of YC were measured using the same methods for YPC, as described in Part 1 of this study (Yi et al., 2021). The delivery of YC was numerically simulated following the same model development procedure of the YPC model as well.

5.7.2.1. Characterization of antimicrobial yeast microparticles YC

Reaction parameters of the YC model were measured by the same experimental methods for the YPC model described in Part 1 of this study (Yi et al., 2021). However, instead of using 0.01 g or 0.01 g/mL of yeast microparticle–polyethylenimine in the measurements, 0.03 g or 0.03 g/mL of yeast microparticles (without encapsulation of polyethylenimine) were used. This level was determined based on the preliminary results (data not shown), where it was observed that yeast microparticles could charge three times less chlorine than yeast microparticle–polyethylenimine. All experiments were performed in triplicates at room temperature.

Table 5.5. Experimentally measured parameters for the targeted antimicrobial delivery systems

Symbol	Description	Model	Value & units
k_{b}	Binding rate of free yeast microparticles to biofilm	YPC	6.16×10^{-4} s^{-1}
		YC	4.40×10^{-4} s^{-1}
k_{r1}	Passive chlorine release rate from free yeast microparticles in the aqueous phase	YPC	1.06×10^{-5} s^{-1}
		YC	3.62×10^{-5} s^{-1}
k_{r2}	Apparent active chlorine release rate from biofilm-bound yeast microparticles	YPC	4.13×10^{-3} s^{-1}
		YC	3.09×10^{-3} s^{-1}
$S_{\mathrm{b},\infty}$	Maximum concentration of biofilm-bound yeast microparticles within 1 h incubation	YPC	0.054 kg/m^2
		YC	0.024 kg/m^2

YPC: yeast microparticle–polyethylenimine–chlorine. YC: Yeast microparticle–chlorine. Rate parameters were measured as described in Part 1 of this study.

5.7.2.2. Biofilm inactivation assay

The ability of the selected antimicrobial yeast microparticles to inactivate *Escherichia coli* O157:H7 (*E. coli*) biofilm was assessed using the biofilm formed on a sterile polystyrene surface. This biofilm was prepared following the methods described in Part 1 of this study (Yi et al., 2021). The chlorine-charged yeast microparticles were suspended at a concentration of 0.01 g/mL or 0.03 g/mL in sterile Milli-Q water for further use, for the YPC and YC model, respectively. 1 mL of each type of antimicrobial yeast microparticles was added to each well of biofilm and incubated at room temperature. After incubation for 0, 15, 30, 45, and 60 min, the biofilms were gently washed twice by sterile phosphate-buffered saline (PBS) to remove residual chlorine and yeast microparticles.

The viable bacteria in the biofilm were recovered and then enumerated by the plate counting method. After the treatment, 0.1 mL of 0.1 M sodium thiosulfate was added to each well of the 24-well plate to quench the residual chlorine, followed by 1 mL of sterile maximum recovery diluent supplemented with 0.1% v/v Tween 20. The 24-well plate was then sealed with sterile Parafilm to prevent leakage of the recovery solution and vortexed vigorously for 30 s, followed by bath sonication (Branson 2510 Ultrasonic Cleaner, Branson Ultrasonics, Danbury, CT, USA) for 2 min. After the recovery process, the solution containing viable bacteria was subjected to quantification by serial dilution with sterile PBS and spread plating onto and tryptic soy agar (TSA) plates supplemented with 50 μg/mL rifampicin. Bacterial counts were determined after incubation of the TSA plates at 37 °C for 24 h. All experiments were performed in triplicates at room temperature.

5.7.2.3. Statistical analysis

Statistical analysis was performed using the SPSS Statistics software (version 27, IBM SPSS, Chicago, IL, USA) to evaluate the measured datasets. All the experiments were performed in triplicates. The t-test, one-way analysis of variance, and Tukey's multiple comparison were used to determine the significant differences among the values of the selected measurements ($p < 0.05$).

5.8. Results

5.8.1. Simulation results: free chlorine and YPC models

5.8.1.1. Chlorine distribution and biofilm inactivation in the presence of organic matter in the aqueous phase

The simulation results in Figure 5.6 illustrate the spatiotemporal changes in chlorine concentrations within the biofilm in the presence of organic matter in the aqueous phase (chemical oxygen demand, COD = 2 kg/m^3). To compare the chlorine delivery efficiency of two selected models, the initial chlorine concentration in the free chlorine model was set to be equivalent to the total chlorine level initially charged to yeast microparticles in the YPC model. Moreover, the rate parameters for the inactivation of bacteria in the biofilm upon interaction with released chlorine were kept the same in both YPC and free chlorine models. For the free chlorine model (conventional system), the results in Figure 5.6a show that chlorine was rapidly depleted in the presence of organic matter in the aqueous phase. The initial chlorine concentration at the top section of the biofilm was 0.03 kg/m^3, and it decreased to 0.1-fold (0.003 kg/m^3) in 0.5 min. This 0.1-fold decrease was achieved in 1.5 min without the aqueous-phase organic matter, according to the results in Part 1 of this study (Yi et al., 2021). In contrast, the results in Figure 5.6b show a sustained level of chlorine in the case of the YPC model (targeted delivery system) in the presence

of aqueous-phase organic matter. The maximum chlorine concentration of 0.004 kg/m^3 was achieved within the first 6 min, and this was similar to the results in Part 1 of this study without the aqueous-phase organic matter (Yi et al., 2021). This maximum level was then decreased to 0.001 kg/m^3 after 42.8 min. Overall, rapid depletion of free chlorine was enhanced in the presence of organic matter in the aqueous phase, but the use of yeast microparticles protected chlorine from this nonspecific reaction so that a sustained chlorine concentration was delivered within the biofilm.

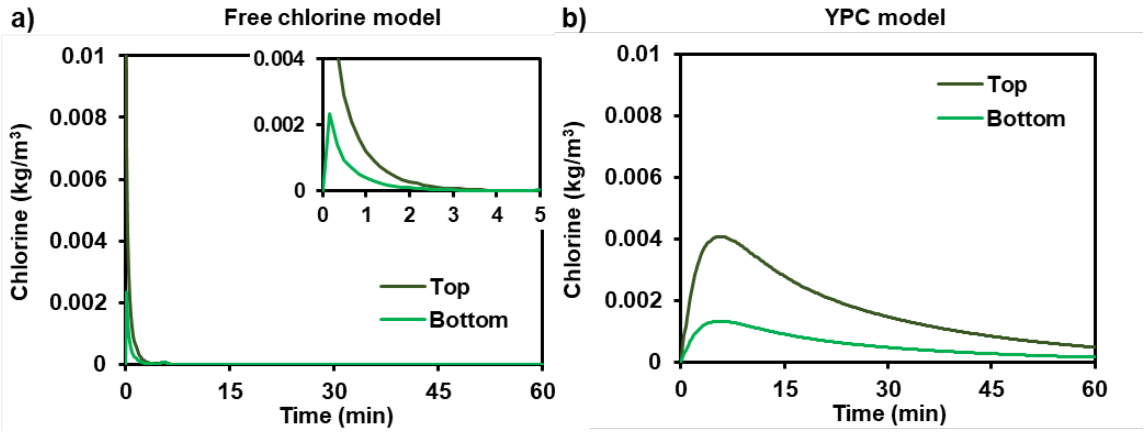

Figure 5.6. Simulated chlorine concentrations as a function of time at different locations in the *Escherichia coli* O157:H7 (*E. coli*) biofilm for (a) the free chlorine model and (b) the YPC model in the presence of organic matter (chemical oxygen demand = 2 kg/m^3) in the aqueous phase. YPC: yeast microparticle–polyethylenimine–chlorine.

Similarly, the results in Figure 5.7 illustrate the respective simulated bacterial inactivation in the biofilm for each model. As described in Part 1 of this study (Yi et al., 2021), the inactivation level of *E. coli* in the biofilm was calculated by subtracting the mean log CFU/mL value after the treatment from the initial log CFU/mL value (7 log CFU/mL), and the details of the unit conversion of bacterial counts in the biofilm are described in Part 1 of this study (Yi et al., 2021). The results in Figure 5.7a show that the biofilm inactivation efficacy of the free chlorine model was remarkably reduced in the presence of organic matter in the aqueous phase. The volumetric average inactivation level of *E. coli* in the biofilm was 0.8 log after 3 min of free chlorine treatment in the presence of aqueous-phase organic matter, and no further bacterial inactivation was achieved within 60 min of treatment time. On the contrary, the results in Figure 5.7b illustrate that the enhanced level of biofilm inactivation of the YPC model was maintained even in the presence of aqueous-phase organic matter. The volumetric average inactivation level of *E. coli* in the biofilm reached 7 log within 18.2 min in this case. Overall, YPC enhanced the delivery and chemical stability of chlorine and resulted in improved inactivation of the biofilm, with or without the presence of organic matter in the aqueous phase.

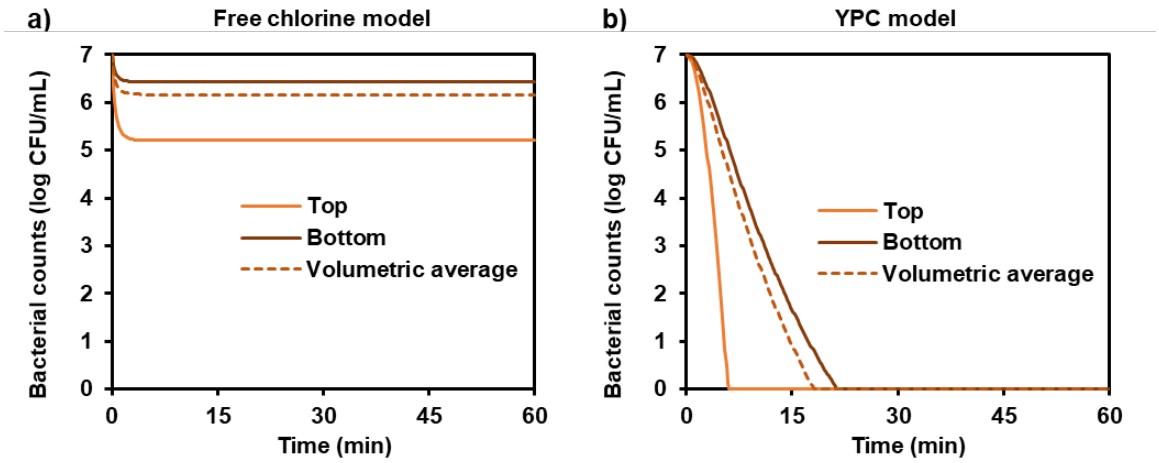

Figure 5.7. Simulated bacterial inactivation in the *E. coli* biofilm of (a) the free chlorine model and (b) the YPC model in the presence of organic matter (chemical oxygen demand = 2 kg/m^3) in the aqueous phase.

5.8.1.2. Influences of binding and release rates on biofilm inactivation efficacy

The results in Figure 5.8a show that with an increase in the binding rate of YPC by 10-fold ($10k_b$), complete biofilm inactivation was achieved in 3.8 min, whereas 16.2 min was required for complete biofilm inactivation based on the original binding rate (k_b) of YPC. Thus, the results show a 4.2-fold increase in the rate of biofilm inactivation with a 10-fold increase in the binding rate. In contrast, reducing the binding rate to 0.1-fold ($0.1k_b$) resulted in only 3.6 log CFU/mL of the *E. coli* cells in the biofilm being inactivated after a 60-min treatment.

On the other hand, the results in Figure 5.8b show the influence of the apparent active release rate of chlorine. With an increase in this release rate of YPC by 10-fold ($10k_{r2}$), complete biofilm inactivation was achieved in 15.7 min. This inactivation time was similar to the original inactivation time acquired for the YPC without changing rate parameters. However, reducing the apparent active chlorine release rate to 0.1-fold ($0.1k_{r2}$) resulted in complete biofilm inactivation within 36 min. Thus, the rate of biofilm inactivation decreased 2.2 times compared to the original YPC microparticles. Overall, the results showed that the binding affinity was a key factor for improving biofilm inactivation, as changes in binding rate could lead to a more critical effect on biofilm inactivation efficacy.

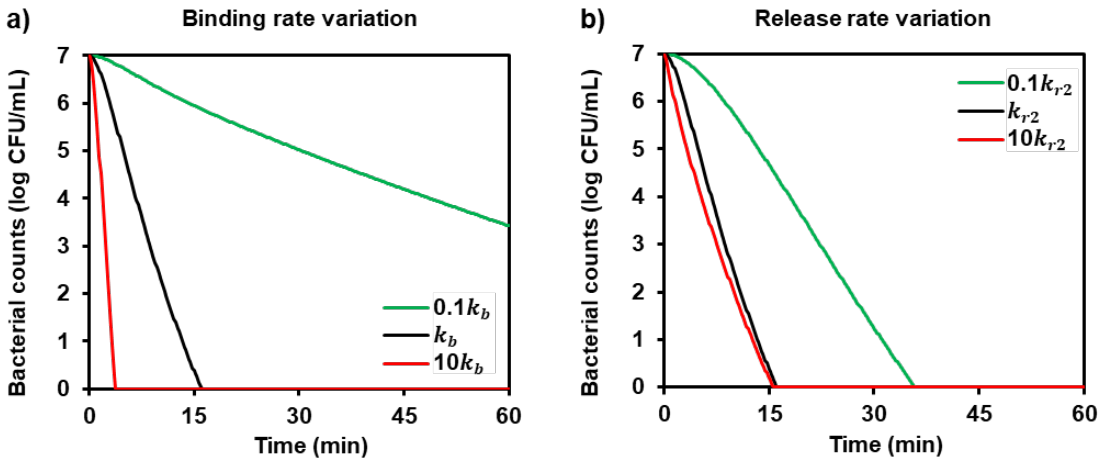

Figure 5.8. Influences of binding affinity and apparent active release rate on simulated biofilm inactivation of the YPC model. Simulated bacterial counts in the biofilm were computed for different (a) binding rates of microparticles to the biofilm (k_b) and (b) apparent active chlorine release rates from the biofilm-bound microparticles at the aqueous/biofilm interface (k_{r2}).

5.8.2. Experimental validation: YPC and YC models

As the parameter evaluation of simulation demonstrated that antibiofilm efficacy was influenced by the binding of yeast microparticles and release of chlorine from them, experimental validation using two different types of yeast microparticles was performed. Both binding and release rates of yeast microparticles can be changed by modifying the formulation using chemical and biological approaches. In this study, YC was achieved by chemical hydrolysis of yeasts, while YPC was further modified by encapsulation of polyethylenimine.

5.8.2.1. Characterization of binding and release properties of YPC and YC particles

The results in Figures 5.9–5.10, and Table 5.2 show the kinetics parameters of the YPC and YC models, which were experimentally measured following the methods in Part 1 of this study (Yi et al., 2021). Results in Figure 5.9 show that approximately 95% and 42% of the fluorescence-YPC and YC particles were bound to the *E. coli* biofilm within 1 h of incubation, respectively. These results demonstrate significant differences ($p < 0.05$) in the binding affinity of two selected yeast microparticles. The binding ratio data were then fitted to the pseudo-first-order kinetics equation (Figure 5.10a) to obtain the binding rates. As indicated in Table 5.2, the binding rate of YPC (6.16×10^{-4} s^{-1}) was 1.4 times faster than that of YC (4.40×10^{-4} s^{-1}). The maximum concentration of biofilm-bound yeast microparticles within 1 h incubation was also measured, and YPC showed a 2.25-times higher level (0.054 kg/m^2) than that of YC (0.024 kg/m^2). The passive release of chlorine was determined by the rate of decrease of chlorine remaining in free yeast microparticles in the aqueous phase. As shown in Figure 5.10b, the data were fitted to the first-order kinetics equation to obtain the passive chlorine release rates. As indicated in Table 5.2, YC showed a faster passive chlorine release rate in the aqueous phase (3.62×10^{-5} s^{-1}) than YPC (1.06×10^{-5} s^{-1}). On the contrary, the apparent active chlorine release rate from biofilm-bound

yeast microparticles was determined by measuring the time and equivalent free chlorine concentration required to inactivate bacteria. The data were fitted to the first-order kinetics equation to calculate the apparent active release rate of chlorine, and the results in Table 5.2 indicate that YPC had a faster apparent active chlorine release rate (4.13×10^{-3} s^{-1}) than YC (3.09×10^{-3} s^{-1}).

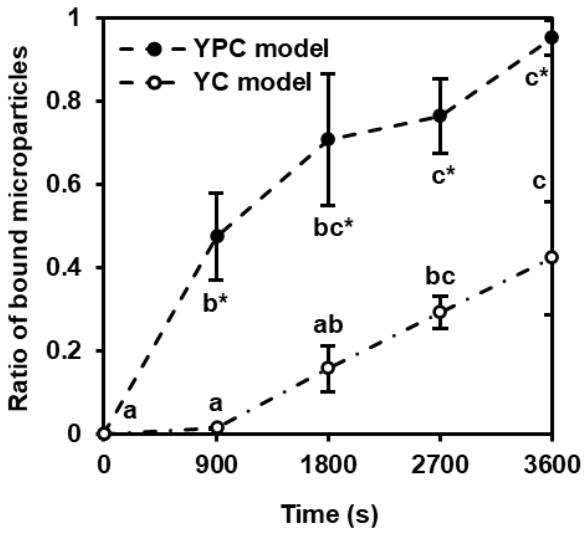

Figure 5.9. Initial binding of the selected yeast microparticles to *E. coli* biofilm. YC: Yeast microparticle–chlorine. The data are mean values and their standard deviations ($n = 3$). Different letters indicate significant differences ($p < 0.05$) between the values within the same model and the asterisks indicate significant differences ($p < 0.05$) among the models.

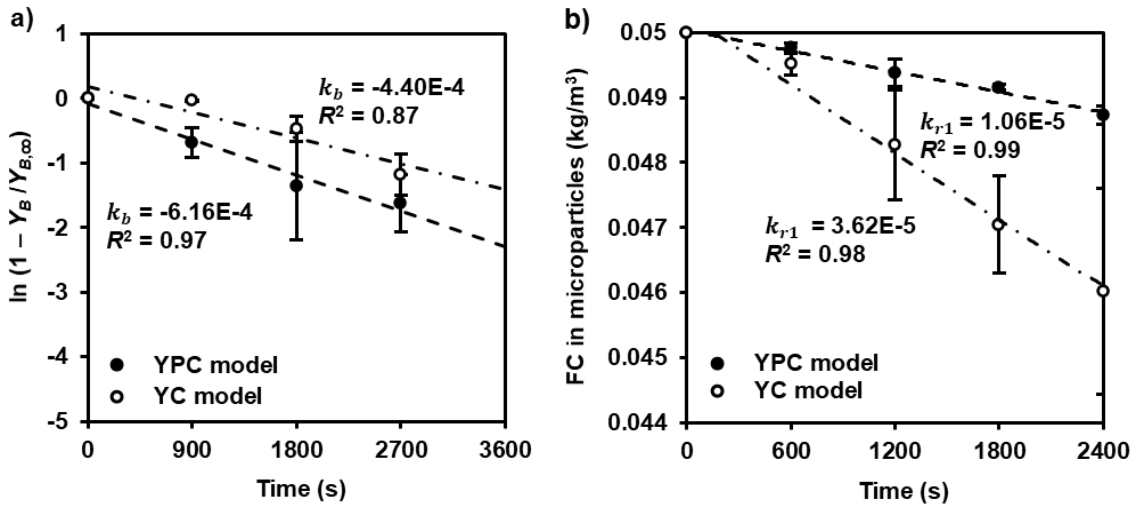

Figure 5.10. Reaction kinetics of the selected antimicrobial yeast microparticles as a function of incubation time: (a) binding of yeast microparticles to *E. coli* biofilms and (b) passive release of chlorine from free yeast microparticles in the aqueous phase. Data were fitted to (a) the pseudo-first-order kinetics equation (dotted lines) with the binding rate k_b, and (b) the first-order kinetics equation (dotted lines) to attain the passive release rate parameter in the aqueous phase k_{r1}. The data are mean values and their standard deviations (n = 3).

5.8.2.2. Simulated and experimental biofilm inactivation

The biofilm inactivation using two different types of yeast microparticles was experimentally measured to validate the model predictions acquired by the simulation results. The results in Figures 5.11a–b illustrate that the overall trends of biofilm inactivation rates acquired by numerical simulation matched the experimental data. The results in Figure 5.11c show strong linear correlations between these simulation and experimental results, with a slope of 1.04 (R^2 = 0.97) and 1.16 (R^2 = 0.89) for the YPC and YC model, respectively. In addition, the time required to achieve bacterial counts under 1 log CFU/mL (the detection limit of experimental measurement) was compared. As shown in Figure 5.11a, simulation results of the YPC model required 13.5 min to obtain bacterial counts under 1 log CFU/mL, while 54.2 min was required for the YC model. Similarly, experimental data in Figure 5.11b shows that the bacterial counts under 1 log CFU/mL were achieved within the first 15 min in the YPC model and approximately 60 min in the YC model. Thus, the mechanistic models developed in this study were experimentally validated, and they supported the dominant influence of binding affinity on antibiofilm activity.

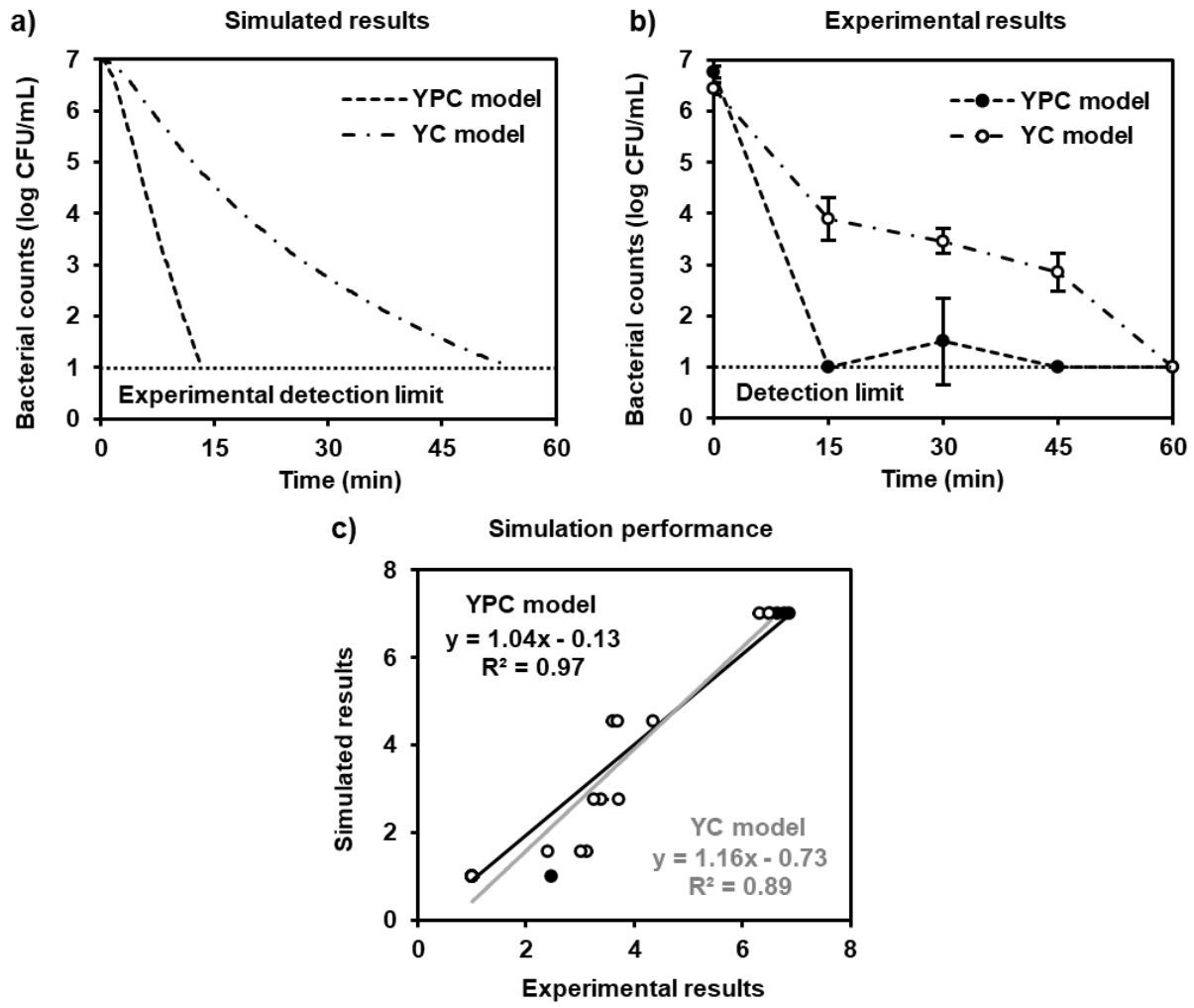

Figure 5.11. *E. coli* biofilm inactivation efficacy of the selected antimicrobial yeast microparticles with different binding affinities: (a) Simulation results, (b) experimental results, and (c) simulation performance. YC: Yeast microparticle–chlorine.

5.9. Discussion

5.9.1. A validated mechanistic model of targeted delivery systems for biofilm inactivation

The mechanistic mathematical model developed in this study combines the influences of chemical stability, binding affinity, and controlled release properties of the particle composition to predict the inactivation of bacteria in a biofilm. The simulation results matched with the experimental results obtained using two different compositions of yeast microparticles. As shown in Figure 5.11, the simulation results using two types of yeast microparticles matched the experimental results, suggesting good reliability of the developed model. Minor differences found between simulated and experimental results may result due to uncertainties in physical and biological properties of the model biofilm, such as porosity, density, and antimicrobial resistance of bacteria to chlorine. Future modeling efforts may be designed to include and validate the role of these factors in influencing the antimicrobial efficacy of the particle-based delivery systems. In general, the results in our study suggest that the mechanistic modeling approach would help to understand the simultaneous effect of each factor on antibiofilm activity, motivate the rational design of the targeted delivery systems for biofilm inactivation, and guide the experimental plans by reducing the number of factors to be considered.

5.9.2. Role of chemical stability of chlorine charged to yeast microparticles

Despite its wide usage in microbial inactivation as an effective sanitizer, chlorine is highly susceptible to organic matter, so that it has been much less effective in inactivating bacteria in biofilms (Meireles, Ferreira, Melo, & Simões, 2017). It was reported that chlorine could be depleted by nonspecific reactions with organic matter both in the biofilm matrix (extracellular polymeric substances and dead bacteria) (Lin, Zhu, Wang, & Yu, 2017) and the aqueous phase

(Ayebah, Hung, Kim, & Frank, 2006; Korany et al., 2018). Conventional approaches to solving this chemical instability of chlorine focused on increasing the total chlorine level in the system (Luo et al., 2011), or adding stabilizers such as T-128 (composed of phosphoric acid and propylene glycol) (Shen et al., 2012). However, the effect of these approaches was limited by the organic matter of high concentration or lettuce extracts and soils (Nou et al., 2011). In contrast, chlorine could be protected from nonspecific reactions with the organic matter when charged to yeast microparticles (Huang et al., 2019). Moreover, the simulation results in Part 1 of this study illustrate that a sufficient level of chlorine was available for biofilm inactivation. Although the released chlorine reacted with organic matter of the biofilm, a highly concentrated source of chlorine in the form of yeast microparticles compensated for this loss. Furthermore, the simulation results in Figures 5.6–5.7 illustrate that the presence of organic matter in the aqueous phase increased the chlorine depletion, and this led to dramatically reduced biofilm inactivation in the free chlorine model when compared to the results in Part 1 of this study. In contrast, there was not much change in the YPC model with or without the presence of organic matter in the aqueous phase. Therefore, it could be concluded that yeast microparticles can reduce challenges with chemical instability of chlorine and improve its delivery to biofilms in the presence of soluble organic matter.

5.9.3. Role of binding affinity of yeast microparticles to the biofilm

In addition to the increased chlorine stability, the binding affinity of yeast microparticles to the biofilm is a key factor in achieving a high chlorine level at the aqueous/biofilm interface. Due to the particle size, the use of yeast microparticles can reduce chlorine mobility compared to its free form. Therefore, it is important to have enough binding affinity that compensates for the reduced mobility by guiding the yeast microparticles to their target destination (Pakulska, Miersch,

& Shoichet, 2016). The results in Figure 5.8a support this idea as the biofilm inactivation efficacy was reduced when the binding rate was reduced to 0.1-fold. Moreover, these results were compared to the results in Figure 5.8b, showing that the binding affinity was a key factor in improving biofilm inactivation. This dominant influence of the binding rate was further validated experimentally using yeast microparticles with varying binding affinities (Figure 5.11). A previous study on mathematical modeling of drug delivery systems reported a similar finding that the binding affinity and the diffusion coefficient of drug carriers were the key parameters in optimizing the drug delivery to the target tumor (Ying, Wang, Lamm, & Kamei, 2013). Experimental studies on biofilm control have also reported the effectiveness of the affinity-based targeted delivery systems; however, none of these biofilm studies has quantitatively addressed the effect of binding affinity (Kim, 2016; Rukavina & Vanić, 2016; Smith, 2005; Suci, Kang, Gmür, Douglas, & Young, 2010). Overall, the results in this study provide a novel quantitative insight into understanding the role of binding affinity in biofilm inactivation.

Moreover, the binding affinity of yeast microparticles can be further increased by modifying the particle formulations. Numerous interactions, including ionic, hydrophobic, van der Waals, hydrogen bonding, are generally associated with the nonspecific binding affinity (Pakulska et al., 2016; Wang & von Recum, 2011). Thus, yeast microparticles can be modified to have a better affinity with target cells based on one of these interactions. In the case of yeast microparticles used in this study, YPC microparticles had a faster binding rate than YC microparticles (Figure 5.10 and Table 5.2) since polyethylenimine encapsulated in YPC contributed to an additional nonspecific electrostatic binding between the particles and negatively charged bacteria in the biofilm (Soto & Ostroff, 2008). For another example, yeast strains with different surface charge and hydrophobicity can be selected as potential biobased particles, and

their binding rates could be compared using our mechanistic modeling approach. Surface modification of yeast microparticles can be an alternative method, where a simple acid washing is known to alter the surface hydrophobicity of an ale-producing *S. cerevisiae* NCYC 1119 (Wilcocks & Smart, 1995). In addition, it was reported that the binding affinity could be affected by the media, pH, and temperature, especially when macromolecules are used (Wang & von Recum, 2011). Thus, future studies may be designed to include the change in binding affinity in different environments.

5.9.4. Role of controlled release of chlorine from yeast microparticles

Unlike the binding process, the apparent active release of chlorine was less influential since it was limited by the diffusion of chlorine. The results in Figure 5.8b show that the rate of biofilm inactivation increased when the apparent active chlorine release rate was raised from $0.1k_{r2}$ to k_{r2}. However, this increase was saturated after that, as the biofilm inactivation rate simulated by using $10k_{r2}$ was similar to the results obtained with the apparent active chlorine release rate of k_{r2}. To address this observation further, the Damköhler number was calculated as follows (Coffel, Gandhi, & Nuxoll, 2016):

$$\mathrm{Da} = \frac{\text{reaction rate}}{\text{mass transport rate}} = \frac{k_{r2} C_0^{n-1} z^2}{D_C} \tag{5.13}$$

Where k_{r2} is the apparent active chlorine release rate from biofilm-bound yeast microparticles (s^{-1}), C_0 is the initial concentration of chlorine, n is the order of reaction ($n = 1$ in this case), z is the thickness of the system (m) ($= z_b + z_w$), and D_C is the diffusivity of chlorine (m^2/s).

The Damköhler number with the apparent active chlorine release rates of $0.1k_{r2}$, k_{r2}, and $10k_{r2}$ were 12.8, 128, and 1280, respectively, which means that the rates of release reaction were faster than the diffusion rate in all three cases ($\mathrm{Da} \geq 10$). Therefore, bacterial inactivation in a

biofilm was limited by the diffusion process, and thus changes in the apparent active chlorine release rate had a limited impact on biofilm inactivation.

5.10. Conclusions

In summary, a mechanistic modeling approach developed in Part 1 of this study was utilized to assess the roles of different factors in the targeted antimicrobial delivery system to *E. coli* biofilms, including the chemical stability of chlorine charged to yeast microparticles, binding affinity of the yeast microparticles to biofilms, and controlled release of chlorine. The binding affinity and chemical stability were key factors influencing the biofilm inactivation efficacy, and this was experimentally validated. The results in this study illustrate the potential use of the validated mechanistic model in evaluating the role of each factor in improving biofilm inactivation. This mechanistic modeling approach could be further extended to design targeted delivery systems using various combinations of antimicrobials other than chlorine and particles with bioaffinity. It would save time and resources by replacing the conventional trial-and-error approaches, as the simulation results may guide experimental plans and enable innovations in material design by focusing on the key factors. This would eventually facilitate the implementation of novel antimicrobial delivery systems for biofilm inactivation in water, food, and environmental applications.

Acknowledgements

This work was supported by the United States Department of Agriculture National Institute of Food and Agriculture [grant number 2015-68003-23411].

References

Ayebah, B., Hung, Y. C., Kim, C., & Frank, J. F. (2006). Efficacy of electrolyzed water in the inactivation of planktonic and biofilm *Listeria monocytogenes* in the presence of organic matter. *Journal of Food Protection*, *69*(9), 2143–2150. https://doi.org/10.4315/0362-028X-69.9.2143

Choi, O., Yu, C. P., Esteban Fernández, G., & Hu, Z. (2010). Interactions of nanosilver with *Escherichia coli* cells in planktonic and biofilm cultures. *Water Research*, *44*(20), 6095–6103. https://doi.org/10.1016/j.watres.2010.06.069

Coffel, J., Gandhi, S., & Nuxoll, E. (2016). Unified polymer erosion model for pulsatile drug delivery. *Journal of Membrane Science*, *512*, 61–72. https://doi.org/10.1016/j.memsci.2016.03.055

Ferreira, C., Rosmaninho, R., Simoes, M., Pereira, M. C., Bastos, M. M., Nunes, O. C., … Melo, L. F. (2010). Biofouling control using microparticles carrying a biocide. *Biofouling*, *26*(2), 205–212. https://doi.org/10.1080/08927010903419630

Ferreira, Carla, Pereira, A. M., Pereira, M. C., Simões, M., & Melo, L. F. (2013). Biofilm control with new microparticles with immobilized biocide. *Heat Transfer Engineering*, *34*(8–9), 712–718. https://doi.org/10.1080/01457632.2012.739040

Forier, K., Raemdonck, K., De Smedt, S. C., Demeester, J., Coenye, T., & Braeckmans, K. (2014). Lipid and polymer nanoparticles for drug delivery to bacterial biofilms. *Journal of Controlled Release*, *190*, 607–623. https://doi.org/10.1016/j.jconrel.2014.03.055

Huang, K., Dou, F., & Nitin, N. (2019). Biobased sanitizer delivery system for improved sanitation of bacterial and fungal biofilms. *ACS Applied Materials & Interfaces*, *11*, 17204–17214. https://doi.org/10.1021/acsami.9b02428

Hwang, G., Liu, Y., Kim, D., Li, Y., Krysan, D. J., & Koo, H. (2017). *Candida albicans* mannans mediate *Streptococcus mutans* exoenzyme GtfB binding to modulate cross-kingdom biofilm development *in vivo*. *PLoS Pathogens*, *13*(6), 1–25. https://doi.org/10.1371/journal.ppat.1006407

Jing, H., Mezgebe, B., Aly Hassan, A., Sahle-Demessie, E., Sorial, G. A., & Bennett-Stamper, C. (2014). Experimental and modeling studies of sorption of ceria nanoparticle on microbial biofilms. *Bioresource Technology*, *161*, 109–117. https://doi.org/10.1016/j.biortech.2014.03.015

Kim, M. H. (2016). Nanoparticle-based therapies for wound biofilm infection: Opportunities and challenges. *IEEE Transactions on Nanobioscience*, *15*(3), 294–304. https://doi.org/10.1109/TNB.2016.2527600

Kogan, G., & Kocher, A. (2007). Role of yeast cell wall polysaccharides in pig nutrition and health protection. *Livestock Science*, *109*, 161–165. https://doi.org/10.1016/j.livsci.2007.01.134

Korany, A. M., Hua, Z., Green, T., Hanrahan, I., El-Shinawy, S. H., El-Kholy, A., … Zhu, M. J. (2018). Efficacy of ozonated water, chlorine, chlorine dioxide, quaternary ammonium compounds and peroxyacetic acid against *Listeria monocytogenes* biofilm on polystyrene surfaces. *Frontiers in Microbiology*, *9*, 1–10. https://doi.org/10.3389/fmicb.2018.02296

Kuroda, K., Ueda, M., Shibasaki, S., & Tanaka, A. (2002). Cell surface-engineered yeast with ability to bind, and self-aggregate in response to, copper ion. *Applied Microbiology and Biotechnology*, *59*, 259–264. https://doi.org/10.1007/s00253-002-1014-8

Li, Q., Mahendra, S., Lyon, D. Y., Brunet, L., Liga, M. V., Li, D., & Alvarez, P. J. J. (2008). Antimicrobial nanomaterials for water disinfection and microbial control: Potential

applications and implications. *Water Research*, *42*(18), 4591–4602. https://doi.org/10.1016/j.watres.2008.08.015

Lin, H., Zhu, X., Wang, Y., & Yu, X. (2017). Effect of sodium hypochlorite on typical biofilms formed in drinking water distribution systems. *Journal of Water and Health*, *15*(2), 218–227. https://doi.org/10.2166/wh.2017.141

Lisle, J. T., Broadaway, S. C., Prescott, A. M., Pyle, B. H., Fricker, C., & Mcfeters, G. A. (1998). Effects of starvation on physiological activity and chlorine disinfection resistance in *Escherichia coli* O157:H7. *Applied and Environmental Microbiology*, *64*(12), 4658–4662. https://doi.org/10.1128/aem.64.12.4658-4662.1998

Loo, C. Y., Rohanizadeh, R., Young, P. M., Traini, D., Cavaliere, R., Whitchurch, C. B., & Lee, W. H. (2016). Combination of silver nanoparticles and curcumin nanoparticles for enhanced anti-biofilm activities. *Journal of Agricultural and Food Chemistry*, *64*(12), 2513–2522. https://doi.org/10.1021/acs.jafc.5b04559

Luo, Y., Nou, X., Yang, Y., Alegre, I., Turner, E., Feng, H., … Conway, W. (2011). Determination of free chlorine concentrations needed to prevent *Escherichia coli* O157:H7 cross-contamination during fresh-cut produce wash. *Journal of Food Protection*, *74*(3), 352–358. https://doi.org/10.4315/0362-028X.JFP-10-429

Meireles, A., Ferreira, C., Melo, L., & Simões, M. (2017). Comparative stability and efficacy of selected chlorine-based biocides against *Escherichia coli* in planktonic and biofilm states. *Food Research International*, *102*, 511–518. https://doi.org/10.1016/j.foodres.2017.09.033

Murphy, H. M., Payne, S. J., & Gagnon, G. A. (2008). Sequential UV- and chlorine-based disinfection to mitigate *Escherichia coli* in drinking water biofilms. *Water Research*, *42*(8–9), 2083–2092. https://doi.org/10.1016/j.watres.2007.12.020

Nam, J. M., Fujita, Y., Arai, T., Kondo, A., Morikawa, Y., Okada, H., … Tanaka, A. (2002). Construction of engineered yeast with the ability of binding to cellulose. *Journal of Molecular Catalysis - B Enzymatic*, *17*(3–5), 197–202. https://doi.org/10.1016/S1381-1177(02)00028-0

Nou, X., Luo, Y., Hollar, L., Yang, Y., Feng, H., Millner, P., & Shelton, D. (2011). Chlorine stabilizer T-128 enhances efficacy of chlorine against cross-contamination by *E. coli* O157:H7 and *Salmonella* in fresh-cut lettuce processing. *Journal of Food Science*, *76*(3). https://doi.org/10.1111/j.1750-3841.2011.02046.x

Pakulska, M. M., Miersch, S., & Shoichet, M. S. (2016). Designer protein delivery: From natural to engineered affinity-controlled release systems. *Science*, *351*(6279). https://doi.org/10.1126/science.aac4750

Peulen, T. O., & Wilkinson, K. J. (2011). Diffusion of nanoparticles in a biofilm. *Environmental Science and Technology*, *45*(8), 3367–3373. https://doi.org/10.1021/es103450g

Rukavina, Z., & Vanić, Ž. (2016). Current trends in development of liposomes for targeting bacterial biofilms. *Pharmaceutics*, *8*(2), 1–26. https://doi.org/10.3390/pharmaceutics8020018

Sharma, P., Panghal, A., Gaikwad, V., Jadhav, S., Bagal, A., Jadhav, A., & Chhikara, N. (2019). Nanotechnology: A Boon for Food Safety and Food Defense. In R. Prasad, V. Kumar, M. Kumar, & D. Choudhary (Eds.), *Nanobiotechnology in Bioformulations* (pp. 225–242). Cham: Springer.

Shen, C., Luo, Y., Nou, X., Bauchan, G., Zhou, B., Wang, Q., & Millner, P. (2012). Enhanced inactivation of *Salmonella* and *Pseudomonas* biofilms on stainless steel by use of T-128, a fresh-produce washing aid, in chlorinated wash solutions. *Applied and Environmental Microbiology*, *78*(19), 6789–6798. https://doi.org/10.1128/AEM.01094-12

Singh, R. S., Bhari, R., & Kaur, H. P. (2011). Characteristics of yeast lectins and their role in cell-cell interactions. *Biotechnology Advances*, *29*(6), 726–731. https://doi.org/10.1016/j.biotechadv.2011.06.002

Smith, A. W. (2005). Biofilms and antibiotic therapy: Is there a role for combating bacterial resistance by the use of novel drug delivery systems? *Advanced Drug Delivery Reviews*, *57*(10), 1539–1550. https://doi.org/10.1016/j.addr.2005.04.007

Soto, E. R., & Ostroff, G. R. (2008). Characterization of multilayered nanoparticles encapsulated in yeast cell wall particles for DNA. *Bioconjugate Chemistry*, *19*(4), 840–848. https://doi.org/10.1021/bc700329p

Srey, S., Jahid, I. K., & Ha, S. Do. (2013). Biofilm formation in food industries: A food safety concern. *Food Control*, *31*(2), 572–585. https://doi.org/10.1016/j.foodcont.2012.12.001

Stratford, M., & Bond, C. J. (1992). Selective separation of microorganisms by lectins: Yeast and concanavalin A as a model system. *Biotechnology and Bioengineering*, *40*(7), 835–843. https://doi.org/10.1002/bit.260400711

Suci, P., Kang, S., Gmür, R., Douglas, T., & Young, M. (2010). Targeted delivery of a photosensitizer to *Aggregatibacter actinomycetemcomitans* biofilm. *Antimicrobial Agents and Chemotherapy*, *54*(6), 2489–2496. https://doi.org/10.1128/AAC.00059-10

Touhami, A., Hoffmann, B., Vasella, A., Denis, F. A., & Dufrêne, Y. F. (2003). Aggregation of yeast cells: Direct measurement of discrete lectin-carbohydrate interactions. *Microbiology*, *149*(10), 2873–2878. https://doi.org/10.1099/mic.0.26431-0

Wang, N. X., & von Recum, H. A. (2011). Affinity-based drug delivery. *Macromolecular Bioscience*, *11*(3), 321–332. https://doi.org/10.1002/mabi.201000206

Wilcocks, K. L., & Smart, K. A. (1995). The importance of surface charge and hydrophobicity for the flocculation of chain-forming brewing yeast strains and resistance of these parameters to acid washing. *FEMS Microbiology Letters*, *134*(2–3), 293–297. https://doi.org/10.1016/0378-1097(95)00422-8

Williams, M. M., & Braun-Howland, E. B. (2003). Growth of *Escherichia coli* in model distribution system biofilms exposed to hypochlorous acid or monochloramine. *Applied and Environmental Microbiology*, *69*(9), 5463–5471. https://doi.org/10.1128/AEM.69.9.5463-5471.2003

Yadav, M. K., Song, J.-J., Singh, B. P., & Vidal, J. E. (2020). Microbial biofilms and human disease: A concise review. In M. K. Yadav & B. P. Singh (Eds.), *New and Future Developments in Microbial Biotechnology and Bioengineering: Microbial Biofilms* (Vol. 1, pp. 1–13). Elsevier. https://doi.org/10.1016/b978-0-444-64279-0.00001-3

Yi, J., Huang, K., & Nitin, N. (2021). Modeling bioaffinity-based targeted delivery of antimicrobials to *Escherichia coli* biofilms using yeast microparticles. Part 1: model development and numerical simulation. Manuscript submitted for publication.

Ying, C. T., Wang, J., Lamm, R. J., & Kamei, D. T. (2013). Mathematical modeling of vesicle drug delivery systems 2: Targeted vesicle interactions with cells, tumors, and the body. *Journal of Laboratory Automation*, *18*(1), 46–62. https://doi.org/10.1177/2211068212458265

CHAPTER 6:

The Role of Leaf Surface Topography at Different Spatial Scales in Antimicrobial Efficacy of Chlorine-Based Sanitizers: Numerical Simulation and Experimental Study

Abstract

The role of leaf surface topography in microbial inactivation by chlorine-based sanitizers was mechanistically characterized. Topomimetic leaf replicasts were developed using polydimethylsiloxane to replicate baby spinach surface structures at different scales, including veins, stomata, and epidermal pavement cells. Based on 3D geometries obtained by leaf replicasts, mass transport and reaction kinetics of chlorine-based sanitizers on the leaf surface were modeled using COMSOL Multiphysics®. The model included passive diffusion of chlorine and its reactions with plant organic matter and *Escherichia coli* O157:H7. Moreover, the model was adapted to evaluate a stabilized chlorine composition using biobased microparticles. Both experimental and computational results showed significant differences ($p < 0.05$) in bacterial reduction on the leaf surfaces with different topographical features. Bacteria in the grooves of the leaf surface were protected against the sanitizers. The stabilized chlorine enhanced antimicrobial efficacy (> 1.3 log reduction, 30 min) by targeted delivery derived from chemical stability and bioaffinity of the microparticles.

Keywords: Surface topography; Leafy greens; *Escherichia coli* O157:H7; Mechanistic modeling; Chlorine; Yeast microparticle

6.1. Introduction

One of the major food safety challenges in fresh produce is the limited effectiveness of sanitizers on bacteria attached to the leaf surface (Gil, Selma, López-Gálvez, & Allende, 2009; Olaimat & Holley, 2012; Wang, Feng, Liang, Luo, & Malyarchuk, 2009). This lack of antimicrobial efficacy on the leaf surface has been attributed to various factors, including sanitizer dose, mass transport of sanitizers by diffusion or fluid flow, leaf surface composition, and leaf surface topography (Fu, Li, Awad, Zhou, & Liu, 2018; Olaimat & Holley, 2012; Zhang et al., 2014). Specifically, the surface properties of leafy greens (i.e., surface composition and topography) may vary with the plant type and could not easily be modified since they are intrinsic factors. However, previous studies had reported that these intrinsic factors could have significant influences on the effectiveness of antimicrobial treatment (Chiu, Shen, Farnham, & Ku, 2020; Palma-Salgado et al., 2020; Wang et al., 2009). These studies demonstrated that despite the use of the same level of sanitizers, bacterial reductions on the leaf surface varied among different plant types. Another study showed that the antimicrobial efficacy of chlorine-based sanitizers was significantly reduced on a leaf-patterned surface compared to a flat one (Zhang et al., 2014). Nevertheless, the individual influences of leaf surface properties on antimicrobial efficacy have not been well addressed because of the entangled complexity of the leaf surface composition and topography.

The surface topography of leafy greens is complex and has multi-scale structures (Doan, Antequera-Gómez, Parikh, & Leveau, 2020; Doan, Ngassam, et al., 2020). In prior studies, researchers have evaluated the influence of these topographical features on the attachment and removal of bacteria (Macarisin, Patel, Bauchan, Giron, & Ravishankar, 2013; Palma-Salgado et al., 2020; Zhang et al., 2014). A conventional way to represent the surface topography of leafy

greens was to use the average surface roughness (Macarisin et al., 2013; Palma-Salgado et al., 2020). However, the average roughness may oversimplify the leaf surface complexity since the interactions between bacteria and leaf surface could be affected by variations in microscale surface structures (Zhang et al., 2014). Macarisin et al. (2013) examined the stomata density of leaf surface to supplement the topographical information represented by the average roughness, but larger-scale surface structures, including veins, were not examined. Moreover, these prior studies used real leaves so that the results could have been influenced by other factors such as epicuticular wax composition. Thus, to assess the influence of leaf surface topography as an individual factor and reflect heterogeneous topographical features, diverse artificial leaf surfaces were developed in previous studies, including solidified agar, micropatterned plastics, and isolated leaf compositions (Doan & Leveau, 2015; Soffe, Bernach, Remus-Emsermann, & Nock, 2019). More recently, several studies reported that leaf replicasts prepared using polydimethylsiloxane (PDMS) could capture the surface topography at a submicron scale (Doan & Leveau, 2015; Doan, Ngassam, et al., 2020; Zhang et al., 2014). Utilizing these leaf replicasts, Zhang et al. (2014) studied *Escherichia coli* inactivation on a spinach leaf surface by chlorine-based sanitizers, and their results showed that bacteria were protected in the grooves and stomata. Similarly, Doan et al. (2020a) reported that *E. coli* survival on a spinach leaf surface was influenced by the leaf venation (the percentage of the surface area of veins). However, despite these advanced efforts to characterize the role of surface topography in bacterial inactivation, there is a limited mechanistic understanding of sanitizer delivery and its chemical interaction with bacteria on the leaf surface.

To the best of our knowledge, experimental studies have been actively conducted to understand the leaf topographical effects on bacterial inactivation, but only one mechanistic study has been done so far (Kinsinger, Mayton, Luth, & Walker, 2017). In this prior study, isolated

epicuticle layers of spinach leaf surfaces were used to investigate the mechanisms of bacterial adhesion and disinfection in a microfluidic flow cell. To further evaluate these mechanisms across the leaf surface, its topographical features were characterized by atomic force microscopy (AFM) and used to model mass transport during a simulated washing process. They reported that the antimicrobial efficacy of chlorine-based sanitizers was influenced by leaf surface topography and was significantly reduced in crevices. This finding highlights the need for understanding the spatial distribution of sanitizers across the leaf surface and their respective microbial inactivation. However, temporal changes by sanitizer reactions were not examined in their model and treated as an initial experimental condition term to describe the bacterial attachment and detachment. Moreover, this prior study used a simplified 2D geometry regenerated from the microscale AFM images acquired near a single stoma where other major leaf surface structures (i.e., veins and epidermal pavement cells) were not included. Since previous experimental studies reported that these structures might also influence the antimicrobial efficacy on the leaf surface (Doan, Antequera-Gómez, et al., 2020; Zhang et al., 2014), it is highly desirable to explore fully represented leaf surface topography. Therefore, there is an unmet need for a mechanistic understanding of the role of leaf surface topography at different spatial scales in the inactivation of bacteria on the leaf surface.

In this study, a mechanistic modeling approach was developed by diffusion mass transport with surface reaction kinetics of chlorine-based sanitizers on distinct sections of the leaf surface. The objectives of this study were to: (i) develop a topomimetic leaf replicast and characterize the multi-scale surface topography; (ii) determine the role of this topography in bacterial inactivation on the leaf surface by numerical approaches and experimental validation; and (iii) evaluate enhanced antimicrobial delivery on the leaf surface using the stabilized chlorine. Different sections

of the leaf surface were characterized using a PDMS-based leaf replicast and represented major topographical features, including veins, stomata, and epidermal pavement cells. *E. coli* O157:H7 was selected as a model pathogen since it is one of the major sources of foodborne outbreaks associated with leafy greens (Marshall et al., 2020; Olaimat & Holley, 2012; Yeni, Yavaş, Alpas, & Soyer, 2016). Free chlorine was selected as a conventional chlorine-based sanitizer. A stabilized chlorine composition was prepared with yeast-derived carriers (yeast microparticles hereafter) following our previous method (Huang, Dou, & Nitin, 2019). This stabilized chlorine was reported to be stable in the presence of organic matter (Huang et al., 2019), preventing nonspecific reactions between plant organic matter and chlorine that could occur when free chlorine is used (Fu et al., 2018; Shen, Luo, Nou, Wang, & Millner, 2013; Weng et al., 2016; Zhou, Luo, Nou, Lyu, & Wang, 2015). Overall, the results of this study demonstrate the role of leaf surface topography in antimicrobial efficacy based on an understanding of the chlorine mass transport and chemical reactions on multi-scale geometries. This would ultimately guide the design of improved antimicrobial systems for washing and sanitation of leafy greens.

6.2. Material and Methods

6.2.1. *Chemicals and reagents*

Acetic acid, acetone, ethanol, glycerol, hydrochloric acid (HCl), isopropanol, n-octadecyltrichlorosilane (OTS), phosphate-buffered saline (PBS), potassium phosphate dibasic (K_2HPO_4), potassium phosphate monobasic (KH_2PO_4), sodium hydroxide (NaOH), sodium thiosulfate, toluene, tryptic soy broth (TSB), and tryptic soy agar (TSA) were purchased from Fisher Scientific (Waltham, MA, USA). Branched polyethylenimine (PEI), calcofluor white stain, maximum recovery diluent (MRD), 10% sodium hypochlorite, and Triton-X 100 were purchased

from Millipore Sigma (St. Louis, MO, USA). Dow Corning Sylgard 184 PDMS elastomer kit was purchased from Ellsworth Adhesive (Germantown, WI, USA). Fleischmann's Active Dry Yeast (*Saccharomyces cerevisiae*) was purchased from a local grocery store. Rifampicin was purchased from TCI America (Portland, OR, USA). Ultrapure water (18 MΩ cm) was obtained using the in-lab Milli-Q RG water ultrapurification system from EMD Millipore (Billerica, MA, USA).

6.2.2. *Fabrication of baby spinach surface topography*

The surface topography of a baby spinach leaf was analyzed using a topomimetic leaf replicast and a combination of microscopy and image analysis. The leaf replicasts were used since they capture all the main features of the real leaf surfaces at a submicron scale (Doan, Ngassam, et al., 2020). In addition, these leaf replicasts could control light scattering caused by pigments on real leaf surfaces that are heterogeneously distributed (Vogelmann and Evans, 2002). Thus, the leaf replicasts could enable the understanding of the individual effect of topographical features on microbial behaviors (Doan, Ngassam, et al., 2020; Soffe et al., 2019).

6.2.2.1. *Preparation of topomimetic baby spinach leaf replicasts*

Baby spinach (*Spinacia oleracea* L. variety Catalina) leaves were grown in the lab in Sunshine mix #1 (Sun Gro Horticulture, Bellevue, WA, USA) under sunlight at an ambient temperature of 23 ± 2 °C and an ambient relative humidity of 50 ± 5%. These leaves were harvested during the daytime under sunlight, and the abaxial sides were used to produce topomimetic leaf replicasts. The abaxial side was chosen in this study since several studies reported that more bacteria attach and survive on this side (Doan, Antequera-Gómez, et al., 2020; Doan, Ngassam, et al., 2020; Olaimat & Holley, 2012; Soffe et al., 2019). For example, the abaxial side

of spinach leaves had significantly ($p < 0.01$) more bacteria attached to the surface than the adaxial side by dip-inoculation (Doan, Ngassam, et al., 2020). Bacteria on abaxial surfaces were also significantly more resistant to removal by water (Doan, Antequera-Gómez, et al., 2020).

The leaf replicasts were prepared using PDMS in a two-step replica casting process (Figure 6.1a), following the method in a prior study (Doan, Ngassam, et al., 2020). First, a negative mold of a baby spinach leaf was obtained using a Sylgard 184 PDMS elastomer kit with mixing ratio of 10:1 (base:curing agent). A freshly harvested leaf was cleaned with a gentle stream of N_2 gas and attached to a plastic Petri dish using 3M double-sided masking tape, with the abaxial side facing upwards. The PDMS mixture was degassed for 15 min in a vacuum desiccator and poured onto the attached leaf surfaces. Any air bubbles trapped in the PDMS mixture were removed with a gentle stream of N_2 gas, and the PDMS mixture was covered and cured at 23 ± 2 °C overnight. After the negative mold was cured, it was cut along the border of the leaf sample and separated from the sample. The trimmed negative molds was washed in a dilute Triton-X 100 solution (1% v/v), rinsed with DI water, and dried with a gentle stream of N_2 gas. Subsequently, this mold was exposed to UV light (UV-F 400 F, 450 W, λ = 187–254 nm) at a distance of 100 mm (UVP, Upland, CA, USA) for 1 h. Right after this treatment, the UV-exposed negative mold was submerged in an OTS/toluene solution (0.1% v/v) for 5 min, rinsed in ethanol for 2 min, and dried at 23 ± 2 °C for > 10 h. This negative mold was then rinsed with DI water, dried, and placed at a glass Petri dish. The degassed PDMS mixture prepared in the same way as above was poured onto the negative mold and cured at 23 ± 2 °C overnight after removing air bubbles.

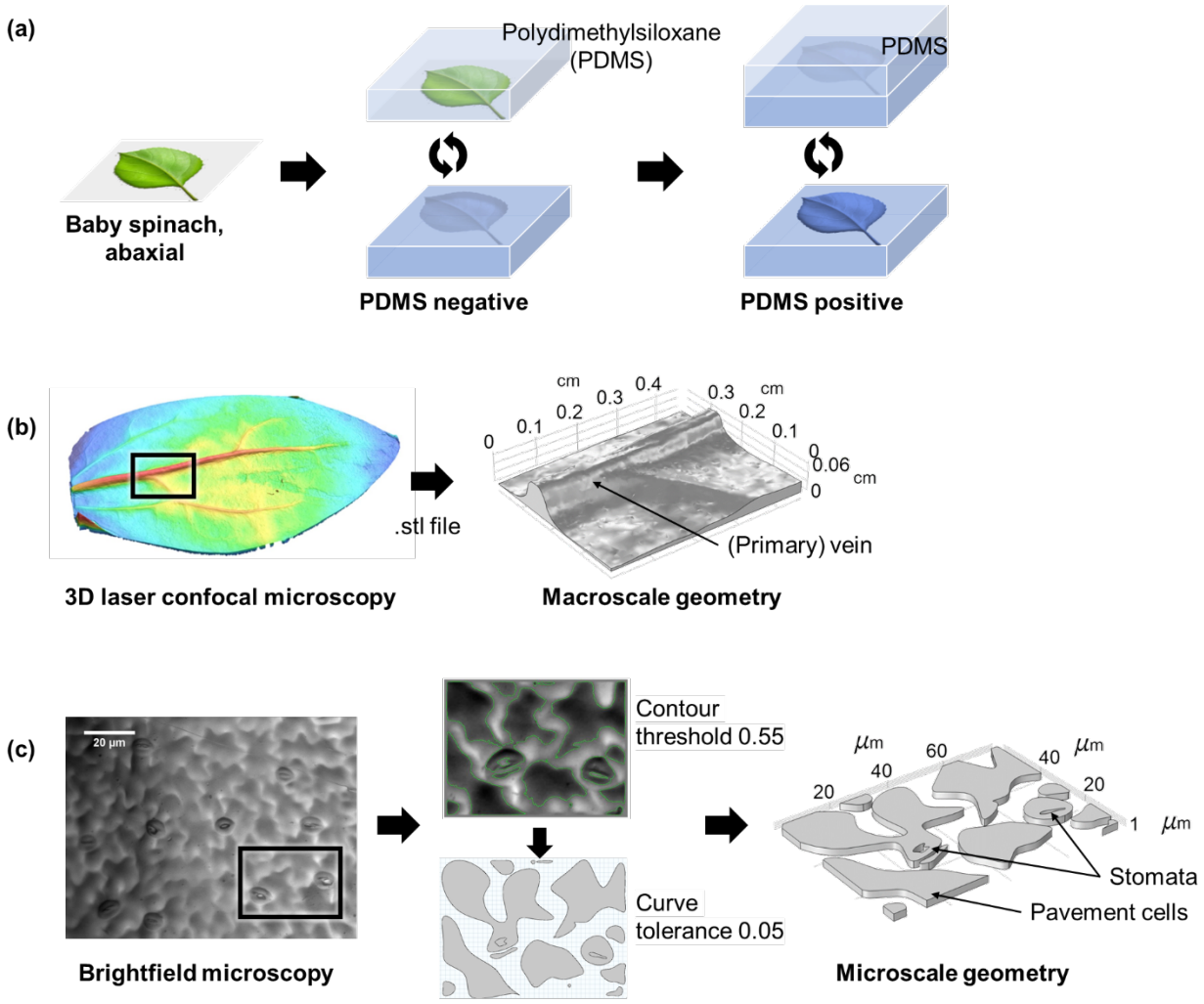

Figure 6.1. Fabrication processes of leaf surface topography. (a) Preparation of baby spinach leaf replicasts using polydimethylsiloxane. (b) Macroscale geometry acquired by 3D laser confocal microscopy (a major structure: primary vein). (c) Microscale geometry acquired by brightfield microscopy (major structures: stomata and epidermal pavement cells).

6.2.2.2. *Geometry acquisition for numerical simulation*

The leaf surface was divided into two sections, i.e., one containing macroscale surface features and the other with only microscale features, for further analyses. The imaging results of this study as well as the literature showed that a leaf surface has multiple scales of topographical features, and the major leaf surface structures include veins, stomata, and epidermal pavement cells (Doan, Ngassam, et al., 2020; Wang et al., 2009). Since primary veins have a much larger scale than stomata or pavement cells, the leaf surface section that contained a primary vein (cm-scale) was referred to as "macroscale geometry", and the one without any veins (μm-scale roughness only) as "microscale geometry" hereafter (Figures 6.1b–6.1c). These macro-and microscale structures were independently examined to understand the influence of the leaf surface heterogeneity on the antimicrobial efficacy.

6.2.2.2.1. *Macroscale geometry*

The macroscale geometry was obtained by scanning a 3D laser confocal microscopic image of the leaf replicast using a 3D profilometer (VR-5000, Keyence, Campbell, CA, USA). A small section of the acquired image representing the primary vein structure was selected and converted to an STL file (Figure 6.1b). This STL file was then imported to COMSOL Multiphysics® software version 5.6 (or simply COMSOL) as a leaf surface. This leaf surface was enclosed by a block and then partitioned to achieve the final geometry shown in Figure 6.1b ($0.46 \times 0.38 \times 0.066$ cm^3). In this macroscale geometry, leaf surface structures in micro-size (i.e., stomata and pavement cells) were smoothed due to the selected imaging resolution.

6.2.2.2.2. *Microscale geometry*

As shown in Figure 6.1c, the microscale geometry was obtained from a 2D brightfield microscopic image of the leaf replicast (top view) using an optical microscope (Olympus IX-7, Olympus, Center Valley, PA, USA) with a 20× objective (Olympus UPlanFL, Olympus). A small section of the image containing the stomata and pavement cells was selected and imported as a JPG file to COMSOL. The Image to Curve add-in of COMSOL was used to convert the microscopic image to a geometry where differential equations could be computed. Briefly, the image was simplified and the edges were smoothed yet representing the major structures by using the Gaussian blur, applying the contour threshold of 0.55 and the curve tolerance of 0.05. The converted 2D geometry was then extruded using the average roughness of the baby spinach to acquire the final geometry, as shown in Figure 6.1c ($77 \times 55 \times 2.27$ μm^3).

6.2.3. *Model development*

The transport processes of chlorine-based sanitizers and inactivation of bacteria on the leaf surface were numerically simulated using COMSOL based on natural diffusion and reaction kinetics. A conventional system was represented by a free chlorine model, while a targeted delivery system was represented by a stabilized chlorine model. In the latter case, yeast microparticles were used to charge chlorine, which could increase the chemical stability of chlorine but slow down diffusion (Huang et al., 2019). In both cases, geometries with two different scales acquired from Section 6.2.2.2 were used. The microbial concentration was modeled as a surface concentration term uniformly distributed on the leaf surface. All the variables and parameters used in Eqs. 6.1–6.6 are indicated in Tables 6.1 and 6.2, respectively. For the results, spatiotemporal chlorine concentration was computed in terms of free chlorine or equivalent free chlorine (See

Section 6.2.3.2.1) for the free chlorine model and the stabilized chlorine model, respectively. The resulting bacterial counts on the leaf surfaces were also computed.

Table 6.1. List of variables

Symbol	Description	Units
$B(t)$	Live bacterial concentration on the leaf surface	kg/m^2
$C(t)$	Free chlorine concentration in the aqueous phase	kg/m^3
$O_B(t)$	Organic matter concentration from dead bacteria on the leaf surface	kg/m^2
$S(t)$	Stabilized chlorine concentration in the aqueous phase	kg/m^3
$S_{\mathrm{b}}(t)$	Concentration of stabilized chlorine bound to bacteria on the leaf surface	kg/m^2

All the variables are nonnegative.

Table 6.2. List of input parameters used in the numerical models

Symbol	Description	Value	Units	Source
B_0	Initial bacterial load on the leaf surface	9.5×10^{-7}	kg/m^2	Calculated [a]
C_0	Initial concentration of free chlorine	0.1	kg/m^3	Assumed
D_C	Diffusivity of free chlorine	1.0489×10^{-9}	m^2/s	(Chao, 1968)
D_S	Diffusivity of stabilized chlorine [b]	8.584×10^{-14}	m^2/s	(Ju, Liu, Yang, & Sun, 2014)
k_0	Natural decay rate of free chlorine	2.83×10^{-5}	s^{-1}	(Munther, Luo, Wu, Magpantay, & Srinivasan, 2015)
k_1	Free chlorine depletion rate by nonspecific reactions with organic matter	8.97×10^{-3}	m^3/(kg·s)	(Munther et al., 2015)
k_b	Binding rate of stabilized chlorine to bacteria	7×10^{-4}	s^{-1}	(Yi, Huang, & Nitin, 2021a)
k_C	Bacterial inactivation rate by free chlorine	12.5	m^3/(kg·s)	(Munther et al., 2015)
k_S	Bacterial inactivation rate by stabilized chlorine	5.789	m^2/(kg·s)	(Huang et al., 2019)
m_B	Mass of an *E. coli* cell	9.5×10^{-16}	kg	(Neidhardt, Ingraham, & Schaechter, 1990)
O_l	Plant organic matter on the leaf surface	1.41×10^{-2}	kg/m^2	Estimated [c]
S_0	Initial concentration of stabilized chlorine [d]	20	kg/m^3	(Huang et al., 2019)
$z_{\mathrm{l}1}$	Maximum height of leaf surface in macroscale geometry	6.52×10^{-4}	m	Measured
$z_{\mathrm{l}2}$	Maximum height of leaf surface in microscale geometry [e]	2.27×10^{-6}	m	(Kinsinger et al., 2017)
$z_{\mathrm{w}1}$	Height of aqueous phase in macroscale geometry	6.52×10^{-3}	m	Assumed [f]
$z_{\mathrm{w}2}$	Height of aqueous phase in microscale geometry	2.27×10^{-5}	m	Assumed [f]

[a] $B_0 = 10^9$ CFU $\times m_B$ [b] Diffusivity of yeast cells was used since the stabilized chlorine was composed of yeast microparticles. [c] The value was derived by the level of plant organic matter of an entire baby spinach leaf, 46400 mg/L COD (Weng et al., 2016), and the leaf thickness of 303 ± 50 μm (measured). [d] Equivalent to the initial concentration of free chlorine. [e] Average roughness of baby spinach without major leaf veins. [f] 10-fold of the maximum height of leaf surface.

As shown in Tables 6.1–6.2, the units of the variables and parameters used in this study were based on the mass concentration. However, COMSOL only allowed molar concentrations in computing chemical reactions. Thus, all the input parameters and output results were treated as mass concentrations using the following method: (i) A factor of 1 mol/kg was multiplied to input parameters with units of mass concentration, i.e., initial conditions; and (ii) a factor of 1 kg/mol was multiplied to second-order reaction rate parameters or the simulation results. This process crossed out molar concentration units and enabled mass-based computation using COMSOL. For bacterial counts on the leaf surface, the final results were further converted to be compared with experimental results. The data obtained in the simulation were expressed in the unit of mass concentration on the leaf (kg/m^2), and these were converted to the standard unit in the experimental microbiological analysis (CFU/cm^2) based on the mass of an *E. coli* cell (see Table 6.2).

6.2.3.1. *Free chlorine model – a conventional system*

The overall model descriptions of the free chlorine model are shown in Figure 6.2, including geometry, assumptions, governing equations, boundary conditions, and mesh.

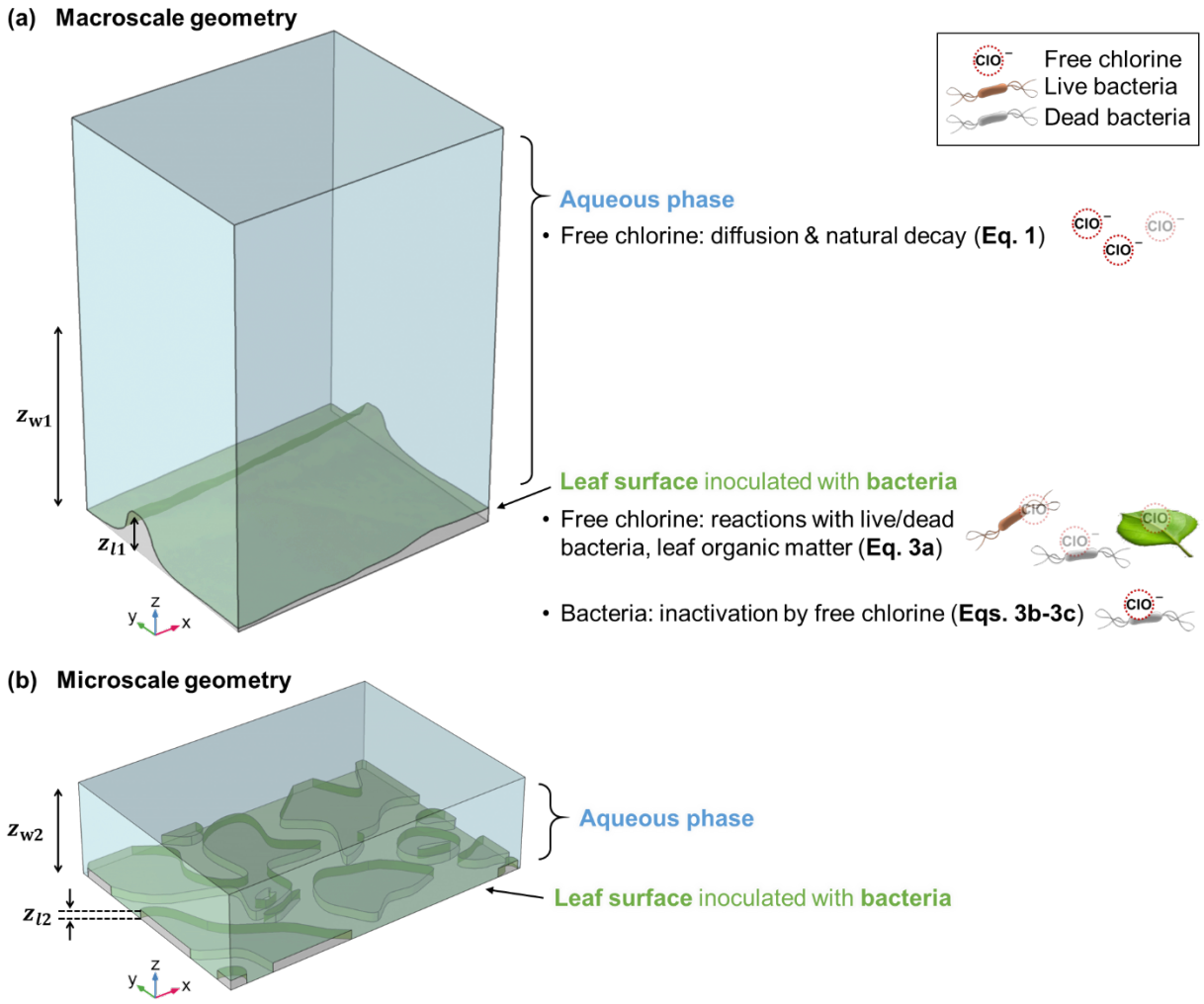

Figure 6.2. Geometry, assumptions, and mesh of the free chlorine model. (a) Macroscale geometry and (b) microscale geometry. The assumptions used in (a) were applied to the corresponding domain and boundaries of (b). In both cases, no flux condition was applied to the boundaries except the leaf surface.

6.2.3.1.1. *Governing equations*

The mass balance of free chlorine in the aqueous phase was expressed as a combination of diffusion and reaction. In the aqueous domain, the reaction term included natural decay of free chlorine, and the rate of change of free chlorine in this domain was as follows:

$$\frac{\partial C(t)}{\partial t} = D_C \nabla^2 C(t) - k_0 C(t) \tag{6.1}$$

where $C(t)$ is the free chlorine concentration in the aqueous phase (kg/m^3), t is the time (s), D_C is the diffusivity of free chlorine (m^2/s), and k_0 is the natural decay rate of free chlorine (s^{-1}).

6.2.3.1.2. *Initial and boundary conditions*

It was assumed that free chlorine [$C(t)$] was homogeneously distributed in the aqueous domain, bacteria were inoculated on the leaf surface, and there were no dead bacteria at $t = 0$. Thus, the initial conditions in the aqueous phase (Eq. 6.2a) and on the leaf surface (Eqs. 6.2b–c) were as follows:

$$\begin{cases} C(t=0) = C_0 & (6.2a) \\ B(t=0)|_{\text{leaf}} = B_0 & (6.2b) \\ O_B(t=0)|_{\text{leaf}} = 0 & (6.2c) \end{cases}$$

Where $B(t)$ is the live bacterial concentration on the leaf surface (kg/m^2), and $O_B(t)$ is the organic matter concentration from dead bacteria on the leaf surface (kg/m^2). The values for C_0 and B_0 are indicated in Table 6.2.

On the leaf surface, the following reactions were modeled: (i) Free chlorine [$C(t)$] consumption by reactions with live bacteria, dead bacteria, and plant organic matter (Eq. 6.3a); (ii) Inactivation of live bacteria [$B(t)$] by free chlorine (Eq. 6.3b); (iii) Increase of dead bacteria [$O_B(t)$] by bacterial inactivation (Eq. 6.3c). The net growth and death of bacteria were assumed to be negligible since the treatment times in this study were no longer than 30 min.

$$\begin{cases} \left.\frac{\partial C(t)}{\partial t}\right|_{\text{leaf}} = -k_1\,[B(t) + O_B(t) + O_l]C(t) & (6.3a) \\ \left.\frac{\partial B(t)}{\partial t}\right|_{\text{leaf}} = -k_C C(t)B(t) & (6.3b) \\ \left.\frac{\partial O_B(t)}{\partial t}\right|_{\text{leaf}} = k_C C(t)B(t) & (6.3c) \end{cases}$$

where O_l is the plant organic matter concentration on the leaf surface (kg/m^2), k_1 is the free chlorine depletion rate by nonspecific reactions with organic matter (live/dead bacteria and plant materials) [m^3/(kg·s)], and k_C is the bacterial inactivation rate by free chlorine [m^3/(kg·s)]. For the boundaries other than the leaf surface, no flux condition was applied.

6.2.3.2. *Stabilized chlorine model – a targeted delivery system*

The stabilized chlorine used in this study was prepared by forming *N*-halamine compositions with yeast microparticles to chemically bind chlorine (See Section 6.2.4.2). The major differences of this stabilized chlorine compared to the conventional free chlorine are as follows: (i) It does not react with organic matter; (ii) It has a specific binding affinity to bacteria; (iii) Its bacterial inactivation rate is different from that of free chlorine (Huang et al., 2019), and this depends on the concentration of stabilized chlorine bound to bacteria (see Section 6.2.3.2). The overall model descriptions of the stabilized chlorine model are shown in Figure 6.3.

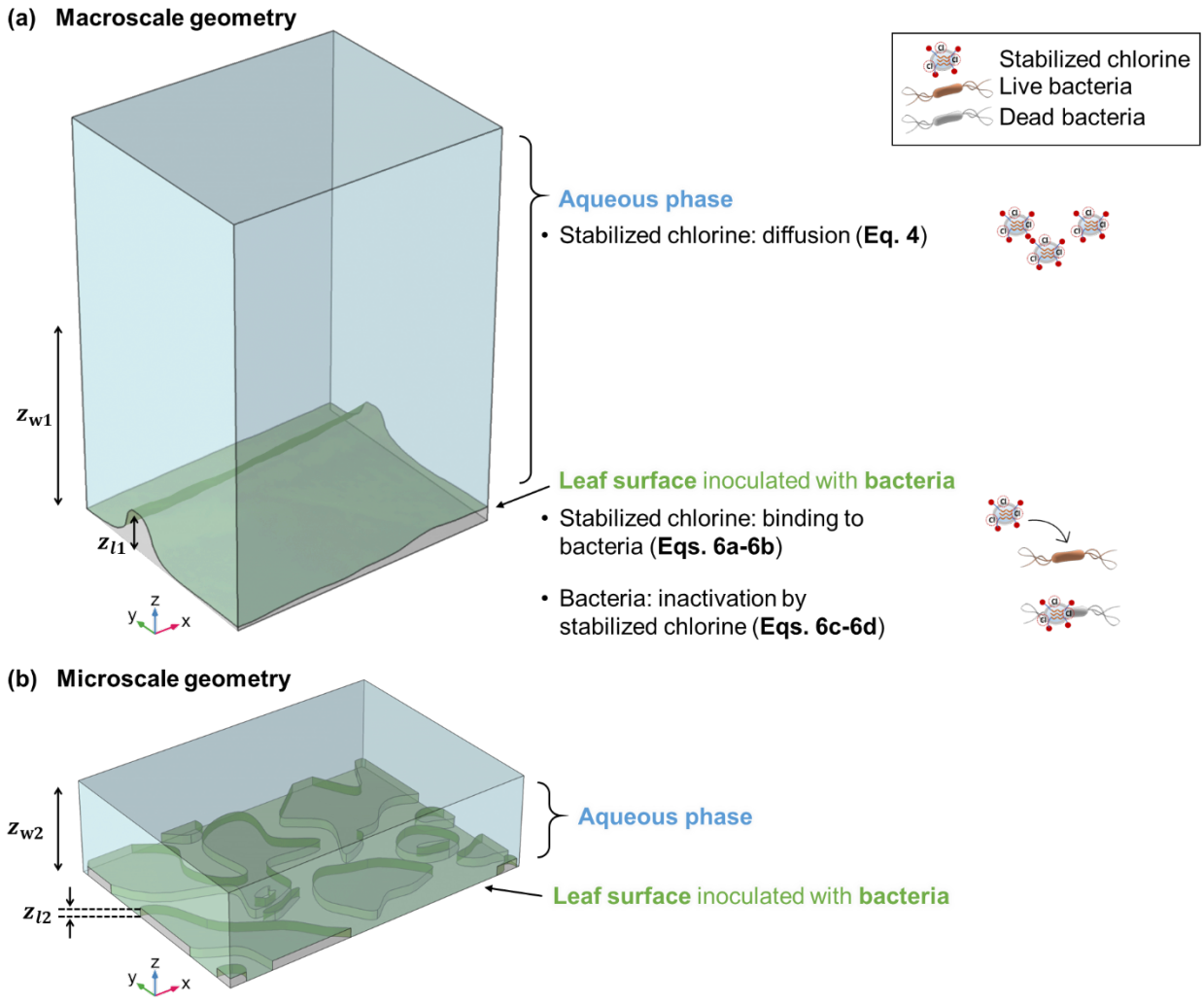

Figure 6.3. Geometry, assumptions, and mesh of the stabilized chlorine model. (a) Macroscale geometry and (b) microscale geometry. The assumptions used in (a) were applied to the corresponding domain and boundaries of (b). In both cases, no flux condition was applied to the boundaries except the leaf surface.

6.2.3.2.1. *Governing equations*

The mass balance of the stabilized chlorine in the aqueous domain was expressed by its diffusion, where the diffusivity followed that of yeasts (See Table 6.2). and the reaction term was omitted in this case since the natural loss of the stabilized chlorine was negligible within the treatment time of < 30 min (Yi, Huang, & Nitin, 2021a, 2021b):

$$\frac{\partial S(t)}{\partial t} = D_S \nabla^2 S(t) \tag{6.4}$$

where $S(t)$ is the stabilized chlorine concentration in the aqueous phase (kg/m^3), and D_S is the diffusivity of the stabilized chlorine (m^2/s).

6.2.3.2.2. *Initial and boundary conditions*

It was assumed that the stabilized chlorine [$S(t)$] was homogeneously distributed in the aqueous domain, and none of them were bound to bacteria on the leaf surface at $t = 0$. Assumptions for inoculated live bacteria [$B(t)$] and initial dead bacteria [$O_B(t)$] were the same as the free chlorine model (See Section 6.2.3.1.2). Thus, the initial conditions in the aqueous phase (Eq. 6.5a) and on the leaf surface (Eqs. 6.5b–d) were as follows:

$$\begin{cases} S(t=0) = S_0 & (6.5a) \\ S_b(t=0)|_{\text{leaf}} = 0 & (6.5b) \\ B(t=0)|_{\text{leaf}} = B_0 & (6.5c) \\ O_B(t=0)|_{\text{leaf}} = 0 & (6.5d) \end{cases}$$

where $S_b(t)$ is the concentration of the stabilized chlorine bound to bacteria on the leaf surface (kg/m^2) (see Table 6.2 for S_0 and B_0).

On the leaf surface, the following reactions were modeled based on our prior experimental observations (Yi, Huang, & Nitin, 2021a, 2021b): (i) A specific binding reaction of the stabilized chlorine to bacteria on the leaf surface followed first-order kinetics. The concentration of the

stabilized chlorine in the aqueous phase [$S(t)$] decreased due to this binding, and the bacteria-bound concentration of the stabilized chlorine on the leaf surface [$S_b(t)$] increased accordingly (Eqs. 6.6a–b); (ii) Live bacteria [$B(t)$] were then inactivated by direct contact with by the bacteria-bound stabilized chlorine (Eq. 6.6c); (iii) The concentration of dead bacteria [$O_B(t)$] increased as a result of bacterial inactivation (Eq. 6.6d). The bacterial inactivation by the stabilized chlorine can be attributed to both direct contact of chlorine-bound yeast microparticles with bacteria and chlorine actively released from the microparticles upon binding the bacteria (Dong, Wang, Gao, Gao, & Gao, 2017; Huang et al., 2019). Since the treatment time in this study was relatively short (< 30 min), these two mechanisms were combined and simplified to represent the apparent bacterial inactivation rate (see Table 6.2). It was assumed that the stabilized chlorine did not react with the organic matter based on preliminary study (data not shown).

$$\begin{cases} \left.\frac{\partial S(t)}{\partial t}\right|_{\text{leaf}} = -k_b S(t) & (6.6a) \\ \left.\frac{\partial S_b(t)}{\partial t}\right|_{\text{leaf}} = k_b S(t) & (6.6b) \\ \left.\frac{\partial B(t)}{\partial t}\right|_{\text{leaf}} = -k_S S_b(t) B(t) & (6.6c) \\ \left.\frac{\partial O_B(t)}{\partial t}\right|_{\text{leaf}} = k_S S_b(t) B(t) & (6.6d) \end{cases}$$

where k_b is the binding rate of the stabilized chlorine to bacteria (s^{-1}), k_S is the bacterial inactivation rate by the stabilized chlorine [$m^2/(kg \cdot s)$]. For the boundaries other than the leaf surface, no flux condition was applied.

The bacterial inactivation rate of the stabilized chlorine was measured by assuming second-order kinetics (Eq. 6.6c) with excess stabilized chlorine. The second-order kinetics was used as an analogy to the bacterial inactivation of the conventional free chlorine (Eq. 6.3b). The results in our prior study showed that the bacterial inactivation of the stabilized chlorine could follow first-order

kinetics, but this could be attributed to the highly localized chlorine concentration of the stabilized chlorine composition. Thus, assuming that the stabilized chlorine is in excess (i.e., a constant S_b), the first-order reaction rate parameters for bacterial inactivation (k_S' of Eq. 6.7a) were further measured at different S_b concentrations (1, 3, 5, 10, and 20 kg/m^3). Then, the concentration dependency of these parameters was determined (Eq. 6.7b) to obtain the second-order reaction rate parameter (k_S).

$$\left.\frac{\partial B(t)}{\partial t}\right|_{\text{leaf}} = -k_S S_b(t) B(t) = -(k_S S_b) B(t) = -k_S' B(t) \tag{6.7a}$$

$$k_S' = k_S S_b \tag{6.7b}$$

In this model, the resulting level of the stabilized chlorine on the leaf surface [$S_b(t)$] was converted to the equivalent free chlorine concentration for comparison purposes. This conversion was achieved by multiplying the ratio of the concentration of free chlorine initially bound to yeast microparticles (C_0) to that of yeast microparticles (S_0), i.e., $S_b(t) \times C_0/S_0$.

6.2.3.3. *Computational mesh convergence*

The mesh convergence was tested to confirm that simulation results are independent of the meshes, and the convergence criteria were set to 0.005 (the difference between simulation results from two sequential meshes be less than 0.5%). For both the geometries, the initial computational meshes were designed using free tetrahedral meshes with the predefined size of normal and fine in the aqueous domain and at the leaf surface boundary, respectively. These initial meshes were further refined by a COMSOL-provided adaptive mesh refinement algorithm (longest edge refinement method). This algorithm determines the longest edge of the mesh elements that have the largest errors, and then bisect this longest edge to increase the mesh element number (Chandler et al., 2011; COMSOL, 2008). The final mesh for each model is indicated in Table 6.3.

Table 6.3. The final mesh information used in numerical simulation

Geometry	Number of elements				Average element quality [a]
	Tetrahedral	Triangular	Edge	Vertex	
Macroscale	45396	8474	304	9	0.6276
Microscale	66440	14947	1515	101	0.5296

[a] The mesh quality greater than 0.3 should not affect the quality of the solution (COMSOL, 2008; Lin et al., 2017; Santos et al., 2011).

6.2.4. *Experimental validation*

6.2.4.1. *Bacterial strain, media, and culture*

A rifampicin-resistant and Shiga toxin-negative *E. coli* O157:H7 (ATCC 700728) (*E. coli*) was provided by Dr. Linda Harris (University of California-Davis, USA) and stored frozen (–80 °C) in sterile TSB supplemented with 15% v/v glycerol. The bacteria were then streaked onto TSA supplemented with 50 μg/mL rifampicin and grown at 37 °C for 24 h before use. One colony was isolated from the agar plate, cultured in 10 mL of sterile TSB with a constant shaking of 250 rpm at 37 °C for 18 h to reach the stationary phase. This bacterial culture was then washed three times using centrifugal separation at 3100 × g/23 °C for 8 min, and the pellet was resuspended in 10 mL of sterile PBS between each cycle. The concentration of the bacterial suspension assessed by plate counting was approximately 9 log CFU/mL, and this was serially diluted with sterile PBS to achieve the inoculation level of 6 log CFU/mL for further use.

6.2.4.2. *Preparation of the stabilized chlorine*

The stabilized chlorine was prepared using yeast-derived carriers by the methods described in our previous studies (Huang et al., 2019; Yi, Huang, & Nitin, 2021a). Briefly, yeast microparticles were obtained by chemical hydrolysis of baker's yeast (Fleischmann's Active Dry Yeast) using NaOH and HCl. Polyethylenimine was then encapsulated into these yeast microparticles by vacuum infusion to acquire the high chlorine loading capacity and binding affinity to target bacteria. These polyethylenimine-encapsulated yeast microparticles were immersed in a dilute sodium hypochlorite solution (1% v/v) for 1 h to charge chlorine by forming *N*-halamine compositions. The final form of the stabilized chlorine was obtained as yeast microparticles–polyethylenimine–chlorine.

6.2.4.3. *Baby spinach inoculation and chlorine-based treatments*

In this section, real baby spinach leaves were used to account for the reactions between free chlorine and the plant organic matter. The leaves were inoculated with *E. coli* by droplet-spreading, following the method in our prior study (Yi, Huang, Ma, et al., 2021). Briefly, the leaves washed with sterile deionized (DI) water (5 × 5 cm^2) were inoculated with 0.5 mL of bacterial suspension (6 log CFU/mL) using a sterile cell spreader. After 1-h incubation at 23 °C to allow bacterial attachment, the leaves were cut into discs with a 1-cm diameter using a sterile borer. The discs were taken at different spots of the leaves to represent each geometry. A zone near the stem containing the primary vein was selected for the macroscale geometry, while a relatively smooth and flat zone without any veins was chosen for the microscale geometry. The leaf samples were rinsed with 1 mL of sterile DI water by a quick dip to wash off loosely attached bacteria prior to treatment.

The inoculated leaf samples were placed in each well of a sterile 24-well plate (Corning Inc., Corning, NY, USA) for chlorine-based treatments. To achieve the datasets corresponding to the free chlorine or stabilized chlorine model, respectively, 100 mg/L (or 10 kg/m^3 in SI unit) of sodium hypochlorite solution or 20 g/L (or 20 kg/m^3 in SI unit) of the stabilized chlorine was used. The concentration of the stabilized chlorine was set to be equivalent to that of free chlorine in terms of total chlorine concentration, and this was determined based on the experimental results of our prior study (Huang et al., 2019). 1 mL of these chlorine-based treatment solutions were added to each well for different times (0, 5, 10, 20, and 30 min), and the leaf samples were collected for microbiological assay. For the negative controls, 1 mL of sterile DI water was used instead of

the chlorine-based sanitizers. These were used to normalize the datasets to reflect the bacterial loss caused by experimental conditions other than the chlorine effect.

6.2.4.4. *Microbiological assay*

The number of viable bacteria on the leaf surface was determined by the MRD-based bacterial recovery and the plate counting, following the method in our previous study (Yi, Huang, Ma, et al., 2021). To recover the bacteria from the leaf surface and quench the remaining chlorine after the treatment, each leaf sample was immersed in 1 mL of sterile MRD supplemented with 1% w/v sodium thiosulfate for 2 min, and then vortexed at full speed for 1 min. The isolated bacterial suspension was plated on a TSA supplemented with 50 μg/mL rifampicin with serial dilution. The agar plates were incubated at 37 °C for 24 h before enumeration. The colony forming units (CFU) on the plates were counted and then converted to log CFU/cm^2 based on the surface area of the leaf sample. The detection limit was determined by converting 1 CFU/agar plate into log CFU/cm^2, i.e., 1.1 log CFU/cm^2.

6.2.4.5. *Statistical analysis*

The datasets obtained by measurements were evaluated using the SPSS Statistics software (version 27, IBM SPSS, Chicago, IL, USA), and the significant differences ($p < 0.05$) were determined by one-way analysis of variance, followed by Tukey's pairwise comparisons. All the experiments were performed in triplicates.

6.3. Results

6.3.1. *Simulation results of the free chlorine model*

As shown in Figure 6.1b–c, the surface topography of baby spinach leaf was successfully replicated at a submicron scale by following the two-step replica casting process reported in the prior study (Doan, Ngassam, et al., 2020). This topography profile was then coupled with the mass transport of free chlorine to understand its role in the inactivation of bacteria on the leaf surface. The mass transport process of free chlorine was characterized as a combination of diffusion and its competing reactions with bacteria or plant organic matter based on the continuum assumptions (see Section 6.2.3.1).

6.3.1.1. *Bacterial inactivation on the leaf surface with different geometries*

The simulation results in Figure 6.4a show the spatiotemporal free chlorine distribution on the leaf surface in the free chlorine model, which represented a conventional leaf sanitation system (see Section 6.2.3.1). Given the same free chlorine concentration in the aqueous phase, the initial surface average concentrations on the leaf surface for the macro-and microscale geometries were 4.78 and 0.075 μg/cm^2, respectively. These levels were rapidly depleted within the first few seconds (reduced to 0.098 and 0.0011 μg/cm^2 within 1 s, respectively). Similarly, the simulation results in Figure 6.4b show the number of bacteria on the leaf surface exposed to the free chlorine treatment. As a result of the free chlorine delivery to the leaf surface, the surface average number of bacteria on the leaf with the macroscale geometry gradually decreased to 4.3 log CFU/cm^2 from an initial load of 5 log CFU/cm^2, corresponding to 0.7-log reduction. In contrast, due to the rapid depletion of free chlorine on the leaf surface with the microscale geometry, no log reduction was achieved. In sum, a conventional free chlorine system resulted in < 1 log reduction on the

macroscale geometry and did not inactivate bacteria on the microscale geometry, due to the rapid depletion of free chlorine on the leaf surfaces.

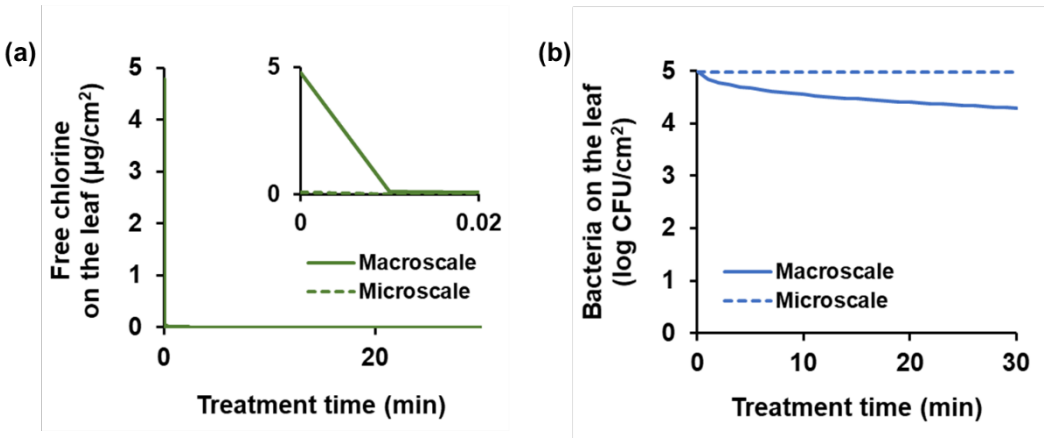

Figure 6.4. Simulated bacterial inactivation on the leaf surface with different geometries using free chlorine: (a) The free chlorine concentration and (b) the number of bacteria on the leaf surface during free chlorine treatment.

6.3.1.2. *Spatial distributions of bacteria remaining on the leaf surface*

Moreover, the simulated spatial distributions of bacteria were mapped for both macro-and microscale geometries to determine the role of leaf surface topography in antimicrobial efficacy. The results in Figure 6.5a show the changes in the number of bacteria on the leaf surfaces after the first 20 min of free chlorine treatment, while Figure 6.5b show their respective surface topography from the top view. For the macroscale geometry, more bacteria survived near the sides of the vein structures. Similarly, as shown in Figure 6.5c, more bacteria survived in the microscale grooves, especially near the walls of the pavement cells and inside the stomata. Overall, bacteria in the macroscale crevices along protruding veins and in the microscale grooves of the leaf surface survived better against free chlorine.

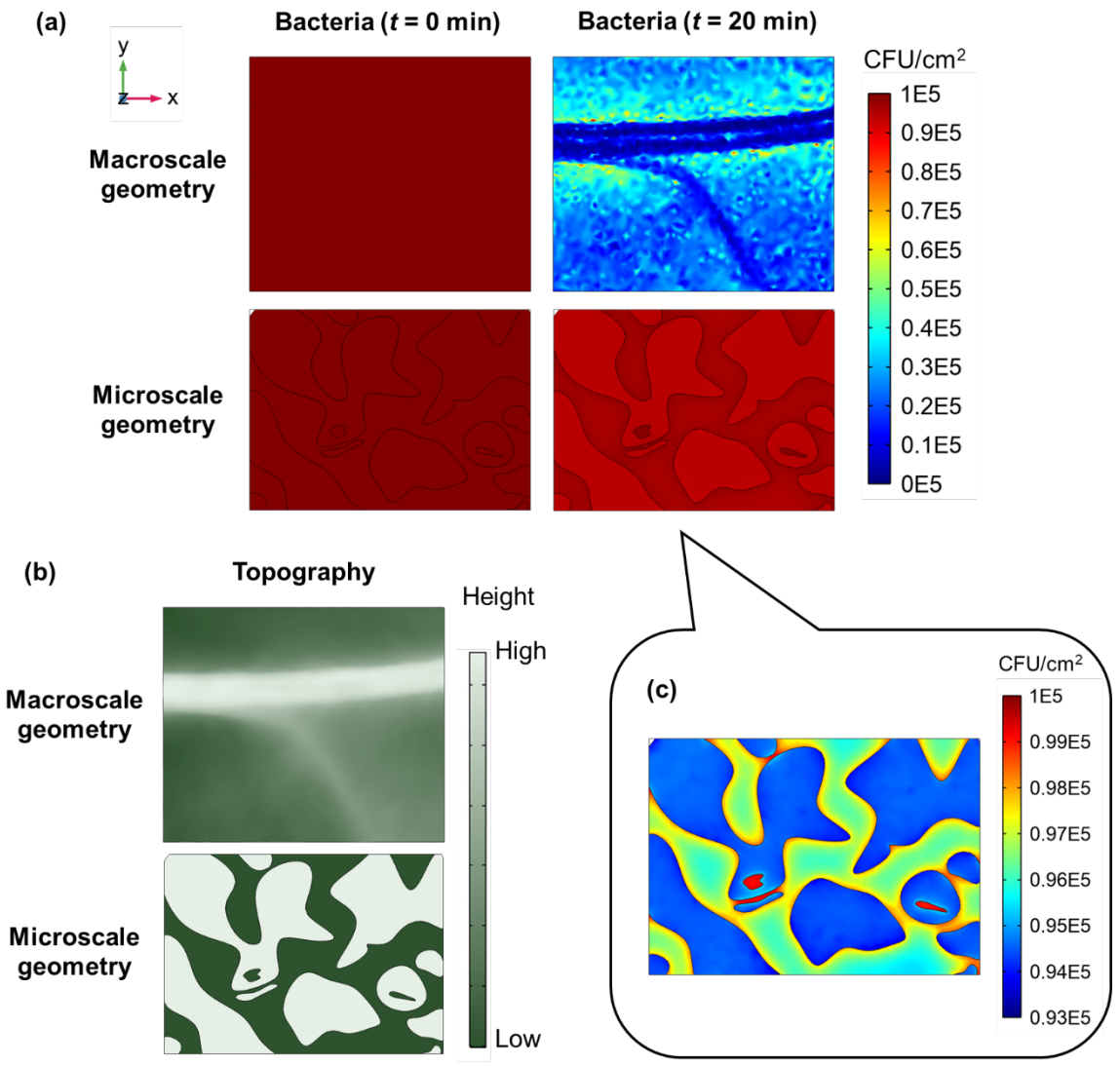

Figure 6.5. Simulated spatial distributions of bacteria remaining on the leaf surface (top view): (a) The changes in the number of bacteria on the leaf surfaces after the first 20 min of free chlorine treatment, (b) their respective surface topography maps from the same angle, and (c) the bacterial distribution on the leaf surface with the microscale geometry at 20 min depicted by a narrower range of color legend.

6.3.2. *Simulation results of the stabilized chlorine model*

The simulation results in Figures 6.6–6.7 show the bacterial inactivation on the leaf surface in the stabilized chlorine model, which represented a targeted delivery system for leaf sanitation using chlorine-charged yeast microparticles (see Section 6.2.3.2). As shown in Figure 6.6a, the maximum surface average concentrations of the equivalent free chlorine for macro-and microscale geometries were 0.35 and 0.11 μg/cm^2, respectively. These concentrations were relatively lower than those of the free chlorine model due to the slower diffusivity, but maintained at a stable level throughout the treatment time, resulting in extended contact time with target bacteria. Consequently, the results in Figure 6.6b show that the levels of bacterial inactivation on the leaf surface were enhanced for both geometries than those of the free chlorine model. Based on the surface average numbers of bacteria on the leaf, the macro-and microscale geometries resulted in 2.0-and 0.4-log reduction after 30-min treatment, respectively. Thus, the stabilized chlorine resulted in a sustained chlorine level on the leaf surface, which led to enhanced bacterial inactivation.

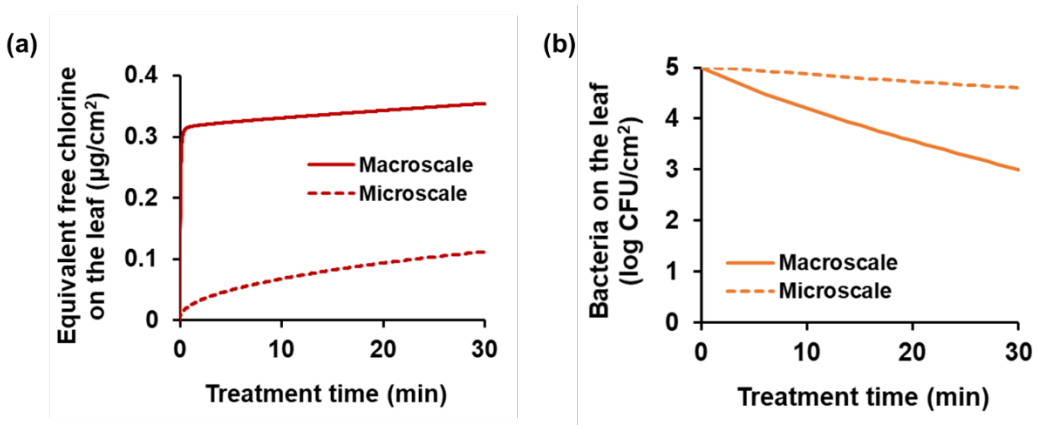

Figure 6.6. Simulated bacterial inactivation on the leaf surface with different geometries using the stabilized chlorine: (a) The equivalent free chlorine concentration and (b) the number of bacteria on the leaf surface during the stabilized chlorine treatment.

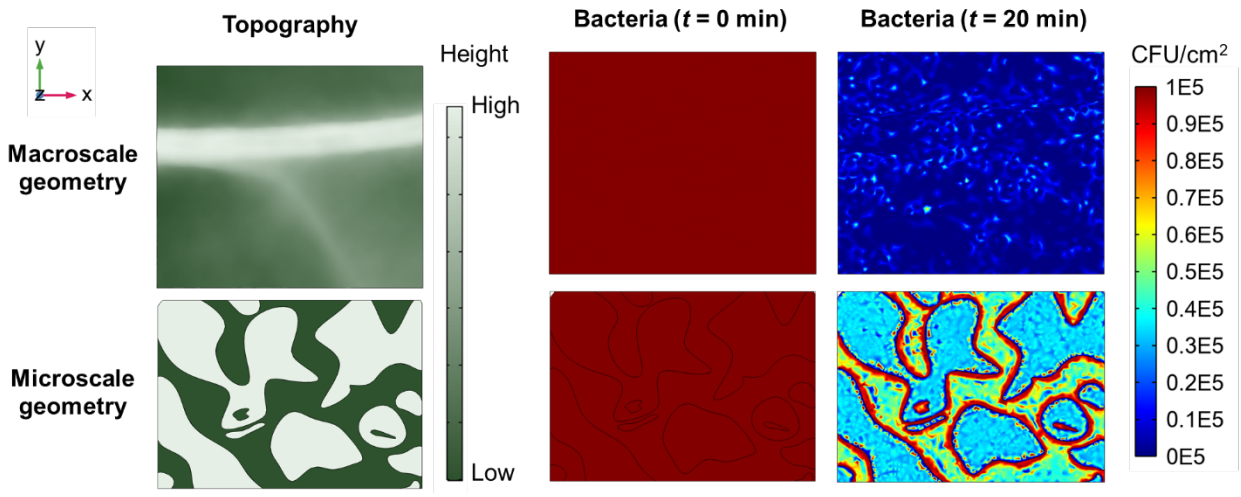

Figure 6.7. Simulated spatial distributions of bacteria remaining on the leaf surface before and after a 20-min of the stabilized chlorine treatment (top view).

6.3.3. *Experimental results*

The data obtained by numerical simulation were further compared with experimental results to validate the models. As shown in Figure 6.8, the overall trends of experimental measurements for bacterial inactivation on the leaf surface matched the simulation results. The experimental results in Figure 6.8a show that the free chlorine and stabilized chlorine treatments on the macroscale geometry resulted in a 0.6-and 2.0-log reduction, respectively. These values were in agreement with the simulation results in Figures 6.4b (0.7 log reduction) and 6.6b (2.0 log reduction), respectively. In contrast, the experimental results in Figure 6.8b show no significant differences ($p > 0.05$) among the values acquired by the free chlorine treatment on the microscale geometry. Similarly, the respective simulation results in Figure 6.4b illustrate that there was no bacterial inactivation. However, the experimental results for the stabilized chlorine treatment on the microscale geometry resulted in a 0.7 log reduction (Figure 6.8b), and this was 0.5-log higher than the value measured for the free chlorine treatment. The respective simulation also illustrated that the stabilized chlorine model resulted in an additional 0.4 log reduction compared to the free chlorine. Overall, the simulation results from the mechanistic models developed in this study matched experimental measurements for both free chlorine and the stabilized chlorine treatment within 30 min..

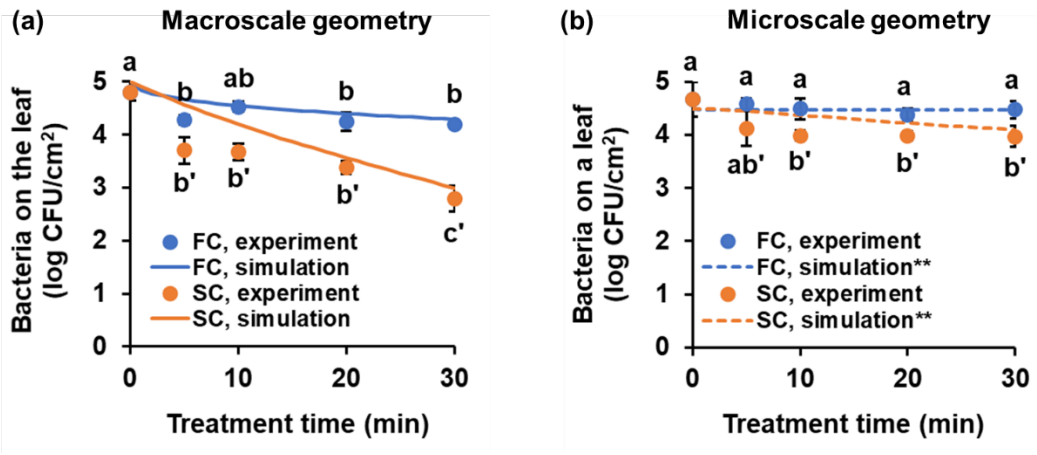

Figure 6.8. Experimental measurements for model validation: Bacterial inactivation on the leaf surface using chlorine-based sanitizers for (a) macroscale and (b) microscale geometries. The dot points are experimental results (the mean values and their standard deviations, $n = 3$), and the lines are simulation results. FC: Free chlorine. SC: Stabilized chlorine. Different letters indicate significant differences between the mean values for the same sanitizer ($p < 0.05$). **The initial bacterial concentration for the microscale simulation was adjusted based on the experimental observation of the loss of loosely attached bacteria after inoculation.

6.4. Discussion

6.4.1. *Influence of the leaf surface microstructure on the antimicrobial efficacy of free chlorine*

The results in Figures 6.4–6.5 illustrate that the effectiveness of free chlorine on bacterial inactivation on the leaf varied depending on the surface topography. In the case of the macroscale geometry, it was shown that bacteria in the crevices along protruding veins survived more than elsewhere (Figure 6.5a). This could be due to the harborages created by the leaf surface structure that enable bacteria to hide from free chlorine. Experimental results from a prior study on spinach leaf surface topography support this finding (Doan, Antequera-Gómez, et al., 2020). This prior study reported that *E. coli* survival on a leaf surface increased with a greater leaf venation upon free chlorine treatment. They also reported that very few bacteria remained on flat PDMS surfaces, so they concluded this observation as a result of structural protection of bacteria from free chlorine. Thus, the results in the present study supplement the prior experimental observation and mechanistically explain the influence of surface topography on chemical reactions of free chlorine. Furthermore, it was reported that leaf veins were the main path of water dispersion, which was associated with bacterial distribution (Doan, Ngassam, et al., 2020). Considering that the present study assumed homogeneous inoculation throughout the leaf surface, the results of bacterial survival against free chlorine may become even worse if more bacteria were accumulated in the macroscale crevices along the veins. Thus, future studies may include the integration of a topography-dependent initial distribution of bacteria.

Similarly, more bacteria survived in the grooves of the microscale geometry, especially in stomata and near the walls created by the patterns of pavement cells (Figure 6.5c). This was consistent with previous studies of plant surface roughness and chlorine treatment (Fransisca &

Feng, 2012; Wang et al., 2009; Zhang et al., 2014). These studies reported that *E. coli* cells inside the micro-or submicron scale grooves were protected from direct contact with free chlorine to survive better than the *E. coli* on a flat section of leaf surfaces. Moreover, the microscale roughness of the leaf surface may increase the rate of free chlorine consumption due to increased surface area of leaf surface to react with plant organic matter. Overall, the leaf surface topography affected the accessibility of free chlorine to bacteria in different sections of the leaf surface, and more bacteria persisted in the macroscale crevices along protruding veins or microscale grooves along pavement cells.

6.4.2. *Enhanced bacterial inactivation on the leaf surface using the stabilized chlorine*

The results in Figure 6.4 show that free chlorine was depleted instantaneously on the leaf surface, resulting in inefficient bacterial inactivation for both macro-and microscale geometries. In the free chlorine model of this study, the plant organic matter concentration was estimated using the literature value of baby spinach extract (Weng et al., 2016). Assuming a homogeneous distribution of plant organic matter within the entire leaf, its surface concentration was computed using the leaf thickness (see Table 6.2). As a result of the exposure to this plant organic matter on the leaf surface, free chlorine was rapidly consumed to form chloramines and organochloramines (Zhou et al., 2015). As shown in Figure 6.4a, despite the high initial concentration of free chlorine in the aqueous phase, a limited amount of free chlorine was presented on the leaf surface after the first few seconds. This rapid depletion of free chlorine by the organic matter of leafy greens was in agreement with previous experimental studies on chlorine-based sanitation (Fu et al., 2018; Shen et al., 2013; Weng et al., 2016; Zhou et al., 2015). Thus, we could conclude that the reaction

between free chlorine and the plant organic matter is dominant compared to its competing reaction between free chlorine and bacteria on the leaf.

In contrast, both simulation and experimental results in Figures 6.6 and 6.8 illustrate that bacterial inactivation on the leaf surface was enhanced when using the stabilized chlorine. The results in Figures 6.4a and 6.6a show that the maximum surface average concentration of equivalent free chlorine in the stabilized chlorine model was lower (0.35 μg/cm^2) than that of the free chlorine model (4.78 μg/cm^2) within 30 min of treatment. This could be due to the slower diffusivity of the stabilized chlorine since it was chemically bound to yeast microparticles that have a larger size (Table 6.2). However, the contact time between the stabilized chlorine and bacteria was longer than that of free chlorine treatment, which led to an enhanced bacterial inactivation of more than 1-log reduction (Figures 6.6b and 6.8). This was consistent with previous studies on the chlorine-based treatment of bacteria (Bremer, Monk, & Butler, 2002; Helbling & VanBriesen, 2007; Shen et al., 2013). These studies reported that bacterial inactivation efficacy of chlorine-based sanitizers was determined by a combination of the chlorine concentration and contact time, i.e., a longer contact time compensated for a lower chlorine concentration. The prolonged contact time of the stabilized chlorine was achieved by the chemical stability against plant organic matter on the leaf surface. Our prior study reported that the stabilized chlorine used in this study had a minimal reactivity with high organic matter in the simulated wash water (Huang et al., 2019). Similarly, there was no significant chlorine loss when the stabilized chlorine was mixed with a non-inoculated leaf (data not shown). Furthermore, the binding affinity to target bacteria contributed to a constant increase of the stabilized chlorine concentration on the leaf surface (Figure 6.6a). It was notable that the maximum surface average concentration of equivalent free chlorine of the stabilized chlorine model with the microscale geometry was higher

(0.11 μg/cm^2) than that of the free chlorine model (0.075 μg/cm^2) after 30 min. These results imply that the stabilized chlorine, which has a specific affinity to bind target cells, could lead to more inactivation of bacteria on the leaf if the treatment time is extended further. Overall, the sustained concentration and extended contact time of the stabilized chlorine improved the bacterial inactivation on the leaf surface.

6.4.3. *Potential application of the mechanistic modeling approach to design targeted antimicrobial delivery systems*

The mechanistic modeling approach proposed in this study could be used to understand the major limitations of current sanitizers and guide the design of targeted antimicrobial delivery systems for the sanitation of leafy greens. For example, the results in Figure 6.9 illustrate the predicted simulation results of the stabilized chlorine with varying binding rates or diffusivities. These results suggest that the stabilized chlorine model was sensitive to the diffusivity of the sanitizers. Since the formulation of the stabilized chlorine could be varied by exploring different biobased carriers with natural binding affinity to bacteria (Huang et al., 2019; Hwang et al., 2017; Kuroda, Ueda, Shibasaki, & Tanaka, 2002; Nam et al., 2002), it would be desirable for future experimental studies to focus on developing smaller carriers that would have a faster diffusivity. In addition, this study concluded that leaf surface topography controlled the antimicrobial efficacy. However, there have been variations in the selection of leaf surface topography for experimental studies: Previous studies on the influence of leaf surface roughness on bacterial behaviors mainly focused on relatively smooth sections excluding major veins (Fransisca & Feng, 2012; Horikawa, Chai, Zhao, Wikle, & Chin, 2014; Palma-Salgado et al., 2020; Zhang et al., 2014), which corresponds to the microscale geometry of the present study; In contrast, studies on the sanitation

of leafy greens used leaves without veins (Palma-Salgado et al., 2020), including veins (Doan, Antequera-Gómez, et al., 2020; Nou & Luo, 2010; Weng et al., 2016), or random pieces (Gómez-López, Marín, Medina-Martínez, Gil, & Allende, 2013; Huang & Nitin, 2019). Thus, the approach proposed in the present study could also provide an insight into the integration of these topographic discrepancies.

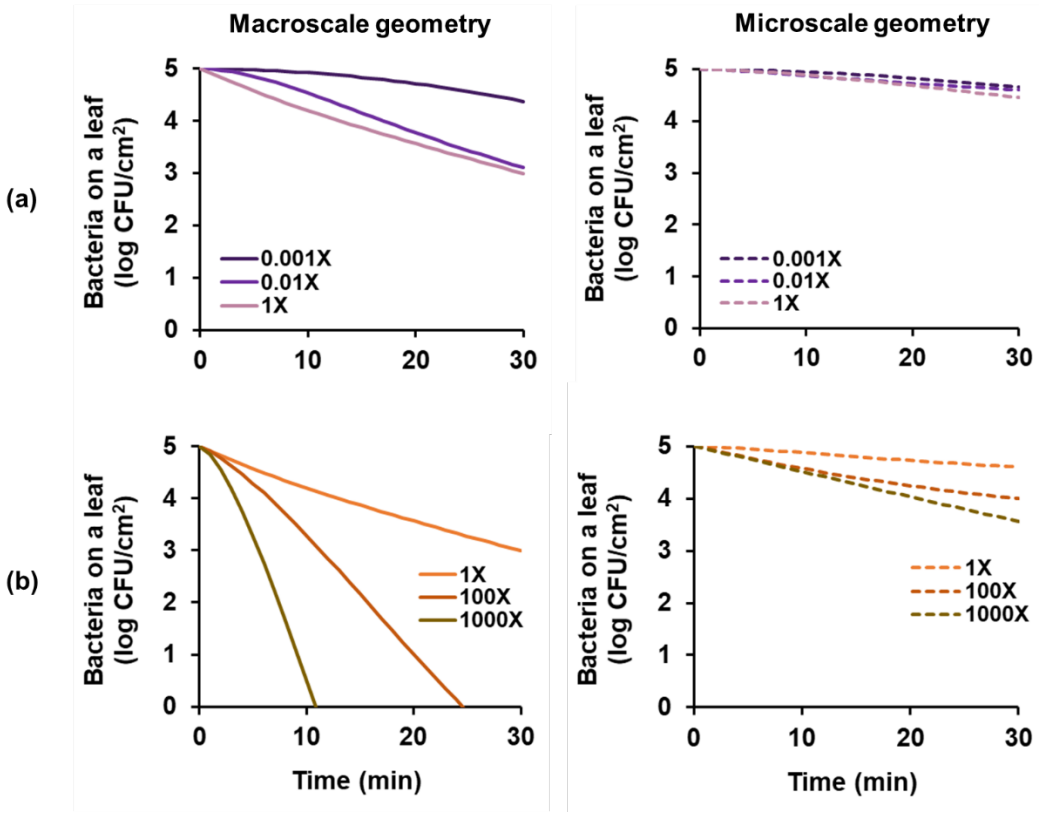

Figure 6.9. Simulated bacterial inactivation on the leaf surface using the stabilized chlorine model with varying (a) binding rates or (b) diffusivities. 1X indicates the original parameter value of the stabilized chlorine for each case.

6.5. Conclusions

This study illustrates the role of multi-scale leaf surface topography in limiting the antimicrobial efficacy of chlorine-based sanitizers by mechanistic modeling. The simulation results show that leaf surface structures of baby spinach at different scales contributed to the chlorine delivery and its respective bacterial survival. Specifically, bacteria in the macroscale crevices or microscale grooves created by the adjacent leaf surface structures, i.e., veins, stomata, epidermal pavement cells, were protected from chlorine-based sanitizers. The use of yeast microparticles enhanced chemical stability and mass transport by a specific bioaffinity to target bacteria, and therefore, this form of stabilized chlorine showed a better antimicrobial efficacy on the leaf surface. Furthermore, the experimental observations of the same set of conditions well-validated these simulation results. Thus, the mechanistic modeling approach developed in this study could be used to design improved antimicrobial systems for washing and sanitation of leafy greens.

Acknowledgements

This work was supported by the United States Department of Agriculture National Institute of Food and Agriculture [grant number 2015-68003-23411]. The authors thank Dr. Atul N. Parikh in the Department of Biomedical Engineering and the Department of Material Science and Engineering at the University of California, Davis for providing laboratory space to prepare leaf replicasts, and Mr. Trevor Quiel from Keyence for his assistance with 3D laser confocal microscopy.

References

Bremer, P. J., Monk, I., & Butler, R. (2002). Inactivation of *Listeria monocytogenes*/*Flavobacterium* spp. biofilms using chlorine: Impact of substrate, pH, time and concentration. *Letters in Applied Microbiology*, *35*(4), 321–325. https://doi.org/10.1046/j.1472-765X.2002.01198.x

Chandler, D., Maldonado, G. I., Primm, R. T., & Freels, J. D. (2011). Neutronics modeling of the high flux isotope reactor using COMSOL. *Annals of Nuclear Energy*, *38*(11), 2594–2605. https://doi.org/10.1016/j.anucene.2011.06.002

Chao, M. S. (1968). The diffusion coefficients of hypochlorite, hypochlorous acid, and chlorine in aqueous media by chronopotentiometry. *Journal of The Electrochemical Society*, *115*(11), 1172. https://doi.org/10.1149/1.2410933

Chiu, Y. C., Shen, C., Farnham, M. W., & Ku, K. M. (2020). Three-dimensional epicuticular wax on plant surface reduces attachment and survival rate of *Salmonella* during storage. *Postharvest Biology and Technology*, *166*, 111197. https://doi.org/10.1016/j.postharvbio.2020.111197

COMSOL. (2008). *COMSOL Multiphysic User's Guide Version 3.5a*.

Doan, H. K., Antequera-Gómez, M. L., Parikh, A. N., & Leveau, J. H. J. (2020). Leaf surface topography contributes to the ability of *Escherichia coli* on leafy greens to resist removal by washing, escape disinfection with chlorine, and disperse through splash. *Frontiers in Microbiology*, *11*, 1–14. https://doi.org/10.3389/fmicb.2020.01485

Doan, H. K., & Leveau, J. H. J. (2015). Artificial surfaces in phyllosphere microbiology. *Phytopathology*, *105*(8), 1036–1042. https://doi.org/10.1094/PHYTO-02-15-0050-RVW

Doan, H. K., Ngassam, V. N., Gilmore, S. F., Tecon, R., Parikh, A. N., & Leveau, J. H. J. (2020). Topography-driven shape, spread, and retention of leaf surface water impacts microbial dispersion and activity in the phyllosphere. *Phytobiomes Journal*, *4*(3), 268–280. https://doi.org/10.1094/PBIOMES-01-20-0006-R

Dong, A., Wang, Y. J., Gao, Y., Gao, T., & Gao, G. (2017). Chemical insights into antibacterial *N*-halamines. *Chemical Reviews*, *117*(6), 4806–4862. https://doi.org/10.1021/acs.chemrev.6b00687

Fransisca, L., & Feng, H. (2012). Effect of surface roughness on inactivation of *Escherichia coli* O157:H7 87-23 by new organic acid-surfactant combinations on alfalfa, broccoli, and radish seeds. *Journal of Food Protection*, *75*(2), 261–269. https://doi.org/10.4315/0362-028X.JFP-11-279

Fu, T., Li, Y., Awad, D., Zhou, T., & Liu, L. (2018). Factors affecting the performance and monitoring of a chlorine wash in preventing *Escherichia coli* O157:H7 cross-contamination during postharvest washing of cut lettuce. *Food Control*, *94*, 212–221. https://doi.org/10.1016/j.foodcont.2018.06.035

Gil, M. I., Selma, M. V., López-Gálvez, F., & Allende, A. (2009). Fresh-cut product sanitation and wash water disinfection: Problems and solutions. *International Journal of Food Microbiology*, *134*(1–2), 37–45. https://doi.org/10.1016/j.ijfoodmicro.2009.05.021

Gómez-López, V. M., Marín, A., Medina-Martínez, M. S., Gil, M. I., & Allende, A. (2013). Generation of trihalomethanes with chlorine-based sanitizers and impact on microbial, nutritional and sensory quality of baby spinach. *Postharvest Biology and Technology*, *85*, 210–217. https://doi.org/10.1016/j.postharvbio.2013.05.012

Helbling, D. E., & VanBriesen, J. M. (2007). Free chlorine demand and cell survival of microbial suspensions. *Water Research*, *41*(19), 4424–4434. https://doi.org/10.1016/j.watres.2007.06.006

Horikawa, S., Chai, Y., Zhao, R., Wikle, H. C., & Chin, B. A. (2014). Effects of food surface topography on phage-based magnetoelastic biosensor detection. *Sensing for Agriculture and Food Quality and Safety VI*, *9108*(May 2014), 910802. https://doi.org/10.1117/12.2049852

Huang, K., Dou, F., & Nitin, N. (2019). Biobased sanitizer delivery system for improved sanitation of bacterial and fungal biofilms. *ACS Applied Materials & Interfaces*, *11*, 17204–17214. https://doi.org/10.1021/acsami.9b02428

Huang, K., & Nitin, N. (2019). Antimicrobial particle-based novel sanitizer for enhanced decontamination of fresh produce. *Applied and Environmental Microbiology*, *85*(8), e02599-18. https://doi.org/10.1128/AEM.02599-18

Hwang, G., Liu, Y., Kim, D., Li, Y., Krysan, D. J., & Koo, H. (2017). *Candida albicans* mannans mediate *Streptococcus mutans* exoenzyme GtfB binding to modulate cross-kingdom biofilm development *in vivo*. *PLoS Pathogens*, *13*(6), 1–25. https://doi.org/10.1371/journal.ppat.1006407

Ju, T., Liu, S., Yang, J., & Sun, D. (2014). Rapidly exploring random tree algorithm-based path planning for robot-aided optical manipulation of biological cells. *IEEE Transactions on Automation Science and Engineering*, *11*(3), 649–657. https://doi.org/10.1109/TASE.2013.2289311

Karalis, K., Karkalos, N., Antipas, G. S. E., & Xenidis, A. (2015). Electromagnetic phenomena in an electric submerged arc furnace. *METAL 2015 - 24th International Conference on Metallurgy and Materials*, *Conference Proceedings*, 60–66.

Kinsinger, N. M., Mayton, H. M., Luth, M. R., & Walker, S. L. (2017). Efficacy of post-harvest rinsing and bleach disinfection of *E. coli* O157:H7 on spinach leaf surfaces. *Food Microbiology*, *62*, 212–220. https://doi.org/10.1016/j.fm.2016.10.019

Kuroda, K., Ueda, M., Shibasaki, S., & Tanaka, A. (2002). Cell surface-engineered yeast with ability to bind, and self-aggregate in response to, copper ion. *Applied Microbiology and Biotechnology*, *59*, 259–264. https://doi.org/10.1007/s00253-002-1014-8

Lin, B., Li, H., Chen, Z., Zheng, C., Hong, Y., & Wang, Z. (2017). Sensitivity analysis on the microwave heating of coal: A coupled electromagnetic and heat transfer model. *Applied Thermal Engineering*, *126*, 949–962. https://doi.org/10.1016/j.applthermaleng.2017.08.012

Macarisin, D., Patel, J., Bauchan, G., Giron, J. A., & Ravishankar, S. (2013). Effect of spinach cultivar and bacterial adherence factors on survival of *Escherichia coli* O157:H7 on spinach leaves. *Journal of Food Protection*, *76*(11), 1829–1837. https://doi.org/10.4315/0362-028X.JFP-12-556

Marshall, K. E., Hexemer, A., Seelman, S. L., Fatica, M. K., Blessington, T., Hajmeer, M., … Gieraltowski, L. (2020). Lessons learned from a decade of investigations of Shiga toxin–producing *Escherichia coli* outbreaks linked to leafy greens, United States and Canada. *Emerging Infectious Diseases*, *26*(10), 2319–2328. https://doi.org/10.3201/eid2610.191418

Munther, D., Luo, Y., Wu, J., Magpantay, F. M. G., & Srinivasan, P. (2015). A mathematical model for pathogen cross-contamination dynamics during produce wash. *Food Microbiology*, *51*, 101–107. https://doi.org/10.1016/j.fm.2015.05.010

Nam, J. M., Fujita, Y., Arai, T., Kondo, A., Morikawa, Y., Okada, H., … Tanaka, A. (2002). Construction of engineered yeast with the ability of binding to cellulose. *Journal of Molecular Catalysis - B Enzymatic*, *17*(3–5), 197–202. https://doi.org/10.1016/S1381-1177(02)00028-0

Neidhardt, F. C., Ingraham, J. L., & Schaechter, M. (1990). *Physiology of the Bacterial Cell*. Sinauer Associates, Sunderland, MA.

Nou, X., & Luo, Y. (2010). Whole-leaf wash improves chlorine efficacy for microbial reduction and prevents pathogen cross-contamination during fresh-cut lettuce processing. *Journal of Food Science*, *75*(5), M283–M290. https://doi.org/10.1111/j.1750-3841.2010.01630.x

Olaimat, A. N., & Holley, R. A. (2012). Factors influencing the microbial safety of fresh produce: A review. *Food Microbiology*, *32*(1), 1–19. https://doi.org/10.1016/j.fm.2012.04.016

Palma-Salgado, S., Ku, K. M., Dong, M., Nguyen, T. H., Juvik, J. A., & Feng, H. (2020). Adhesion and removal of *E. coli* K12 as affected by leafy green produce epicuticular wax composition, surface roughness, produce and bacterial surface hydrophobicity, and sanitizers. *International Journal of Food Microbiology*, *334*, 108834. https://doi.org/10.1016/j.ijfoodmicro.2020.108834

Santos, T., Valente, M. A., Monteiro, J., Sousa, J., & Costa, L. C. (2011). Electromagnetic and thermal history during microwave heating. *Applied Thermal Engineering*, *31*(16), 3255–3261. https://doi.org/10.1016/j.applthermaleng.2011.06.006

Shen, C., Luo, Y., Nou, X., Wang, Q., & Millner, P. (2013). Dynamic effects of free chlorine concentration, organic load, and exposure time on the inactivation of *Salmonella*, *Escherichia coli* O157:H7, and non-O157 Shiga toxin–producing *E. coli*. *Journal of Food Protection*, *76*(3), 386–393. https://doi.org/10.4315/0362-028X.JFP-12-320

Soffe, R., Altenhuber, N., Bernach, M., Remus-Emsermann, M. N. P., & Nock, V. (2019). Comparison of replica leaf surface materials for phyllosphere microbiology. *PLoS ONE*, *14*(6). https://doi.org/10.1371/journal.pone.0218102

Soffe, R., Bernach, M., Remus-Emsermann, M. N. P., & Nock, V. (2019). Replicating *Arabidopsis* model leaf surfaces for phyllosphere microbiology. *Scientific Reports*, 9(1), 1–12. https://doi.org/10.1038/s41598-019-50983-7

Vogelmann, T. C., & Evans, J. R. (2002). Profiles of light absorption and chlorophyll within spinach leaves from chlorophyll fluorescence. *Plant, Cell and Environment*, *25*(10), 1313–1323. https://doi.org/10.1046/j.1365-3040.2002.00910.x

Wang, H., Feng, H., Liang, W., Luo, Y., & Malyarchuk, V. (2009). Effect of surface roughness on retention and removal of *Escherichia coli* O157:H7 on surfaces of selected fruits. *Journal of Food Science*, *74*(1), 1–8. https://doi.org/10.1111/j.1750-3841.2008.00998.x

Weng, S., Luo, Y., Li, J., Zhou, B., Jacangelo, J. G., & Schwab, K. J. (2016). Assessment and speciation of chlorine demand in fresh-cut produce wash water. *Food Control*, *60*, 543–551. https://doi.org/10.1016/j.foodcont.2015.08.031

Yeni, F., Yavaş, S., Alpas, H., & Soyer, Y. (2016). Most common foodborne pathogens and mycotoxins on fresh produce: A review of recent outbreaks. *Critical Reviews in Food Science and Nutrition*, *56*(9), 1532–1544. https://doi.org/10.1080/10408398.2013.777021

Yi, J., Huang, K., Ma, Y., Sun, G., Young, G. M., & Nitin, N. (2021). Antimicrobial *N*-halamine incorporated poly(vinyl alcohol-co-ethylene) films for reducing cross-contamination of fresh produce. *Food Control*, *124*, 107880. https://doi.org/10.1016/j.foodcont.2021.107880

Yi, J., Huang, K., & Nitin, N. (2021a). Modeling bioaffinity-based targeted delivery of antimicrobials to *Escherichia coli* biofilms using yeast microparticles. Part 1: model development and numerical simulation. Manuscript submitted for publication.

Yi, J., Huang, K., & Nitin, N. (2021b). Modeling bioaffinity-based targeted delivery of antimicrobials to *Escherichia coli* biofilms using yeast microparticles. Part 2: parameter evaluation and validation. Manuscript submitted for publication.

Zhang, B., Luo, Y., Pearlstein, A. J., Aplin, J., Liu, Y., Bauchan, G. R., … Millner, P. D. (2014). Fabrication of biomimetically patterned surfaces and their application to probing plant-bacteria interactions. *ACS Applied Materials and Interfaces*, *6*(15), 12467–12478. https://doi.org/10.1021/am502384q

Zhou, B., Luo, Y., Nou, X., Lyu, S., & Wang, Q. (2015). Inactivation dynamics of *Salmonella enterica*, *Listeria monocytogenes*, and *Escherichia coli* O157: H7 in wash water during simulated chlorine depletion and replenishment processes. *Food Microbiology*. https://doi.org/10.1016/j.fm.2015.03.004

CHAPTER 7:

Conclusions

In this research, novel antimicrobial compositions and mechanistic mathematical models were investigated to reduce microbial contamination of fresh produce and food contact surfaces. The research focused on evaluating physicochemical factors in cross-contamination of fresh produce, chemical modification of food contact surfaces with *N*-halamine formulations, and modeling targeted antimicrobial delivery systems for inactivation of persistent microbes (i.e., microbes in biofilms or on leaf surfaces). In addition, multi-scale leaf surface topography was analyzed to characterize the sanitation of fresh produce.

Chapter 2 quantitatively assessed the risk potential of microbial cross-contamination from a contaminated leaf surface to biotic surfaces (leafy greens) or abiotic surfaces (food contact surfaces). The results show that leaf-to-leaf cross-contamination was instantaneous (< 5 s) and bi-directional. Moreover, a single contaminated leaf could transfer microbes to multiple leaves, highlighting the risk potential of cross-contamination. The increase in the applied contact force enhanced microbial transfer efficiency of *L. innocua*, but this effect was limited for *P. fluorescens*, which is a plant-associated bacterium that has a higher affinity to the leaf surface. Furthermore, the results illustrate the significance of hydrophobicity of a substratum surface that microbes are attached or transferred. Overall, the methodology developed in this chapter could give reproducible results with precise control on physical contact conditions, and it was further applied in Chapters 3–4 to examine the efficacy of novel antimicrobial food contact surfaces.

Chapters 3 and 4 evaluated the effects of reducing cross-contamination of leafy greens using antimicrobial surfaces modified with *N*-halamine compositions. The results from Chapter 3

demonstrate *N*-halamine incorporated hydrophilic plastic [poly(vinyl alcohol-co-ethylene)] films' ability to rapidly inactivate microbes and reduce cross-contamination of leafy greens. The chlorine-charged plastic films showed self-cleaning activity and reduced leaf-to-surface-to-leaf cross-contamination efficiently (approximately 2 log reduction) in 10 min without deteriorating food quality. This effect was reduced with a higher applied contact force due to enhanced exposure to organic matter on the leaf surface. The results from Chapter 4 show that *N*-halamine compositions could also be deposited on hydrophobic plastic (polypropylene) surfaces with food-grade coatings. A commercial yeast-derived *N*-halamine precursor called Bio-Mos was used as an antimicrobial compound, and beeswax was a coating base that provides hydrophobicity. The chlorine-charged Bio-Mos/beeswax coatings on plastic surfaces demonstrated rapid bacterial inactivation (> 4 log reduction in 2 min), and their antimicrobial activity was effective under simulated processing conditions, i.e., aqueous and organic-rich environments. These coatings also reduced leaf-to-surface-to-leaf cross-contamination efficiently (> 2 log reduction) in 10 min.

Chapter 5 investigated targeted delivery systems for *E. coli* biofilm treatment based on a mechanistic modeling approach. Both experimental and numerical simulation results illustrate improved biofilm inactivation by utilizing yeast microparticles that form *N*-halamine compositions. Moreover, the roles of the following factors in biofilm inactivation were determined by parameter evaluation of the developed model: (i) the chemical stability of chlorine-charged yeast microparticles, (ii) binding affinity of yeast microparticles to the biofilms, and (iii) controlled release of chlorine. The results show that the chemical stability and binding affinity were key factors in improving antibiofilm efficacy. This conclusion was further supported by experimental validation using two types of yeast microparticles. The mechanistic modeling framework

developed in this chapter was applied in Chapter 6 to understand the antimicrobial efficacy of chlorine-charged yeast microparticles on more complex geometries (i.e., leaf surface).

Chapter 6 combined experimental and mathematical modeling approaches to understand the sanitizer efficacy on the leaf surface considering multi-scale surface topography. The results demonstrate that leaf surface structures at different scales (μm to cm) controlled the sanitizer delivery and *E. coli* survival. Limited antimicrobial efficacy was observed for the microbes placed in the crevices and grooves created by the leaf surface structures, including veins, stomata, and epidermal pavement cells. In addition, chlorine-charged yeast microparticles improved the sanitizer efficacy on the leaf surface by enhanced chemical stability and binding affinity that increased mass transport to target microbes. The simulation results in this chapter were also validated by experimental observations.

Overall, the novel antimicrobial compositions and mechanistic modeling approaches developed in this research demonstrate the effective strategies to reduce microbial contamination of fresh produce and food contact surfaces. Based on the findings in this research, potential follow-on studies may include:

- Development of antimicrobial surfaces using *N*-halamine compositions with advanced chemical stability in the presence of high organic load by increasing the surface area (e.g., use of fiber structure)
- Design of biobased targeted antimicrobial delivery systems by utilizing the mechanistic modeling approach to guide experimental plans (e.g., reduced particle size to increase diffusivity, encapsulation of food-grade polymers to enhance binding affinity)
- Integration of mechanistic modeling approach and artificial intelligence-based parameter optimization for real-time food processing control

- Quantitative risk assessment approach in evaluating the implementation of novel antimicrobial compositions in postharvest processing based on measurement of microbial transfer efficiency